AGH University of Krakow

FIELD OF SCIENCE: NATURAL SCIENCES

SCIENTIFIC DISCIPLINE : PHYSICAL SCIENCES

DOCTORAL DISSERTATION

Unconventional superconductivity, topology and strong electronic correlations in two dimensional transition-metal dichalcogenide moiré bilayers

Author: *WASEEM AKBAR*

Supervisor: Dr. hab. inż. Michał Zegrodnik, Prof. AGH
Auxiliary supervisor: Dr. hab. Andrzej Biborski, Prof. AGH

AGH University of Kraków
Academic Centre for Materials and Nanotechnology

Kraków, 2026

Dedication

To my beloved wife, **Rubab Ashraf** for her patience, understanding and unwavering encouragement throughout this journey; to my beloved **parents, brothers and sisters**, whose constant support and care for my children during my PhD have been the foundation of my strength; and to my children, **Muhammad Eisa**, **Umm E Aiman** and **Muhammad Ibrahim**, whose love sustained me even from afar.

This dedication is especially for my Father **Akbar Khan Shad** and daughter **Umm E Aiman**.

Declaration

Declaration of the Author of this dissertation:

Aware of legal responsibility for making untrue statements I hereby declare that I have written this dissertation myself and all the contents of the dissertation have been obtained by legal means.

.....

Date, Author's signature

Declaration of Supervisor:

This dissertation is ready to be reviewed.

.....

Date, Supervisor's signature

Declaration of Auxilliary Supervisor:

This dissertation is ready to be reviewed.

.....

Date, Auxilliary Supervisor's signature

Acknowledgements

Pursuing a PhD in Physics has been a long term goal for me, achieved through dedication, hard work and persistence. This achievement reflects years of continuous effort, learning and personal growth in my journey toward knowledge.

I am sincerely grateful to my supervisor, Prof. Michał Zegrodnik and Auxiliary supervisor Prof. Andrzej Biborski, for their continuous guidance, support and encouragement throughout my PhD studies. Their valuable insights and mentorship greatly contributed to the shaping of this work. I truly appreciate your support in helping me overcome challenges and grow as a researcher. I am indebted to research Collaborator Prof. Louk Rademaker for insightful discussions that helped shape the direction of this research. I would also like to thank Prof. Michał Nowak for the valuable group discussions during the weekly meeting, which created a supportive and intellectually engaging atmosphere.

On the occasion of submitting my PhD thesis, I also appreciate my Master's supervisor, Prof. Safdar Nazir. The discipline and passion for research that I developed under his supervision have remained with me throughout the years.

I express my sincere gratitude to the administrative staff of the ACMiN Centre, especially the former Director Prof. Marek Przybylski, Prof. Piotr Bała (current Director), Ms. Anna Wójcikowska and Ms. Paulina Dudek for their excellent support and continuous cooperation in efficiently handling administrative procedures and documentation.

Although it would be unfair to single out only a few individuals. First, I would like to recall the wonderful time here in Kraków, especially the memorable moments shared with Fasih Zareef, Ahsan Soomro, Hafeez Ur Rehman, Abu Sarhan, Junaid Ur Rehman, Amir Sultan, Ms. Mehr Un Nisa, Piotr Osada, Grzegorz and Ms. Laiba Amir. I also acknowledge my dear friends Sajid Elahi, Tasadduq Niaz, Irfan Elahi, Ms. Tahira Liaqat and Abdul Khaliq for their thoughtful discussions, valuable advice and constant encouragement throughout this journey. My heartiest thanks to my dear friend Ms. Sabina, You have always been such a wonderful and close friend. I truly appreciate all the meaningful conversations we have about so many different topics. I also cherish the wonderful moments shared with my friends Adnan Zahoor, Qasim Bilal, Ahtasham Ali, Fahad Khan, Rafeeq Hasan and Hafiz Bilal,

whose companionship and constant support helped me through many challenging situations. In addition, I am also deeply grateful for the intellectually stimulating conversations with Junaid Ur Rehman, Hafeez Ur Rehman and Abu Sarhan, covered a wide range of topics greatly enriched my critical thinking and perspective. I fondly recall the pleasant time with colleagues in our research group particularly with Dibyendu Kuiri, Ms. Shalini Maji, Jorge Correa, Palash Saha, Arindam Pramanik and members of the research centre. I am highly thankful to the research centre's administration for providing such an excellent and supportive environment for academic and personal growth.

Highly important, I would like to acknowledge the National Science Centre, Poland (NCN) for financial support under decision No.2021/42/E/ST3/00128. I also acknowledge the PLGrid infrastructure (ACK Cyfronet AGH) and tera ACMiN cluster for providing computational resources and support.

Abstract

Two dimensional (2D) moiré superlattices provide a highly controllable environment for exploring the intertwined effects of strong electronic correlations, nontrivial topology and unconventional superconductivity. Here we focus on the transition-metal dichlacogenide (TMD) bilayers which lead to a moiré pattern when two identical monolayers such as WSe_2 are stacked with a small twist angle or when different monolayers such as WS_2 and WSe_2 are combined even in the absence of twisting. The main aim of this study is to develop a unified theoretical understanding of unconventional superconducting state in TMD bilayers based on the effective low energy $t-J$ and $t-J-U$ models where the pairing mechanism originates from kinetic exchange in the moderately and strongly correlated regimes. In order to take into account the significant role of electron-electron interactions, we apply the Gutzwiller approximation method. Our analysis reveal several key features: (i) The emergence of topological superconductivity in twisted bilayer WSe_2 in the strongly correlated regime, revealing two topologically non-trivial superconducting domes characterized by mixed singlet $(d+id)$-wave and triplet $(p-ip)$-wave symmetry and a Mott insulating state at half-filling which is consistent with the early experimental report; (ii) In the moderately correlated regime and in the presence of intersite Coulomb repulsion term (V-term) we demonstrate that superconductivity emerges only within a narrow window of displacement field values, specifically when the Van Hove singularity aligns with half-filling, in qualitative agreement with the subsequent experimental data; (iii) We show that the negative U-Hubbard model, which results in conventional form of the paired state, does not fully resembles the experimental situation which additionally suggests that unconventional character of the paired state and significant role of electron correlations should be viewed as necessary ingredients of the theoretical description of superconductivity in WSe_2 homobilayer; (iv) Our numerical calculations show, that due to renormalization effects the considered pairing mechanism allows the superconductivity to persist even for relatively large values of V which are characteristic to WS_2/WSe_2 heterostructure, what emphasizes the potential of this system as another candidate for unconventional SC in the family of moiré flat band systems. Overall, this study establishes that the theoretical framework based on the t-J-U model provides a promising route towards unified description of SC in moiré TMD bilayers.

Streszczenie

Dwuwymiarowe (2D) supersieci moiré stanowią wysoce kontrolowalną platformę do badania wzajemnie powiązanych efektów silnych korelacji elektronowych, nietrywialnej topologii oraz niekonwencjonalnego nadprzewodnictwa. W niniejszej pracy koncentrujemy się na dwuwarstwach dichalkogenków metali przejściowych (TMD), które prowadzą do powstania struktury moiré, gdy dwie identyczne monowarstwy, takie jak WSe_2, są połączone z niewielkim kątem skręcenia lub gdy różne monowarstwy, takie jak WS_2 i WSe_2, są połączone nawet bez skręcenia. Głównym celem pracy jest opracowanie spójnego opisu teoretycznego niekonwencjonalnego stanu nadprzewodzącego w dwuwarstwach TMD w oparciu o efektywne niskoenergetyczne modele t–J oraz t–J–U, w których mechanizm parowania wynika z kinetycznej wymiany w reżimach umiarkowanych i silnych korelacji. Aby uwzględnić istotną rolę oddziaływań elektron-elektron, zastosowano metodę przybliżenia Gutzwillera. Nasza analiza ujawnia kilka kluczowych wyników: (i) pojawienie się topologicznego nadprzewodnictwa w skręconej dwuwarstwie WSe_2 w reżimie silnych korelacji, z dwiema topologicznie nietrywialnymi kopułami nadprzewodzącymi o mieszanej symetrii singletowej ($d+id$) oraz trypletowej ($p-ip$), a także stan izolatora Motta przy połowicznym zapełnieniu, co jest zgodne z wczesnymi wynikami eksperymentalnymi; (ii) w reżimie umiarkowanych korelacji oraz w obecności oddziaływania kulombowskiego między węzłami (V) wykazujemy, że nadprzewodnictwo pojawia się jedynie w wąskim zakresie wartości prostopadłego pola elektrycznego, gdy osobliwość Van Hove'a pokrywa się z połowicznym zapełnieniem, co jakościowo zgadza się z późniejszymi danymi eksperymentalnymi; (iii) pokazujemy, że model Hubbarda z ujemnym U, prowadzący do konwencjonalnego stanu sparowanego, nie odtwarza w pełni sytuacji eksperymentalnej, co wskazuje, że niekonwencjonalny charakter parowania oraz istotna rola korelacji elektronowych są kluczowymi elementami opisu teoretycznego nadprzewodnictwa w dwuwarstwie WSe_2; (iv) nasze obliczenia numeryczne pokazują, że dzięki efektom renormalizacji rozważany mechanizm parowania pozwala na utrzymanie nadprzewodnictwa nawet dla stosunkowo dużych wartości V, charakterystycznych dla heterostruktury WS_2/WSe_2, co podkreśla potencjał tego układu jako kolejnego kandydata do niekonwencjonalnego nadprzewodnictwa w rodzinie układów z wąskimi pasmami moiré. Podsumowując, niniejsza praca pokazuje, że formalizm teoretyczny oparty na modelu t-J-U stanowi obiecującą drogę do spójnego opisu nadprzewodnictwa w dwuwarstwach moiré opartych o TMD.

Table of contents

Abbreviations

SC	Superconductivity
AFM	Antiferromagnetic
U	Onsite Coulomb repulsion
J	Superexchange interactions
TMD	Transition-metal dichalcogenide
TBG	Twisted bilayer graphene
SOC	Spin orbit coupling
D	Displacement field
VHS	Van Hove singularity
tWSe_2	Twisted WSe_2
DOS	Density of states
V	Intersite Coulomb repulsion

Chapter 1

Introduction

In recent years, moiré systems have attracted considerable interest because they offer access to a range of remarkable phenomena driven by electron correlations including unconventional superconductivity (SC), correlated insulating phases, exotic magnetic features and topological states [1–7]. The key advantage of moiré superlattice systems lies in their ability to allow precise tuning of the electron density through gate voltage, thus avoiding the disruptive effects associated with chemical doping. Moreover by changing the twist angle, one can also tune the strength of electron-electron correlations [8–10]. These systems combine versatile physical properties with exceptional tunability, making them promising platforms for next generation superconducting electronics and quantum information technologies. At the same time, they provide a controlled setting for understanding correlated electron phenomena and uncovering the microscopic origins of unconventional SC where topology, symmetry and strong electronic correlations cooperate to produce novel states.

In this chapter, we briefly review the historical development of unconventional SC before turning to moiré flat band physics, which shares key features with strongly correlated systems such as high-T_c cuprates [11].

1.1 Unconventional Superconductivity and Strong Correlations

The discovery of SC by Kamerlingh Onnes in 1911 marked a milestone in condensed matter physics [12] that was later complemented by the Meissner effect in 1933, which demonstrated the expulsion of magnetic fields from superconductors and established SC as a distinct thermodynamic phase [13]. Early theories including the London equations and Ginzburg Landau theory described superconducting properties phenomenologically but did not explain

the microscopic origin of electron pairing. A major breakthrough occurred in 1957 with the Bardeen Cooper Schrieffer (BCS) theory, which explained SC as phonon mediated electron pairing with an isotropic s-wave gap and the corresponding thermodynamic properties [14]. From the late 1970s onward, a series of superconductors have been discovered that could not be explained within the BCS framework and led to the concept of unconventional SC. The first evidence of unconventional pairing was reported in the heavy fermion compound $CeCu_2Si_2$ in 1979 [15]. In these materials, strong hybridization between conduction electrons and localized f orbitals gives rise to heavy quasiparticles with effective masses hundreds of times that of free electrons. Heavy fermions are characterized by unconventional gap symmetries and a strong interplay with magnetism indicating a pairing mechanism beyond conventional phonon mediation. In these systems, SC often coexists or competes with antiferromagnetism and is widely believed to arise from spin fluctuation mediated pairing [16, 17]. A transformative breakthrough came in 1986 with the discovery of high T_c cuprate superconductors by Bednorz and Müller [18], whose transition temperatures exceeded the limits of conventional BCS theory (above liquid nitrogen). Subsequent experiments established a d-wave order parameter with gap nodes and sign changes in the superconducting wave function [19], clearly distinguishing them from conventional isotropic s-wave superconductors. In addition, strontium ruthenate is a superconductor with spin triplet pairing [20] while iron based superconductors exhibit unconventional SC arises from anisotropic s-wave pairing [21]. More recently, nickelates [22] and kagome metals AV_3Sb_5 (A = K, Rb, Cs) [23] have emerged as cuprate analogs, exhibiting intertwined SC, charge order and topological phenomena. Together, these discoveries highlight the diversity of unconventional SC across materials with varying lattice structures and electronic environments. Such systems are typically characterized by strong or moderate electronic correlations and competing orders. Unconventional superconductors are distinguished by nontrivial gap symmetries (d-, p-, or extended s-wave), spin-triplet or mixed parity pairing states, proximity to competing fluctuations (magnetic, charge, or nematic), and pairing mechanisms dominated by spin or orbital interactions rather than phonons. In these systems, BCS theory fails to explain the characteristic features of the superconducting state.

One of the most prominent examples of strongly correlated systems as well as unconventional superconductors are copper-based compounds. Their characteristic temperature–doping phase diagram exhibits a dome-shaped dependence on T_c and the emergence of competing electronic orders such as antiferromagnetism and pseudogap see Fig. 1.1(a) (adopted from [24]). The undoped parent compounds are antiferromagnetic (AFM) charge transfer insulators with high Néel temperatures. The antiferromagnetism is rapidly suppressed on both electron and hole doping, giving way to a superconducting dome with a

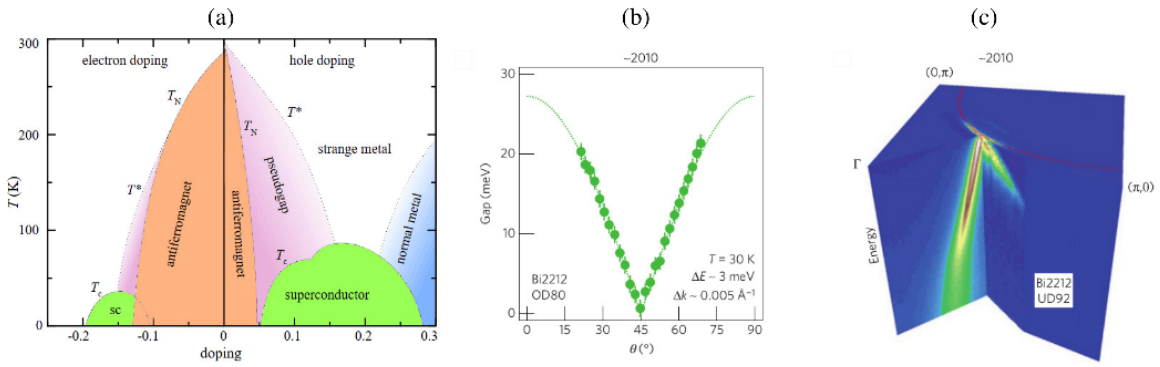

Fig. 1.1 (a) Phase diagram of cuprate superconductors as a function of doping, showing the evolution from the antiferromagnetic Mott insulator to the superconducting dome and strange metal phase. Taken from Ref. [24].
(b) Momentum dependence of the superconducting gap measured by ARPES, illustrating the anisotropic gap structure and its evolution along the Fermi surface. This figure is obtained from Nat. Phys. **10**, 483–495 (2014). (c) Three dimensional ARPES intensity plot showing quasiparticle dispersion near the nodal direction, with linear energy-momentum relation and well-defined quasiparticle velocity. Sourced from Phys. Rev. Lett. **104**, 207002 (2010).

maximum T_c near optimal hole doping ($\delta \approx 0.1$–0.2). As identified by APRES measurements, the gap exhibits strong angular depedance reaching its maximum near the antinodal region and continuosly decreasing toward the nodal direction (cf. Fig. 1.1 b,c). On the hole-doped side, a broad pseudogap regime extends above the superconducting dome and terminates at a critical doping, while charge and spin density modulations develop in the underdoped region and may coexist or compete with SC. At higher doping, the normal (strange) metallic state emerges above T_c, evolving toward conventional metallic behavior [24]. Further, the hole doped cuprates exhibit charge density wave and incommensurate spin density wave correlations in the underdoped regime, where they coexist and compete with SC. Beyond optimal doping, the pseudogap phase terminates and the system gradually evolves toward a more conventional Fermi-liquid like metallic state at low temperatures [25]. Despite decades of research, a unified theoretical picture remains elusive, with proposed mechanisms ranging from Coulomb driven pairing and magnetic spin fluctuations to more conventional phonon mediated scenarios.

To capture these complex phenomena, modern theoretical approaches very often employ strongly correlated lattice models that explicitly incorporate Coulomb interactions and competing electronic orders. These studies are based on the *Hubbard model*, which describes the competition between kinetic energy and onsite Coulomb repulsion (U) [26], and its extension, the *extended Hubbard model* which accounts charge and spin instabilities [27]. In the strong coupling limit, the Hubbard model leads to the t–J model framework, where

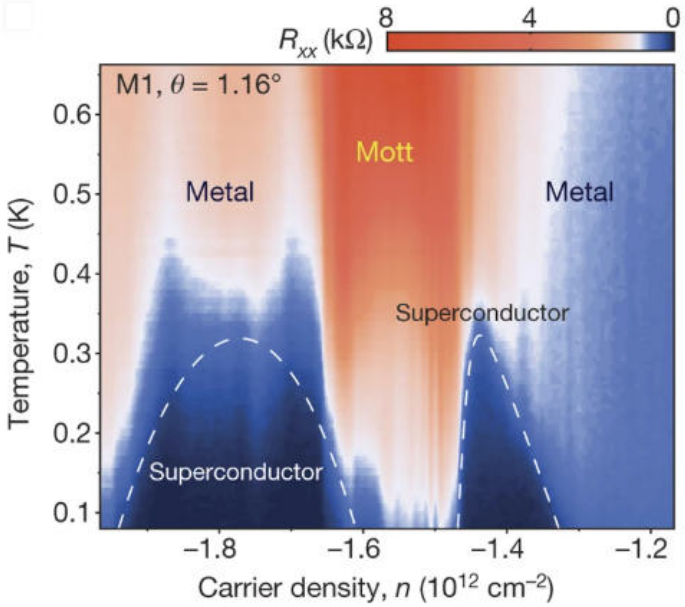

Fig. 1.2 Temperature–carrier density phase diagram of magic-angle twisted bilayer graphene (M1, $\theta = 1.16°$), showing the longitudinal resistance R_{xx}. A correlated Mott-like insulating state emerges near half-filling, flanked by metallic regions. Superconducting domes appear adjacent to the insulating phase, as indicated by the dashed boundaries. (Adopted from Ref. [1]).

double occupancy is prohibited and superexchange interactions (J) provide an effective AFM coupling between neighboring spins, potentially driving electron pairing with d-wave gap symmetry [28]. Together, these theoretical frameworks provide a coherent foundation for understanding unconventional SC in strongly correlated electron systems, a central focus of modern condensed matter physics. Within such approaches, strong electronic correlations play a central role in unconventional SC, which often emerges near Mott insulating phases, as in the cuprates, where large U localizes electrons near half filling, and doping induces phenomena such as pseudogaps [29], nematicity [30] and strange metal behavior [31] (cf. Fig. 1.1(a)).

1.2 Moiré Superlattices: From Twisted Bilayer Graphene to Twisted Transition Metal Dichalcogenides

In recent years another group of correlated systems has gathered significant interest in the context of unconventional SC. These systems are formed by stacking two monolayers with a small twist angle or lattice mismatch, resulting in a long wavelength moiré superlattice. The size of the unit cell depends on the twist angle. Moreover in the momentum space

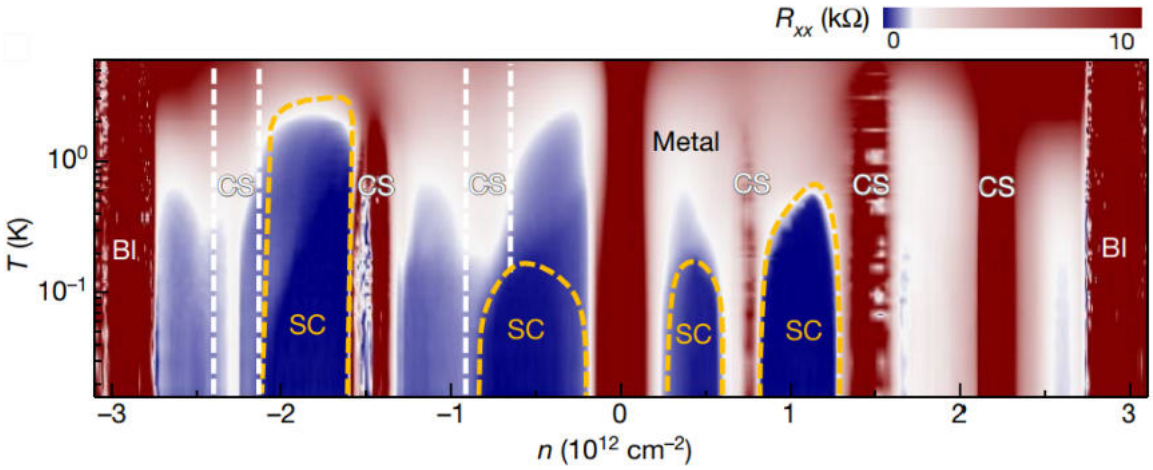

Fig. 1.3 Schematic carrier density-temperature phase diagram of the magic angle twisted bilayer graphene. As one can see the superconducting state appears in close proximity to the correlated insulating state, which resides at all integer moiré band filling factors.
(Extracted from Ref. [32]).

a minibrillouin zone is created but most importantly for proper twist angles, flat bands appear on the electronic structure which points to the role of strong correlations. The emergence of correlated insulating (commonly known as mott insulating) state and SC phases in moiré materials has opened a new era for exploring strongly interacting quantum phases in condensed matter physics. Currently, the vast majority of moiré quantum materials are mostly graphene and transition-metal dichalcogenide (TMD) based [1, 2, 8, 33–35].

Twisted bilayer graphene (TBG) marked the first experimental realization in which moiré engineering dramatically flattened electronic bands near the magic angle (1.1°), strongly enhancing electron electron interactions and giving rise to correlated (Mott) insulating states and SC [1, 2]. In addition, interaction driven topological phases, including Chern insulating states with quantized anomalous Hall response, have been experimentally observed at certain integer fillings [36, 37], highlighting the rich interplay between strong correlations and topology in moiré systems. These findings provided the first clear evidence that band flattening in moiré materials can drive strong correlation effects, establishing TBG as a highly tunable model system for studying the interplay of electron correlations, SC and nontrivial topology. Interestingly, similarly as in cuprates, the correlated insulating phases emerge at integer moiré band filling factors while superconducting domes appear upon slight doping away from these insulating states as depicted in Fig. 1.2 and 1.3. This intimate relationship suggests that SC in TBG is strongly influenced by electronic correlations and may arise from the same underlying interaction driven physics that stabilizes the insulating phases. Moreover, experiments on twisted double bilayer graphene proximitized by WSe_2 have demonstrated

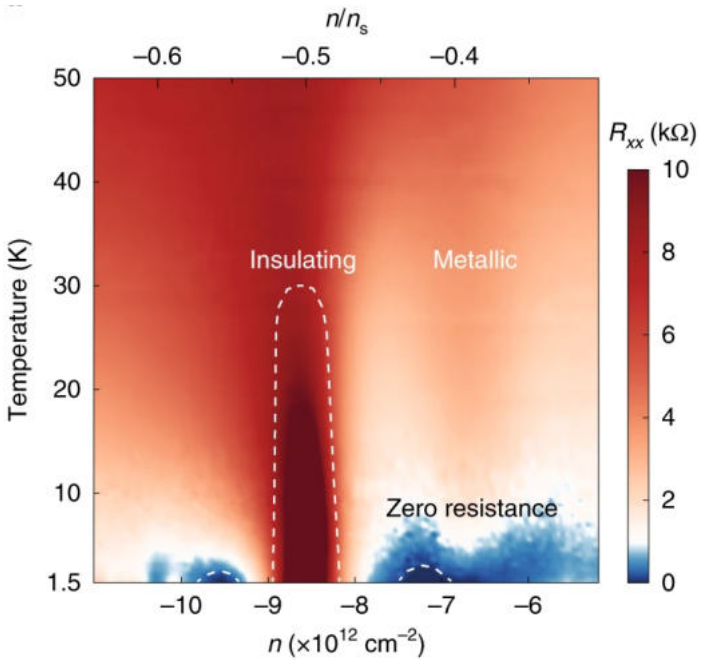

Fig. 1.4 Resistance as a function of temperature and density for a twist angle of 5.1° at D= 0.45 V/nm^{-1}. The density is varied with V_bg, while V_tg ia at -12.25 V. Two zero-resistance regions, which suggests a transition to superconducting behavior, appear when doping away from the insulating state (adopted from Ref. [8]).

gate tunable SC domes in both valence and conduction bands near van Hove singularities (VHS) [38]. These include interaction driven ferromagnetism and anomalous Hall effects near fractional fillings [36], the intrinsic quantized anomalous Hall (Chern insulating) state [37], nematicity and rotational symmetry breaking [39], orbital magnetism/valley polarization [32] and correlated Chern insulators in aligned graphene/hBN structures [40]. These fundamental discoveries paved the way for correlated insulating and superconducting states in magic-angle TBG and naturally extend to twisted TMD systems, where stronger moiré potentials and intrinsic spin orbit coupling (SOC) give rise to even richer correlated and topological phenomena.

The second prominent family of moiré systems are the TMD-based multilayers formed from twisted or stacked MoS_2, $MoSe_2$, WS_2 and WSe_2 monolayers [41–43]. Compared to graphene, flat bands in TMD moiré systems are more robust to twist angle variations, possess sizeable band gaps, and exhibit spin valley locking due to broken inversion symmetry which are absent in graphene based moiré materials [35, 44–48]. Despite these differences, Mott insulating states and SC have also been observed in twisted WSe_2 ($tWSe_2$) [8, 10, 49, 50] and $tMoTe_2$ [51, 52]. Rapid advances in TMD fabrication and synthesis continue to expand the study in these systems [53]. Experimentally, twisted TMD bilayers have revealed a

variety of correlation driven phases emerging due to moiré physics [8, 10, 42, 46, 49, 50]. These studies show that the emergent phases in twisted TMD bilayers are governed by strong electron electron interactions, valley physics and symmetry breaking rather than weak coupling mechanisms [41, 48, 54]. An exotic quantum phases driven primarily by electron–electron interactions in the $tWSe_2$ bilayers is also theoretically observed [41, 55]. Continuum and Hubbard based models reveal chiral and topological characteristics in this system [56, 57]. Mapping $tWSe_2$ onto effective triangular lattice Hubbard models establishes a direct connection between continuum descriptions and lattice Hamiltonians, enabling systematic studies to already experimentally exploited exotic quantum phases [42].

Beyond twist engineering, moiré superlattices have also been realized via lattice mismatch in vertically stacked WS_2/WSe_2 heterobilayers leading to correlated insulating states and excitonic localization [35, 58, 59]. The heterobilayers have stronger interactions than the homobilayers [60]. An additional motivation for studying the heterobilayer system is that both experimental observations and theoretical analyzes indicate that on-site and intersite Coulomb repulsion play a significant role [35, 58, 61–65]. In particular, a significant value of V (intersite repulsion integral) in WS_2/WSe_2 heterobilayers drive charge ordering and generalized Wigner crystallization as experimentally observed at certain fractional fillings [35, 58, 63–65]. However, SC has not been experimentally verified in this system.

Chapter 2

Experimental Data and Motivation

The past half decade has witnessed remarkable progress in the exploration of correlated phases in moiré TMD bilayers, notably $tWSe_2$ and WS_2/WSe_2. In this chapter, we systematically analyze the experimental data and key phenomenology related with the physics of moiré bilayers with the emphasis placed on the superconducting state. This will set the stage for next chapters, where we develop many body theoretical frameworks and compare our theoretical results with these experiments.

For the first time, Wang *et al.* reported low-energy flat bands with signatures of collectively correlated phases in $tWSe_2$ bilayers within the twist angle range of approximately 4°–5.1°. The system was precisely tuned by controlling the carrier density n, dual gating (displacement field D) and twist angle. They identified a correlated insulating state at half filling and observed signatures of two superconducting domes, corresponding to electron and hole doping, away from half filling, with SC appearing below 3 K at 5.1° (cf. Fig. 2.1) twist. They further showed that the insulating state remains unchanged under increasing magnetic field, indicating a non-ferromagnetic ground state identified as an AFM insulating phase. In addition, they mapped the phase diagram and demonstrated that the position of the VHS evolves continuously as a function of D. With increasing D, the VHS shifts from low filling $|n/n_s| < 0.5$ to higher filling $|n/n_s| > 0.5$, passing through half filling. It should be noted that, despite the important discoveries reported by *Wang* in 2020, the superconducting state was not unambiguously detected at that time.

Few years after, a strong experimental evidence of the superconducting state in $tWSe_2$ has been reported by *Xia et al.,* and *Guo et al.,* [10, 49]. Fig. 2.2 compiles experimental results from those two independent studies. The left panel (a) reports SC at a twist angle of 3.65° in which a well defined Mott insulating state is observed precisely at half filling at some non-zero values of the displacement field and SC emerges in close proximity to this insulating phase, appearing at half-filling end near zero or small vertical displacement

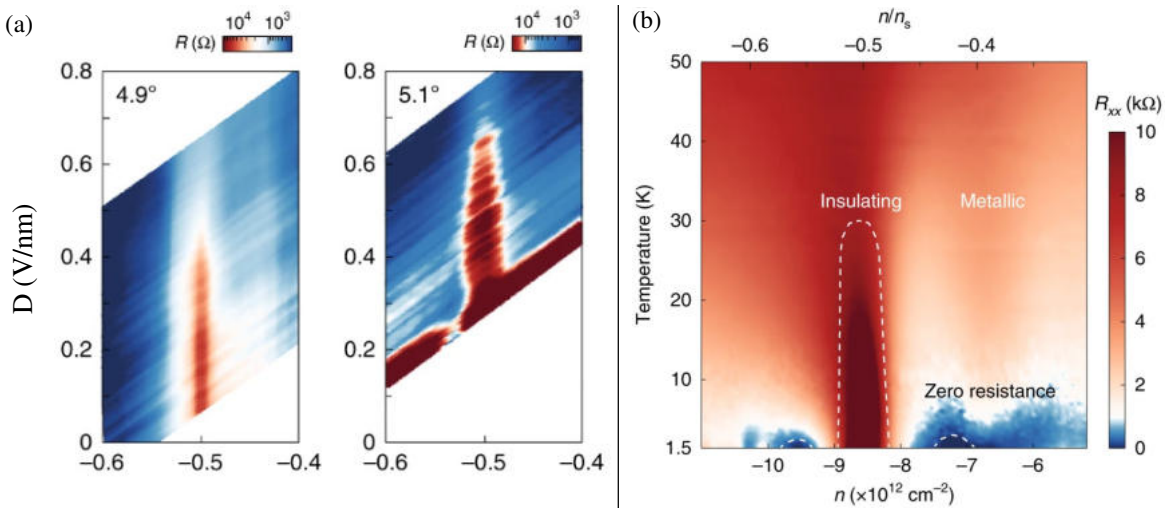

Fig. 2.1 (a) Resistance versus displacement field and normalized density near half filling for all the measured angles (b) Resistance as a function of temperature and density for a twist angle of 5.1° at D= 0.45 V/nm^{-1}. The density is varied with V_bg, while V_tg ia at -12.25 V. Two zero-resistance regions, which suggests a transition to superconducting behavior, appear when doping away from the insulating state (adopted from Ref. [8]).

field [49]. In contrast in the second study, SC is not found exactly at half filling but instead develops on the hole doped side at larger twist angle of ~ 5.0°, slightly away from the half filled Mott state and requires a relatively larger D [10]. This apparent shift of the SC/Mott insulating state away from the half filling may arise from uncertainty in the determination of the band filling, as indicated in the right corner of Fig. 2.2 (c). Taken together, these experiments demonstrate that although SC consistently emerges in close proximity to a correlated (likely AFM) insulating state, its precise location in band filling and displacement field strongly depends on the twist angle. This highlights the delicate interplay between moiré band structure, strong electronic correlations and electric field tunability in tWSe_2 moiré systems.

A key advance characteristic reported recently in another experimental paper is the systematic dependence of the correlated phases on the twist angle in the tWSe_2 moiré bilayers (cf. Fig. 2.3) [50]. In this experiment, they revealed a rich phase diagram including an AFM insulator, superconducting domes and strange metal. As shown in Fig. 2.3, the ground state evolves systematically with hole filling and displacement field. At small twist angles, the half filled insulating state is robust and centered near small E, whereas increasing the twist angle weakens the correlated insulating phase, shifts it to higher displacement fields. This observation is consistent with the theoretical study which shows broadening of the upper valence moiré band with increasing twist angle. As shown in Fig. 2.3, SC begins to emerge around twist angles of 3.5°–3.6° and at higher angles (~ 4.6°–4.7°), it appears around half

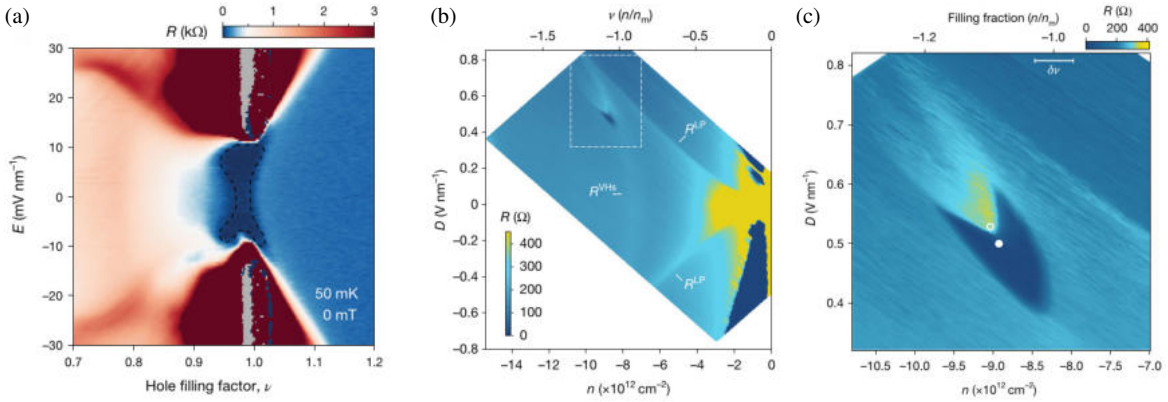

Fig. 2.2 Zero bias resistance R as a function of temperature T and filling factor ν at $E \approx 8\,\mathrm{mV\,nm^{-1}}$ and $B = 0$. Superconductivity appears only in the vicinity of $\nu = 1$, while the corresponding normal state exhibits a pronounced resistance peak around 10 K
((a) panel taken from Refs. [49] and (b), (c) [10]).

filling under large E. Although Guo *et al.,* observed SC slightly away from half filling at high D, their filling fraction was uncertain. Here, we clearly see resolve an insulating state exactly at half filling for small D and at larger angles for higher D, SC arises near the AFM Mott insulating phase (see magnified phase diagram), underscoring the interplay of strong correlations and SC in $tWSe_2$ moiré systems. It should also be noted that according to this experimental analysis, the SC state can also be stable at half-filling for small enough D, leading to single dome behavior. Despite these advances, a microscopic understanding of the superconducting mechanism in $tWSe_2$ remains incomplete, particularly with regard to the role of electronic correlations, VHS and their interplay with emergent magnetic phases.

Another moiré material that shows some similarities with $tWSe_2$ is WS_2/WSe_2 where moiré pattern emerges due to lattice mismatch. Most importantly, correlated insulating states have been identified at half filling of WS_2/WSe_2. Moreover, the system exhibits correlated insulating phases at a variety of fractional band fillings (cf. Fig. 2.4), consistent with interaction driven charge ordering or Wigner crystal formation [34, 35, 63, 66]. These experimental data indicates that in WS_2/WSe_2 not only the onsite repulsion but also the longer range Coulomb interaction plays the central role. It should be noted that SC has not yet been experimentally observed in WS_2/WSe_2 heterobilayer moiré system. However, the strong tendency towards interaction driven ordering provides a clear motivation to theoretically investigate whether and under what conditions SC may emerge in this lattice mismatch induced moiré platform.

This PhD thesis aims to develop a unified theoretical understanding of unconventional superconducting state in $tWSe_2$ homobilayer within the t-J and t-J-U model-based approaches where pairing is induced by substantial kinetic exchange. We determine the fundamental

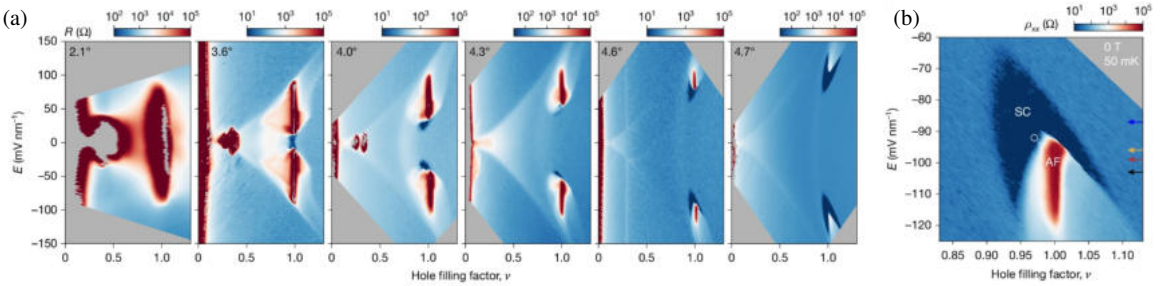

Fig. 2.3 **Longitudinal resistance of $tWSe_2$ across twist angles.** Maps of the longitudinal resistance R measured at $T = 1.6\,\mathrm{K}$ and $B = 0\,\mathrm{T}$ as a function of displacement field E and hole filling factor ν for twist angles spanning 2.1° to 4.7°. Pronounced correlated insulating states are visible at $\nu = 1$, $1/3$, and $1/4$ for the smaller twist angles. These insulating features weaken with increasing twist and become indiscernible near $\theta = 4.7°$, consistent with a reduction in correlation strength as the moiré period decreases. Close-up view of the dashed box in panel showing the longitudinal resistivity ρ_{00} as a function of filling factor ν and vertical electric field E (at $T = 50$ mK and $B = 0$ T) for device (4.6° twisted WSe_2). The white circle marks the location of the highest superconducting transition temperature T_c. The grey region indicates experimentally inaccessible values of ρ_{00}. (Sourced from Ref. [50]).

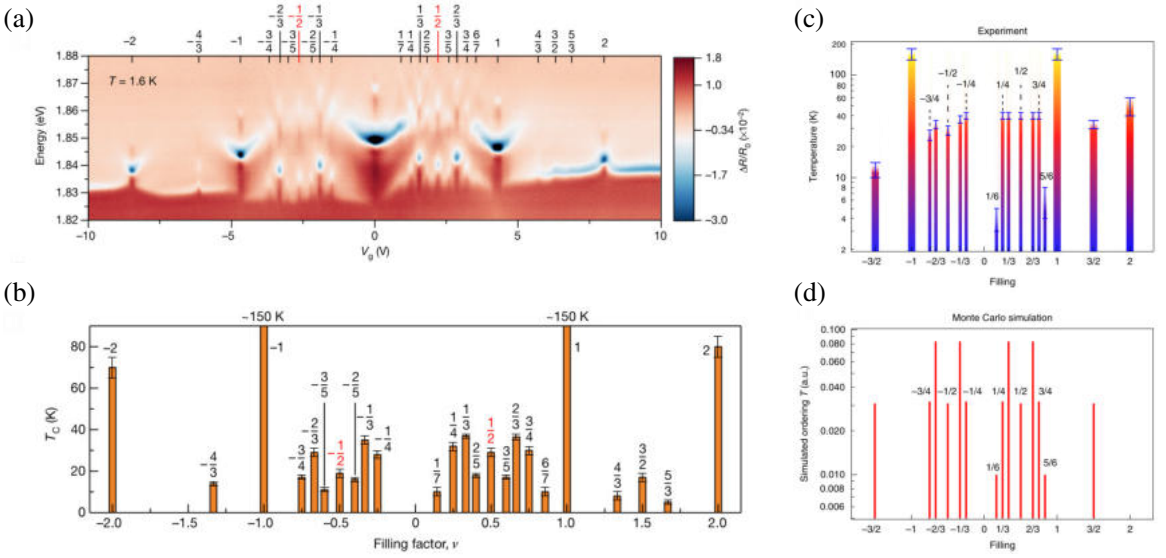

Fig. 2.4 (a,b) Representative measurements from Ref. [63] illustrating the emergence of strongly correlated insulating states and tunable electronic phases in moiré superlattices. Here (a) The colorbar $\Delta R/R_0$ represents the relative reflectance contrast, which probes changes in the optical conductivity and excitonic resonances, and thereby provides information about the underlying electronic structure and correlated states and Panel (b) presents $\Delta R/R_0$ highlighting correlated insulating states at integer and fractional fillings and their temperature dependent evolution. (c,d) Results from Ref. [58] demonstrating interaction driven phenomena and signatures of nontrivial band topology in WS_2/WSe_2 moiré heterostructure.

features of the paired state such as pairing symmetry, topological properties as well as the response to experimentally controlable parameters. We analyze the role of SOC and the effect of density of states (DOS) evolution on the obtained results. An important part of our study is the reconstruction and understanding of the experimentally observed phase diagram in the band filling-displacement field plane. Additionally, we compare the results obtained in the main part of the analysis with an alternative approarch based on the negative-U Hubbard model which generates a more conventional type of paired state.

Due to similarities between tWSe_2 homobilayer and WS_2/WSe_2 heterobilayer, we also analyze the possibility of the paired phase appearance in the latter. Due to enhanced amplitude of the intersite Coulomb repulsion (V) in this system, we focus here on the t-J-V and t-J-U-V models. Therefore, we aim at determining the influence of such circumstances on the paired state and most importantly analyzing if the considered unconventional superconducting state can still persist in the range of significant values of the intersite Coulomb integral within the real-space pairing scenario. We also investigate the role of long range hopping and exchange interactions in shaping the SC. As SOC plays a central role in determining the topological character of the phases, we also find the topological features in both systems, as it constitutes a key ingredient for the realization of experimentally robust and technologically relevant topological SC.

Chapter 3

Models and Methods

In this chapter, we discuss the basics of theoretical description appropriate for correlated electron systems. In particular, we provide the theoretical framework which is used in this thesis to investigate the unconventional superconducting phase in moiré TMD systems.

3.1 Models for Strongly Correlated Electron Systems

The simplest minimal model for correlated electrons in a narrow band is the single-band Hubbard model

$$\hat{H}_{\text{Hub}} = \sum_{\langle ij\rangle,\sigma} t_{ij}\hat{c}^{\dagger}_{i\sigma}\hat{c}_{j\sigma} + U\sum_{i}\hat{n}_{i\uparrow}\hat{n}_{i\downarrow} \tag{3.1}$$

where $\hat{c}^{\dagger}_{i\sigma}$ ($\hat{c}_{i\sigma}$) are the operators of creation (annihilation) of an electron with spin σ at the lattice site i and $\hat{n}_{i\sigma} = \hat{c}^{\dagger}_{i\sigma}\hat{c}_{i\sigma}$. The first term describes the kinetic part with so-called hopping amplitudes t_{ij}, while the second term corresponds to onsite electron-electron repulsion. The competition between kinetic delocalization and Coulomb repulsion governs the physics of the model. Despite its apparent simplicity, the Hubbard model exhibits a wide range of physical phenomena. In the weak coupling regime ($U \ll t$), the system behaves as a metal with renormalized quasiparticles, whereas in the strong coupling limit ($U \gg t$), charge fluctuations are suppressed which means that electrons stop moving freely between sites, and additionally the system can develop magnetic order [68–70]. Furthermore, it has been extensively studied as a prototype model for unconventional SC. In particular, numerical and analytical studies have reported the emergence of superconducting phases within the Hubbard model, especially in two dimensional lattices [71–74]. The schematic phase diagram of the Hubbard model on a square lattice as a function of Coulomb repulsion and hole doping δ is shown here in Fig. 3.1 which has been obtained with the use of Diagrammatic Expansion of

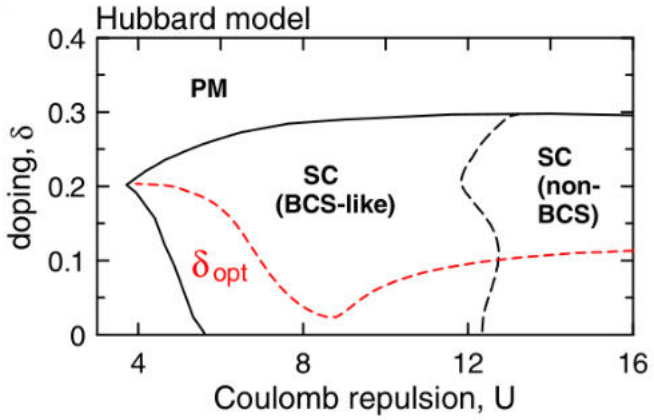

Fig. 3.1 Schematic phase diagram of the Hubbard model as a function of Coulomb repulsion U and hole doping δ ($\delta = 0$ corresponds to half-filling). The diagram shows the paramagnetic (PM) metallic phase at weak coupling, a BCS-like superconducting (SC) region at intermediate interactions, and a non-BCS superconducting phase in the strong-correlation regime. The red dashed line denotes the evolution of optimal doping δ_{opt} for which the SC gap amplitude is the largest for a given U. Adopted from Ref. [67].

the Gutzwiller Wave Function method. As one can see according to this study the system remains in a paramagnetic metallic phase in the weak coupling regime (small U). However, with increasing U and finite doping, a superconducting phase emerges. Note that for the case of moderate correlations ($U \approx W$, where $W \approx 8t$ is the bandwidth), the superconducting state is already stable but relatively weak. The BCS-like and non-BCS regions correspond to positive and negative kinetic energy gain at the transition to the superconducting state (for details see Ref. [67]). At half filling ($\delta = 0$) and for strong correlations $U \gtrsim W$ a Mott insulating state is formed which suppresses pairing and moves the optimal doping away from $\delta = 0$ with further increase of U.

Numerous other studies have shown that the Hubbard model can support unconventional SC with $d_{x^2-y^2}$ pairing symmetry [24, 75, 76]. Thus, the model unifies the description of insulating, magnetic and superconducting phases across varying interaction strength and carrier concentration. On a 2D square lattice, SC emerging from the Hubbard model is most commonly associated with $d_{x^2-y^2}$ pairing symmetry. This pairing state reflects the underlying lattice geometry, where the superconducting order parameter changes sign between the x and y directions and the resulting gap function has nodes along the diagonals of the Brillouin zone ($\Delta(\mathbf{k}) \sim \cos k_x - \cos k_y$). Such a structure is favored by repulsive interactions, as it allows electrons to pair while minimizing U. The $d_{x^2-y^2}$-wave paired state is particularly relevant for cuprate superconductors where the dome like behavior and the *d-wave* character of the order parameter have been reported experimentally.

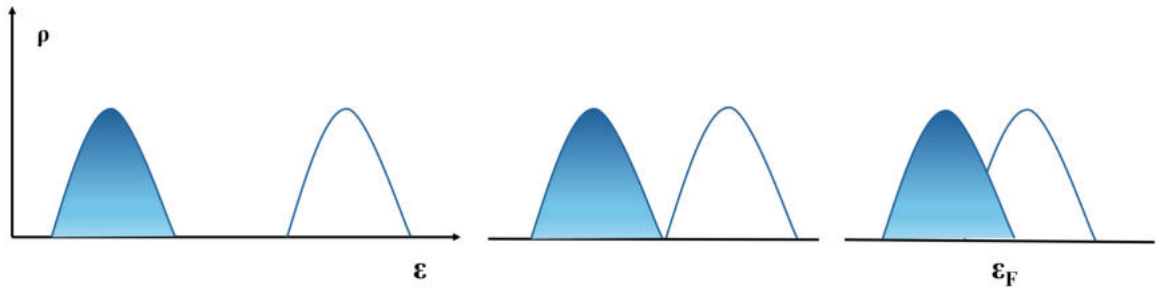

Fig. 3.2 Schematic illustration of the evolution of Hubbard subbands across the Mott transition. With increasing interaction strength, the single-particle spectrum splits into lower and upper Hubbard bands, separated by an interaction-driven gap. The three panels represent the regimes of weak, intermediate, and strong correlations, highlighting the formation and separation of spectral weight. The shaded regions indicate the occupied states, with the Fermi level ε_F shown for reference. This figure is made by me, inspired by the schematic representation in Ref. [77]

An important feature of the Hubbard model is the formation of Hubbard subbands at half-filling which correspond to the Mott-Hubbard metal-insulator transition. For $t \ll U$, added electrons (holes) occupy well-separated Hubbard subbands of width zt, where t is the nearest neighbour hopping amplitude and z is the lattice coordination number. The lower and upper Hubbard band is separated by an energy scale of order U. This splitting reflects the cost of double occupancy and leads to a profound restructuring of the electronic DOS. The schematic illustration of this band splitting is represented in Fig. 3.2, where the spectral weight is redistributed into two distinct subbands corresponding to singly occupied and doubly occupied configurations. The figure illustrates the evolution of the electronic structure within the Hubbard model as a function of the interaction strength U/t. For small U/t, the system behaves as a metal, while increasing U leads to band splitting. Beyond a critical interaction strength, a Mott gap opens, resulting in a transition to an insulating state. In practice the Mott insulating state often exhibits magnetic ordering leading to AFM Mott insulator.

In the limit $U \gg t$, charge fluctuations are suppressed and double occupancy is projected out, yielding an effective t-J Hamiltonian [78] derived via a second-order Schrieffer Wolff transformation.

$$\hat{H}_{tJ} = \sum_{\langle ij\rangle,\sigma} t_{ij}\tilde{c}^{\dagger}_{i\sigma}\tilde{c}_{j\sigma} + J\sum_{\langle ij\rangle}\left(\hat{\mathbf{S}}_i\cdot\hat{\mathbf{S}}_j - \frac{1}{4}\hat{n}_i\hat{n}_j\right) \tag{3.2}$$

A central feature of the t-J model is its natural tendency towards the AFM order at half filling. In the absence of doping, the kinetic term is ineffective *i.e.,* projected fermionic operators $\tilde{c}_{i\sigma}$ act in a restricted Hilbert space that forbids double occupancy and the Hamiltonian

reduces to the Heisenberg model. The exchange coupling $J = \frac{4t^2}{U}$ originates from second order virtual hopping processes, although electrons cannot permanently occupy the same site due to the large U, they can temporarily hop to form a doubly occupied intermediate state and then return. These virtual processes lower the energy when neighboring spins are antiparallel, giving rise to an AFM superexchange interaction leading to a long-range Néel AFM ground state on bipartite lattices. The t-J model thus captures the essential low energy physics of doped Mott insulators, where charge motion and spin correlations are strongly intertwined, and has played a foundational role in theoretical descriptions of high-T_c cuprates. Its formal derivation is strictly valid in the limit $U \to \infty$, where double occupancy is completely excluded, although it is often used as an effective model in very large but finite U. This reflects the strong correlation-driven localization of electrons, where charge degrees of freedom are frozen and low-energy physics is governed entirely by spin fluctuations.

Upon doping mobile holes are introduced into the system and the interplay between kinetic energy and spin exchange becomes highly nontrivial. The motion of holes frustrates the underlying AFM background, as each hopping process tends to disrupt the spin alignment favored by the J-term. This competition gives rise to rich physics, including the suppression of long-range AFM order and the emergence of short range spin correlations. One of the most remarkable consequences of this interplay is the appearance of unconventional SC. Within the t-J framework, the same J responsible for antiferromagnetism can mediate an effective attractive interaction between electrons. This leads to the formation of singlet pairs with predominantly d-wave symmetry, as supported by variational and numerical studies. Unlike SC originated from conventional BCS, where pairing is driven by phonons. Here, the pairing mechanism is purely electronic in origin and arises from strong correlations.

As already described, starting from the Hubbard model and considering the large-U limit, double occupancy is projected out, and an effective kinetic exchange interaction emerges leading to the t-J model. However, in the regime of weak U, double occupancy remains allowed even near half-filling, and the kinetic exchange mechanism becomes less significant. The t-J-U model is considered an effective approach dedicated to the situation when U is in between the two limiting situations. If U is substantial and not infinite, the double occupancies are small but non zero, therefore U term should be present in the Hamiltonian. At the same time, the spin-spin kinetic exchange interaction already starts to develop. In order to explicitly take into account both effects, the t-J-U model is used. The t-J-U model has been proposed already some time ago and discussed in the context of general properties of correlated electron systems [79–83]. The concept is very much related to the so-called Gossamer superconductivity introduced by Laughlin [84] and discussed by F. C. Zhang [85]. It has also been shown that the approach based on the t-J-U model allows to reproduce

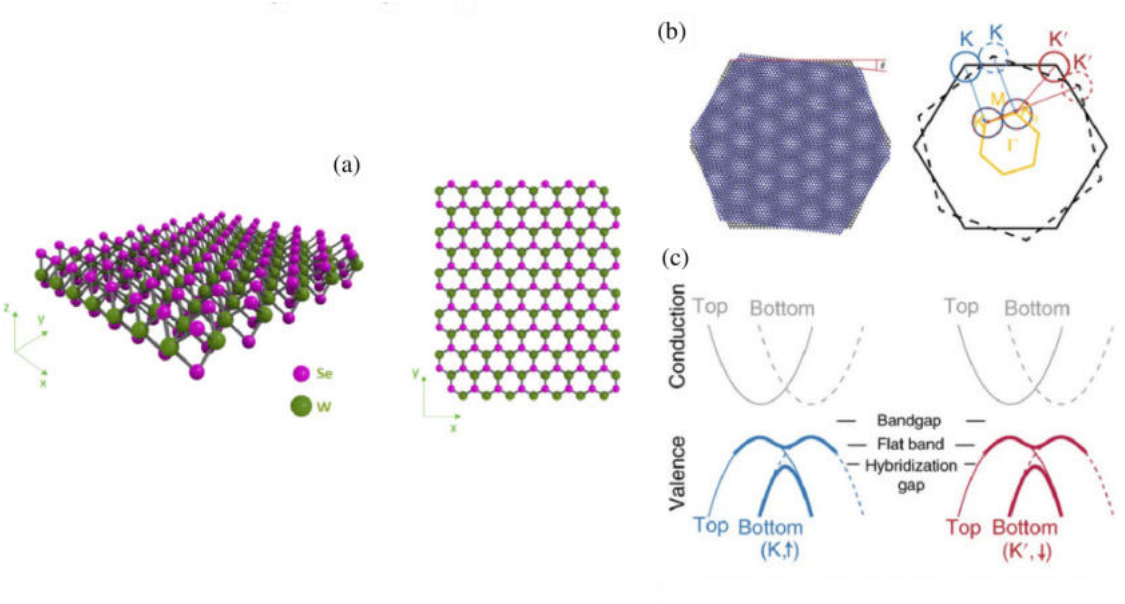

Fig. 3.3 (a) Atomic structure of a monolayer WSe_2 shown in side and top views, illustrating its hexagonal lattice. The lattice constant is $a \approx 0.33\,\text{nm}$. The monolayer consists of a tungsten (W) layer sandwiched between two selenium (Se) layers. (b) Moiré superlattice formed in twisted bilayer WSe_2, along with the corresponding Brillouin zone reconstruction. The figure is sourced from Ref. [8]

selected fundamental properties of cuprates quantitatively [67]. The t-J-U model corresponds to the following form of hamiltonian

$$\hat{H} = \sum_{\langle ij\rangle,\sigma} t_{ij}\hat{c}^{\dagger}_{i\sigma}\hat{c}_{j\sigma} + J\sum_{\langle ij\rangle}\hat{\mathbf{S}}_i\cdot\hat{\mathbf{S}}_j + U\sum_i \hat{n}_{i\uparrow}\hat{n}_{i\downarrow} \tag{3.3}$$

Thus, the t-J-U model provides a controlled and flexible theoretical framework to describe correlated phases in the presence of explicit kinetic exchange term and possible non-zero double occupancies which are significantly suppressed by the U-term.

3.2 Modeling of Moiré Superlattices

Here we discuss the theoretical approach to modeling of TMD moiré superlattices by focusing on the two particular systems which are $tWSe_2$ homobilayer and WS_2/WSe_2 heterobilayer. In the following we start with the homobilayer and than move to the heterobilyer case.

It should be noted that a WSe_2 monolayer forms a hexagonal structure (see Fig. 3.3(a)) and is a semiconductor with a direct band gap of ~ 1.7 eV. After joining two such monolayers with the application of some small twist angle, a moiré structure is formed, characterized by a miniBrillioun zone and flat electronic bands formed at the top of the valence band

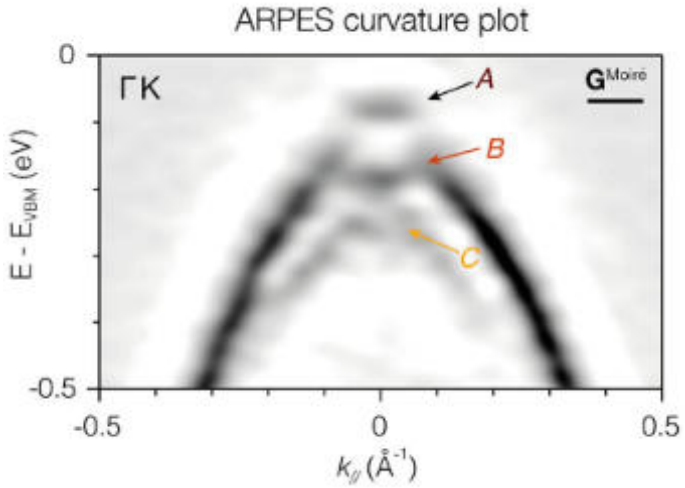

Fig. 3.4 ARPES curvature plot of twisted WSe_2 bilayer showing the valence band dispersion near the Γ–K direction. The enhanced contrast highlights the band structure features, with representative dispersive branches indicated by arrows (A, B, and C). The horizontal axis corresponds to the in-plane momentum $k_{\parallel}$, while the vertical axis shows the binding energy relative to the valence band maximum. This figure is adopted from Phys. Rev. Lett. **131**, 046401 (2023).

(Fig. 3.3(b) and (c)). The creation of such bands has been reported experimentally with the use of ARPES (Fig. 3.4). The flat electonic bands indicate the significant role played by electronic interaction. At the same time calculation methods dedicated for interacting electron systems are characterized by relatively high complexity and/or they require large computational resources. Therefore, an important point of any theoretical approach aimed at understanding the electron correlation effects begins with the determination of minimal effective model. In general, for the case of moiré systems one can distinguish between two approaches. The first one can be considered as more standard one and has been extensively applied to previously known correlated systems like cuprates. Namely, this approach is based on first principle calculation according to Density Functional Theory, which allows one to determine the band structure as well as to project the obtained result onto a simplified tight binding Hamiltonian in real space which takes into account only the most relevant degrees of freedom. The obtained minimal model supplemented with various interaction terms, due to their simplicity allow to account for significant electronic correlations as well as analyze various exotic states. The projection itself can be carried out with the use of Wannierization procedure or by simply fitting the tight binding hopping parameters so as the resulting bands reconstruct the ab initio result. This approach has been applied by Wang et al [8] in order to determine an effective model that describes the single flat moiré band of $tWSe_2$. The resulting tight-binding Hamiltonian on a triangular lattice with spin and direction dependent

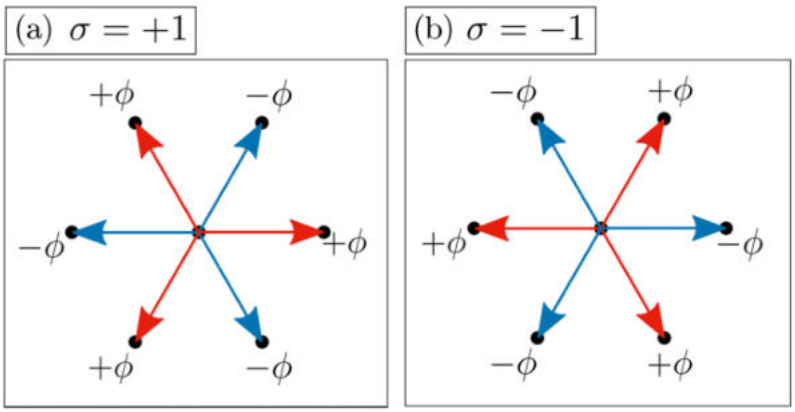

Fig. 3.5 Phase of the complex hoppings to the nearest neighbors for spin up (a) and spin down (b) electrons

complex hoppings parameters is given by

$$H_0 = \sum_{ij\sigma} t_{ij\sigma}\, \hat{c}^{\dagger}_{i\sigma} \hat{c}_{j\sigma}, \tag{3.4}$$

where $\sigma = \pm 1$ represents spin up/down, $\hat{c}^{\dagger}_{i\sigma}$ and $\hat{c}_{i\sigma}$ are the creation and anihilation operators for the electron with spin σ at the site i of a triangular lattice, and $t_{ij\sigma}$ denotes the hopping amplitude between neighboring sites i and j. As Wang *et al.,* considered hoppings up to the fifth nearest neighbors in this $tWSe_2$ moiré bilayer [8]. However, the interactions are taken into account up to the third nearest neighbor in our theoretical analysis. These hopping parameters have complex, spin dependent phases reflecting the underlying spin-valley locking which comes as a result of Ising type SOC. The complex hopping parameters, $t_{ij\sigma}$, satisfy the hermiticity requirement ($t_{ij\sigma} = t^{*}_{ij\sigma}$), the time-reversal symmetry condition ($t_{ij\sigma} = t^{*}_{ij\bar{\sigma}}$), the threefold rotational symmetry (C_3), and can be explicitly expressed in the following form

$$t_{ij\sigma} = |t_l| e^{i\phi_{ij\sigma}} = |t_l| e^{i\sigma \nu_{ij}\phi}, \tag{3.5}$$

Here, the index $l = 1, 2, 3$ labels the distance from the neighbor where t_1, t_2 and t_3 correspond to the first, second and third nearest neighbor hopping amplitudes, respectively. The hopping strength $|t_l|$ depends on the distance between lattice sites and the phase is given by $\phi_{ij\sigma} = \sigma \nu_{ij}\phi$, with $\nu_{ij} = \pm 1$ set by the bond direction. The resulting complex phases of the hoppings for all the six nearest neighbors and for both spins are shown schematically in Fig. 3.5. It should be noted that D affects both the absolute values and the complex phase of the hoppings (cf. Fig. 3.6). In Fig. 3.7 we show how the variation of D impacts the spin splitting of the resulting Fermi surface and shifts the VHS from higher to lower band fillings. This

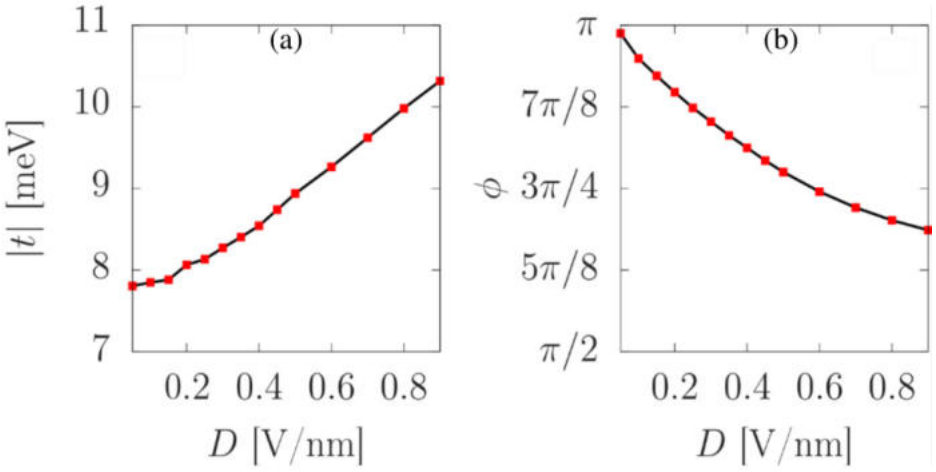

Fig. 3.6 (a) Magnitude of the hopping and (b) Phase factor ϕ as a function of the displacement field D. The data shown in (a) and (b) are taken from Ref. [8] calculated for a twist angle of $\theta = 5.08°$ and are used in the present analysis.

behavior is primarily governed by the D-dependent phase factor ϕ. In the limit of very small D, where $\phi \approx \pi$, the hopping amplitudes are nearly real. As a result, the distinction between spin up and spin down Fermi surfaces remains minimal as can be seen in panel (f), indicating negligible spin splitting and an approximate C_6 rotational symmetry. With increasing D, ϕ progressively deviates from π, introducing a growing spin dependent imaginary component to the hopping terms. This enhances the spin splitting of the Fermi surface and drives a reduction in symmetry from C_6 to C_3, which becomes clearly manifested at larger D. Such simple model given by Eq. (3.4) allows to reconstruct the single moiré band of $tWSe_2$ in an effective manner.

An alternative approach which, however, leads to the same structure of the single particle hamiltonian is based on the so-called continuum model. For the case of moiré systems where relevant physics occurs on length scales much larger than the atomic lattice spacing, the continuum model provides a natural framework for low-energy degrees of freedom. This approach allows us to reconstruct the band structure resulting from the characteristic moiré pattern with the unit cell consisting of tens or even hundreds of atoms without explicitly taking them into account in our calculations. Instead, an effective continuous periodic potential and position dependent tunneling term are introduced mimicking the effect of the moiré pattern of atoms. Such an approach has been applied by Pan et al [86] in connection with the maximally localized Wannier functions in order to derive a minimal single band of $tWSe_2$. At low energies, the continuum model thus serves as a bridge between microscopic lattice physics and effective many body descriptions.

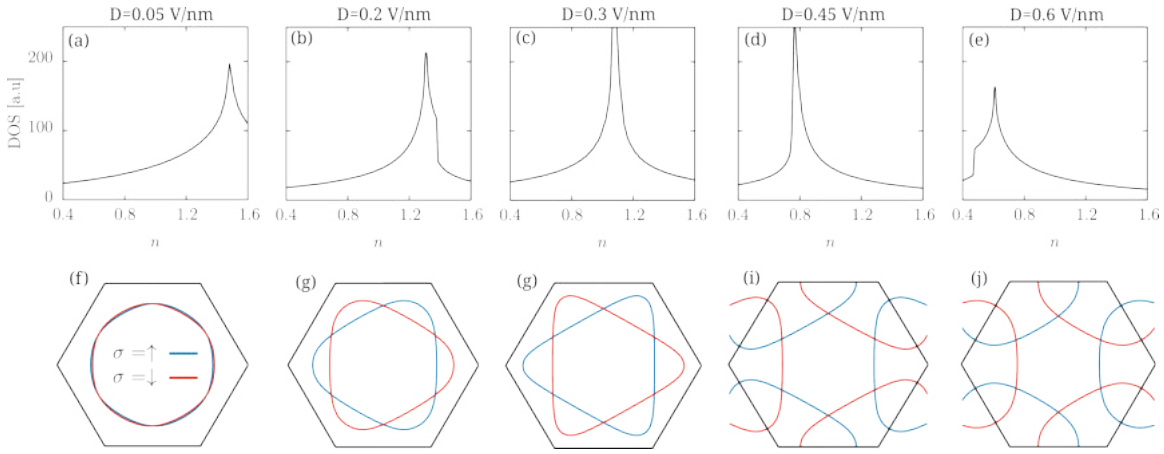

Fig. 3.7 Evolution of the electronic structure and Fermi surface topology in $tWSe_2$ homobilayers as a function of displacement field D.

The basics of such continuum model approach is provided in the following for the case of $tWSe_2$ homobilayer. It should be noted that the two valleys (K_+ and K_-) of such a system are well separated in the momentum space (cf. Fig. 3.3). The non interacting continuum Hamiltonian for the K valley is given by:

$$H_\uparrow = \begin{pmatrix} -\frac{\hbar^2(\mathbf{k}-\boldsymbol{\kappa}_+)^2}{2m^*} + \Delta_+(\mathbf{r}) & T(\mathbf{r}) \\ T^\dagger(\mathbf{r}) & -\frac{\hbar^2(\mathbf{k}-\boldsymbol{\kappa}_-)^2}{2m^*} + \Delta_-(\mathbf{r}) \end{pmatrix}, \tag{3.6}$$

The above Hamiltonian is expressed on the basis of the two layers, where the diagonal terms describe the individual layers and the off-diagonal terms account for interlayer coupling. The kinetic energy terms $-\frac{\hbar^2(\mathbf{k}-\boldsymbol{\kappa}_\pm)^2}{2m^*}$ correspond to the motion of carriers within each layer, where m^* is the effective mass of the valence band. The momentum shifts $\boldsymbol{\kappa}_\pm$ arise due to the relative twist between the two layers and represent the displacement of the K-points in momentum space for the upper (+) and lower (−) layers. The terms $\Delta_\pm(\mathbf{r})$ denote the moiré potentials experienced by electrons in each layer. These potentials originate from the spatial modulation induced by the moiré pattern and vary periodically in real space. They play a crucial role in reconstructing the electronic structure and giving rise to moiré minibands. The off-diagonal terms $T(\mathbf{r})$ and $T^\dagger(\mathbf{r})$ describe the interlayer tunneling between the two layers. This coupling allows electrons to hop from one layer to the other and leads to hybridization of the layer resolved states. As a result, the electronic bands are no longer purely layer-localized, and new moiré bands emerge. The continuum Hamiltonian defined above leads to the band structure provided in Fig. 3.8 (a), (b) for selected model parameters and can serve as the

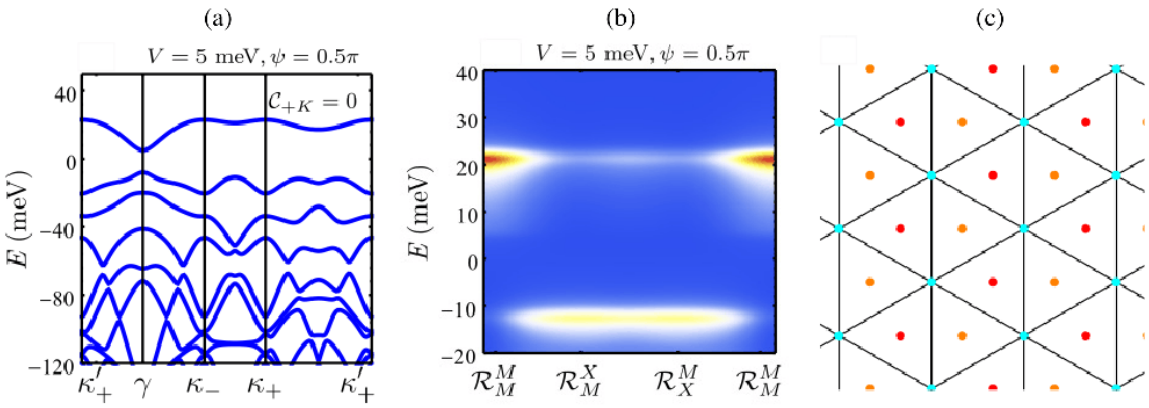

Fig. 3.8 (a) Band dispersions along high symmetry directions of the moiré Brillouin zone, showing the formation of minibands and gap openings. (b) Corresponding local density of states, highlighting the redistribution of spectral weight and the emergence of localized states. (c) Effective triangular lattice model for the first moiré band shown in (a). The cyan, red, and orange markers denote the $\mathcal{R}_M^M$, $\mathcal{R}_M^X$ and $\mathcal{R}_X^M$ positions in the $tWSe_2$ moiré superlattice, respectively. This figure is extracted from [86].

starting point for Wannierization of the isolated moiré valence bands, producing localized orbitals on the triangular moiré lattice shown schematically in Fig. 3.8 (c).

When the first moiré valence band is topologically trivial, a localized Wannier state centered at $\mathbf{R} = 0$ in the $+K$ valley is constructed from the Bloch eigenstates of the continuum Hamiltonian $H_\uparrow$ as

$$W(\mathbf{r}) = \frac{1}{\sqrt{N}} \sum_{\mathbf{k}\in \mathrm{BZ}} \psi_{\mathbf{k}}(\mathbf{r}), \tag{3.7}$$

Here $\psi_{\mathbf{k}}(\mathbf{r})$ is the Bloch wave function and N is the number of k points in the moiré Brillouin zone. The flat bands are Wannierized using maximally localized Wannier functions centered at real space maxima. Projecting $H_\uparrow$ onto these functions gives a tight-binding model with well defined hoppings. As shown in Ref. [86], in order to construct an effective description of the topmost moié valence band, a triangular lattice of Wannier orbitals leads to the same structure of the single particle Hamiltonian as the one resulting from ab initio approach given by Eq. 3.4. Wannierization of the moiré valence bands in the $tWSe_2$ bilayer has also been carried out in other studies [41, 57]. The resulting Wannier models accurately reproduce the narrow valence band dispersion and provide a reliable low energy framework for correlated many body studies.

The comparison between the ab initio DFT-based calculations and the continuum model approach has been carried out in Ref. [41] for the case of twist angle $\theta = 5.08°$. In Fig. 3.9 we provide the result of this study where the black dots represent the DFT band structure, while the solid curves denote the fitted continuum model. For the top two isolated moiré valence bands, the agreement is essentially exact with the fitted band lying directly on top of the

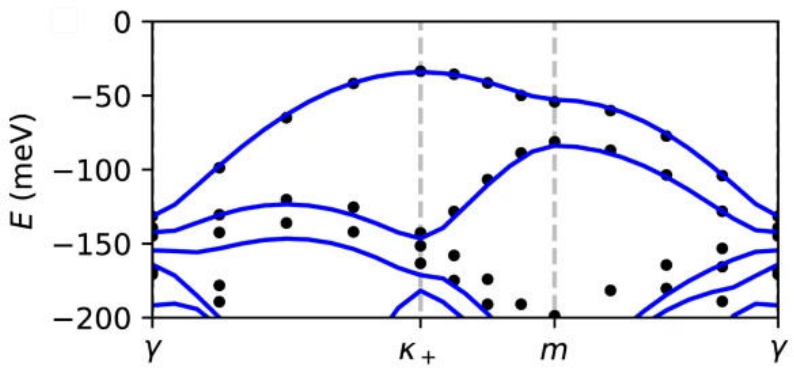

Fig. 3.9 The continuum band structure (blue lines) is plotted in comparison with large scale density functional theory calculations (black dots) at twist angle $\theta = 5.08°$ showing excellent agreement in $tWSe_2$ moiré bilayer. This figure is Chosen from Ref. [41].

DFT data. This near perfect matching justifies the use of the corresponding Wannierization parameters within a single and two band model for low energy physics. In contrast, for three-band descriptions, small deviations appear in the lower energy bands, indicating that these models provide only qualitative, rather than fully quantitative agreement. As discussed by Devakul *et al.*, this supports the validity of the single and two-band approximation at low energies.

While the tight binding Hamiltonian H_0 successfully captures the single particle band structure, it does not include electron-electron interactions, which are expected to play a crucial role due to the narrow bandwidth of the moiré band. In particular, both the onsite and intersite Coulomb interaction (U and V) become relevant in such systems. To capture both finite U and kinetic exchange effects, the t-J-U model supplemented by the V-term can be regarded as an effective framework appropriate for the intermediate regime between weak to strong correlations. Our considerations corresponding to the $tWSe_2$ are based on the t-J-U model adopted to the single moiré band given by Eq. 3.4

$$\begin{aligned}\hat{H} = & \sum_{\langle ij\rangle,\sigma} t_{ij\sigma}\, \hat{c}^{\dagger}_{i\sigma}\hat{c}_{j\sigma} \\ & + J\sum_{\langle ij\rangle}{}' \left(\hat{S}^z_i\hat{S}^z_j + \frac{1}{2}e^{i2\nu_{ij}\phi}\hat{S}^+_i\hat{S}^-_j + \frac{1}{2}e^{-i2\nu_{ij}\phi}\hat{S}^-_i\hat{S}^+_j \right) \\ & + U\sum_i \hat{n}_{i\uparrow}\hat{n}_{j\downarrow} + V\sum_{\langle ij\rangle}{}' \hat{n}_i\hat{n}_j,\end{aligned} \tag{3.8}$$

Here S^z_i, S^+_i, S^-_i are the spin component $\frac{1}{2}$ z, rising and lowering operators, respectively, $\hat{n}_{i\sigma}$ is the occupancy operator and $\hat{n}_i = \sum_\sigma \hat{n}_{i\sigma}$. The summation over $\langle i, j\rangle$ means that we limit to

nearest neighbors only. The prime summation means that each bond between the lattice sites appears only once. The subsequent terms of the above Hamiltonian correspond to electron hopping, intersite exchange interaction and intrasite/intersite Coulomb repulsion.

An effective low-energy model of similar structure can also be constructed for the WS_2/WSe_2 heterobilayer moiré system by Wannierization of the continuum valence bands. For this, L. Rademaker derived an effective tight binding model for the flat valence bands of WS_2/ WSe_2 heterobilayer using the continuum moiré band structure onto a localized basis (Wannier-like orbitals) [87]. It is observed that a single TMD monolayer (WX_2 with X = S, Se) creates a hexagonal lattice with rotational symmetry C_3 and corresponds to a relatively large direct band gap at the K and K′ points. After two different TMD monolayers are joined in a heterobilayer, a moiré pattern emerges with a new lattice constant

$$a_M = \frac{1}{\sqrt{\frac{1}{a_1^2} + \frac{1}{a_2^2} - 2\cos\theta/(a_1 a_2)}}, \tag{3.9}$$

where a_1 and a_2 are the monolayer lattice constants and θ is the twist angle. Moreover, a mini Brillouin zone is created with the high-symmetry points $\Gamma = (0,0)$, $\kappa = \left(\frac{4\pi}{\sqrt{3}a_M}, 0\right)$, $\kappa' = \left(\frac{2\pi}{3a_M}, \frac{2\pi}{3a_M}\right)$. Because the two monolayers have different band gaps, the top of the valence band of the resulting structure consists of states localized in a single layer. Within the continuum model approach, the valence band states can be described per spin/valley by using a moiré potential $V(\mathbf{r})$. This leads to the following continuum Hamiltonian for the valence band states [87]:

$$H = -\frac{\hbar^2 Q^2}{2m^*} + V(\mathbf{r}), \quad V(\mathbf{r}) = \sum_j g_j V_j \exp(i\mathbf{g}_j \cdot \mathbf{r}), \tag{3.10}$$

where $\mathbf{Q}$ is the momentum relative to the K and K′ points of the monolayer and $\mathbf{g}_j = \frac{4\pi}{\sqrt{3}}\left(-\sin\frac{2\pi(j-1)}{6}, \cos\frac{2\pi(j-1)}{6}\right)$ are the reciprocal moiré vectors. Due to the C_3 symmetry of the moiré lattice one obtains: $V_1 = V_3 = V_5$ and $V_2 = V_4 = V_6 = V_1^*$, with $V_1 = Ve^{i\psi}$. After carrying out a proper momentum backfolding procedure to the moiré miniBrillouin zone, the moiré band structure can be calculated and then used during the Wannierization procedure to obtain the hopping parameters of an effective single band description given by Eq. 3.4. However, in this case the absolute values and the complex phases of the hoppings for the top valence moiré flat band of the aligned AA-stacking of the WS_2/WSe_2 heterobilayer with the continuum model parameters $(V, \psi) = (7.8\ \text{meV}, -106°)$, are

$$
\begin{aligned}
|t_1| &= 1.81 \text{ meV}; \quad \phi_1 = 2\pi/3, \\
|t_2| &= 0.28 \text{ meV}; \quad \phi_2 = \pi, \\
|t_3| &= 0.11 \text{ meV}; \quad \phi_3 = \pi/3.
\end{aligned} \tag{3.11}
$$

The values of the hopping parameters are adopted from the literature [87] and are used in our theoretical analysis to reconstruct the single moié band of the WS_2/WSe_2 heterobilayer. Similarly as in the homobilayer case we supplement the single particle part of the Hamiltonian with the Coulomb repulsion and kinetic exchange interaction terms which leads to a t-J-U model based description (cf. 3.8). For the heterobilayer case, we include hoppings and interactions up to the third nearest neighbors. Accordingly, the hopping amplitudes and associated phases are taken as $|t_1|$, $|t_2|$, $|t_3|$ and ϕ_1, ϕ_2, ϕ_3 corresponding to the first, second and third nearest neighbors, respectively.

3.3 Gutzwiller Approximation

The Gutzwiller approximation is a variational method designed to incorporate strong local electronic correlations beyond conventional mean field theory. It systematically incorporates correlation effects by renormalizing hopping and interaction terms. It is particularly well suited for lattice models of correlated electrons such as Hubbard and related models, where U plays a dominant role.

In order to take into account electron-electron correlations, we apply the variational wave function of the Gutzwiller type which is defined in the following manner

$$
|\Psi_G\rangle = \hat{P}|\Psi_0\rangle, \tag{3.12}
$$

where $|\Psi_0\rangle$ is the non-correlated (mean-field) state and $\hat{P}$ is the correlation operator

$$
\hat{P} = \prod_i \sum_\Gamma \lambda_{i,\Gamma} |\Gamma\rangle_{i\,i}\langle\Gamma|, \tag{3.13}
$$

where i runs over all the lattice sites, $|\Gamma\rangle \in \{|\varnothing\rangle, |\uparrow\rangle, |\downarrow\rangle, |\uparrow\downarrow\rangle\}$, and $\lambda_{i,\Gamma}$ are the corresponding variational parameters. It has been shown that for such a form of the correlation operator it is convenient to impose an additional condition on the $\hat{P}_i$ operator[88], i.e.,

$$
\hat{P}_i^2 = 1 + x\hat{d}_i^{HF}, \tag{3.14}
$$

where $\hat{d}_i^{HF} = \hat{n}_{i\uparrow}^{HF}\hat{n}_{i\downarrow}^{HF}$, $\hat{n}_{i\sigma}^{HF} = \hat{n}_{i\sigma} - n_{i\sigma}$, with $n_{i\sigma} = \langle\Psi_0|\hat{n}_{i\sigma}|\Psi_0\rangle$, and x is yet another variational parameter. It is straightforward to show that

$$\begin{aligned}
\lambda_{\uparrow\downarrow}^2 &= 1 + x(1-n_s)^2, \\
\lambda_s^2 &= 1 - xn_s(1-n_s)^2, \\
\lambda_\varnothing^2 &= 1 + xn_s^2,
\end{aligned} \tag{3.15}$$

where for simplicity we have assumed a homogeneous system with no magnetic or charge ordering. Hence, $\lambda_{i,\Gamma} \equiv \lambda_\Gamma$ and $\lambda_\uparrow = \lambda_\downarrow = \lambda_s$, $n_{i\uparrow} = n_{i\downarrow} \equiv n_s$.

In order to obtain the formula for the expectation value of our hamiltonian per lattice site,

$$E_G = \frac{\langle\Psi_G|\hat{H}|\Psi_G\rangle}{N\langle\Psi_G|\Psi_G\rangle} = \frac{1}{N}\langle\hat{H}\rangle_G, \tag{3.16}$$

we apply the diagrammatic expansion of the Gutzwiller wave function [89] in the zeroth order which is equivalent to the *Statistically consistant Gutzwiller Approximation* (SGA)[83]. As a result one obtains

$$\begin{aligned}
\langle\hat{H}_0\rangle_G &= \sum_{ij} q^2 t_{ij\sigma}\langle\hat{c}_{i\sigma}^\dagger\hat{c}_{j\sigma}\rangle_0, \\
\langle\hat{H}_J\rangle_G &= \lambda_s^4 {\sum_{\langle ij\rangle}}' J_{ij}\left(\frac{1}{2}\sum_\sigma e^{i\sigma 2\phi_{ij}}\langle\hat{c}_{i\sigma}^\dagger\hat{c}_{i\bar{\sigma}}\hat{c}_{j\bar{\sigma}}^\dagger\hat{c}_{j\sigma}\rangle_0 + \frac{1}{4}\sum_{\sigma\sigma'}\sigma\sigma'\langle\hat{n}_{i\sigma}^{HF}\hat{n}_{j\sigma'}^{HF}\rangle_0\right), \\
\langle\hat{H}_{UV}\rangle_G &= \lambda_{\uparrow\downarrow}^2 U\sum_i\langle n_{i\uparrow}n_{j\downarrow}\rangle_0 + V{\sum_{\langle ij\rangle}}'\left((1-g_v^2)\langle\hat{n}_i\rangle_0\langle\hat{n}_j\rangle_0 + g_v^2\langle\hat{n}_i\hat{n}_j\rangle_0\right),
\end{aligned} \tag{3.17}$$

where,

$$\begin{aligned}
q &= \lambda_s\left(\lambda_d n_s + \lambda_\varnothing(1-n_s)\right), \\
g_v &= 1 + xn_s(1-n_s),
\end{aligned} \tag{3.18}$$

while $q = \lambda_s\left(\lambda_d n_s + \lambda_\varnothing(1-n_s)\right)$ and $\langle\hat{o}\rangle_0$ stands for the expectation value of the $\hat{o}$ operator in the state $|\psi\rangle_0$. As one can see, the expectation value of a given energy term in the correlated state $|\psi_G\rangle$, can be expressed in terms of the expectation values in the non-correlated state $|\psi_0\rangle$. However, factors q, λ_s^4, $\lambda_{\uparrow\downarrow}$ and g_v^2 renormalize the hopping amplitudes as well as the coupling constants J, U and V, respectively. Moreover, by applying the standard Wick's theorem decomposition one can express all the four-operator expectation values which appear on the right-hand side of the above equation. Hence, the obtained E_G becomes a function of

n_s as well as the electron hopping and Cooper pairing mean field parameters,

$$P_{ij\sigma} = \langle \hat{c}^{\dagger}_{i\sigma} \hat{c}_{j\sigma} \rangle_0, \quad S^{\sigma\sigma'}_{ij} = \langle \hat{c}_{i\sigma} \hat{c}_{j\sigma'} \rangle_0, \tag{3.19}$$

respectively. It should be noted that the expectation values in the non-correlated state together with the variational parameters determine the corresponding expectation values in the correlated state. Namely,

$$\begin{aligned} \Delta^{\sigma\sigma'}_{ij} &= \langle \hat{c}_{i\sigma} \hat{c}_{j\bar{\sigma}} \rangle_G = q^2 \langle \hat{c}_{i\sigma} \hat{c}_{j\sigma'} \rangle_0, \\ \Lambda_{ij\sigma} &= \langle \hat{c}^{\dagger}_{i\sigma} \hat{c}_{j\sigma} \rangle_G = q^2 \langle \hat{c}^{\dagger}_{i\sigma} \hat{c}_{j\sigma} \rangle_0. \end{aligned} \tag{3.20}$$

Within our analysis, we treat $S^{\uparrow\downarrow}_{ij}$ and $S^{\downarrow\uparrow}_{ij}$ separately allowing for both pure spin-singlet pairing ($S^{\uparrow\downarrow}_{ij} = -S^{\downarrow\uparrow}_{ij}$), pure spin-triplet pairing ($S^{\uparrow\downarrow}_{ij} = S^{\downarrow\uparrow}_{ij}$) as well as their mixture ($|S^{\uparrow\downarrow}_{ij}| \neq |S^{\downarrow\uparrow}_{ij}|$). At the same time, we neglect the possibility of $\uparrow\uparrow$ and $\downarrow\downarrow$ pairing due to the fact that here the pairing mechanism is based on the kinetic exchange term which is of AFM type. Additionally the $S^z = \pm 1$ pairing channels would lead to a Fermi wave vector mismatch, which is detrimental when it comes to the formation of the superconducting state.

In order to determine the values of the mean fields we apply the Effective Hamiltonian Scheme[90]. Within such approach the minimization condition of the ground state energy (3.16) leads to an effective Hamiltonian, which for our case has the following form

$$\begin{aligned} \hat{\mathcal{H}}_{\text{eff}} = &\sum_{ij\sigma} \tilde{t}_{ij\sigma} \hat{c}^{\dagger}_{i\sigma} \hat{c}_{j\sigma} - \tilde{\mu} \sum_{i\sigma} \hat{n}_{i\sigma} \\ &+ \sum_{<ij>\sigma}{}' \left((\tilde{\Delta}_{ij\sigma\bar{\sigma}})^* \hat{c}_{j\sigma} \hat{c}_{i\bar{\sigma}} + h.c. \right), \end{aligned} \tag{3.21}$$

where the effective hopping, effective chemical potential, and the effective superconducting gap parameters are defined through the corresponding relations

$$\tilde{t}_{ij\sigma} \equiv \frac{\partial \mathcal{F}}{\partial P_{ij\sigma}}, \quad (\tilde{\Delta}_{ij\sigma\bar{\sigma}})^* \equiv \frac{\partial \mathcal{F}}{\partial S^{\sigma\bar{\sigma}}_{ji}}, \quad \tilde{\mu} \equiv -\frac{\partial \mathcal{F}}{\partial n_s}, \tag{3.22}$$

where $\mathcal{F} = E_G - 2\mu_G n_s$ with μ_G being the chemical potential determined in the correlated state. For completeness, we explicitly present the effective model parameters below

$$\tilde{t}_{ij\sigma} = q^2 \, t_{ij\sigma} - J \, \frac{\lambda_s^4}{4} \left[2(P_{ij\bar{\sigma}})^* \, e^{i2\phi^{\sigma}_{ij}} + (P_{ij\sigma})^* \right] + g_v^2 V (P_{ij\sigma})^*, \tag{3.23}$$

$$(\tilde{\Delta}_{ij}^{\sigma\bar{\sigma}})^* = -J\,\frac{\lambda_s^4}{2}\left[2(S_{ij}^{\sigma\bar{\sigma}})^*\, e^{i2\phi_{ij}^{\sigma}} - (S_{ij}^{\bar{\sigma}\sigma})^*\right] + 2V g_V^2 (S_{ij}^{\bar{\sigma}\sigma}), \tag{3.24}$$

$$\tilde{\mu} = \mu_G - U\lambda_d^2 n_s - 6V n_s. \tag{3.25}$$

After the transformation to the reciprocal space we write down the effective hamiltonian in the matrix form

$$\begin{aligned}\hat{\mathcal{H}}_{\text{eff}} = \sum_{\mathbf{k}\sigma} & \begin{pmatrix} \hat{c}_{\mathbf{k}\sigma}^{\dagger} & \hat{c}_{-\mathbf{k}\bar{\sigma}} \end{pmatrix} \begin{pmatrix} \tilde{\varepsilon}_{\mathbf{k}\sigma} - \tilde{\mu} & \tilde{\Delta}_{\mathbf{k}\bar{\sigma}\sigma} \\ (\tilde{\Delta}_{\mathbf{k}\bar{\sigma}\sigma})^* & -\tilde{\varepsilon}_{\mathbf{k}\sigma} + \tilde{\mu} \end{pmatrix} \begin{pmatrix} \hat{c}_{\mathbf{k}\sigma} \\ \hat{c}_{-\mathbf{k}\bar{\sigma}}^{\dagger} \end{pmatrix} \\ & + \sum_{\mathbf{k}\sigma} (\tilde{\varepsilon}_{\mathbf{k}\sigma} - \tilde{\mu}),\end{aligned} \tag{3.26}$$

where $\bar{\sigma} = -\sigma$ and we have used the relation $\tilde{\varepsilon}_{\mathbf{k}\sigma} = \tilde{\varepsilon}_{-\mathbf{k}\bar{\sigma}}$ (time reversal symmetry condition). The effective dispersion relations as well as the superconducting gaps in $\mathbf{k}$-space are related with their real-space counterparts in the following manner

$$\begin{aligned}\tilde{\varepsilon}_{\mathbf{k}\sigma} &= \sum_{i(j)} \tilde{t}_{ij} e^{ik(\mathbf{R}_i - \mathbf{R}_j)} \\ \tilde{\Delta}_{\mathbf{k}\bar{\sigma}\sigma} &= \sum_{i(j)} \tilde{\Delta}_{ji\sigma\bar{\sigma}} e^{ik(\mathbf{R}_j - \mathbf{R}_i)},\end{aligned} \tag{3.27}$$

where i index runs over the nearest neighbor lattice sites of site j. The $\mathbf{R}_i$ and $\mathbf{R}_j$ vectors point to the i and j lattice sites, respectively. The left-hand sites of the equations above do not depend on j since we assume spaciously homogeneous state. The eigenvalues of the hamitlonian matrix in Eq. (3.26) are the following

$$\lambda_{\mathbf{k}\sigma} = \pm\sqrt{(\tilde{\varepsilon}_{\mathbf{k}\sigma} - \tilde{\mu})^2 + |\tilde{\Delta}_{\mathbf{k}\bar{\sigma}\sigma}|^2}. \tag{3.28}$$

From the above equation, one can see that in the SC state the gap $\tilde{\Delta}_{\mathbf{k}\downarrow\uparrow}$ ($\tilde{\Delta}_{\mathbf{k}\uparrow\downarrow}$) opens up at the spin up (spin down) Fermi surface. Moreover, the $\tilde{\Delta}_{\mathbf{k}\downarrow\uparrow}$ and $\tilde{\Delta}_{\mathbf{k}\uparrow\downarrow}$ SC gaps can be transformed

Table 3.1 The six possible values of the symmetry factor M and the corresponding values of the parity factor p (second column), appearing in Eq. (3.31). The corresponding six symmetries of the superconducting gap together with their parities are provided in the third and fourth columns. The Cooper pair spin state compatible with a given symmetry is provided in the fifth column.

M	p	gap symmetry	parity	spin state
0	0	*extended s*	even	singlet
1	1	$p_x + i\,p_y$	odd	triplet
2	0	$d_{x^2-y^2} + i\,d_{xy}$	even	singlet
3	1	f	odd	triplet
4	0	$d_{x^2-y^2} - i\,d_{xy}$	even	singlet
5	1	$p_x - i\,p_y$	odd	triplet

into the singlet and triplet components,

$$\begin{aligned}\tilde{\Delta}^s_{\mathbf{k}} &= \frac{1}{\sqrt{2}}\left(\tilde{\Delta}_{\mathbf{k}\uparrow\downarrow} - \tilde{\Delta}_{\mathbf{k}\downarrow\uparrow}\right),\\ \tilde{\Delta}^t_{\mathbf{k}} &= \frac{1}{\sqrt{2}}\left(\tilde{\Delta}_{\mathbf{k}\uparrow\downarrow} + \tilde{\Delta}_{\mathbf{k}\downarrow\uparrow}\right),\end{aligned} \tag{3.29}$$

which we can use to rewrite the expressions for the eigenvalues

$$\lambda_{\mathbf{k}\sigma} = \pm\sqrt{(\tilde{\varepsilon}_{\mathbf{k}\sigma} - \tilde{\mu})^2 + \frac{1}{2}|\tilde{\Delta}^t_{\mathbf{k}} - \sigma\tilde{\Delta}^s_{\mathbf{k}}|^2}. \tag{3.30}$$

The paired state with $\Delta^s_{\mathbf{k}} \neq 0$ and $\Delta^t_{\mathbf{k}} \neq 0$ is referred to here as the mixed singlet-triplet paired state.

The self-consistent equations for the mean field parameters [Eq. (3.19)] can be derived in a standard manner by applying the Bogolubov-de Gennes approach to the effective hamiltonian given by Eq. (3.26). By solving the set of self-consistent equations numerically we determine the hopping and pairing amplitudes to all the six nearest neighbors. Than, in order to obtain the correlated state correspondents we use Eqs. (3.20). Similarly as in our previous study[91], to identify the symmetry of the resultant paired state, we transform the six real-space nearest neighbor pairing amplitudes into six symmetry resolved pairing

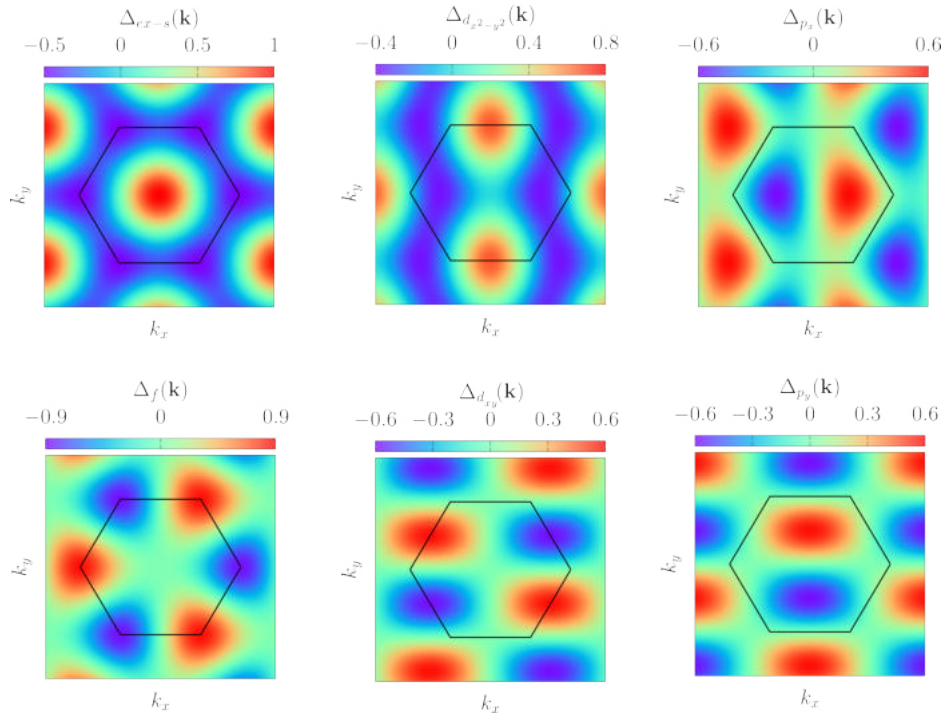

Fig. 3.10 The k-dependent SC gaps corresponding to the six symmetries which appear as real and imaginary parts of the pairing channels listed in Table 3.1. The Brillouin zone is marked by black solid line. The presented distributions have been obtained by setting particular symmetry resolved factors to 1 and all the others to 0.

amplitudes of the following form

$$\Delta^{\sigma\bar{\sigma}}_{M,p} = \frac{i^p}{6} \sum_{i(j)} e^{-iM\theta_{ji}} \Delta^{\sigma\bar{\sigma}}_{ji}, \tag{3.31}$$

where the summation runs over the six nearest neighbor lattice sites j surrounding site i and θ_{ji} are the angles $\{0, \pi/3, 2\pi/3, \pi, 4\pi/3, 5\pi/3\}$ between the positive half-x axis and the $\mathbf{R}_{ji} = \mathbf{R}_j - \mathbf{R}_i$ vector. M is the symmetry factor, which takes integer values and corresponds to six possible pairing symmetries (cf. Table 3.1). The p parameter corresponds to the parity of the particular symmetry. Namely, for even parity symmetries we have $p = 0$ and for odd parities we have $p = 1$.

Finally, similarly as for the case of the momentum space [Eqs. 3.29] one can write down the expressions for the real-space singlet and triplet gap amplitudes in the correlated state,

which will play the central role in our subsequent analysis

$$\begin{aligned}\Delta^{s}_{M,p} &= (\Delta^{\uparrow\downarrow}_{M,p} - \Delta^{\downarrow\uparrow}_{M,p})/\sqrt{2},\\ \Delta^{t}_{M,p} &= (\Delta^{\uparrow\downarrow}_{M,p} + \Delta^{\downarrow\uparrow}_{M,p})/\sqrt{2}.\end{aligned} \tag{3.32}$$

For the sake of clarity, we use the symmetry names ($p \pm ip$, $d \pm id$, f etc.) in the subscripts of the symmetry resolved SC gaps instead of the values of the M and p factors. In Fig. 3.10, we present the six gap symmetries in reciprocal space, corresponding to the real and imaginary parts of the pairing channels listed in Table 3.1. The magnitudes of the extended s-wave and f-wave gaps exhibit full C_6 rotational symmetry, indicating that these channels can exist independently on the triangular lattice. In contrast, the remaining $d_{x^2-y^2}$, d_{xy}, d_{p_x}, and d_{p_y} are not C_6 symmetric. It should be noted that although the lattice itself possesses C_6 symmetry, the Hamiltonian does not fully retain this property due to the spin valley locking through spin- and direction-dependent hopping terms. These lead to a reduction of the symmetry to C_3, which has further consequences for the pairing symmetry.

For calculations a `C++` numerical code has been used, where matrix diagonalization and integration over the Brillouin zone are carried out using efficient linear algebra libraries. The code iteratively solves the coupled nonlinear equations for $\Delta_{\mathbf{k}}$ and μ until self-consistency is achieved. At each iteration, the Gutzwiller renormalization factors are recalculated based on the current filling level. Throughout the code the numerical routines provided by the `GSL` library are used.

For the case of t-J-U model calculations, the procedure for solving the set of self-consistent equations is supplemented with the minimization of the system energy over the variational parameter x. For the case t-J model which is also considered by us in our study, we project out the double occupancies completely meaning that the x parameter is set according to the following conditions

$$\begin{aligned}&\text{for } n_s < 0.5 : \lambda_{\uparrow\downarrow} = 0 \;\Rightarrow x = -\frac{1}{(1-n_s)^2}\\ &\text{for } n_s > 0.5 : \lambda_{\varnothing} = 0 \;\Rightarrow x = -\frac{1}{n_s^2}\end{aligned} \tag{3.33}$$

Chapter 4

Articles overview

4.1 Topological superconductivity with mixed singlet-triplet pairing in moiré transition metal dichalcogenide bilayers

The work is motivated by recent experimental report of correlated insulating states and possible superconductivity in TMD moiré systems [8]. Here, we employ an effective single band t-J model on the triangular lattice in which hopping terms are complex and spin dependent reflecting strong SOC and the influence of an external displacement field. To capture strong electronic correlations, the model is treated within the variational Gutzwiller projection framework. It should be noted that this research has been carried out when the appearence of the SC state in moiré TMDs has not been unambiguously detected. At that time Ref. [8] was the only experimental report which suggested signatures of two superconducting domes residing on both sides of an insulating state. Our theoretical approach allows for the exploration of the SC order parameters, their symmetry and topological properties.

The main finding reported here is the emergence of SC domes characterized by a *mixed singlet triplet* gap structure, combining $d+id$ (spin-singlet) and $p-ip$ (spin-triplet) components. This mixed pairing arises naturally from valley dependent spin splitting and breaks time reversal symmetry. The resulting SC states are topologically nontrivial, with Chern numbers $C = \pm 2, \pm 4$, depending on the filling level and displacement field. This means that in principle it should be possible to drive topological phase transitions between different SC states by using experimentally controlable parameters in an in-situ manner. We also obtained weaker extended s-wave and f-wave topologically trivial phases at low and high electron concentrations for large value of exchange interaction (J= 10 meV) along with spin $d+id$ singlet and $p-ip$ triplet which are energetically stable near half filling. Moreover, we also

found that we can tune the relative strength of singlet and triplet pairing components by changing the displacement field. The two SC domes separated by a mott insulating state at half filling which we have obtained in our calculations are in agreement with experimental observations provided in Ref. [8]. After submitting our theoretical analysis, new experiments reported clear evidence of either two or one superconducting domes in $tWSe_2$ we refer to those new experimental results further on in the subsequent articles.

Topological superconductivity with mixed singlet-triplet pairing in moiré transition metal dichalcogenide bilayers

Waseem Akbar,[1] Andrzej Biborski,[1] Louk Rademaker,[2] and Michał Zegrodnik[1,*]
[1]*Academic Centre for Materials and Nanotechnology, AGH University of Krakow, Al. Mickiewicza 30, 30-059 Krakow, Poland*
[2]*Department of Quantum Matter Physics, University of Geneva, CH-1211 Geneva, Switzerland*

(Received 21 March 2024; revised 16 July 2024; accepted 9 August 2024; published 26 August 2024)

We investigate strong coupling topological superconductivity in twisted moiré bilayer WSe_2. Our approach is based on an effective t-J model with displacement-field-dependent complex hoppings, which is treated with the variational Gutzwiller projection method. The calculated phase diagram contains domes of topologically nontrivial superconducting phases, with Chern numbers $C = \pm 2,\ \pm 4$. The order parameter is characterized by a mixed $(d + id)$-wave (singlet) and $(p$-$ip)$-wave (triplet) gap symmetry. We also report on the appearance of an additional topologically trivial extended s-wave and f-wave paired phases. As we show, by changing the electron density and displacement field, one can tune the singlet and triplet contributions to the pairing, as well as induce topological phase transitions between superconducting states characterized by different values of the Chern number. We analyze the physical origin of the reported effects and discuss it briefly in the view of new possibilities for designing unconventional superconductivity in moiré systems.

DOI: 10.1103/PhysRevB.110.064516

I. INTRODUCTION

In recent years, more and more two-dimensional systems realizing a moiré pattern of atoms have been investigated, as they provide a fertile ground for novel electronic states. The characteristic moiré structure emerges after twisting two or more monolayers with respect to each other, like in the well-known twisted bilayer graphene [1–3]. A similar effect can also be obtained as a result of lattice mismatch in heterostructures without the necessity of rotational misalignment [4,5].

The common feature of moiré systems is the appearance of flat electronic bands, which implies a significant role of electronic interactions. For graphene-based multilayers, the flat bands can be realized only for specific twist angles (so-called magic angles), for which the system exhibits an unusually rich phase diagram [1–3]. For transition metal dichalcogenide (TMD) moiré structures, the appearance of flat bands is more robust with respect to the twist-angle deviations [5–10]. Evidence of strongly correlated phenomena in the moiré TMDs has been reported in recent years: amongst them metal-insulator transitions [6,7], different forms of charge ordering [11,12], as well as signatures of superconductivity [6,13]. We write "signatures" because the supposed superconducting state has not been unambiguously detected experimentally in Ref. [6]. Nevertheless, what distinguishes TMDs from graphene-based moiré systems is that the former have a relatively strong spin-orbit coupling. This would naturally imply that the superconducting state in the TMDs can have some nontrivial pairing symmetry.

The main focus of this paper is a theoretical exploration of the possible superconducting phases in a twisted WSe_2 homobilayer ($tWSe_2$), for which "signatures" of superconductivity were observed [6]. The low-energy physics of $tWSe_2$ is believed to be described by a single-band Hamiltonian on a triangular lattice with both spin- and direction-dependent complex hoppings [6,14]. The Hubbard U resulting from such an approach is approximately $U \gtrsim W$ (W is the bare bandwidth), which suggests that $tWSe_2$ is in a relatively strongly correlated regime [6,14,15]. Indeed, the experimental phase diagram suggests an insulating state at half-filling with adjacent superconducting domes [6]. Even though the pairing mechanism and the symmetry of the superconducting gap are still unknown, the dome structure implies that superconductivity might arise purely from strong electron repulsion through Hubbard or t-J models [16,17]. The Hubbard model as applied to the description of homobilayer and heterobilayer moiré TMDs has been analyzed in the view of spin and charge ordering, as well as the appearance of unconventional superconducting state [15,16,18–21]. For the case of the paired phase these approaches resemble those that have been applied earlier to the single-band models of the well-known cuprates [22]. However, other proposals related to TMD superconductivity, based on the spin-valley fluctuations or interlayer excitonic physics, have also been put forward [23,24].

In this paper we study the t-J model relevant for $tWSe_2$ using the Gutzwiller approximation, and analyze in detail the topological features of the obtained unconventional paired states. The interesting peculiarity about TMD systems is that the moiré pattern generates a triangular lattice system, which allows for quite nontrivial and possible topological order-parameter symmetries. In fact, we predict a two-dome structure of *mixed singlet-triplet superconductivity*

*Contact author: michal.zegrodnik@agh.edu.pl

(with $d + id$ and $p - ip$ gap symmetry mixing), separated by a correlation-induced insulating state at half-filling. This is consistent with our previous work on the t-J-U model as applied to the description of $tWSe_2$ [25]. Additionally, here we show that the obtained mixed state is topologically nontrivial with Chern number values $C = \pm 2,\ \pm 4$. Furthermore, we focus on the effect of the displacement field by explicitly taking into account the appropriate complex hopping parameters. By tuning the displacement field one can induce topological phase transitions between phases with different Chern numbers, as well as control the balance between the singlet and triplet contributions to the pairing. Additionally, for low- and high-electron concentration regimes we have obtained a topologically trivial extended s-wave and f-wave paired state. Our results show the TMD homobilayers as promising candidates for topological superconductors characterized by a high degree of tunability.

It should be noted that during the process of submission of the current theoretical analysis, two experimental papers have appeared, showing strong evidence of the superconducting state in the same system [26,27]. There are some differences between the two very recent experimental papers and the original one by Wang *et al.* [6], to which we are mainly referring here. Namely, the measurements presented in Ref. [6] suggest two superconducting domes residing on both sides of the half-filled case, where the insulating state is located. Such situation is consistent with the physical picture stemming from our theoretical analysis carried out here within the t-J model, which corresponds to a relatively large-U limit. On the other hand, in the recent experimental reports [26,27] only one superconducting (SC) dome is shown in particular range of displacement field. Moreover, in Ref. [26], the SC state is stable at half-filling, indicating that the system is in relatively weaker U limit ($U \lesssim W$). In general, for $tWSe_2$ the value of U is tuned both by the twist angle and the dielectric constant. Therefore, it might be the case that both situations are valid and can be reached in $tWSe_2$ ($U > W$ and $U < W$), depending on the particular parameters of the sample and the experimental setup itself. In order to analyze theoretically the $U \lesssim W$ situation one would have to apply the Hubbard or t-J-U models, which allow for nonzero number of double occupancies unlike the current t-J Hamiltonian. The t-J-U model has already been considered by us in the context of the paired state in $tWSe_2$ recently [25]. In fact, it has been shown by us there that a single SC dome residing at half-filling (as in Ref. [26]) can be reproduced for 50 meV $\lesssim U \lesssim$ 90 meV (see Fig. 5 in Ref. [25]).

The remainder of this paper is organized as follows. In Sec. II we introduce the t-J model relevant for $tWSe_2$ and we describe our method of the Gutzwiller projected variational wave function. In Sec. III A we provide our results on the structure of the mixed singlet-triplet superconducting domes, while in Sec. III B we discuss the topological classification of the phases. Additionally, in Appendix A we briefly discuss the influence of nonzero double occupancies within the t-J-U model and relate the obtained results with the recently reported experimental results [26,27]. Finally, in Sec. IV we provide an outlook on the experimental detection of topologically nontrivial superconductivity in $tWSe_2$.

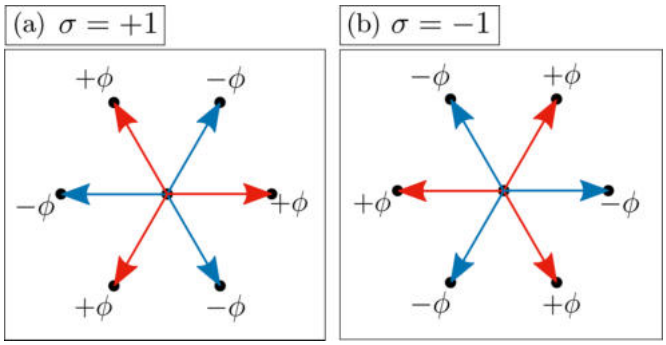

FIG. 1. Phase of the complex hoppings to the nearest neighbors for spin-up (a) and spin-down (b) electrons.

II. MODEL AND METHOD

In this work we apply a moiré band t-J Hamiltonian on a triangular lattice, i.e.,

$$\hat{H} = \sum_{\langle ij\rangle\sigma} t_{ij\sigma}\, \hat{c}^{\dagger}_{i\sigma}\hat{c}_{j\sigma} + J \sum_{\langle ij\rangle}{}' \left(\hat{S}^z_i \hat{S}^z_j + \cos\left(2\phi_{ij\uparrow}\right) \sum_{\alpha=x,y} \hat{S}^{\alpha}_i \hat{S}^{\alpha}_j + \sin\left(2\phi_{ij\uparrow}\right)(\hat{\mathbf{S}}_i \times \hat{\mathbf{S}}_j)\cdot\hat{z} \right), \tag{1}$$

where $\hat{c}^{\dagger}_{i\sigma}$ ($\hat{c}_{i\sigma}$) are the creation (anihilation) operators for electrons at site i with spin $\sigma = \{1, -1\}$, and $\hat{\mathbf{S}}_i = (\hat{S}^x_i, \hat{S}^y_i, \hat{S}^z_i)$ is the spin-$\frac{1}{2}$ operator. The summation over $\langle ij\rangle$ in both terms is restricted to nearest neighbors only since the longer-ranged contributions are expected to be about one order of magnitude smaller [6]. The primed summation in the interaction part means that each bond appears only once. The complex hopping parameters $t_{ij\sigma}$ fulfill the Hermiticity requirement ($t_{ij\sigma} = t^{*}_{ji\sigma}$), time-reversal symmetry condition ($t_{ij\sigma} = t^{*}_{ij\bar{\sigma}}$), threefold rotational symmetry (C_3), and can be explicitly expressed in the form

$$t_{ij\sigma} = |t|e^{i\phi_{ij\sigma}} = |t|e^{i\sigma\nu_{ij}\phi}, \tag{2}$$

with $\nu_{ij} = \pm 1$, depending on the direction of the bond. The resulting complex phases of the hoppings for all the six nearest neighbors are shown schematically in Fig. 1. As one can see from Eq. (1) the exchange interaction $\sim J$ is supplemented with the Dzyaloshinskii-Moriya term which results from the fact that the phase of the hoppings is spin dependent.

This form of the t-J model can be derived from the Hubbard model as applied to the description of the $tWSe_2$ in the large-U limit. As shown in Refs. [6,14], within such approach, both the absolute values of the hoppings ($|t|$) as well as their complex phase (ϕ) depend on the bias voltage across the bilayer (the so-called displacement field D). This provides an experimentally controllable parameter which can be used to tune *in situ* the magnitude of the valley-dependent spin splitting as well as the position of the Van Hove singularity (cf. Fig. 2). The complex hopping parameters for the range of displacement fields $D \in [0, 0.9]$ V/nm, that are used for the analysis provided in Sec. II, have been taken from Ref. [6] and are provided for the sake of clarity in Appendix B.

The t-J model is one of the canonical models used for the description of strongly correlated electron systems. In order

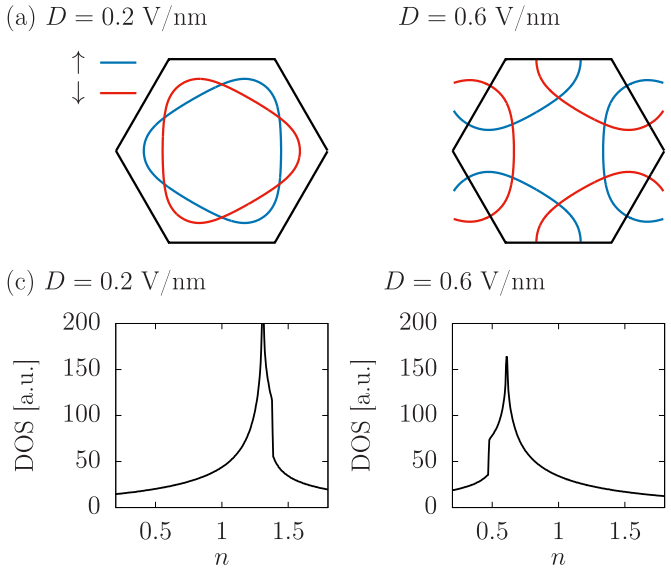

FIG. 2. The spin-dependent Fermi surfaces at half-filling (a), (b) and the density of states (c), (d) for two selected values of the displacement field $D = 0.2$ ($\phi \approx 7\pi/8$) and $D = 0.4$ ($\phi \approx 3\pi/4$). The data have been obtained based on the single-particle part of Hamiltonian given by Eq. (1). Note that by changing the displacement field one can tune the valley-dependent spin splitting as well as the position of the Van Hove singularity. The Fermi surfaces in (a) and (b) are of electronlike and holelike character, respectively.

to take into account electron-electron correlations, we apply the variational wave function of the Gutzwiller type which is defined in the following manner:

$$|\Psi_G\rangle = \hat{P}|\Psi_0\rangle, \tag{3}$$

where $|\Psi_0\rangle$ is the noncorrelated (mean-field) state and $\hat{P}$ is the correlation operator

$$\hat{P} = \prod_i \sum_\Gamma \lambda_{i,\Gamma} |\Gamma\rangle_{i\,i}\langle\Gamma|, \tag{4}$$

where i runs over all the lattice sites, $|\Gamma\rangle \in \{|\emptyset\rangle, |\uparrow\rangle, |\downarrow\rangle, |\uparrow\downarrow\rangle\}$, and $\lambda_{i,\Gamma}$ are the corresponding variational parameters. It has been shown that for such a form of the correlation operator it is convenient to impose an additional condition on the $\hat{P}_i$ operator [28], i.e.,

$$\hat{P}_i^2 = 1 + x\hat{d}_i^{HF}, \tag{5}$$

where $\hat{d}_i^{HF} = \hat{n}_{i\uparrow}^{HF}\hat{n}_{i\downarrow}^{HF}$, $\hat{n}_{i\sigma}^{HF} = \hat{n}_{i\sigma} - n_{i\sigma}$, with $n_{i\sigma} = \langle\Psi_0|\hat{n}_{i\sigma}|\Psi_0\rangle$, and x is yet another variational parameter. It is straightforward to show that

$$\begin{aligned} \lambda_{\uparrow\downarrow}^2 &= 1 + x(1-n_s)^2, \\ \lambda_s^2 &= 1 - xn_s(1-n_s), \\ \lambda_\emptyset^2 &= 1 + xn_s^2, \end{aligned} \tag{6}$$

where for simplicity we have assumed a homogeneous system with no magnetic or charge ordering. Hence, $\lambda_{i,\Gamma} \equiv \lambda_\Gamma$ and $\lambda_\uparrow = \lambda_\downarrow = \lambda_s$, $n_{i\uparrow} = n_{i\downarrow} \equiv n_s$. As a result, we are left with only one variational parameter, x. Now, in order to project out the double occupancies, what is required for the t-J model, one has to set

$$\begin{aligned} &\text{for } n_s < 0.5 : \lambda_{\uparrow\downarrow} = 0 \;\Rightarrow x = -\frac{1}{(1-n_s)^2}, \\ &\text{for } n_s > 0.5 : \lambda_\emptyset = 0 \;\Rightarrow x = -\frac{1}{n_s^2}, \end{aligned} \tag{7}$$

meaning that for electron concentrations below half-filling the double occupancies of electrons are prohibited, and above half-filling the holons are prohibited.

In order to obtain the formula for the expectation value of our Hamiltonian per lattice site,

$$E_G = \frac{\langle\Psi_G|\hat{H}|\Psi_G\rangle}{N\langle\Psi_G|\Psi_G\rangle} = \frac{1}{N}\langle\hat{H}\rangle_G, \tag{8}$$

we apply the diagrammatic expansion of the Gutzwiller wave function (DE-GWF) [22] in the zeroth order which is equivalent to the *statistically consistent Gutzwiller approximation* (SGA) [29]. As a result one obtains

$$\begin{aligned} \langle\hat{H}\rangle_G = &\sum_{ij} q^2 t_{ij\sigma}\langle\hat{c}_{i\sigma}^\dagger\hat{c}_{j\sigma}\rangle_0 \\ &+ \lambda_s^4 J \sum_{\langle ij\rangle}{}' \Bigg(\frac{1}{2}\sum_\sigma e^{i\sigma 2\phi_{ij}}\langle\hat{c}_{i\sigma}^\dagger\hat{c}_{i\bar{\sigma}}\hat{c}_{j\bar{\sigma}}^\dagger\hat{c}_{j\sigma}\rangle_0 \\ &+ \frac{1}{4}\sum_{\sigma\sigma'}\sigma\sigma'\langle\hat{n}_{i\sigma}^{HF}\hat{n}_{j\sigma'}^{HF}\rangle_0 \Bigg), \end{aligned} \tag{9}$$

where $q = \lambda_s[\lambda_d n_s + \lambda_\emptyset(1-n_s)]$ and $\langle\hat{o}\rangle_0$ stands for the expectation value of the $\hat{o}$ operator in the state $|\psi\rangle_0$. By applying the Wick's theorem one can decompose all the four-operator expectation values which appear on the right-hand side of the above equation. Hence, the obtained E_G becomes a function of x, n_s as well as the electron hopping and Cooper pairing mean field parameters

$$P_{ij\sigma} = \langle\hat{c}_{i\sigma}^\dagger\hat{c}_{j\sigma}\rangle_0, \quad S_{ij}^{\sigma\sigma'} = \langle\hat{c}_{i\sigma}\hat{c}_{j\sigma'}\rangle_0, \tag{10}$$

respectively. It should be noted that the expectation values in the noncorrelated state together with the variational parameters determine the corresponding expectation values in the correlated state. Namely,

$$\begin{aligned} \Delta_{ij}^{\sigma\sigma'} &= \langle\hat{c}_{i\sigma}\hat{c}_{j\sigma'}\rangle_G = q^2\langle\hat{c}_{i\sigma}\hat{c}_{j\sigma'}\rangle_0, \\ \Lambda_{ij\sigma} &= \langle\hat{c}_{i\sigma}^\dagger\hat{c}_{j\sigma}\rangle_G = q^2\langle\hat{c}_{i\sigma}^\dagger\hat{c}_{j\sigma}\rangle_0. \end{aligned} \tag{11}$$

Since we are using the zeroth-order expansion of the Gutzwiller wave function and do not consider the standard onsite *s-wave* pairing scenario, the number of particles does not change by the projection procedure ($\langle\hat{n}_{i\sigma}\rangle_G = \langle\hat{n}_{i\sigma}\rangle_0$).

Within our analysis, we treat $S_{ij}^{\uparrow\downarrow}$ and $S_{ij}^{\downarrow\uparrow}$ separately allowing for both pure spin-singlet pairing ($S_{ij}^{\uparrow\downarrow} = -S_{ij}^{\downarrow\uparrow}$), pure spin-triplet pairing ($S_{ij}^{\uparrow\downarrow} = S_{ij}^{\downarrow\uparrow}$) as well as their mixture ($|S_{ij}^{\uparrow\downarrow}| \neq |S_{ij}^{\downarrow\uparrow}|$). At the same time, we neglect the possibility of $\uparrow\uparrow$ and $\downarrow\downarrow$ pairing due to the fact that here the pairing mechanism is based on the kinetic exchange term which is of antiferromagnetic type. Additionally, the $S^z = \pm 1$ pairing channels would lead to a Fermi wave vector mismatch, which is detrimental when it comes to the formation of the superconducting state.

In order to determine the values of the mean fields we apply the effective Hamiltonian scheme [30]. Within such approach the minimization condition of the ground-state energy (8) leads to an effective Hamiltonian, which for our case has the form

$$\hat{\mathcal{H}}_{\text{eff}} = \sum_{ij\sigma} \tilde{t}_{ij\sigma} \hat{c}^{\dagger}_{i\sigma} \hat{c}_{j\sigma} - \tilde{\mu} \sum_{i\sigma} \hat{n}_{i\sigma} + {\sum_{\langle ij\rangle\sigma}}' \left[(\tilde{\Delta}_{ij\sigma\bar{\sigma}})^* \hat{c}_{j\sigma} \hat{c}_{i\bar{\sigma}} + \text{H.c.} \right], \tag{12}$$

where the effective hopping, effective chemical potential, and the effective superconducting gap parameters are defined through the corresponding relations

$$\tilde{t}_{ij\sigma} \equiv \frac{\partial \mathcal{F}}{\partial P_{ij\sigma}}, \quad (\tilde{\Delta}_{ij\sigma\bar{\sigma}})^* \equiv \frac{\partial \mathcal{F}}{\partial S^{\sigma\bar{\sigma}}_{ji}}, \quad \tilde{\mu} \equiv -\frac{\partial \mathcal{F}}{\partial n_s}, \tag{13}$$

where $\mathcal{F} = E_G - 2\mu_G n_s$ with μ_G being the chemical potential determined in the correlated state. For the sake of completeness we show explicitly the form of the effective model parameters below:

$$\tilde{t}_{ij\sigma} = q^2\, t_{ij\sigma} - J\, \frac{\lambda_s^4}{2} \left[2(P_{ij\bar{\sigma}})^*\, e^{i2\phi^{\sigma}_{ij}} + (P_{ij\sigma})^* \right], \tag{14}$$

$$\left(\tilde{\Delta}^{\sigma\bar{\sigma}}_{ij}\right)^* = -J\, \frac{\lambda_s^4}{2} \left[2\left(S^{\sigma\bar{\sigma}}_{ij}\right)^*\, e^{i2\phi^{\sigma}_{ij}} - \left(S^{\bar{\sigma}\sigma}_{ij}\right)^* \right], \tag{15}$$

$$\tilde{\mu} = \mu_G - U\lambda_d^2 n_s. \tag{16}$$

After the transformation to the reciprocal space we write the effective Hamiltonian in the matrix form

$$\hat{\mathcal{H}}_{\text{eff}} = \sum_{\mathbf{k}\sigma} (\hat{c}^{\dagger}_{\mathbf{k}\sigma} \;\; \hat{c}_{-\mathbf{k}\bar{\sigma}}) \begin{pmatrix} \tilde{\epsilon}_{\mathbf{k}\sigma} - \tilde{\mu} & \tilde{\Delta}_{\mathbf{k}\bar{\sigma}\sigma} \\ (\tilde{\Delta}_{\mathbf{k}\bar{\sigma}\sigma})^* & -\tilde{\epsilon}_{\mathbf{k}\sigma} + \tilde{\mu} \end{pmatrix} \begin{pmatrix} \hat{c}_{\mathbf{k}\sigma} \\ \hat{c}^{\dagger}_{-\mathbf{k}\bar{\sigma}} \end{pmatrix} + \sum_{\mathbf{k}\sigma} (\tilde{\epsilon}_{\mathbf{k}\sigma} - \tilde{\mu}), \tag{17}$$

where $\bar{\sigma} = -\sigma$ and we have used the relation $\tilde{\epsilon}_{\mathbf{k}\sigma} = \tilde{\epsilon}_{-\mathbf{k}\bar{\sigma}}$ (time-reversal symmetry condition). The effective dispersion relations as well as the superconducting gaps in $\mathbf{k}$ space are related with their real-space counterparts in the following manner:

$$\tilde{\epsilon}_{\mathbf{k}\sigma} = \sum_{i(j)} \tilde{t}_{ij} e^{ik(\mathbf{R}_i - \mathbf{R}_j)}, \qquad \tilde{\Delta}_{\mathbf{k}\bar{\sigma}\sigma} = \sum_{i(j)} \tilde{\Delta}_{ji\sigma\bar{\sigma}} e^{ik(\mathbf{R}_j - \mathbf{R}_i)}, \tag{18}$$

where i index runs over the nearest-neighbor lattice sites of site j. The $\mathbf{R}_i$ and $\mathbf{R}_j$ vectors point to the i and j lattice sites, respectively. The left-hand sites of the equations above do not depend on j since we assume spaciously homogeneous state.

The eigenvalues of the Hamiltonian matrix in Eq. (17) are

$$\lambda_{\mathbf{k}\sigma} = \pm\sqrt{(\tilde{\epsilon}_{\mathbf{k}\sigma} - \tilde{\mu})^2 + |\tilde{\Delta}_{\mathbf{k}\bar{\sigma}\sigma}|^2}. \tag{19}$$

From the above equation, one can see that in the SC state the gap $\tilde{\Delta}_{\mathbf{k}\downarrow\uparrow}$ ($\tilde{\Delta}_{\mathbf{k}\uparrow\downarrow}$) opens up at the spin-up (spin-down) Fermi surface. Moreover, the $\tilde{\Delta}_{\mathbf{k}\downarrow\uparrow}$ and $\tilde{\Delta}_{\mathbf{k}\uparrow\downarrow}$ SC gaps can be transformed into the singlet and triplet components

$$\tilde{\Delta}^{s}_{\mathbf{k}} = \frac{1}{\sqrt{2}}(\tilde{\Delta}_{\mathbf{k}\uparrow\downarrow} - \tilde{\Delta}_{\mathbf{k}\downarrow\uparrow}), \qquad \tilde{\Delta}^{t}_{\mathbf{k}} = \frac{1}{\sqrt{2}}(\tilde{\Delta}_{\mathbf{k}\uparrow\downarrow} + \tilde{\Delta}_{\mathbf{k}\downarrow\uparrow}), \tag{20}$$

which we can use to rewrite the expressions for the eigenvalues

$$\lambda_{\mathbf{k}\sigma} = \pm\sqrt{(\tilde{\epsilon}_{\mathbf{k}\sigma} - \tilde{\mu})^2 + \frac{1}{2}\left|\tilde{\Delta}^{t}_{\mathbf{k}} - \sigma\tilde{\Delta}^{s}_{\mathbf{k}}\right|^2}. \tag{21}$$

The paired state with $\Delta^{s}_{\mathbf{k}} \neq 0$ and $\Delta^{t}_{\mathbf{k}} \neq 0$ is referred to here as the *mixed singlet-triplet* paired state.

The self-consistent equations for the mean field parameters [Eq. (10)] can be derived in a standard manner by applying the Bogoliubov–de Gennes approach to the effective Hamiltonian given by Eq. (17). By solving the set of self-consistent equations numerically we determine the hopping and pairing amplitudes to all the six nearest neighbors. Then, in order to obtain their correlated state counterparts, we use Eqs. (11). Similarly as in our previous study [25], to identify the symmetry of the resultant paired state, we transform the six real-space nearest-neighbor pairing amplitudes into six symmetry-resolved pairing amplitudes of the following form:

$$\Delta^{\sigma\bar{\sigma}}_{M,p} = \frac{i^p}{6} \sum_{i(j)} e^{-iM\theta_{ji}} \Delta^{\sigma\bar{\sigma}}_{ji}, \tag{22}$$

where the summation runs over the six nearest-neighbor lattice sites j surrounding site i, and θ_{ji} are the angles $\{0,\ \pi/3,\ 2\pi/3,\ \pi,\ 4\pi/3,\ 5\pi/3\}$ between the positive half-x axis and the $\mathbf{R}_{ji} = \mathbf{R}_j - \mathbf{R}_i$ vector. M is the symmetry factor, which takes integer values and corresponds to six possible pairing symmetries (cf. Table I). The p parameter corresponds to the parity of the particular symmetry: for even parity symmetries we have $p = 0$, and for odd parities we have $p = 1$.

Finally, similarly as for the case of the momentum space [Eqs. (20)] one can write the expressions for the real-space singlet and triplet gap amplitudes in the correlated state, which

TABLE I. The six possible values of the symmetry factor M and the corresponding values of the parity factor p (second column), appearing in Eq. (22). The corresponding six symmetries of the superconducting gap together with their parities are provided in the third and fourth columns. The Cooper-pair spin state compatible with a given symmetry is provided in the fifth column.

M	p	Gap symmetry	Parity	Spin state
0	0	Extended s	Even	Singlet
1	1	$p_x + i\, p_y$	Odd	Triplet
2	0	$d_{x^2-y^2} + i\, d_{xy}$	Even	Singlet
3	1	f	Odd	Triplet
4	0	$d_{x^2-y^2} - i\, d_{xy}$	Even	Singlet
5	1	$p_x - i\, p_y$	Odd	Triplet

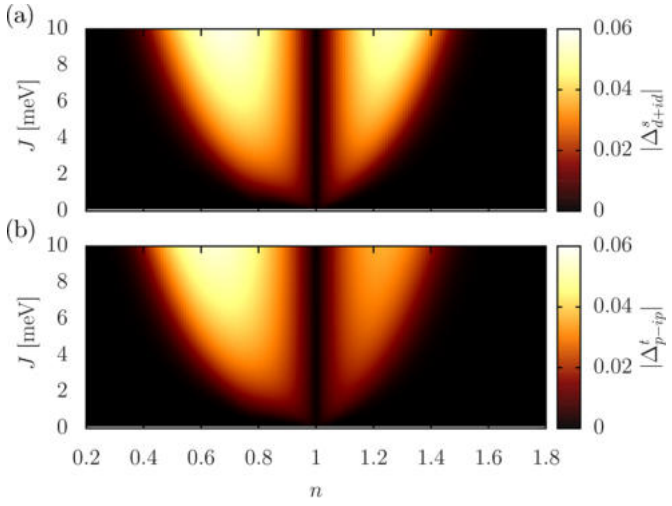

FIG. 3. Superconducting gap amplitudes for the spin-singlet $d + id$ (a) and spin-triplet $p - ip$ (b) symmetries as a function of band filling n and exchange interaction energy J for the selected value of the displacement field $D = 0.4$ V/nm.

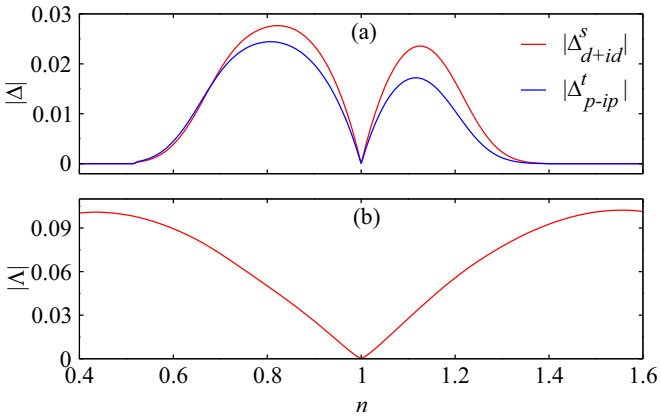

FIG. 4. (a) Superconducting gap amplitudes for the spin-singlet $d + id$ and spin-triplet $p - ip$ symmetries as a function of band filling n for selected values of exchange interaction energy $J = 2.62$ meV and displacement field $D = 0.4$ V/nm. (b) The expectation value of the nearest-neighbor electron hopping for the same model parameters as in (a).

will play the central role in our subsequent analysis:

$$\Delta^s_{M,p} = (\Delta^{\uparrow\downarrow}_{M,p} - \Delta^{\downarrow\uparrow}_{M,p})/\sqrt{2},$$
$$\Delta^t_{M,p} = (\Delta^{\uparrow\downarrow}_{M,p} + \Delta^{\downarrow\uparrow}_{M,p})/\sqrt{2}. \tag{23}$$

For the sake of clarity, in the following sections, we use the symmetry names ($p \pm ip$, $d \pm id$, f, etc.) in the subscripts of the symmetry-resolved superconducting gaps instead of the values of the M and p factors.

III. RESULTS

A. General features of the paired state

We now characterize the unconventional superconducting state within the t-J model description of the WSe_2 homobilayer at twist angle $\theta = 5.08°$. This is the twist angle where, in Ref. [6], "signatures of superconductivity" have been experimentally observed. In particular, they observe an insulating state at half-filling ($n = 1$ in our notation), with possible superconducting domes around $n \approx 0.86$ and $n \approx 1.16$. Note, that in Ref. [6] the band filling is expressed as hole density per spin, in contrast to our paper where we use the total number of electrons per lattice site ($n = 2n_s$).

First, we set the hopping parameters to those corresponding to the displacement field $D = 0.4$ V/nm and determine the stability range and the symmetry of the obtained superconducting state. We scan the whole (n, J) plane. As one can see from Fig. 3 a two-dome structure (similar to the experimental results in Ref. [6]) of an unconventional paired state appears, which is characterized by nonzero $d + id$ spin-singlet as well as $p - ip$ spin-triplet amplitudes. Both gap amplitudes show very similar behavior, though the triplet component is slightly smaller. It should be noted that these are not two separate solutions with different gap symmetries, but a single solution for which both amplitudes are nonzero (a mixed singlet-triplet state) meaning that $|\tilde{\Delta}_{\mathbf{k}\uparrow\downarrow}| \neq |\tilde{\Delta}_{\mathbf{k}\downarrow\uparrow}|$ [compare to Eqs. (19) and (20)]. The appearance of a mixed paired state is a consequence of the valley-dependent spin splitting. Indeed, we verified that if one would have purely real hoppings without spin-orbit coupling, there would be a doubly degenerate Fermi surface with a pure spin-singlet $d + id$ solution. Finally, since the exchange interaction term $\sim J$ is responsible for the appearance of the pairing, the band-filling range for which the SC state is stable is wider for larger values of J.

In order to determine the range of realistic values of J we use the formula $J = 4|t|^2/U$, where U is the Coulomb repulsion integral originating from the Hubbard model, which serves as a starting point for the t-J model derivation. For the case of $tWSe_2$, it has been estimated that U is comparable to the bare bandwidth $W \approx 90$ meV [6,14] what would give us $J \approx 3$ meV. In practice by changing the twist angle one can change the value of U, tuning the strength of the correlations. Also, the dielectric constant which is modified by the three-dimensional dielectric environment also significantly influences U and is not precisely known. Nevertheless, the calculations provided in Ref. [14] for the typical value of dielectric constant $\epsilon = 10$ show that, for the twist angle close to 5°, the onsite Coulomb repulsion should be $U \approx 120$ meV which is larger than the bare bandwidth. Other estimates [6] show that the crossover between the $U < W$ and $U > W$ situations should appear close to the twist angle of 5° for the dielectric constant $\epsilon \approx 6$.

In Fig. 4 we show the band-filling dependence of the SC gap amplitudes for a selected typical value of $J = 2.62$ meV, which corresponds to $U \gtrsim W$ (close to the moderately correlated regime). As can be explicitly seen at half-filling ($n = 1$) both the pairing and the expectation value of the nearest-neighbor electron hopping ($|\Lambda|$) are suppressed, which is a manifestation of the insulating state at half-filling.

Apart from the $(d + id)$- and $(p - ip)$-wave solution visible in Figs. 3 and 4 we have also obtained an extended s- and f-wave solution which, however, is much weaker and requires relatively larger values of the J parameter to become stable. In Fig. 5 we provide the results for $J = 10$ meV, where in the low- and high-electron concentration regimes the mentioned

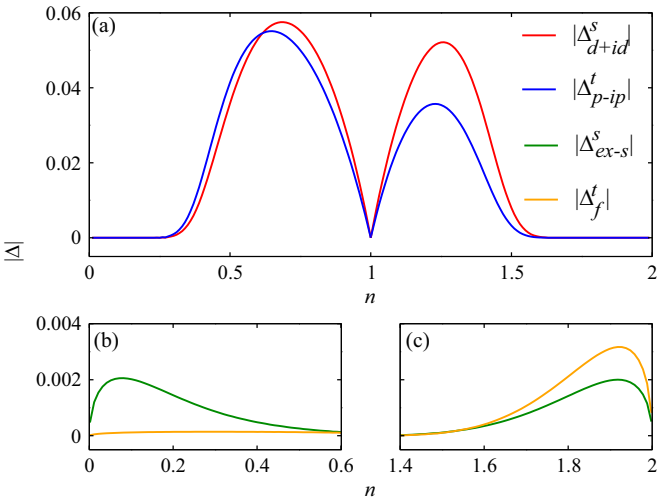

FIG. 5. (a) Superconducting gap amplitudes for the spin-singlet $d+id$ and spin-triplet $p-ip$ symmetries as a function of band filling n for selected values of exchange interaction energy $J=10$ meV and displacement field $D=0.4$. In (b) and (c) we show the low- and high-electron concentration regimes where a mixed singlet *extended s-* and triplet *f-wave* solution becomes stable.

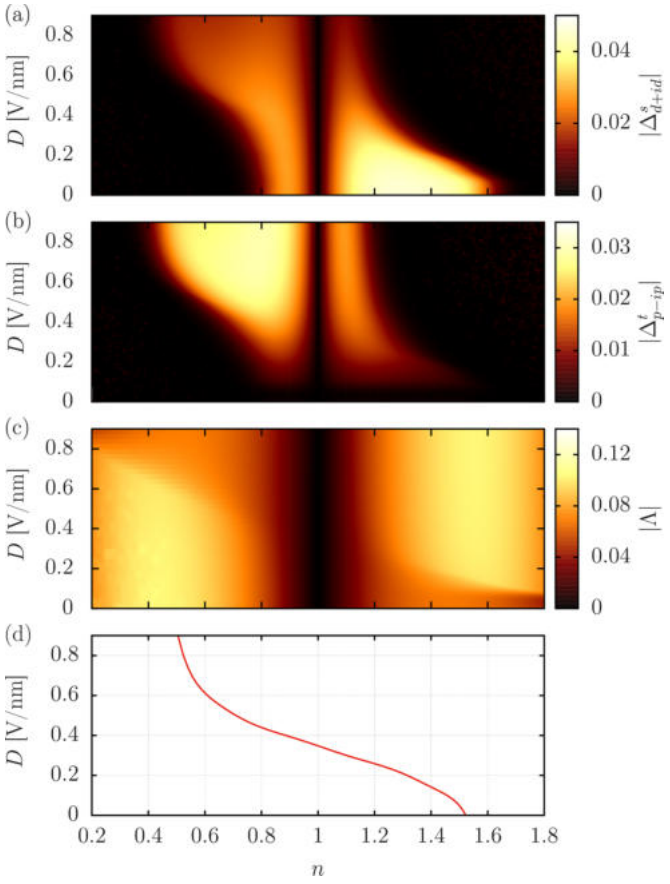

FIG. 6. Superconducting gap amplitudes for the spin-singlet $d+id$ (a) and spin-triplet $p-ip$ (b) symmetries as a function of band filling n and displacement field D for $J=2.62$ meV. In (c) we show the electron hopping expectation value in the correlated state as a function of n and D. The position of the Van Hove singularity which influences the behavior of the superconducting gap is provided in (d).

extended s- and f-wave paired state is shown to create two additional SC domes as a function of band filling. As one can see, the gap amplitudes $\Delta^s_{\text{ex-}s}$ and Δ^t_f are approximately one order of magnitude smaller than the p- and d-wave solutions Δ^s_{d+id}, Δ^t_{p-ip}. This situation resembles the one obtained earlier for a much simpler model with intersite real-space pairing on a square lattice, in which a *d-wave* superconducting state becomes stable around half-filling and an extended s-wave paired state resides in the low- and high-electron concentration regimes (see Fig. 2 in Ref. [31]). In this study, due to the triangular lattice and the complex hoppings, the gap symmetry is more exotic being of mixed singlet-triplet type.

Next, we turn to the analysis of the effect of the displacement field on the paired state. For that, we set the typical value of the exchange interaction $J=2.62$ meV, and solve the set of self-consistent equations for different complex hopping parameters, which correspond to different displacement fields. In order to make the obtained phase diagram more smooth we have applied interpolation to the data provided Ref. [6] where the complex hopping parameters for 14 values of the displacement field in the range $D\in[0,0.9]$ V/nm have been provided. As one can see in Fig. 6, for low values of D, the spin-singlet component to the pairing is dominant while for large D the situation changes in favor of the spin-triplet component. It should be noted that for $D\approx 0$ the imaginary part of the complex hoppings is close to zero, meaning that the valley-dependent spin spitting is very small. This will promote the spin-singlet state. On the other hand, for purely imaginary hoppings one would obtain a pure spin-triplet state (similar to our previous result in Ref. [25]). However, this situation is not reached in the considered range of D values. Nevertheless, the result provided in Fig. 6 shows that by adjusting the displacement field one should be able to tune the balance between the singlet and triplet contributions to the pairing.

Another effect which is visible in the (n,D) diagram is that the stability regime of the SC state moves towards lower concentrations with increasing D. This is caused by the fact that the Van Hove singularity changes its position while increasing the displacement field [see Figs. 6(d), 2(c) and 2(d)]. The superconducting state is stabilized by the high density of states at the Van Hove singularity. Consequently, the behavior of the superconducting gap amplitudes reflects the evolution of the Van Hove singularity with increasing D. Of course, at half-filling ($n=1$) there is still an insulating state with suppressed pairing amplitudes, regardless of the Van Hove singularity. The same applies to the expectation values of the electron hopping which is provided in Fig. 6(c) for completeness. This last result reflects the experimental situation in which also the appearance of the insulating behavior corresponds to the half-filled case in wide range of D values [6].

It should be noted that instabilities toward mixed singlet-triplet pairing of $d+id$ and $p-ip$ as well as extended s- and f-type has been recently reported in the Hubbard model as applied to the description of $tWSe_2$ in the regime of relatively weak correlations ($U\lesssim 0.7\,W$) within functional renormalization group (FRG) method [32]. Also, for very weak Coulomb interactions ($U\lesssim 0.3W$) $p+ip$, $d+id$, and $g+ig$ pairing symmetries have been identified and their interplay with spin-polarized pair density waves has been

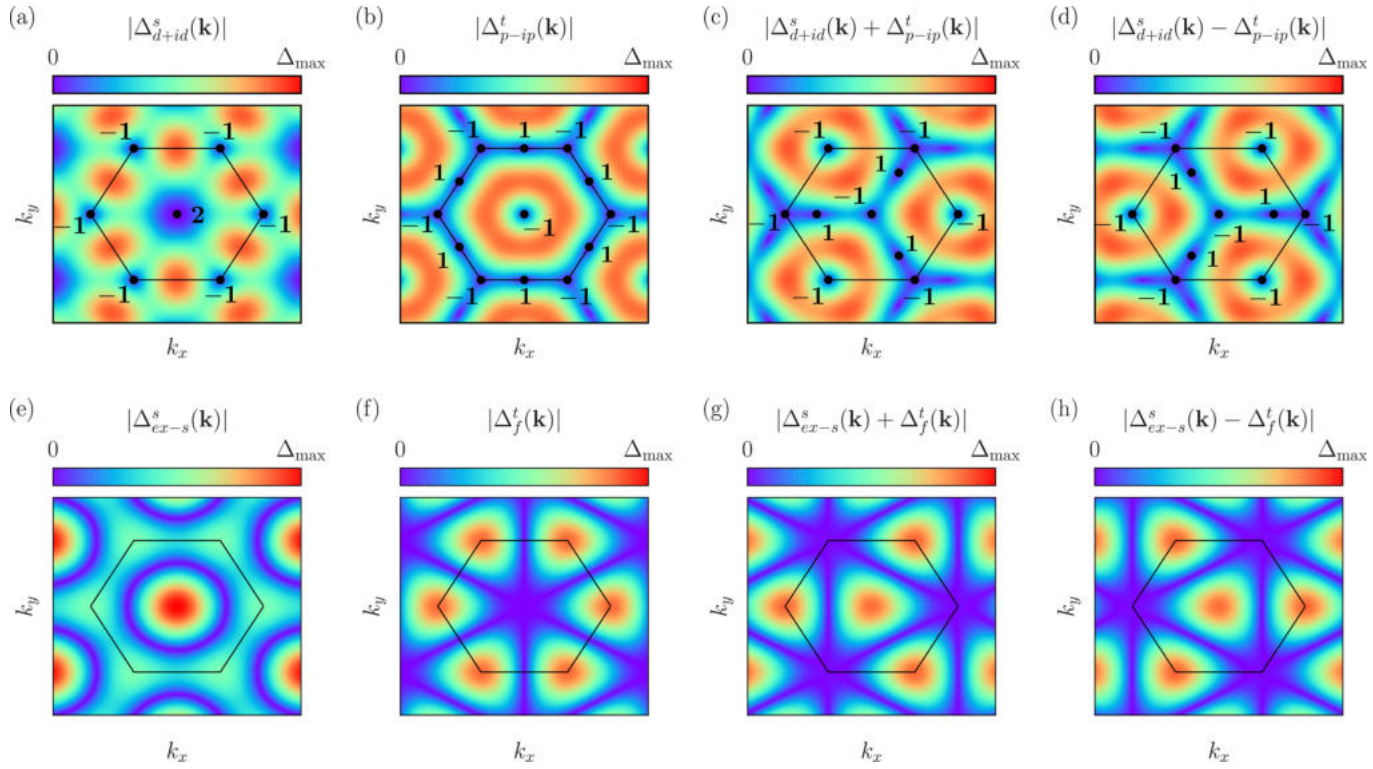

FIG. 7. Superconducting gap as a function of momentum for the pure $(d + id)$-*wave* (a), $(p - ip)$-*wave* (b), *extended-s-wave* (e), and f-*wave* (f) gap symmetries together with the mixed gap symmetries $|\Delta^s(\mathbf{k}) \pm \Delta^t(\mathbf{k})|$ (c), (d), (g), (h). Note that in the mixed states, the $|\Delta^s(\mathbf{k}) - \Delta^t(\mathbf{k})|$ and $|\Delta^s(\mathbf{k}) + \Delta^t(\mathbf{k})|$ gaps open at the spin-up and spin-down Fermi surfaces, respectively [cf. Eq. (21)]. The nodal points (if they appear) are marked by the black dots together with the topological charge (Chern charge) next to it. The Chern charges provided here have been calculated for the case of electronlike normal-state Fermi surface (counterclockwise superconducting gap's phase winding). For the case of holelike Fermi surfaces the sign of the Chern charges changes to opposite.

analyzed, however, without the singlet-triplet mixing appearance [20].

To understand the role of symmetry in the mixed paired state, we provide in Fig. 7 the momentum dependence of the pure $d + id$-, $p - ip$-, extended-s-, and f-wave gap symmetries, together with the mixed gap symmetries that have been obtained by us here in proper parameter ranges. As one can see all the pure gap symmetries fulfill the sixfold rotational symmetry, while for the mixed states the symmetry is reduced to C_3, which is the one obeyed by our Hamiltonian with valley-dependent spin splitting. Hence, the reduction of symmetry due to the spin splitting incorporated in the minimal model naturally leads to singlet-triplet mixing in the superconducting state. Also, it should be noted that for the mixed states, $|\Delta^s(\mathbf{k}) - \Delta^t(\mathbf{k})|$ and $|\Delta^s(\mathbf{k}) + \Delta^t(\mathbf{k})|$, gaps open at the spin-up and spin-down Fermi surfaces, respectively [cf. Eq. (21)].

As can be seen from Fig. 7 the $d + id$ and $p - ip$ gap symmetries as well as their mixtures all have nodal points in the Brillouin zone for which the gap is exactly zero (marked by black dots). This is not the case for the extended-s-, and f-wave gaps, as well as their mixtures, for which only nodal lines appear. Each nodal point comes with a topological charge (Chern charge) which is also provided in the figure and can lead to a nonzero Chern number of a given paired state. A detailed analysis of the topological features of the mixed $d + id$ and $p - ip$ superconducting state is presented in the next subsection.

B. Topological properties of the paired state

We now analyze in detail the topological properties of the mixed singlet-triplet superconducting state. Since the paired states studied here spontaneously break time-reversal symmetry, their classification is given by the Chern number [33]. We calculate the Chern number with the use of the Brillouin zone triangulation method [34]. As mentioned in the previous section, the extended-s- and f-wave paired state does not have any nodal points in the Brillouin zone, and is therefore topologically trivial with $C = 0$. On the other hand, the calculated Chern number for the $d + id$ and $p - ip$ symmetry takes the values of $C = \pm 2,\ \pm 4$, depending on both band filling and displacement field. In Fig. 8 we show the topological phase diagram of the mixed $d + id$ and $p - ip$ paired state in the (n, D) plane. As can be seen according to our calculations, by changing the experimentally controllable parameters one can induce topological phase transitions between regimes characterized by different values of the Chern number. It should be noted that the bare band of the considered model is topologically trivial, therefore, the topological features are introduced by the paired state itself.

While analyzing the data provided in Fig. 8 it is worth emphasizing that the Chern number can be interpreted as the winding number of the superconducting gap's complex phase while going around the normal-state Fermi surface (FS) [35]:

$$C = \frac{1}{2\pi} \oint_{\mathrm{FS}} d\mathbf{l} \cdot \nabla \phi, \tag{24}$$

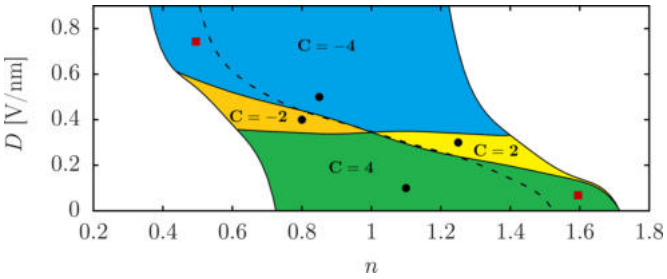

FIG. 8. The topological phase diagram of the mixed $d + id$ (singlet) and $p - ip$ (triplet) superconducting states in the (n, D) plane. The colored regions correspond to the stability of the mixed paired state (cf. Fig. 6). Different colors correspond to different values of the Chern number. The position of the Van Hove singularity in the diagram is marked by the dashed line. By changing the experimentally controllable parameters, like electron concentration (n) and displacement field (D), one can induce topological phase transitions. The black dots correspond to n and D values which have been selected for detailed analysis provided in Fig. 9. Additionally, the red squares mark the two selected situations of relatively high- and low-n values which are analyzed in detail in Fig. 10.

where for the case of electronlike (holelike) FS the integration is carried out counterclockwise (clockwise). Therefore, the shape and size of the FS, which can be tuned by both n and D, may affect the resulting topological features of the SC state. In fact, Eq. (24) can be further simplified, as the Chern number simply counts the Chern charge of the nodal points which are contained within the FS,

$$C = \sum_{i \in \Omega_{\mathrm{FS}}} (-1)^w C_i, \tag{25}$$

where C_i is the Chern charge of a given nodal point which can be determined by calculating the winding number of the order parameter around it. The sign of the Chern charge depends on whether it is enclosed by an electronlike ($w = 0$) or holelike ($w = 1$) Fermi surface. The i index runs only over the nodal points that are contained inside the Fermi surface. In Fig. 7 we provide the Chern charges C_i of all the nodal points for the considered gap symmetries. Once we know the Chern charge of every nodal point, as well as the shape of the FS, we can determine the Chern number (winding number) by simply using Eq. (25). With this procedure one can easily interpret the obtained topological phase diagram by looking at the relative position of the Fermi surface and the Chern charges of the nodal points.

It should be noted that the nodal points of the $d + id$ and $p - ip$ paired state fall into two categories. The first one corresponds to the nodes located at the high-symmetry points (Γ, K, and K') which are fixed and result from the symmetry of the triangular lattice itself. The second category are the points which position in the Brillouin zone depends on the balance between the singlet and triplet components to the pairing. There are three such points per each of the two mixed gaps $[|\Delta^s(\mathbf{k}) - \Delta^t(\mathbf{k})|$ and $|\Delta^s(\mathbf{k}) + \Delta^t(\mathbf{k})|]$ and they lie at the Γ-K and Γ-K' connecting lines. The movement of the mentioned nodal points inside the Brillouin zone, induced by tuning n and D, can affect the topological features as we show in some more detail further on.

In Fig. 9 we show the normal-state Fermi surfaces as well as the momentum-dependent SC gap for four representative points that are marked by black dots in the phase diagram (Fig. 8) and are characterized by different values of the Chern number. The spin-up and -down Fermi surfaces together with the corresponding SC gaps [cf. Eq. (21)] are provided in separate figures in the panel. As one can see, the topological transitions that appear across the phase diagram provided in Fig. 8 are not induced by a change in order-parameter symmetry. But rather, they result from the fact that with changing n and D one influences the normal-state Fermi surface as well as one moves the nodal points that lie in-between the Γ-K and Γ-K' points. This in turn influences the total Chern charge contained inside the Fermi surfaces. In particular, the transitions from $C = 4$ (a) to $C = -2$ (d) as well as from $C = -4$ (b) to $C = 2$ (c), both correspond to moving the three Chern charges laying at the Γ-K and Γ-K' connecting lines outside the interior of the Fermi surfaces. What is also important is that with changing n and D one can induce transitions from electronlike [Figs. 9(a) and 9(d)] to holelike Fermi surface [Figs. 9(b) and 9(c)]. This changes the position of the Fermi surface as well as the signs of the Chern charges what influences the overall Chern number. That is why the transition line between $C = 4$ and 2 as well as $C = -4$ and -2 coincides with the Van Hove singularity line in the regime of moderate displacement fields ($D \sim 0.3$–0.5 V/nm).

However, outside the region of moderate displacement fields the transition between electronlike and holelike Fermi surface no longer induces a topological phase transition. This is caused by the fact that now at the Van Hove singularity a transition between one FS per spin to two FS per spin appears. This prevents from changing the value of the Chern number. In Fig. 10 we show two such situations with two normal-state Fermi surfaces per spin. For example, in the low-D regime, crossing the Van Hove singularity leads to transition from a single electronlike FS centered at the Γ [Fig. 9(a)] to two holelike FS centered at the K and K' [Fig. 10(b)]. Nevertheless, as one can see it does not lead to a change of the total Chern charge contained inside the Fermi surfaces. As a consequence of this effect, the topological transition line in Fig. 8 does not coincide with the Van Hove singularity line at its full extent.

IV. CONCLUSIONS

We have applied the t-J model to the description of the superconducting state in $tWSe_2$ within the Gutzwiller approach. As we show, such an approach reproduces the experimental situation with two superconducting domes as a function of band filling, and a correlation-induced insulating state at half-filling shown in Ref. [6]. Consistent with the experimental data, the insulating state is not affected by the displacement field in wide range of D. According to our calculations the superconducting domes have a mixed $d + id$ (singlet) and $p - ip$ (triplet) symmetry, which is a direct consequence of the valley-dependent spin splitting. If such an exotic paired state is indeed realized in this system, it would possible to tune the balance between the singlet and triplet contributions to the pairing with the use of the displacement field (cf. Fig. 6). Namely, for low values of D, the singlet pairing dominates and for high values of D the triplet pairing takes over. Ad-

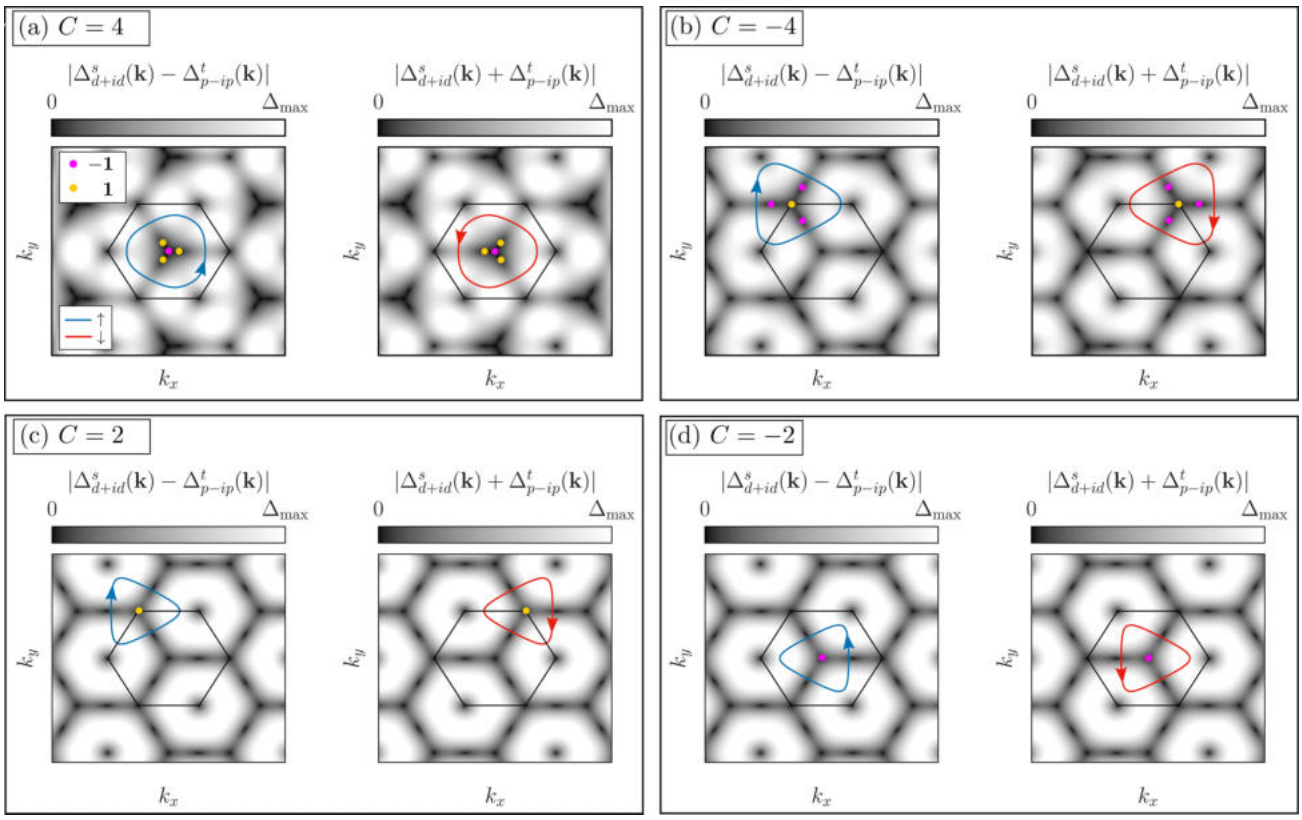

FIG. 9. The normal-state Fermi surfaces for spin-up and -down electrons as well as the **k**-dependent SC gaps for four selected values of n and D, which are marked by black dots in Fig. 8 and correspond to following values of the Chern number: $C = 4$ (a), $C = -4$ (b), $C = 2$ (c), and $C = -2$ (d). Note, that the value of the Chern number is simply the sum of the Chern charges contained inside the spin-up and -down Fermi surfaces (marked by the colored dots). The arrows at the Fermi surfaces represent the winding direction which is counterclockwise (clockwise) for the electronlike (holelike) Fermi surfaces. Note that the signs of the Chern charges depend on the winding direction.

ditionally, due to the evolution of the density of states, with increasing D, the paired state stability regime moves towards lower electron concentrations. Furthermore, our model reveals a weak extended s-wave and f-wave mixed paired state for relatively large values of the J, at low- and high-electron concentrations.

According to our analysis the mixed $d + id$ (singlet) and $p - ip$ (triplet) paired state is topologically nontrivial with Chern numbers $C = \pm 2,\ \pm 4$, depending on the value of band filling and displacement field (see Fig. 8). The changes of the Chern number are caused by (i) changes of the normal-state Fermi surfaces, either due to a change in size or due to a Lifshitz transition from an electronlike to a holelike Fermi surface (cf. Fig. 7); (ii) the movement of the nodal points located at the Γ-K and Γ-K' connecting lines. By tuning the displacement field and electron density one could, according

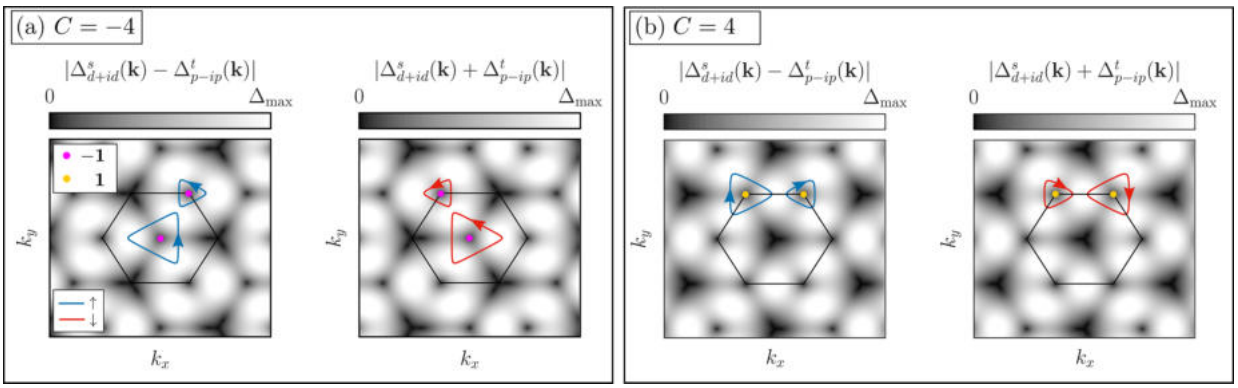

FIG. 10. The same as in Fig. 9 but for n and D values which are represented by the red squares marked in Fig. 8 and correspond to following values of the Chern number: $C = -4$ (a) and $C = 4$ (b). In contrast to Fig. 9, now we have two Fermi surfaces per spin. Note that in the low- and high-D regimes crossing the Van Hove singularity line and the resulting transition from electronlike to holelike Fermi surface no longer leads to topological phase transition.

to our results, induce topological phase transitions between pairing states characterized by different values of the Chern number.

Our methods find the zero-temperature ground state of a relevant t-J model for twisted WSe_2. We can estimate the critical temperature by looking at the maximum magnitude of the gap, $|\tilde{\Delta}|_{\max} \approx 0.06J$. This suggests a critical temperature of the order of $T_c \approx 1$ K, which is at a temperature slightly below the lowest temperature of the transport experiments provided in Ref. [6]. This might explain why so far only "signatures" of superconductivity have been observed in the mentioned experimental report. To experimentally detect the nontrivial nature of the pairing state, we suggest Knight shift measurements to detect the nonsinglet component. A detection of the Kerr effect can reveal the spontaneous broken time-reversal symmetry. Finally, our prediction for topological superconductivity in $tWSe_2$ suggests this system is ideal for observing nontrivial chiral edge states and possible Majorana particles [33].

It should be noted that, in the considered system also magnetically or charge ordered states may appear. In particular, for the half-filled case, it has been shown by various calculation methods that the 120° antiferromagnetic or ferromagnetic states become stable [18,21,36], depending on the complex phase of the hopping parameters. Thus, in some range of parameters the paired phase analyzed here may compete or coexist with other symmetry-broken states. Such study would require much more involved calculations and is beyond the scope of this work. We should see progress along this line soon.

The code which was written to carry out the numerical calculations as well as the data behind the figures are available in the open repository [37].

ACKNOWLEDGMENTS

We acknowledge discussions with M. Fischer. This research was funded by National Science Centre, Poland (NCN) according to Decision No. 2021/42/E/ST3/00128. L.R. is supported by the Swiss National Science Foundation through Starting Grant No. TMSGI2_211296. Research partly supported by program "Excellence initiative–research university" for the AGH University of Krakow.

APPENDIX A: INFLUENCE OF NONZERO DOUBLE OCCUPANCIES WITHIN THE t-J-U MODEL

Both formation and evolution of the paired state with gradual increase of the U value within the t-J-U model, as applied to $tWSe_2$, has been explicitly analyzed by us previously in Ref. [25]. Here, we revisit the results presented in Fig. 5 of that paper and discuss them in the view of the newest experimental findings [26,27], which have appeared at the stage of resubmitting this work. Namely, we select two U values which are of particular interest in this context ($U \lesssim W$ and $U > W$) and discuss the band-filling dependencies of the SC gaps.

For the case of the t-J-U model, the double occupancies are not completely projected out while carrying out the Gutzwiller approximation, and the Hamiltonian given by (1) is supplemented by the onsite Coulomb interaction term

$$\hat{H}_U = U \sum_i \hat{n}_{i\uparrow}\hat{n}_{i\downarrow}, \tag{A1}$$

where $\hat{n}_{i\uparrow}$ ($\hat{n}_{i\downarrow}$) are the number of particle operators on given lattice site with spin up (down), while U corresponds to the Coulomb interaction strength. Since now the double occupancies can be nonzero, one does not impose the conditions given by Eq. (7). Instead, an additional energy minimization over the x variational parameter is carried out during the procedure of solving the self-consistent equations.

As one can see in Fig. 11, within such an approach both one- and two-dome structures of the superconducting order parameter can be obtained as a function of band filling. When $U \lesssim W$ a single SC dome appears as shown in Fig. 11(b), while for $U > W$ a two-dome behavior is reported in Fig. 11(a). The latter case is due to the fact that for relatively large U an insulating state is created which separates the original single dome into two. For the case of the t-J model which is mainly considered in this paper, only the two-dome situation can appear since such approach corresponds to a large-U limit.

As we already mentioned in the Introduction the measurements presented in Ref. [6] suggest two superconducting

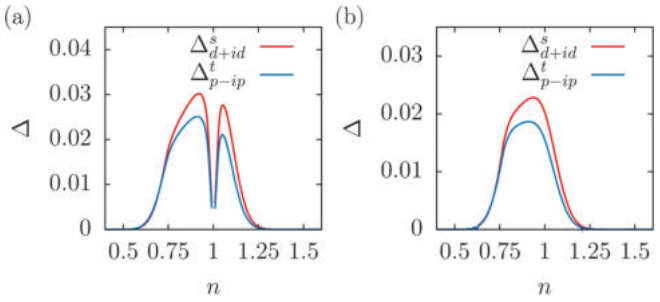

FIG. 11. Superconducting gap amplitudes for the spin-singlet $d + id$ and spin-triplet $p - ip$ symmetries as a function of band filling n for the case of the t-J-U model for two selected values of the Coulomb repulsion strength $U = 120$ meV (a) and $U = 85$ meV (b). The remaining model parameters are $J = 2.54$ meV, $D = 0.45$ V/nm, $W = 90$ meV.

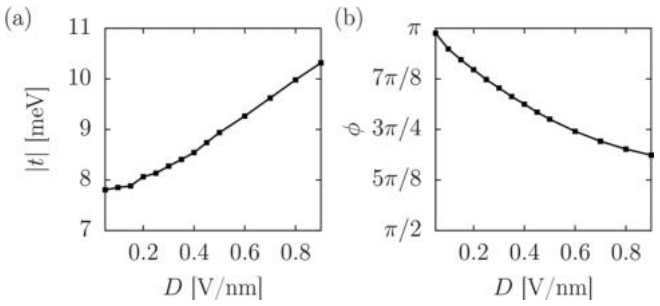

FIG. 12. Absolute value and the phase of the complex hopping parameters as a function of displacement field for the spin-up electrons to the right-hand-side nearest neighbor. In order to reproduce the complex hoppings to the remaining nearest neighbors as well as the spin-down corespondents one needs to use Eq. (2). The data used for this figure have been taken from Ref. [6].

domes residing on both sides of the half-filled case, where the insulating state is located. However, in the recent experiments [26,27] only one SC dome is shown in particular range of displacement field. Moreover, in Ref. [26], the SC state is stable at half-filling. In general, for $tWSe_2$ the value of U is tuned both by the twist angle and the dielectric constant. Therefore, it might be the case that both situations (two SC domes for $U \lesssim W$ and single SC dome for $U > W$) can be valid and reached in $tWSe_2$, depending on the particular parameters of the sample and the experimental setup itself which influence the actual value of U.

APPENDIX B: HOPPING PARAMETERS AS A FUNCTION OF DISPLACEMENT FIELD

Here we show how the displacement field influences the absolute value and the phase of the complex hopping parameters. As one can see for $D = 0$ the hoppings approach purely real and negative ($\phi \approx -\pi$) values. With increasing D the values of the hoppings acquire an imaginary component leading to the valley-dependent spin spitting and C_6 symmetry breaking (cf. Fig. 2). If the trend shown in Fig. 12(b) would not change even for larger D values, it would be theoretically possible to reach a purely imaginary hopping scenario.

[1] Y. Cao, V. Fatemi, A. Demir, S. Fang, S. L. Tomarken, J. Y. Luo, J. D. Sanchez-Yamagishi, K. Watanabe, T. Taniguchi, E. Kaxiras, R. C. Ashoori, and P. Jarillo-Herrero, Nature (London) **556**, 43 (2018).

[2] Y. Cao, V. Fatemi, S. Fang, K. Watanabe, T. Taniguchi, E. Kaxiras, and P. Jarillo-Herrero, Nature (London) **556**, 80 (2018).

[3] L. Balents, C. R. Dean, D. K. Efetov, and A. F. Young, Nat. Phys. **16**, 725 (2020).

[4] Y. Tang, L. Li, T. Li, Y. Xu, S. Liu, K. Barmak, K. Watanabe, T. Taniguchi, A. H. MacDonald, J. Shan, and K. F. Mak, Nature (London) **579**, 353 (2020).

[5] T. Li, S. Jiang, L. Li, Y. Zhang, K. Kang, J. Zhu, K. Watanabe, T. Taniguchi, D. Chowdhury, L. Fu, J. Shan, and K. F. Mak, Nature (London) **597**, 350 (2021).

[6] L. Wang, E.-M. Shih, A. Ghiotto, L. Xian, D. A. Rhodes, C. Tan, M. Claassen, D. M. Kennes, Y. Bai, B. Kim, K. Watanabe, T. Taniguchi, X. Zhu, J. Hone, A. Rubio, and C. R. Pasupathy, Abhay N. amd Dean, Nat. Mater. **19**, 861 (2020).

[7] A. Ghiotto, E.-M. Shih, G. S. S. G. Pereira, D. A. Rhodes, J. Kim, Bumho Zang, A. J. Millis, K. Watanabe, T. Taniguchi, J. C. Hone, L. Wang, C. R. Dean, and A. N. Pasupathy, Nature (London) **597**, 345 (2021).

[8] G. Gatti, J. Issing, L. Rademaker, F. Margot, T. A. de Jong, S. J. van der Molen, J. Teyssier, T. K. Kim, M. D. Watson, C. Cacho, P. Dudin, J. Avila, K. C. Edwards, P. Paruch, N. Ubrig, I. Gutiérrez-Lezama, A. F. Morpurgo, A. Tamai, and F. Baumberger, Phys. Rev. Lett. **131**, 046401 (2023).

[9] D. M. Kennes, M. Claassen, L. Xian, A. Georges, A. J. Millis, J. Hone, C. R. Dean, D. N. Basov, A. N. Pasupathy, and A. Rubio, Nat. Phys. **17**, 155 (2021).

[10] K. F. Mak and J. Shan, Nat. Nanotechnol. **17**, 686 (2022).

[11] C. Jin, Z. Tao, T. Li, Y. Xu, Y. Tang, J. Zhu, S. Liu, K. Watanabe, T. Taniguchi, J. C. Hone, L. Fu, J. Shan, and K. F. Mak, Nat. Mater. **20**, 940 (2021).

[12] A. Ghiotto, E.-M. Shih, G. S. S. G. Pereira, D. A. Rhodes, J. Kim, Bumho Zang, A. J. Millis, K. Watanabe, T. Taniguchi, J. C. Hone, L. Wang, C. R. Dean, and A. N. Pasupathy, Nat. Phys. **17**, 715 (2021).

[13] L. An, X. Cai, D. Pei, M. Huang, Z. Wu, Z. Zhou, J. Lin, Z. Ying, Z. Ye, X. Feng, R. Gao, C. Cacho, M. Watson, Y. Chen, and N. Wang, Nanoscale Horiz. **5**, 1309 (2020).

[14] H. Pan, F. Wu, and S. Das Sarma, Phys. Rev. Res. **2**, 033087 (2020).

[15] Y. Tan, P. K. H. Tsang, V. Dobrosavljević, and L. Rademaker, Phys. Rev. Res. **5**, 043190 (2023).

[16] M. Bélanger, J. Fournier, and D. Sénéchal, Phys. Rev. B **106**, 235135 (2022).

[17] F. Chen and D. N. Sheng, Phys. Rev. B **108**, L201110 (2023).

[18] J. Zang, J. Wang, J. Cano, A. Georges, and A. J. Millis, Phys. Rev. X **12**, 021064 (2022).

[19] J. Motruk, D. Rossi, D. A. Abanin, and L. Rademaker, Phys. Rev. Res. **5**, L022049 (2023).

[20] Y.-M. Wu, Z. Wu, and H. Yao, Phys. Rev. Lett. **130**, 126001 (2023).

[21] A. Biborski, P. Wójcik, and M. Zegrodnik, Phys. Rev. B **109**, 125144 (2024).

[22] J. Spałek, M. Fidrysiak, M. Zegrodnik, and A. Biborski, Phys. Rep. **959**, 1 (2022).

[23] C. Schrade and L. Fu, arXiv:2110.10172.

[24] V. Crépel, D. Guerci, J. Cano, J. H. Pixley, and A. Millis, Phys. Rev. Lett. **131**, 056001 (2023).

[25] M. Zegrodnik and A. Biborski, Phys. Rev. B **108**, 064506 (2023).

[26] Y. Xia, Z. Han, K. Watanabe, T. Taniguchi, J. Shan, and K. F. Mak, arXiv:2405.14784.

[27] Y. Guo, J. Pack, J. Swann, L. Holtzman, M. Cothrine, K. Watanabe, T. Taniguchi, D. Mandrus, K. Barmak, J. Hone, A. J. Millis, A. N. Pasupathy, and C. R. Dean, arXiv:2406.03418.

[28] J. Bünemann, T. Schickling, and F. Gebhard, Europhys. Lett. **98**, 27006 (2012).

[29] M. Abram, J. Kaczmarczyk, J. Jędrak, and J. Spałek, Phys. Rev. B **88**, 094502 (2013).

[30] J. Kaczmarczyk, Philos. Mag. **95**, 563 (2015).

[31] M. Zegrodnik and P. Wójcik, Phys. Rev. B **106**, 184508 (2022).

[32] L. Klebl, A. Fischer, L. Classen, M. M. Scherer, and D. M. Kennes, Phys. Rev. Res. **5**, L012034 (2023).

[33] X.-L. Qi and S.-C. Zhang, Rev. Mod. Phys. **83**, 1057 (2011).

[34] T. Fukui, Y. Hatsugai, and H. Suzuki, J. Phys. Soc. Jpn. **74**, 1674 (2005).

[35] *Topology, Entanglement, and Strong Correlations*, Schriften des Forschungszentrums Jülich, Reihe modeling and simulation, Autumn School on Correlated Electrons, Jülich (Germany), edited by E. Pavarini and E. Koch (Forschungszentrum Jülich GmbH Zentralbibliothek, Verlag, Jülich, 2020), Vol. 10.

[36] D. Kiese, Y. He, C. Hickey, A. Rubio, and D. M. Kennes, APL Mater. **10**, 031113 (2022).

[37] M. Zegrodnik, Topological superconductivity in twisted bilayer WSe_2: single band t-j model, Zenodo (2024), doi:10.5281/zenodo.10793686.

4.2 Optimal superconductivity in twisted bilayer WSe_2 where the Van Hove singularity crosses half-filling

In this article, we present a theoretical investigation of unconventional SC in $tWSe_2$ homobilayer, motivated by recent experimental observations, which appeared after the first paper by Wang *et al*. These new reports showed strong evidence of SC domes near half fillings [10, 49, 50]. The study focuses on the role of VHS and displacement field in stabilizing the SC state. To capture the effects of electron electron interactions, we implement an effective moiré t-J-U model supplemented by V and analyze it within the variational Gutzwiller approximation. This approach allows us to go beyond simple mean field treatment by including correlation induced renormalizations of the Hamiltonian parameters, which play a decisive role in determining the stability of SC.

The results show that SC is stabilized only in a narrow range of displacement fields and near half-filling. This finding is in qualitative agreement with experiments reporting a single SC dome close to half-filling [10, 49, 50]. Similarly as in our previous study the SC order parameter has a mixed character, combining spin-singlet $d + id$ and spin-triplet $p - ip$ components and the resulting paired state is topologically nontrivial. We find that SC is stable when the system exhibits large density of states due to VHS and additionally correlation induced renormalization is maximized. Both effects peak near half filling and in narrow range of displacement fields, creating optimal conditions for superconductivity. It is also discussed here that the number of SC domes depends on the strength of correlations. In the weak to moderate correlation regime ($U \lesssim W$) only a single dome appears with no Mott insulating state at half filling, however in the stronger correlation regime ($U > W$), a Mott insulating state emerges at half filling, which splits the SC region into two domes [8]. The calculated SC gaps correspond to estimated transition temperatures of order $T_c \sim 0.1$–0.5 K, consistent with experimental data, though somewhat underestimated due to the ground state nature of the Gutzwiller method.

 Originally published as M. Zegrodnik, W. Akbar, A. Biborski, and L. Rademaker, *Physical Review Research* **8**, L012070 (2026). DOI: 10.1103/pkf3-fkv4.

Letter

Optimal superconductivity in twisted bilayer WSe_2 where the Van Hove singularity crosses half-filling

Michał Zegrodnik,[1,*] Waseem Akbar,[1] Andrzej Biborski,[1] and Louk Rademaker[2,3]

[1]*Academic Centre for Materials and Nanotechnology, AGH University of Krakow, Al. Mickiewicza 30, 30-059 Krakow, Poland*

[2]*Department of Theoretical Physics, University of Geneva, CH-1211 Geneva, Switzerland*

[3]*Institute-Lorentz for Theoretical Physics, Leiden University, P.O. Box 9506, Leiden NL-2300, The Netherlands*

(Received 2 June 2025; accepted 28 January 2026; published 25 March 2026)

The recent discovery of unconventional superconductivity has pointed to twisted WSe_2 bilayer as a versatile platform for studying the correlated and topological phases of matter. Here, we analyze the effect of the displacement field and electron interactions on the formation of a topological paired state in twisted WSe_2. Our approach is based on the effective single band t-J-U model supplemented with intersite Coulomb interaction term and treated within the Gutzwiller approximation. We show that the superconducting phase is stabilized in a small range of displacement fields where the Van Hove singularity crosses half-filling, which is in qualitative agreement with recent experimental data. According to our analysis, such a circumstance comes as a result of a subtle interplay between the large density of states of the Van Hove singularity, in combination with the renormalization effects that appear in the weak-to-moderate correlation regime. The two factors create favorable conditions for the superconducting pairing only in a small area of the phase diagram.

DOI: 10.1103/pkf3-fkv4

Introduction. Transition-metal dichalcogenide bilayers have recently attracted a significant amount of interest due to their rich physics and exceptional tunability. It has been established experiementally that those systems host a number of correlated and topological states such as Mott insulators [1,2], magnetically ordered states [3,4], generalized Wigner crystals [5–9], quantum anomalous and spin quantum anomalous Hall states [4,10,11], and Kondo effects [12]. Moreover, in recent years signatures of unconventional superconducting (SC) state have been reported, first by Wang *et al*. for the case of the twisted WSe_2 bilayer ($tWSe_2$) [2]. It has been suggested that for this system two superconducting domes reside on both sides of a Mott insulating state, which is located at half-filling similarly to that in the well-known cuprates [13] or twisted bilayer graphene [14,15]. Interestingly, strong evidence of the paired state in $tWSe_2$ has been shown in very recent experimental papers, which, however, report one SC dome close to or at the half-filling for a certain range of displacement fields [16,17].

Depending on the twist angle (θ) between the two WSe_2 monoatomic layers, a moiré pattern emerges, which leads to the creation of a mini-Brillouin zone and, most importantly, to flat electronic bands [18]. This points to a significant role played by electron-electron interactions. It is believed that $tWSe_2$ is in the moderately correlated regime, with the on-site Coulomb integral being comparable to the flat band width ($U \approx W$) [2,19]. However, the actual strength of the electron-electron correlations is influenced by the twist angle and the dielectric environment of the sample. The experimental absence of the Mott insulating state at half-filling in Ref. [17] indicates that most probably a weak-to-moderate correlation regime ($U \lesssim W$) has been achieved in this particular study. Moreover, it has been established that the paired state emerges only in a relatively small range of displacement fields and band fillings, whose exact location depends on the twist angle.

The original experimental report as well as the most recent ones related with SC state in $tWSe_2$ has motivated theoretical analysis that considered effective single- and multiband models as well as different forms of pairing mechanisms [20–32]. Many of the those considerations lead to a mixed singlet and triplet symmetry of the order parameter, due to the presence of the Ising-type spin-orbit coupling in the system. Both the theoretical study and the experimental reports point to the role of the Van Hove singularity (VHS) in the stabilization of the paired state. However, the physical mechanism that determines the characteristic form of the phase diagram is still under ongoing debate and has not been completely resolved so far.

In our previous study, we have employed an effective single-band t-J-U model to the description of SC state of $tWSe_2$, which leads to the stability of a topological mixed $d + id$ and p-ip pairing scenario [23,33]. Within such a description, the single-particle physics is described by a tight binding Hamiltonian with complex hoppings that incorporate the spin-valley locking in the system. Here, we extend our previous considerations by supplementing the Hamiltonian with an *intersite Coulomb interaction term*. We focus on the effect of the displacement field in the formation of the paired

*Contact author: michal.zegrodnik@agh.edu.pl

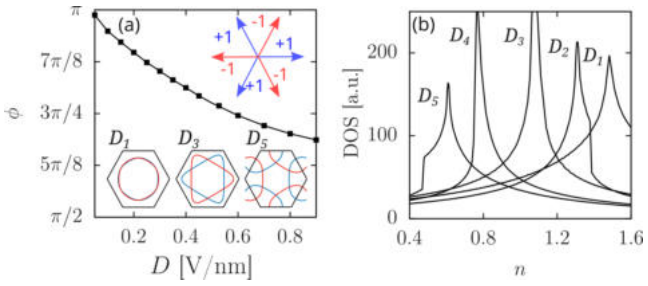

FIG. 1. (a) Phase factor ϕ as a function of displacement field, D, together with spin-up (blue) and spin-down (red) Femi surfaces at half-filling for selected values of D (inset). In the upper right corner, we provide the $\nu_{ij} = \pm 1$ factor corresponding to the six nearest neighbors [cf. Eq. (1)]. (b) Density of states at the Fermi level as a function of band filling for selected values of the displacement field $D_l \in \{0.05,\ 0.2,\ 0.3,\ 0.45,\ 0.6\}$ V/nm, for $l = 1, 2, 3, 4, 5$, respectively.

state in order to discuss the obtained results in the view of the most recent experimental findings. In particular, our main aim here is to reconstruct one of the principal features of the $tWSe_2$, namely, the appearance of an unconventional superconducting state in a relatively small range of displacement fields (D) and band fillings (n) [16,17]. In our study, we apply the Gutzwiller approximation based on which we analyze in detail the electron-correlation-induced renormalization of particular energy terms in the context of the SC state stabilization. As we show explicitly, in the regime of weak-to-moderate correlations, the renormalization effects create favorable conditions for the SC pairing in close proximity of the half-filled situation. This effect, together with the Van Hove singularity evolution induced by the displacement field, determines the stability regime of the SC state in the (n, D) phase diagram.

Model and method. We employ the moiré t-J-U model supplemented with the intersite Coulomb repulsion term, i.e.,

$$\begin{aligned}\hat{H} =& t \sum_{\langle ij\rangle\sigma} e^{i\sigma\nu_{ij}\phi}\, \hat{c}^{\dagger}_{i\sigma}\hat{c}_{j\sigma} \\ &+ J \sum_{\langle ij\rangle}{}' \left(\hat{S}^z_i \hat{S}^z_j + \frac{1}{2} e^{i2\nu_{ij}\phi} \hat{S}^+_i \hat{S}^-_j + \frac{1}{2} e^{-i2\nu_{ij}\phi} \hat{S}^-_i \hat{S}^+_j \right) \\ &+ U \sum_i \hat{n}_{i\uparrow}\hat{n}_{i\downarrow} + V \sum_{\langle ij\rangle}{}' \hat{n}_i \hat{n}_j, \end{aligned} \tag{1}$$

where $\sigma = \pm 1$ represents spin up/down, $\hat{c}^{\dagger}_{i\sigma}$ and $\hat{c}_{i\sigma}$ are the creation and annihilation operators for electron with spin σ at site i of a triangular lattice, $\langle i, j\rangle$ correspond to nearest neighbors, S^z_i, S^+_i, and S^-_i are the spin-$\frac{1}{2}$ z component and rising and lowering operators, respectively, $\hat{n}_{i\sigma}$ is the occupancy operator, and $\hat{n}_i = \sum_\sigma \hat{n}_{i\sigma}$. The primed summation means that each bond between the lattice sites appears only once. The subsequent terms of the above Hamiltonian correspond to electron hopping, intersite exchange interaction, and intra/intersite Coulomb repulsion. The phase factors of the exponents have an alternating sign introduced by $\nu_{ij} = \pm 1$, which depends on the bond direction (cf. inset of Fig. 1). The resultant spin- and direction-dependent complex hoppings account for the Ising-type spin-orbit coupling in the system. As shown in Refs. [2,19], the single-particle part constitutes an effective description of the flat moiré band of twisted WSe_2/WSe_2 homobilayer. It should be noted that in the experimental situation the $tWSe_2$ structure is usually placed in between two electrodes that allow to control both the electron concentration (n) and the displacement field (D) in an *in situ* manner. The effect of the latter tunes the spin-valley splitting and enters the effective model via a D-dependent t and ϕ, which have been calculated for the twist angle of $\theta = 5.08^\circ$ in Ref. [2] and are used by us here. For the sake of completeness in Fig. 1, we provide the D dependence of ϕ as well as Fermi surfaces and density of states as a function of band filling for selected values of displacement field.

Motivated by the experimental result provided in Ref. [17], we focus on the weak-to-moderate correlation regime ($U/W \lesssim 1$) by taking $U = 80$ meV, where the bandwidth is $W \approx 90$ meV. The value of the exchange interaction integral is set to $J = 4t^2/U$. We apply the Gutzwiller approximation method, which takes into account the electron-electron interactions above the level of a standard mean-field approach. At the same time, the considered method allows us to access the renormalization factors corresponding to subsequent energy terms appearing in our Hamiltonian and analyze them in the context of the SC state formation. The considered variational wave function of the Gutzwiller type has the following form $|\Psi_G\rangle = \hat{P}|\Psi_0\rangle$, where $|\Psi_0\rangle$ is the uncorrelated (mean-field) state and $\hat{P}$ denotes the correlation operator, i.e.,

$$\hat{P} = \prod_i \sum_\Gamma \lambda_{i,\Gamma} |\Gamma\rangle_{i\,i}\langle\Gamma|, \tag{2}$$

while $|\Gamma\rangle$ are states from the local basis $\{|\emptyset\rangle, |\uparrow\rangle, |\downarrow\rangle, |\uparrow\downarrow\rangle\}$ and $\lambda_{i,\Gamma}$ represent variational parameters determined via energy minimization. Since we consider a homogeneous system without magnetic or charge ordering, we take $\lambda_{i,\uparrow\downarrow} \equiv \lambda_{\uparrow\downarrow}$, $\lambda_{i,\uparrow} = \lambda_{i,\downarrow} \equiv \lambda_s$, and $\lambda_{i,\emptyset} \equiv \lambda_\emptyset$.

It is important to note that, when it comes to stabilization of the superconducting state, the exchange interaction term (J) and the intersite Coulomb interaction term (V) have positive and negative effects, respectively. Within the Gutzwiller approximation, the expectation values in the $|\Psi_G\rangle$ state of the two mentioned terms is the following:

$$\begin{aligned} E_J =& \lambda_s^4 J \sum_{\langle ij\rangle}{}' \left(\frac{1}{2} \sum_\sigma e^{i\sigma 2\phi_{ij}} \langle \hat{c}^{\dagger}_{i\sigma}\hat{c}_{i\bar{\sigma}}\hat{c}^{\dagger}_{j\bar{\sigma}}\hat{c}_{j\sigma}\rangle_0 \right. \\ &\left. + \frac{1}{4} \sum_{\sigma\sigma'} \sigma\sigma' \left(\langle \hat{n}_{i\sigma}\hat{n}_{j\sigma'}\rangle_0 - n_s^2 \right) \right), \\ E_V =& V \sum_{\langle ij\rangle}{}' \left(g_v^2 \langle \hat{n}_i \hat{n}_j\rangle_0 - \left(1 - g_v^2\right) n_s^2 \right), \end{aligned} \tag{3}$$

where $g_v = (1 - (2 - \lambda^2_{\uparrow\downarrow})n_s)/(1 - n_s)$, $n_{i\uparrow} = n_{i\downarrow} \equiv n_s$, $n_{i\sigma} = \langle \hat{n}_{i\sigma}\rangle_0$, and $\langle\hat{o}\rangle_0$ refers to an expectation value of operator $\hat{o}$ in the $|\Psi_0\rangle$ state. As one can see, the expectation value of a given energy term in the correlated state, $|\psi_G\rangle$, can be expressed in terms of the expectation values in the uncorrelated state, $|\psi_0\rangle$. However, factors λ_s^4 and g_v^2 renormalize the coupling constants J and V, respectively. Therefore, the

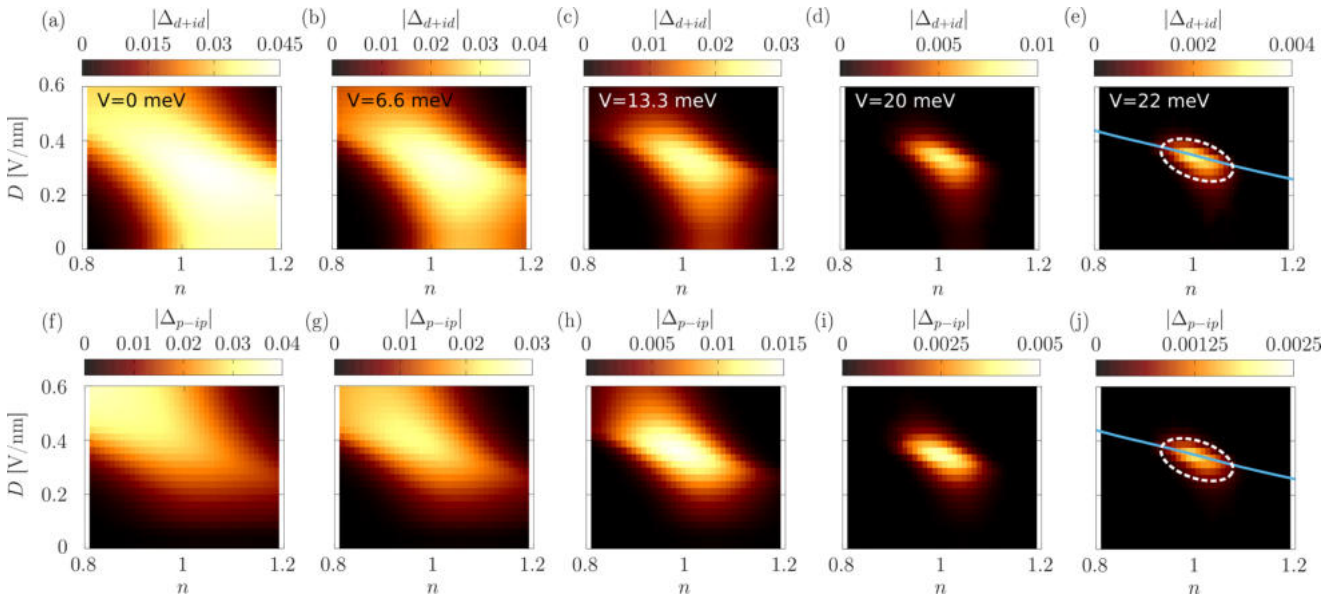

FIG. 2. Symmetry resolved superconducting gap amplitudes corresponding to the obtained mixed spin-singlet $d + id$ and spin-triplet $p - ip$ paired state as a function of band filling n and displacement field D for gradually increasing value of the intersite Coulomb repulsion V (a – j). The on-site Coulomb repulsion and the exchange interaction parameters are set to $U = 80$ meV and $J = 4t^2/U$, respectively. The solid blue line in panels (e) and (j) mark the evoulution of the Van Hove singularity across the phase diagram. The white dashed line is a guide to the eye denoting the stability range of the SC state.

relative balance between the two energy terms is going to be affected by the significant on-site Coulomb repulsion via the renormalization factors possibly having a decisive influence on the stabilization of the superconducting state.

To determine the values of the real-space superconducting gap amplitudes in the correlated state, $\Delta_{ij}^{\sigma\bar{\sigma}} = \langle \hat{c}_{i\sigma}^{\dagger} \hat{c}_{j\bar{\sigma}}^{\dagger} \rangle_G$, we apply the effective Hamiltonian scheme [34] and then extract the symmetry-resolved SC gaps [23], which allow us to analyze the principal features of the paired state. Also, following Bünemann *et al.*, we impose an additional condition to the correlation operator, which reduces the complexity of the numerical calculations [35]. More details related to the applied theoretical approach are provided in the Supplemental Material [36], which includes Refs. [37–50]. In the following, we refer to the average number of electrons per lattice site as band filling $n = 2n_s$.

Results. In order to discuss our theoretical approach in the context of the available experimental data, we calculate the symmetry-resolved SC amplitudes across the (n, D) diagram. In Fig. 2, we provide the results obtained for the gradually increasing value of the intersite Coulomb repulsion, V. Our calculations lead to the stabilization of a mixed $d + id$ (singlet) and p-ip (triplet) paired state. Singlet-triplet mixing has also been reported in other theoretical descriptions of $tWSe_2$ [21,22,25,30,32] and is a straightforward consequence of the spin-valley locking as we discuss in more detail in the Appendix and/or Supplemental Material [36]. As one can see, for the $V = 0$ case the SC state is relatively robust, with the spin-singlet pairing dominating the low displacement field regime and gradually increasing contribution resulting from the triplet component as D increases. Such robust SC state covering a significant area of the phase diagram is in contradiction with the experimental situation. However, as the value of V is increased, the stability area of the paired state shrinks. It should be noted that the negative effect of the V term on the pairing has been previously reported in other theoretical considerations [51–53]. For $V = 22$ meV, the SC phase covers only a small part of the (n, D) plane, which is located in the proximity of the half-filled situation, and for $D \approx 0.2$–0.4 V/nm. The SC phase shown in Figs. 2(e) and 2(j) is characterized by a Chern number $C = \pm 4$ indicating a topological character. The sign change of C appears exactly at the Van Hove singularity line, which is due to the transition from the electronlike to holelike Fermi surfaces. For more details related with the topological features, see the Appendix and/or Supplemental Material [36]. It should be noted that a similar form of the phase diagram has recently been reported experimentally for $tWSe_2$ in Ref. [17]. However, due to uncertainty in experimental determination of band filling, it is not completely clear whether the SC phase stability range has reached the half-filled situation. Another experimental report has shown the SC phase stability at half-filling but in very low displacement field range [16].

In order to analyze why the particular small area of the (n, D) plane seen in Figs. 2(e) and 2(j) creates favorable conditions for the SC state to be stable, we first study the evolution of Van Hove singularity across the phase diagram. The solid blue line marks the band fillings that for a given value of D correspond to the Van Hove singularity being located at the Fermi level. As one can see, the area covered by the SC state is located around the Van Hove singularity line. Such an effect is expected since high values of the density of states at the Fermi energy stabilize superconductivity in the weak-coupling theory. The second effect that is of significant importance here originates from the electron-electron correlations. In Fig. 3, we provide the (n, D) dependence of the g_v^2 and λ_s^4 factors,

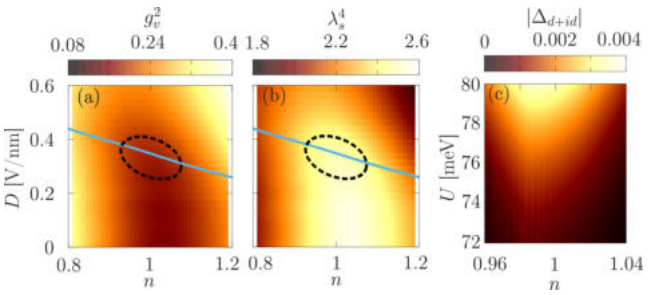

FIG. 3. The g_v^2 [panel (a)] and λ_s^4 [panel (b)] factors that renormalize the intersite Coulomb interaction term and the exchange interaction term [cf. Eq. (3)], respectively, as a function of n and D. The blue line marks the Van Hove singularity evolution across the phase diagram. The black dashed line corresponds to the stability of the SC state as in Figs. 2(e) and 2(j). Note that SC phase is located at the crossing of the Van Hove singularity line and the area where the renormalization is the strongest. (c) The SC gap as a function of U and n for $D = 0.35$ V/nm with $J = 4t^2/U$, $V = U/3.635$. We provide only the singlet component since the triplet one shows the same behavior but is approximately twice smaller.

which renormalize the intersite Coulomb interaction term and the exchange interaction term, respectively [cf. Eq. (3)]. For $g_v^2 = \lambda_s^4 \equiv 1$, our variational Gutzwiller state would become equivalent to the Hartree-Fock solution ($|\psi_0\rangle = |\psi_G\rangle$), which is not the case here. More importantly, the region of maximized renormalization is located roughly around half-filling where g_v^2 is small, significantly diminishing the destructive character of the V term on the paired phase. Moreover, λ_s^4 is relatively large in the same region, which enhances the positive effect of the J term on the pairing. At the same time, since we are dealing with the weak-to-moderate correlation regime, there is no Mott insulating state located at half-filling that would suppress the SC state there. As a result, the stability of the SC state lies exactly at the crossing of the Van Hove singularity line and the maximized renormalization area at half-filling. This allows for the two positive effects to act simultaneously, which as a result create favorable conditions for the paired phase only in a particular region of the (n, D) plane. Additionally, in Fig. 3(c) we show that the SC phase vanishes while the electron-electron correlations are weakened.

For comparison, in Fig. 4 we provide the results for both weak-to-moderate and strong correlations. Namely, panels (a)

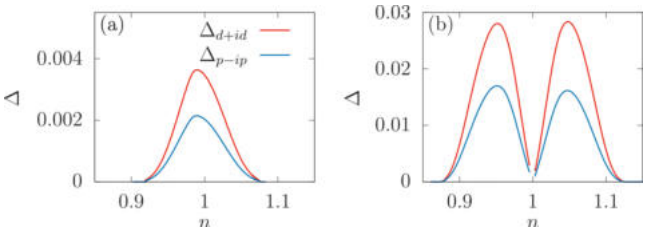

FIG. 4. Symmetry-resolved gap amplitudes of the mixed singlet-triplet solution as a function of n for $D = 0.35$ V/nm and for two selected values of the on-site Coulomb repulsion, $U = 80$ meV [panel (a)] and $U = 120$ meV [panel (b)]. In both cases, we keep $J = 4t^2/U$ and $V = U/3.635$.

and (b) correspond to $U = 80$ meV and $U = 120$ meV, respectively, while the bandwidth is $W \approx 90$ meV. In the second situation, instead of having a single SC dome, we actually obtain two of them with the SC gap reaching values one order of magnitude larger than those in the first case. This is due to the fact that for $U \gtrsim W$ strong electron-electron correlations enhance the positive effect of the renormalization parameters g_v^2 and λ_s^4 on the pairing. However, due to the fact that U is already larger than W in panel (b), a Mott insulating state starts to develop at half-filling, which suppresses the SC amplitudes there, leading to a two-dome behavior.

It should be noted that recent measurements carried out for $\theta = 5.0^\circ$ and $\theta \approx 3.5^\circ$ twisted WSe_2 show a single SC dome not separated by a Mott state in a certain D range [16,17]. However, the original experimental report referring to the same system with a twist angle $\theta = 5.1^\circ$ shows signatures of two SC domes and a Mott insulator at half-filling [2]. It might be possible that depending on the dielectric environment and the actual twist angle the two regimes ($U \lesssim W$ and $U \gtrsim W$) can be reached in $tWSe_2$ leading to two different forms of the phase diagram. It should be noted that our results lead to a significantly larger maximal SC gap in the two-dome case, which would agree with the experimental situation where $T_C \approx 200$–300 mK and $T_C \approx 1$ K correspond to single-dome and two-dome behaviors, respectively [2,16,17]. During the resubmission process of this Letter, an experimental report has appeared [54] showing the stability of the SC phase close to the crossing between the Van Hove singularity and the half-filling, which is consistent with our approach. However, above a certain value of D, an antiferromagnetic Mott insulator begins to develop at $n = 1$.

Our Gutzwiller approach is limited to the ground state only. Therefore, we are not able to reach nonzero temperatures. Nevertheless, in order to provide a rough estimate of the maximal critical temperature in the two considered situations, we use the formulas $\Delta(T = 0) = 1.764\, k_B T_C$ and $\Delta(T = 0) = J\Delta_{\max}$, with $\Delta_{\max}$ being the maximal SC gap amplitude value obtained in our calculations. Such an estimate gives us $T_C \approx 100$ mK and $T_C \approx 450$ mK for the $U = 80$ meV (a) and $U = 120$ meV (b), respectively. The obtained values underestimate the experimentally obtained critical temperatures; however, they are of the same order.

Final remarks. We have analyzed the principal features of the unconventional superconducting state in $tWSe_2$ within an effective t-J-U model supplemented with the intersite Coulomb repulsion term. As we show, for the weak-to-moderate correlation regime the topological mixed singlet-triplet superconducting state covers a relatively small area of the (n, D) phase diagram, which is located where the Van Hove singularity line crosses half-filling. We show that this precise region optimizes the conditions for superconductivity: The VHS causes a large density of states, whereas the electron-correlation-induced renormalization is maximized at half-filling. This allows the two effects to act simultaneously, creating favorable conditions for the paired state as seen in experiments [16,17,54]. To explore the unconventional nature of the SC state experimentally, we propose using Knight shift measurements to identify any nonsinglet pairing. Observing the Kerr effect could indicate spontaneous breaking of time-reversal symmetry. Finally, our prediction of topolog-

ical superconductivity in $tWSe_2$ highlights it as a promising platform for detecting chiral edge states through scanning techniques or transport measurements [55].

Additionally, we show that a single SC dome and two SC domes can be reproduced within a single theoretical framework. The former corresponds to weaker correlations and the latter to stronger correlations. The two-dome scenario comes as a result of the fact that the Mott insulating state located at half-filling separates the SC stability range into two. Nevertheless, the maximal values of the gap amplitudes are larger for the stronger correlations and the two-dome scenario. This is in qualitative agreement with the available experimental data [2,16,17].

For the flat band of cuprate superconductors, it has been shown that the t-J-U and Hubbard models lead to a roughly similar physical picture of the superconducting phase [56]. However, since the J term does not appear explicitly in the latter, either a higher order diagrammatic expansion of the Gutzwiller wave function or a density martix renormalization group (DMRG) method would be necessary to obtain the stability of the paired phase. As we have shown very recently, the DMRG approach can indeed lead to the presence of the SC phase in the effective single-band model of $tWSe_2$ [57].

Acknowledgments. This research was funded by National Science Centre, Poland (NCN) according to decision 2021/42/E/ST3/00128. We gratefully acknowledge Polish high-performance computing infrastructure PLGrid (HPC Center: ACK Cyfronet AGH) for providing computer facilities and support within computational Grant No. PLG/2024/017372. L.R. was funded by the Swiss National Science Foundation through Starting Grant No. TMSGI2_-211296.

Data availability. The code that was written to perform the numerical calculations and the data behind the figures are available in the open repository [58].

Appendix. Here, we provide a detailed extension related to the method of determination of the superconducting gap symmetry, the influence of the spin-valley locking, and the topological features of the superconducting state.

Symmetry of the paired state. Within the presented Gutzwiller wave function approach, the unprojected wave function, $|\Psi_0\rangle$, contains the superconducting order parameter, $S_{ij}^{\sigma\sigma'} = \langle \hat{c}_{i\sigma}\hat{c}_{j\sigma'}\rangle_0$, which is related to the correlated wave function counterpart $\Delta_{ij}^{\sigma\sigma'} = \langle \hat{c}_{i\sigma}\hat{c}_{j\sigma'}\rangle_G = q^2 S_{ij}^{\sigma\sigma'}$, where $q = \lambda_s(\lambda_d n_s + \lambda_\emptyset(1-n_s))$. In our numerical scheme, we do not limit ourselves to one specific symmetry of the SC gap. Instead, we consider all possible pairing symmetries that are allowed for the case of a triangular lattice within the nearest-neighbor real-space pairing scenario. This requires solving the set of self-consistent equations for all the six complex nearest-neighbor gap amplitudes without any additional constraints. We allow for spin-singlet pairing ($S_{ij}^{\uparrow\downarrow} = -S_{ij}^{\downarrow\uparrow}$), spin-triplet pairing ($S_{ij}^{\uparrow\downarrow} = S_{ij}^{\downarrow\uparrow}$), and their mixture ($|S_{ij}^{\uparrow\downarrow}| \neq |S_{ij}^{\downarrow\uparrow}|$). We neglect the possibility of triplet $S^z = \pm 1$ pairing, as these pairing channels lead to a Fermi wave vector mismatch, which significantly suppresses superconductivity.

After we determine the gap amplitudes $\Delta_{ij}^{\bar{\sigma}\sigma}$ to all nearest neighbors, we transform them into the so-called symmetry-resolved gap amplitudes, given by

$$\Delta_{M,p}^{\sigma\bar{\sigma}} = \frac{i^p}{6}\sum_{i(j)} e^{-iM\theta_{ji}}\Delta_{ji}^{\sigma\bar{\sigma}}, \tag{A1}$$

where the summation runs over the nearest-neighbor lattice sites j surrounding site i, and θ_{ji} are angles $\{0,\ \pi/3,\ 2\pi/3,\ \pi,\ 4\pi/3,\ 5\pi/3\}$ between the positive half-x axis and the $\mathbf{R}_{ji} = \mathbf{R}_j - \mathbf{R}_i$ vector. M and p correspond to particular symmetries and are provided in Table I.

TABLE I. Symmetries of the SC gap together with their parities and Cooper pair spin state. The symmetry factor, M, and the parity factor p are provided in the first and the second column, respectively [cf. Eq. (A1)].

M	p	Gap symmetry	Parity	Spin state
0	0	Extended s	Even	Singlet
1	1	$p_x + i\,p_y$	Odd	Triplet
2	0	$d_{x^2-y^2} + i\,d_{xy}$	Even	Singlet
3	1	f	Odd	Triplet
4	0	$d_{x^2-y^2} - i\,d_{xy}$	Even	Singlet
5	1	$p_x - i\,p_y$	Odd	Triplet

Finally, we can write down the expressions for the real-space singlet and triplet gap amplitudes in the correlated state:

$$\begin{aligned}\Delta_{M,p}^{s} &= (\Delta_{M,p}^{\uparrow\downarrow} - \Delta_{M,p}^{\downarrow\uparrow})/\sqrt{2},\\ \Delta_{M,p}^{t} &= (\Delta_{M,p}^{\uparrow\downarrow} + \Delta_{M,p}^{\downarrow\uparrow})/\sqrt{2}.\end{aligned} \tag{A2}$$

For the sake of clarity, in the main text of the Letter, we use the symmetry names ($p \pm ip$, $d \pm id$, f, etc.) instead of the values of the M and p factors.

In Fig. 5, we show the $\mathbf{k}$ dependence of the SC gap corresponding to the symmetries listed in Table I. As one can see, all the symmetries fulfill the C_6 symmetry of the underlaying trianlular lattice. However, due to the presence of spin-valley locking, the Hamiltonian breaks the C_6 symmetry, which has further consequences for the pairing symmetry, as we show in the next section.

Influence of spin-valley locking on the pairing. The presence of spin-valley locking leads to two spin-split Fermi surfaces and a reduction of the symmetry from C_6 to C_3. According to our calculations, for this case, a stable SC solution corresponds to a mixed $d + id$ and $p - ip$ symmetry of the gap in the relevant range of model parameters. As one can see in Fig. 6, this particular composition of the symmetry components leads to a situation in which the SC gap fulfills the C_3 symmetry of the Hamiltonian. Moreover, there are two different SC gap distributions realized in $\mathbf{k}$ space. This allows for the SC gap to adjust to the shape of the two separate Fermi surfaces resulting from the spin-valley locking. Therefore, the mixed symmetry of the gap is a straightforward result of the spin-valley locking, which leads to reduction of the systems' symmetry and to two separate Fermi surfaces.

*Details of the topological paired state.*According to our calculations in the range of parameters corresponding to Figs. 2(e) and 2(j), the superconducting state is nontrivial topologically with the Chern number $C = \pm 4$. For clarity, we revisit here the mentioned diagram in Fig. 7. As one can see,

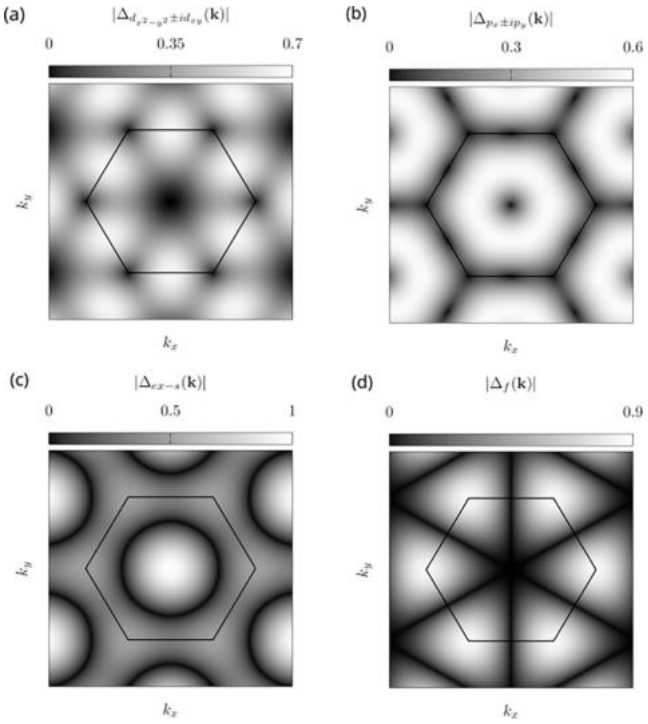

FIG. 5. The absolute value of the **k**-dependent SC gaps for the pairing channels listed in Table I. The Brillouin zone is marked by black solid line. The presented distributions have been obtained by setting particular symmetry-resolved factors to 1 and all the others to 0.

the sign change of C appears at the line representing the Van Hove singularity.

In Fig. 8, we provide the corresponding **k**-dependent SC gap as well as the normal state Fermi surfaces for two representative sets of parameters, which are marked by green dots in Fig. 7. As one can see, the obtained value of the Chern number can be understood as a total topological charge contained inside the spin-up and spin-down Fermi surfaces.

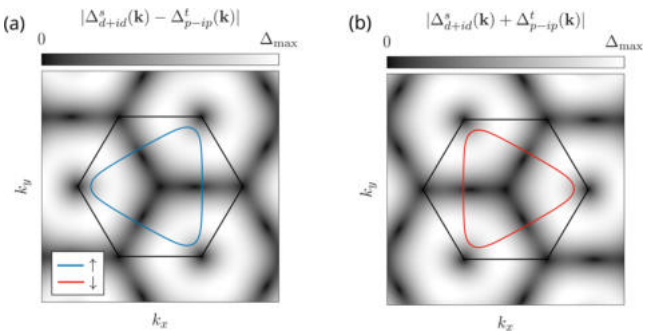

FIG. 6. The absolute value of the **k**-dependent SC gaps corresponding to mixed $d + id/p - ip$ symmetry obtained for $n = 1, U = 80\,\text{meV}$, $J = 4t^2/U$, and $D = 0.3\,\text{V/nm}$. The normal state Fermi surfaces are marked by solid blue and red lines in panels (a) and (b), respectively.

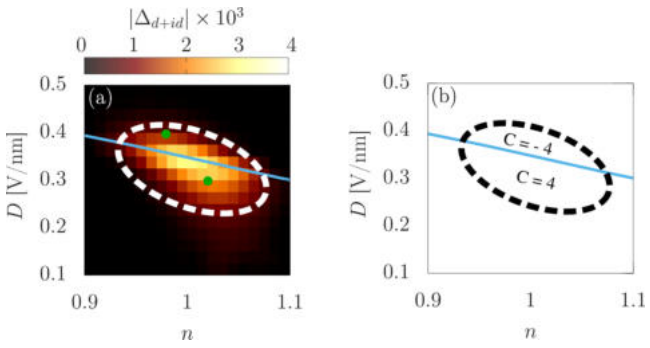

FIG. 7. (a) The SC gap amplitude as a function of band filling and displacement field for the same model parameters as in Fig. 2(e). The two green points correspond to the two representative n and D values leading to $C = \pm 4$ and selected for the detailed analysis provided in Fig. 8. (b) The phase diagram that shows the calculated values of the Chern number of the SC state.

Namely,

$$C = \sum_{i \in \Omega_{\text{FS}}} (-1)^w C_i, \tag{A3}$$

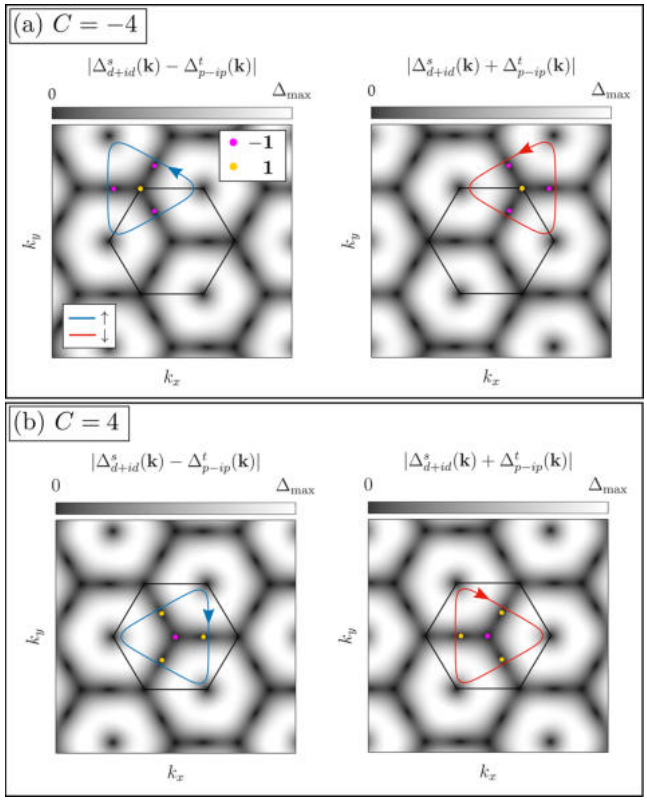

FIG. 8. The normal-state Fermi surfaces for spin-up and spin-down (blue and red solid lines) electrons as well as the **k**-dependent SC gaps for the two points marked by green dots in Fig. 7, which correspond to Chern number: $C = -4$ [panel (a)] and $C = 4$ [panel (b)]. The arrows at the Fermi surfaces represent the winding direction, which is counterclockwise (clockwise) for the electronlike (holelike) Fermi surfaces.

where C_i is the topological charge of a given nodal point, which can be determined by calculating the winding number of the order parameter around it. The sign of the Chern charge depends on whether it is enclosed by an electron- ($w = 0$) or holelike ($w = 1$) Fermi surface. The i index runs only over the nodal points that are contained inside the Fermi surface.

[1] A. Ghiotto, E.-M. Shih, G. S. S. G. Pereira, D. A. Rhodes, B. Kim, J. Zang, A. J. Millis, K. Watanabe, T. Taniguchi, J. C. Hone, L. Wang, C. R. Dean, and A. N. Pasupathy, Quantum criticality in twisted transition metal dichalcogenides, Nature (London) **597**, 345 (2021).

[2] L. Wang, E.-M. Shih, A. Ghiotto, L. Xian, D. A. Rhodes, C. Tan, M. Claassen, D. M. Kennes, Y. Bai, B. Kim, K. Watanabe, T. Taniguchi, X. Zhu, J. Hone, A. Rubio, A. N. Pasupathy, and C. R. Dean, Correlated electronic phases in twisted bilayer transition metal dichalcogenides, Nat. Mater. **19**, 861 (2020).

[3] E. Anderson, F.-R. Fan, J. Cai, W. Holtzmann, T. Taniguchi, K. Watanabe, D. Xiao, W. Yao, and X. Xu, Programming correlated magnetic states with gate-controlled moiré geometry, Science **381**, 325 (2023).

[4] Z. Tao, B. Shen, S. Jiang, T. Li, L. Li, L. Ma, W. Zhao, J. Hu, K. Pistunova, K. Watanabe, T. Taniguchi, T. F. Heinz, K. F. Mak, and J. Shan, Valley-coherent quantum anomalous Hall state in AB-stacked $MoTe_2/WSe_2$ bilayers, Phys. Rev. X **14**, 011004 (2024).

[5] E. C. Regan, D. Wang, C. Jin, M. I. Bakti Utama, B. Gao, X. Wei, S. Zhao, W. Zhao, Z. Zhang, K. Yumigeta, M. Blei, J. D. Carlström, K. Watanabe, T. Taniguchi, S. Tongay, M. Crommie, A. Zettl, and F. Wang, Mott and generalized Wigner crystal states in WSe_2/WS_2 moiré superlattices, Nature (London) **579**, 359 (2020).

[6] Y. Xu, S. Liu, D. A. Rhodes, K. Watanabe, T. Taniguchi, J. Hone, V. Elser, K. F. Mak, and J. Shan, Correlated insulating states at fractional fillings of moiré superlattices, Nature (London) **587**, 214 (2020).

[7] X. Huang, T. Wang, S. Miao, C. Wang, Z. Li, Z. Lian, T. Taniguchi, K. Watanabe, S. Okamoto, D. Xiao, S.-F. Shi, and Y.-T. Cui, Correlated insulating states at fractional fillings of the WS_2/WSe_2 moiré lattice, Nat. Phys. **17**, 715 (2021).

[8] H. Li, S. Li, E. C. Regan, D. Wang, W. Zhao, S. Kahn, K. Yumigeta, M. Blei, T. Taniguchi, K. Watanabe, S. Tongay, A. Zettl, M. F. Crommie, and F. Wang, Imaging two-dimensional generalized Wigner crystals, Nature (London) **597**, 650 (2021).

[9] H. Zhou, K. Liang, L. Bi, Y. Shi, Z. Wang, and S. Li, Spotlight: Visualization of moiré quantum phenomena in transition metal dichalcogenide with scanning tunneling microscopy, ACS Appl. Electron. Mater. **6**, 1530 (2024).

[10] T. Li, S. Jiang, B. Shen, Y. Zhang, L. Li, Z. Tao, T. Devakul, K. Watanabe, T. Taniguchi, L. Fu, J. Shan, and K. F. Mak, Quantum anomalous Hall effect from intertwined moiré bands, Nature (London) **600**, 641 (2021).

[11] Z. Tao, B. Shen, W. Zhao, N. C. Hu, T. Li, S. Jiang, L. Li, K. Watanabe, T. Taniguchi, A. H. MacDonald, J. Shan, and K. F. Mak, Giant spin Hall effect in AB-stacked $MoTe_2/WSe_2$ bilayers, Nat. Nanotechnol. **19**, 28 (2024).

[12] W. Zhao, B. Shen, Z. Tao, Z. Han, K. Kang, K. Watanabe, T. Taniguchi, K. F. Mak, and J. Shan, Gate-tunable heavy fermions in a moiré Kondo lattice, Nature **616**, 61 (2023).

[13] J. Spałek, M. Fidrysiak, M. Zegrodnik, and A. Biborski, Superconductivity in high-T_c and related strongly correlated systems from variational perspective: Beyond mean field theory, Phys. Rep. **959**, 1 (2022).

[14] Y. Cao, V. Fatemi, A. Demir, S. Fang, S. L. Tomarken, J. Y. Luo, J. D. Sanchez-Yamagishi, K. Watanabe, T. Taniguchi, E. Kaxiras, R. C. Ashoori, and P. Jarillo-Herrero, Correlated insulator behaviour at half-filling in magic-angle graphene superlattices, Nature (London) **556**, 80 (2018).

[15] Y. Cao, V. Fatemi, S. Fang, K. Watanabe, T. Taniguchi, E. Kaxiras, and P. Jarillo-Herrero, Unconventional superconductivity in magic-angle graphene superlattices, Nature (London) **556**, 43 (2018).

[16] Y. Xia, Z. Han, K. Watanabe, T. Taniguchi, J. Shan, and K. F. Mak, Superconductivity in twisted bilayer WSe_2, Nature (London) **637**, 833 (2025).

[17] Y. Guo, J. Pack, J. Swann, L. Holtzman, M. Cothrine, K. Watanabe, T. Taniguchi, D. G. Mandrus, K. Barmak, J. Hone, A. J. Millis, A. Pasupathy, and C. R. Dean, Superconductivity in 5.0° twisted bilayer WSe_2, Nature (London) **637**, 839 (2025).

[18] M. Brzezińska, S. Grytsiuk, M. Rösner, M. Gibertini, and L. Rademaker, Pressure-tuned many-body phases through Γ-k valleytronics in moiré bilayer WSe_2, 2D Mater. **12**, 015003 (2025).

[19] H. Pan, F. Wu, and S. Das Sarma, Band topology, Hubbard model, Heisenberg model, and Dzyaloshinskii-Moriya interaction in twisted bilayer WSe_2, Phys. Rev. Res. **2**, 033087 (2020).

[20] M. Bélanger, J. Fournier, and D. Sénéchal, Superconductivity in the twisted bilayer transition metal dichalcogenide WSe_2: A quantum cluster study, Phys. Rev. B **106**, 235135 (2022).

[21] L. Klebl, A. Fischer, L. Classen, M. M. Scherer, and D. M. Kennes, Competition of density waves and superconductivity in twisted tungsten diselenide, Phys. Rev. Res. **5**, L012034 (2023).

[22] F. Chen and D. Sheng, Singlet, triplet and pair density wave superconductivity in the doped triangular-lattice moiré system, Phys. Rev. B **108**, L201110 (2023).

[23] M. Zegrodnik and A. Biborski, Mixed singlet-triplet superconducting state within the moiré t–J–U model applied to twisted bilayer WSe_2, Phys. Rev. B **108**, 064506 (2023).

[24] Y.-M. Wu, Z. Wu, and H. Yao, Pair-density-wave and chiral superconductivity in twisted bilayer transition metal dichalcogenides, Phys. Rev. Lett. **130**, 126001 (2023).

[25] C. Schrade and L. Fu, Nematic, chiral, and topological superconductivity in twisted transition metal dichalcogenides, Phys. Rev. B **110**, 035143 (2024).

[26] V. Crépel, D. Guerci, J. Cano, J. H. Pixley, and A. Millis, Topological superconductivity in doped magnetic moiré semiconductors, Phys. Rev. Lett. **131**, 056001 (2023).

[27] F. Xie, L. Chen, S. Sur, Y. Fang, J. Cano, and Q. Si, Superconductivity in twisted WSe_2 from topology-induced quantum fluctuations, Phys. Rev. Lett. **134**, 136503 (2025).

[28] W. Qin, W.-X. Qiu, and F. Wu, Kohn-Luttinger mechanism of superconductivity in twisted bilayer WSe_2: Gate-tunable unconventional pairing symmetry Phys. Rev. Lett. **135**, 246002 (2025).

[29] C. Tuo, M.-R. Li, Z. Wu, W. Sun, and H. Yao, Theory of topological superconductivity and antiferromagnetic correlated

insulators in twisted bilayer WSe_2 Nat. Commun. **16**, 9525 (2025).
[30] D. Guerci, D. Kaplan, J. Ingham, J. H. Pixley, and A. J. Millis, Topological superconductivity from repulsive interactions in twisted WSe_2, arXiv:2408.16075 [cond-mat.supr-con].
[31] J. Zhu, Y.-Z. Chou, M. Xie, and S. Das Sarma, Superconductivity in twisted transition metal dichalcogenide homobilayers, Phys. Rev. B **111**, L060501 (2025).
[32] A. Fischer, L. Klebl, V. Crépel, S. Ryee, A. Rubio, L. Xian, T. O. Wehling, A. Georges, D. M. Kennes, and A. J. Millis, Theory of intervalley-coherent AFM order and topological superconductivity in $tWSe_2$ Phys. Rev. X **15**, 041055 (2025).
[33] W. Akbar, A. Biborski, L. Rademaker, and M. Zegrodnik, Topological superconductivity with mixed singlet-triplet pairing in moiré transition metal dichalcogenide bilayers, Phys. Rev. B **110**, 064516 (2024).
[34] J. Kaczmarczyk, Comparison of two approaches for the treatment of Gutzwiller variational wave functions, Philos. Mag. **95**, 563 (2015),.
[35] J. Bünemann, T. Schickling, and F. Gebhard, Variational study of Fermi surface deformations in Hubbard models, Europhys. Lett. **98**, 27006 (2012).
[36] See Supplemental Material at https://link.aps.org/supplemental/10.1103/pkf3-fkv4 for more details related to the model, method, considered pairing symmetries, and topological features of the obtained superconducting state.
[37] D. Xiao, G.-B. Liu, W. Feng, X. Xu, and W. Yao, Coupled spin and valley physics in monolayers of MoS_2 and other group-VI dichalcogenides, Phys. Rev. Lett. **108**, 196802 (2012).
[38] Y. Zhang, L. Li, J.-H. Sun, D.-H. Xu, R. Lü, H.-G. Luo, and W.-Q. Chen, Kondo effect in monolayer transition metal dichalcogenide Ising superconductors, Phys. Rev. B **101**, 035124 (2020).
[39] Y.-T. Hsu, F. Wu, and S. Das Sarma, Spin-valley locked instabilities in moiré transition metal dichalcogenides with conventional and higher-order Van Hove singularities, Phys. Rev. B **104**, 195134 (2021).
[40] J. Zang, J. Wang, J. Cano, and A. J. Millis, Hartree-Fock study of the moiré Hubbard model for twisted bilayer transition metal dichalcogenides, Phys. Rev. B **104**, 075150 (2021).
[41] F. Wu, T. Lovorn, E. Tutuc, and A. H. MacDonald, Hubbard model physics in transition metal dichalcogenide moiré bands, Phys. Rev. Lett. **121**, 026402 (2018).
[42] Y. Huang and D. N. Sheng, Topological chiral and nematic superconductivity by doping Mott insulators on triangular lattice, Phys. Rev. X **12**, 031009 (2022).
[43] S. Daul, D. J. Scalapino, and S. R. White, Pairing correlations on t–U–J ladders, Phys. Rev. Lett. **84**, 4188 (2000).
[44] S. Basu, R. J. Gooding, and P. W. Leung, Enhanced bound-state formation in two dimensions via stripelike hopping anisotropies, Phys. Rev. B **63**, 100506 (2001).
[45] E. Plekhanov, S. Sorella, and M. Fabrizio, Increasing d-wave superconductivity by on-site repulsion, Phys. Rev. Lett. **90**, 187004 (2003).
[46] T. Xiang, H. G. Luo, D. H. Lu, K. M. Shen, and Z. X. Shen, Intrinsic electron and hole bands in electron-doped cuprate superconductors, Phys. Rev. B **79**, 014524 (2009).
[47] M. Abram, J. Kaczmarczyk, J. Jędrak, and J. Spałek, d-wave superconductivity and its coexistence with antiferromagnetism in the t–j–u model: Statistically consistent Gutzwiller approach, Phys. Rev. B **88**, 094502 (2013).
[48] R. B. Laughlin, Gossamer superconductivity, arXiv:cond-mat/0209269 [cond-mat.supr-con].
[49] F. C. Zhang, Gossamer superconductor, Mott insulator, and resonating valence bond state in correlated electron systems, Phys. Rev. Lett. **90**, 207002 (2003).
[50] T. Fukui, Y. Hatsugai, and H. Suzuki, Chern numbers in discretized Brillouin zone: Efficient method of computing (spin) Hall conductances, J. Phys. Soc. Jpn. **74**, 1674 (2005).
[51] S. Raghu, E. Berg, A. V. Chubukov, and S. A. Kivelson, Effects of longer-range interactions on unconventional superconductivity, Phys. Rev. B **85**, 024516 (2012).
[52] S. Raghu, R. Thomale, and T. H. Geballe, Optimal T_c of cuprates: The role of screening and reservoir layers, Phys. Rev. B **86**, 094506 (2012).
[53] R. Nandkishore, R. Thomale, and A. V. Chubukov, Superconductivity from weak repulsion in hexagonal lattice systems, Phys. Rev. B **89**, 144501 (2014).
[54] Y. Xia, Z. Han, J. Zhu, Y. Zhang, P. Knüppel, K. Watanabe, T. Taniguchi, K. F. Mak, and J. Shan, Bandwidth-tuned Mott transition and superconductivity in moiré WSe_2, Nature **650**, 585 (2026).
[55] X.-L. Qi and S.-C. Zhang, Topological insulators and superconductors, Rev. Mod. Phys. **83**, 1057 (2011).
[56] J. Spałek, M. Zegrodnik, and J. Kaczmarczyk, Universal properties of high-temperature superconductors from real-space pairing: t–J–U model and its quantitative comparison with experiment, Phys. Rev. B **95**, 024506 (2017).
[57] A. Biborski and M. Zegrodnik, Signatures of superconducting pairing driven by electron-electron interactions in moiré WSe_2/WSe_2 homobilayer modeled by Hubbard Hamiltonian, Phys. Rev. B **112**, L161122 (2025).
[58] M. Zegrodnik, Effect of displacement field on unconventional superconductivity in twisted bilayer WSe_2 [dataset], Zenodo (2025), https://doi.org/10.5281/zenodo.15575293.

Supplemental Materials for Optimal superconductivity in twisted bilayer WSe_2 where the Van Hove singularity crosses half-filling

Michał Zegrodnik,* Waseem Akbar, and Andrzej Biborski

Academic Centre for Materials and Nanotechnology,

AGH University of Krakow, Al. Mickiewicza 30, 30-059 Krakow, Poland

Louk Rademaker

Department of Theoretical Physics, University of Geneva, CH-1211 Geneva, Switzerland and

Institute-Lorentz for Theoretical Physics, Leiden University,

PO Box 9506, Leiden, NL-2300, The Netherlands

I. GENERAL FEATURES OF THE MODEL

Here we provide details related with the applied theoretical approach based on the moiré t-J-U model supplemented with the intersite Coulomb repulsion term. As a reminder below we show the complete form of the Hamiltonian from the main text of our analysis

$$\begin{aligned}\hat{H} = & t \sum_{\langle ij \rangle \sigma} e^{i\sigma\nu_{ij}\phi}\, \hat{c}^{\dagger}_{i\sigma}\hat{c}_{j\sigma} \\ & + J \sum_{\langle ij \rangle}{}' \left(\hat{S}^z_i \hat{S}^z_j + \frac{1}{2} e^{i2\nu_{ij}\phi} \hat{S}^+_i \hat{S}^-_j + \frac{1}{2} e^{-i2\nu_{ij}\phi} \hat{S}^-_i \hat{S}^+_j \right) \\ & + U \sum_i \hat{n}_{i\uparrow}\hat{n}_{j\downarrow} + V \sum_{\langle ij \rangle}{}' \hat{n}_i \hat{n}_j,\end{aligned} \tag{S1}$$

where $\sigma = \pm 1$ represents spin up/down, $\hat{c}^{\dagger}_{i\sigma}$ and $\hat{c}_{i\sigma}$ are the creation and anihilation operators for electron with spin σ at site i of a triangular lattice, $\langle i, j \rangle$ correspond to nearest neighbors, S^z_i, S^+_i, S^-_i are the spin-$\frac{1}{2}$ z component, rising and lowering operators, respectively, $\hat{n}_{i\sigma}$ is the occupancy operator and $\hat{n}_i = \sum_\sigma \hat{n}_{i\sigma}$. The primed summation means that each bond between the lattice sites appears only once. The subsequent terms of the above Hamiltonian correspond to electron hopping, intersite exchange interaction, as well as intra-/inter-site Coulomb repulsion. The phase factors of the exponents have an alternating sign introduced by $\nu_{ij} = \pm 1$, which depends on the bond direction (cf. Fig. S1).

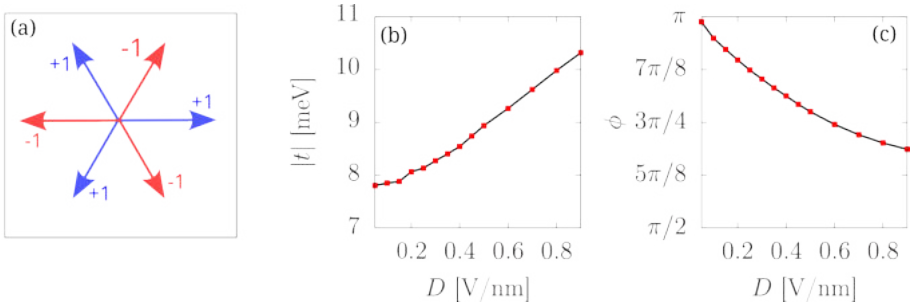

FIG. S1. (a) Values of the direction dependent factor (ν_{ij}) appearing in the hoppings of the effective single-band model. (b) Absolute value of the hoppings as a function of the displacement field. (c) Phase factor ϕ as a function of displacement field, D. The data visualized by Figs. (b) and (c) have been calculated in Ref. [1] for the twist angle of $\theta = 5.08°$ and are used in our analysis.

* michal.zegrodnik@agh.edu.pl

It should be noted that, due to inversion symmetry breaking in transition-metal dichalcogenide quasi-two-dimentional systems, there is a significant valley-dependent spin-orbit coupling, which acts like an effective Zeeman field with opposite out-of-plane directions. Such Ising-type spin-orbit coupling results in spin-momentum locking perpendicular to the two-dimensional crystal near the K and K' valleys (so-called spin-valley locking) [2, 3]. The effect also appears in twisted TMD-based structures and can be tuned by experimentally controllable factors such as the displacement field (D), which is the bias voltage across the layered structure [4, 5]. This is one of the characteristic features which distinguishes the TMD-based moiré systems from those graphene-based.

Here we follow Refs. 1 and 4 where it has been shown that the effect of the Ising type spin-orbit coupling can be taken into account in an effective single-band picture of twisted WSe_2 bilayer by spin- and direction-dependent complex hoppings. As one can see, from Eq. (S1) and Fig. S1(a) the complex phase of the hoppings has opposite signs corresponding to the opposite hopping direction and opposite spin orientation. In principle, this leads to two separate Fermi surfaces corresponding to two values of the spin-valley degree of freedom, $\tau = 1$ for $(K, \uparrow)$ and $\tau = -1$ for $(K', \downarrow)$. As a result of the Ising-type spin orbit coupling the symmetry of the system is reduced from C_6 to C_3. In such a picture, the effect of the displacement field is taken into account via the absolute value of the hoppings (t) and the phase factor (ϕ), which are D-dependent [cf. Fig. S1 (b) and (c)]. As presented in Fig. S2 by increasing the displacement field one enhances the Fermi surface spin splitting as well as changes the position of the Van Hove singularity from higher to lower band fillings. The D-dependant phase factor ϕ plays the major role in this effect. For very low displacement fields where $\phi \approx \pi$ the hopping parameters are nearly real numbers, meaning that the difference between the spin-up and spin-down Fermi surfaces should be minor, as seen in (f). In such a situation, the spin splitting is almost vanishing and the system is nearly C_6 symmetric. However, by increasing the displacement field the phase factor moves away from $\phi \approx \pi$ and spin-dependent imaginary part of the hoppings is increased, which enhances the Fermi surface spin splitting leading to a clear C_3 symmetry realized by the system.

Another visible effect of the displacement field and the Ising-type spin-orbit coupling is that by keeping constant band filling and increasing D a transition occurs from electron-like (closed) to hole-like (opened) Fermi surfaces for some critical value of $D \approx 0.3 - 0.35$ V/nm. This transition corresponds to the Van Hove singularity passing through the Fermi energy

with increasing D. It results from the fact that the Van Hove singularity corresponds to a saddle point in the electronic structure, which connects the electron-like and hole-like Fermi surfaces, which is a characteristic feature of two-dimensional systems.

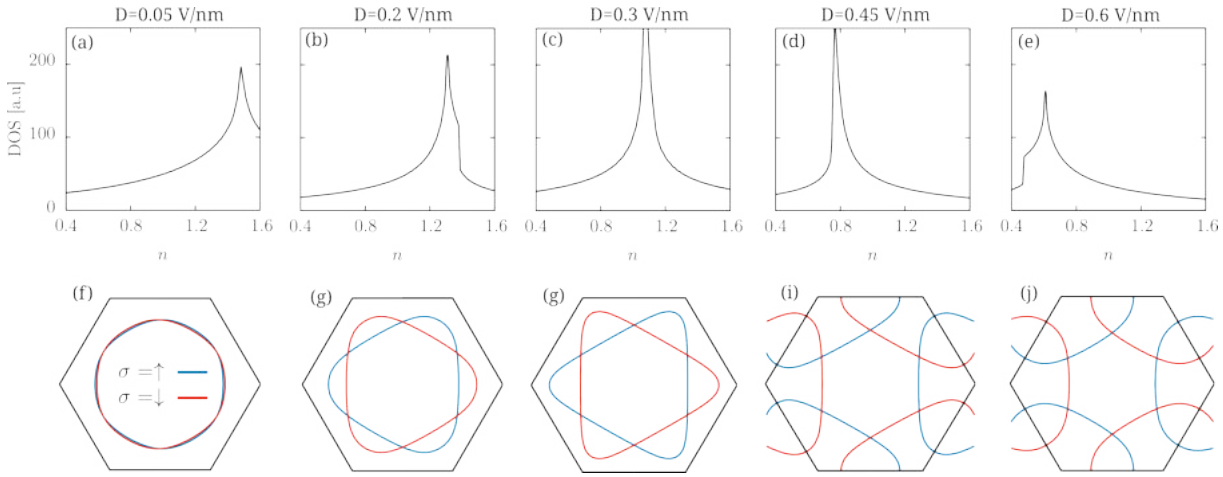

FIG. S2. (a-e) Density of states at the Fermi energy as a function of band filling for five different values of displacement field (provided in the figure). (f-j) the spin-up (blue) and spin-down (red) Fermi surfaces at half-filling corresponding to the subsequent values of the displacement fields provided in (a-e), respectively.

It should be noted that recently both the Hubbard and t-J models have been discussed in the context of $tWSe_2$ [4, 6–10]. Here we use a slightly different approach in which both U- and J- terms are taken into account explicitly. Few methodological remarks related to the model itself are in place here. Namely, starting from the Hubbard model and assuming a large U limit, the double occupancies are projected out, and the kinetic exchange term emerges resulting from virtual double occupancies leading to the t-J model. On the other hand, in the limit of weak onsite Coulomb repulsion, double occupancies are allowed even close to half-filling, but the effect of kinetic exchange is no longer operative. The t-J-U model should be considered as an effective approach dedicated to the situation when the U value is in between the two limiting situations. If U is substantial and not infinite, the double occupancies are small but non-zero, therefore the U term should be present in the Hamiltonian. At the same time, the spin-spin kinetic exchange interaction already starts to develop. In order to explicitly take into account both effects, the t-J-U model is used. Within the Gutzwiller approximation applied here, the effect of onsite correlations induced

by U is taken into account via the variational wave function. However, the effect of spin-spin superexchange is captured by the $\sim J$ term. Additionally, we supplement the model with a V term to take into account the effect of longer-range Coulomb repulsion.

The t-J-U model has been proposed already some time ago and discussed in the context of general properties of correlated electron systems [11–15]. The concept is very much related to the so-called Gossamer superconductivity introduced by Laughlin [16] and discussed by F. C. Zhang [17]. It has also been shown that the approach based on the t-J-U model allows to reproduce selected fundamental properties of the cuprates in a quantitative manner [18].

II. THE VARIATIONAL WAVE FUNCTION

A. The Gutzwiller-type wave function and the effective Hamiltonian

Since we are most interested in the moderately correlated ($U \approx W$) regime, we apply the variational wave function of Gutzwiller type which allows to take into account the electron-electron interactions. The considered variational wave function has the following form

$$|\Psi_G\rangle = \hat{P}|\Psi_0\rangle, \tag{S2}$$

where $|\Psi_0\rangle$ is the uncorrelated (mean-field) state and $\hat{P}$ is the correlation operator

$$\hat{P} = \prod_i \hat{P}_i = \prod_i \sum_\Gamma \lambda_{i,\Gamma} |\Gamma\rangle_{i\,i}\langle\Gamma|, \tag{S3}$$

where i runs over all the lattice sites, $|\Gamma\rangle$ corresponds to the local basis $|\Gamma\rangle \in \{|\emptyset\rangle, |\uparrow\rangle, |\downarrow\rangle, |\uparrow\downarrow\rangle\}$, and $\lambda_{i,\Gamma}$ are the variational parameters. As shown by Bünemann et al., one can impose an additional condition to the correlation operator, in order to reduce the complexity of the numerical calculations [19], i.e.,

$$\hat{P}_i^2 = 1 + x\hat{d}_i^{HF}, \tag{S4}$$

where $\hat{d}_i^{HF} = \hat{n}_{i\uparrow}^{HF}\hat{n}_{i\downarrow}^{HF}$, $\hat{n}_{i\sigma}^{HF} = \hat{n}_{i\sigma} - n_{i\sigma}$, with $n_{i\sigma} = \langle\Psi_0|\hat{n}_{i\sigma}|\Psi_0\rangle$, and x is yet another variational parameter. By using Eqs. (S3) and (S4) one can easily show that

$$\begin{aligned} \lambda_{\uparrow\downarrow}^2 &= 1 + x(1-n_s)^2, \\ \lambda_s^2 &= 1 - xn_s(1-n_s), \\ \lambda_\emptyset^2 &= 1 + xn_s^2, \end{aligned} \tag{S5}$$

where for simplicity we have assumed a homogeneous system with no magnetic or charge ordering. Hence, $\lambda_{i,\uparrow\downarrow} \equiv \lambda_{\uparrow\downarrow}$, $\lambda_{i,\uparrow} = \lambda_{i,\downarrow} \equiv \lambda_s$, $\lambda_{i,\emptyset} \equiv \lambda_\emptyset$, and $n_{i\uparrow} = n_{i\downarrow} \equiv n_s$. Via Eqs. (S5), the parameters $\lambda_{\uparrow\downarrow}$, λ_s, and $\lambda_\emptyset$ which correspond to doubly occupied, singly occupied, and empty lattice sites are all functions of the average number of particles in the system per site per spin and the variational parameter x. As a result, we are left with only one variational parameter, x.

In order to obtain the formula for the expectation value of our hamiltonian

$$E_G = \frac{\langle \Psi_G | \hat{H} | \Psi_G \rangle}{\langle \Psi_G | \Psi_G \rangle} = \langle \hat{H} \rangle_G, \tag{S6}$$

we apply the diagrammatic expansion of the Gutzwiller wave function (DE-GWF) [20] in the zeroth order which is equivalent to the *Statistically consistent Gutzwiller Approximation* (SGA) [15]. As a result, one can obtain the explicit form of all the energy contributions to E_G resulting from subsequent terms appearing in Eq. (S1)

$$\begin{aligned}
E_0 &= \sum_{ij} q^2 t_{ij\sigma} \langle \hat{c}^\dagger_{i\sigma} \hat{c}_{j\sigma} \rangle_0, \\
E_J &= \lambda_s^4 J \sum_{\langle ij \rangle}{}' \left(\frac{1}{2} \sum_\sigma e^{i\sigma 2\phi_{ij}} \langle \hat{c}^\dagger_{i\sigma} \hat{c}_{i\bar{\sigma}} \hat{c}^\dagger_{j\bar{\sigma}} \hat{c}_{j\sigma} \rangle_0 + \frac{1}{4} \sum_{\sigma\sigma'} \sigma\sigma' \big(\langle \hat{n}_{i\sigma} \hat{n}_{j\sigma'} \rangle_0 - n_s^2 \big) \right), \\
E_U &= \lambda_{\uparrow\downarrow}^2 U \sum_i \langle \hat{n}_{i\uparrow} \hat{n}_{i\downarrow} \rangle_0, \\
E_V &= V \sum_{\langle ij \rangle}{}' \big(g_v^2 \langle \hat{n}_i \hat{n}_j \rangle_0 - (1 - g_v^2) n_s^2 \big),
\end{aligned} \tag{S7}$$

where $q = \lambda_s\big(\lambda_d n_s + \lambda_\emptyset (1 - n_s)\big)$, $g_v = (1 - (2 - \lambda_{\uparrow\downarrow}) n_s)/(1 - n_s)$, and $\langle \hat{o} \rangle_0$ stands for the expectation value of the $\hat{o}$ operator in the state $|\psi\rangle_0$. As one can see, the expectation value of a given energy term in the correlated state, $|\Psi_G\rangle$, can be expressed in terms of the expectation values in the unorrelated state, $|\Psi_0\rangle$. However, factors q^2, λ_s^4, $\lambda_{\uparrow\downarrow}^2$, and g_v^2 renormalize the hopping, exchange interactions J, onsite Coulomb repulsion U, and intersite Coulomb repulsion V, respectively. All the operator terms in Eqs. (S7) can be decomposed by applying the Wick's theorem. Hence, the obtained E_G becomes a function of x, n_s as well as the electron hopping and Cooper pairing mean field parameters,

$$P_{ij\sigma} = \langle \hat{c}^\dagger_{i\sigma} \hat{c}_{j\sigma} \rangle_0, \quad S_{ij}^{\sigma\sigma'} = \langle \hat{c}_{i\sigma} \hat{c}_{j\sigma'} \rangle_0, \tag{S8}$$

respectively. It should be noted that one can also calculate the corresponding quantities in

the correlated state which take the form

$$\begin{aligned}\Lambda_{ij\sigma} &= \langle \hat{c}^{\dagger}_{i\sigma}\hat{c}_{j\sigma}\rangle_G = q^2\langle \hat{c}^{\dagger}_{i\sigma}\hat{c}_{j\sigma}\rangle_0,\\ \Delta^{\sigma\sigma'}_{ij} &= \langle \hat{c}_{i\sigma}\hat{c}_{j\sigma'}\rangle_G = q^2\langle \hat{c}_{i\sigma}\hat{c}_{j\sigma'}\rangle_0.\end{aligned} \tag{S9}$$

The Gutzwiller projection does not change the number of particles ($\langle \hat{n}_{i\sigma}\rangle_G = \langle \hat{n}_{i\sigma}\rangle_0$), due to the fact that we are using the zeroth-order expansion of the Gutzwiller wave function and do not consider the standard on-site *s-wave* pairing scenario.

In order to determine the values of the mean fields given by Eqs. (S8), we apply the Effective Hamiltonian Scheme which is based on the minimization condition of the ground state energy [21]. In the considered case, the resulting form of the effective Hamiltonian is the following

$$\begin{aligned}\hat{\mathcal{H}}_{\text{eff}} = &\sum_{ij\sigma}\tilde{t}_{ij\sigma}\hat{c}^{\dagger}_{i\sigma}\hat{c}_{j\sigma} - \tilde{\mu}\sum_{i\sigma}\hat{n}_{i\sigma}\\ &+ {\sum_{\langle ij\rangle\sigma}}'\big((\tilde{\Delta}_{ij\sigma\bar{\sigma}})^{*}\hat{c}_{j\sigma}\hat{c}_{i\bar{\sigma}} + h.c.\big),\end{aligned} \tag{S10}$$

where the effective hopping, effective chemical potential, and effective superconducting gap parameters are defined through the corresponding relations

$$\tilde{t}_{ij\sigma} \equiv \frac{\partial\mathcal{F}}{\partial P_{ij\sigma}}, \quad (\tilde{\Delta}_{ij\sigma\bar{\sigma}})^{*} \equiv \frac{\partial\mathcal{F}}{\partial S^{\sigma\bar{\sigma}}_{ji}}, \quad \tilde{\mu} \equiv -\frac{\partial\mathcal{F}}{\partial n_s}, \tag{S11}$$

where $\mathcal{F} = E_G - 2\mu_G n_s$ with μ_G being the chemical potential determined in the correlated state.

After the transformation to the $\mathbf{k}$ space, one obtains

$$\begin{aligned}\hat{\mathcal{H}}_{\text{eff}} = &\sum_{\mathbf{k}\sigma}\begin{pmatrix}\hat{c}^{\dagger}_{\mathbf{k}\sigma} & \hat{c}_{-\mathbf{k}\bar{\sigma}}\end{pmatrix}\begin{pmatrix}\tilde{\epsilon}_{\mathbf{k}\sigma}-\tilde{\mu} & \tilde{\Delta}_{\mathbf{k}\bar{\sigma}\sigma}\\ (\tilde{\Delta}_{\mathbf{k}\bar{\sigma}\sigma})^{*} & -\tilde{\epsilon}_{\mathbf{k}\sigma}+\tilde{\mu}\end{pmatrix}\begin{pmatrix}\hat{c}_{\mathbf{k}\sigma}\\ \hat{c}^{\dagger}_{-\mathbf{k}\bar{\sigma}}\end{pmatrix}\\ &+\sum_{\mathbf{k}\sigma}(\tilde{\epsilon}_{\mathbf{k}\sigma}-\tilde{\mu}),\end{aligned} \tag{S12}$$

where $\bar{\sigma} = -\sigma$ and

$$\begin{aligned}\tilde{\epsilon}_{\mathbf{k}\sigma} &= \sum_{i(j)}\tilde{t}_{ij}e^{ik(\mathbf{R}_i-\mathbf{R}_j)}\\ \tilde{\Delta}_{\mathbf{k}\bar{\sigma}\sigma} &= \sum_{i(j)}\tilde{\Delta}_{ji\sigma\bar{\sigma}}e^{ik(\mathbf{R}_j-\mathbf{R}_i)},\end{aligned} \tag{S13}$$

where we have used the time reversal symmetry condition ($\tilde{\epsilon}_{\mathbf{k}\sigma} = \tilde{\epsilon}_{-\mathbf{k}\bar{\sigma}}$) and i index runs over the nearest-neighbor lattice sites of site j. The $\mathbf{R}_i$ and $\mathbf{R}_j$ vectors determine the positions of i and j lattice sites, respectively.

The resulting quasiparticle dispersion relations are the following

$$\lambda_{\mathbf{k}\sigma} = \pm\sqrt{(\tilde{\epsilon}_{\mathbf{k}\sigma} - \tilde{\mu})^2 + |\tilde{\Delta}_{\mathbf{k}\bar{\sigma}\sigma}|^2}. \tag{S14}$$

As one can see from the above equation, the SC gap $\tilde{\Delta}_{\mathbf{k}\downarrow\uparrow}$ ($\tilde{\Delta}_{\mathbf{k}\uparrow\downarrow}$) opens up at the spin up (spin down) Fermi surface. Next, we transform $\tilde{\Delta}_{\mathbf{k}\downarrow\uparrow}$ and $\tilde{\Delta}_{\mathbf{k}\uparrow\downarrow}$ into the singlet and triplet components as follows

$$\begin{aligned} \tilde{\Delta}^s_{\mathbf{k}} &= \frac{1}{\sqrt{2}}\big(\tilde{\Delta}_{\mathbf{k}\uparrow\downarrow} - \tilde{\Delta}_{\mathbf{k}\downarrow\uparrow}\big), \\ \tilde{\Delta}^t_{\mathbf{k}} &= \frac{1}{\sqrt{2}}\big(\tilde{\Delta}_{\mathbf{k}\uparrow\downarrow} + \tilde{\Delta}_{\mathbf{k}\downarrow\uparrow}\big), \end{aligned} \tag{S15}$$

which we can use to rewrite the expressions for the eigenvalues

$$\lambda_{\mathbf{k}\sigma} = \pm\sqrt{(\tilde{\epsilon}_{\mathbf{k}\sigma} - \tilde{\mu})^2 + \frac{1}{2}|\tilde{\Delta}^t_{\mathbf{k}} - \sigma\tilde{\Delta}^s_{\mathbf{k}}|^2}. \tag{S16}$$

As one can see from above, for the singlet-triplet mixed paired state, one can have different SC gaps opening at the spin-up and spin-down Fermi surfaces.

The self-consistent equations for the mean field parameters can be derived in a standard manner by applying the Bogolubov-de Gennes approach to the effective Hamiltonian in $\mathbf{k}$-space with the correlation effects taken into account via the renormalization factors. By solving the set of self-consistent equations numerically, we determine the hopping and pairing amplitudes to all the six nearest neighbors. Then, to obtain their correlated state counterparts, we use Eqs. (S9). It should be noted that the procedure for solving the self-consistent equations must be coupled with the minimization of the total energy of the system with respect to the variational parameter x, which then determines all the parameters λ that appear in the correlated state $|\Psi_G\rangle$ by Eqs. (S5). In practice, this can be done by supplementing the set of self-consistent equations with the following

$$\frac{\partial E_G}{\partial x} = 0, \tag{S17}$$

where in our case the analytical derivative is replaced by a numerical one.

B. The paired state

Note that the unprojected wave function already contains the superconducting order parameter defined by Eq. (S8). However, we do not impose the appearance of pairing on

the level of the wave function itself. Instead, we allow for the anomalous expectation values $S_{ij}^{\sigma\bar{\sigma}}$ to be non-zero during our numerical procedure. Also, we do not limit ourselves to one specific symmetry of the SC gap. Instead, we consider all possible pairing symmetries that are allowed for the case of triangular lattice within the nearest neighbor real-space pairing scenario. This requires solving the set of self-consistent equations for all the six complex nearest-neighbor gap amplitudes without any additional constraints. Moreover, we allow for pure spin-singlet pairing ($S_{ij}^{\uparrow\downarrow} = -S_{ij}^{\downarrow\uparrow}$), pure spin-triplet pairing ($S_{ij}^{\uparrow\downarrow} = S_{ij}^{\downarrow\uparrow}$), as well as their mixture ($|S_{ij}^{\uparrow\downarrow}| \neq |S_{ij}^{\downarrow\uparrow}|$). At the same time, we neglect the possibility of triplet $S^z = \pm 1$ pairing due to the fact that those pairing channels lead to a Fermi wave vector mismatch, which is detrimental when it comes to the formation of the superconducting state.

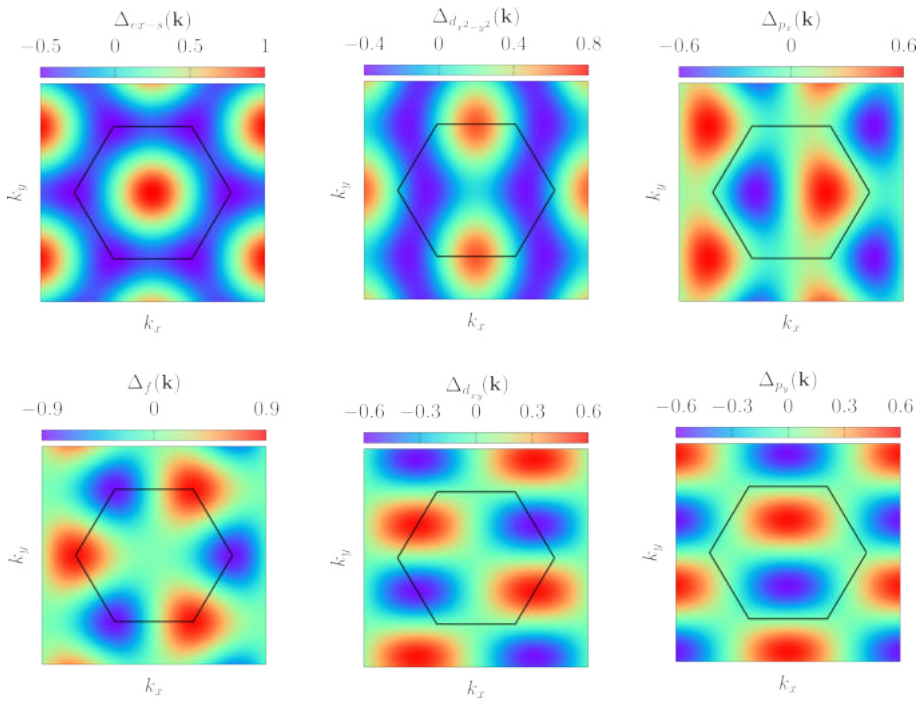

FIG. S3. The **k**-dependent SC gaps corresponding to the six symmetries which appear as real and imaginary parts of the pairing channels listed in Table I. The Brillouin zone is marked by black solid line. The presented distributions have been obtained by setting particular symmetry resolved factors to 1 and all the others to 0.

After we determine all the correlated SC amplitudes $\Delta_{ij}^{\bar{\sigma}\sigma}$ to the nearest neighbors, we transform them into the so-called symmetry resolved gap amplitudes in order to identify the symmetry of the resultant paired state. The symmetry-resolved pairing amplitudes are

M	p	gap symmetry	parity	spin state
0	0	extended s	even	singlet
1	1	$p_x + i\ p_y$	odd	triplet
2	0	$d_{x^2-y^2} + i\ d_{xy}$	even	singlet
3	1	f	odd	triplet
4	0	$d_{x^2-y^2} - i\ d_{xy}$	even	singlet
5	1	$p_x - i\ p_y$	odd	triplet

TABLE I. The six symmetries of the superconducting gap together with their parities and Cooper pair spin state. The symmetry factor, M, and the corresponding values of the parity factor p are provided in the first and the second column, respectively [cf. Eq. (S18)].

defined by the following equation

$$\Delta^{\sigma\bar{\sigma}}_{M,p} = \frac{i^p}{6}\sum_{i(j)} e^{-iM\theta_{ji}}\Delta^{\sigma\bar{\sigma}}_{ji}, \tag{S18}$$

where the summation runs over the six nearest-neighbor lattice sites j surrounding site i, and θ_{ji} are the angles $\{0,\ \pi/3,\ 2\pi/3,\ \pi,\ 4\pi/3,\ 5\pi/3\}$ between the positive half-x axis and the $\mathbf{R}_{ji} = \mathbf{R}_j - \mathbf{R}_i$ vector. M is the symmetry factor, which takes integer values and $p = 0$ for even-parities, and $p = 1$ for odd parities (cf. Table I).

Finally, we can write down the expressions for the real-space singlet and triplet gap amplitudes in the correlated state

$$\begin{aligned}\Delta^{s}_{M,p} &= (\Delta^{\uparrow\downarrow}_{M,p} - \Delta^{\downarrow\uparrow}_{M,p})/\sqrt{2},\\ \Delta^{t}_{M,p} &= (\Delta^{\uparrow\downarrow}_{M,p} + \Delta^{\downarrow\uparrow}_{M,p})/\sqrt{2}.\end{aligned} \tag{S19}$$

For the sake of clarity, in the main text of the paper, we use the symmetry names ($p \pm ip$, $d \pm id$, f etc.) in the subscripts of the symmetry resolved superconducting gaps instead of the values of the M and p factors.

In Fig. S3 we show the six gap symmetries in reciprocal space, which appear as real and imaginary parts of the pairing channels listed in Table I. As one can see, the absolute values of the *extended s-wave* and *f-wave* SC gap is C_6 symmetric; hence those two appear as independent pairing channels possible for the triangular lattice. However, the remaining

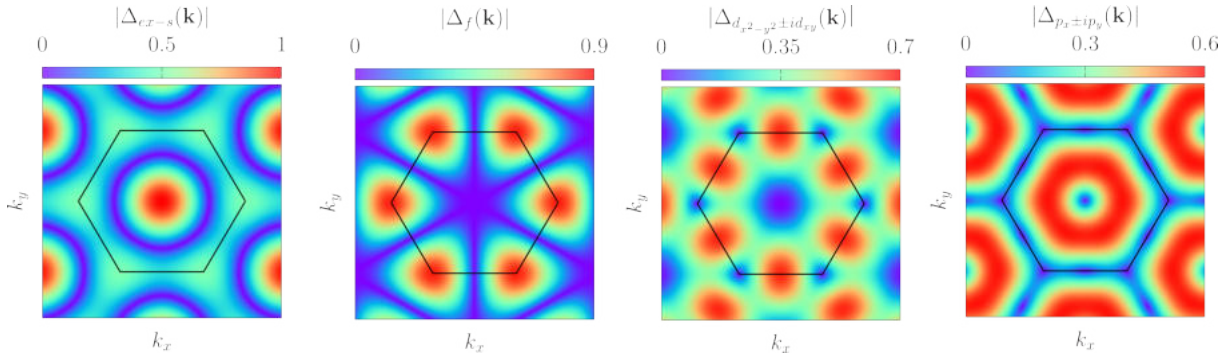

FIG. S4. The absolute value of the **k**-dependent SC gaps corresponding to the six pairing channels listed in Table I. The Brillouin zone is marked by black solid line. The presented distributions have been obtained by setting particular symmetry resolved factors to 1 and all the others to 0.

d_{x^2-y2}, d_{xy}, d_{p_x}, and d_{p_y} are not C_6 symmetric; therefore, those create combinations $d_{x^2-y2} \pm id_{xy}$ and $p_x \pm ip_y$ which result in conserved symmetry of the lattice (cf. Fig. S4). It should be noted that, despite the fact that the lattice itself fulfills the mentioned C_6 symmetry, the Hamiltonian does not due to the spin-valley locking, which is taken into account via spin- and direction-dependent hoppings. Those lead to reduction of the symmetry to C_3 which has further consequences for the pairing symmetry as we show in the next section.

C. Influence of spin-valley locking on the paired state

To show how the Ising-type spin orbit coupling and the resulting spin-valley locking influence the superconducting phase, we consider two representative situations at half-filling ($n = 1$). For the first one, there is no spin-valley locking, hence, we take a single particle term composed of purely real nearest-neighbor hoppings on a triangular lattice. For this case to induce the superconducting state at $n = 1$ we need to completely suppress the V term; therefore, we have carried out calculations for the case of t-J-U model just to analyze the gap symmetry. In this case the stable paired state corresponds to the $d \pm id$ symmetry (two degenerate solutions). The corresponding **k**-dependent SC gap is provided in Fig. S5(a) together with the normal-state Fermi surface. In the absence of SOC the system is C_6 symmetric and the spin-up and spin-down Fermi surfaces are identical (there is no spin-valley locking). As a result, the pairing symmetry is also C_6 symmetric.

In the second case we consider the t-J-U-V model which corresponds to the main result

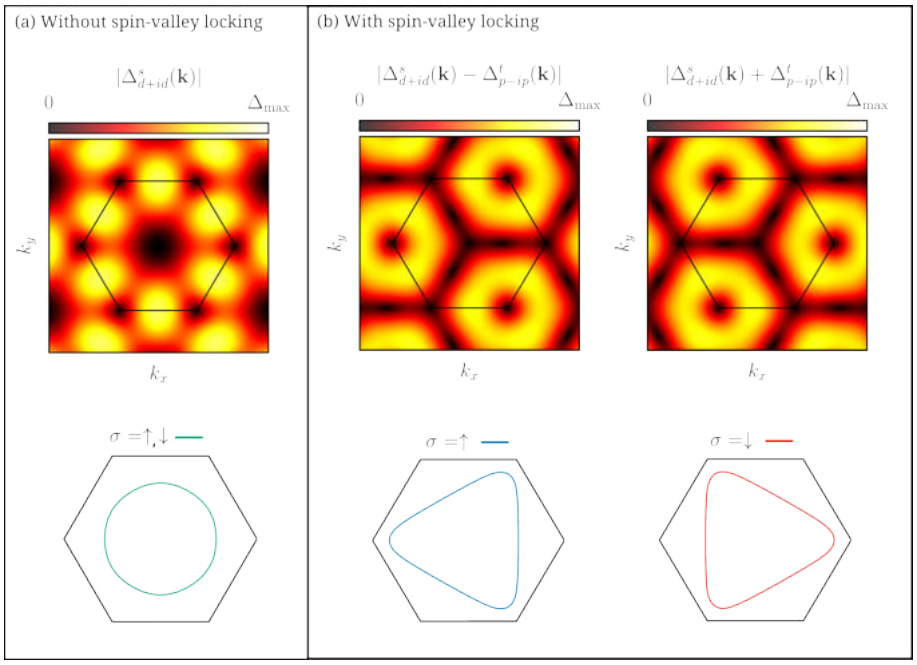

FIG. S5. The **k**-dependent SC gaps and the normal-state Fermi surfaces for two cases: (a) t-J-U model when the Ising-type spin orbit coupling is absent and consequently there is no spin-valley locking (triangular lattice with purely real hoppings conserving C_6 symmetry); (b) t-J-U-V model when the Ising type spin-orbit coupling is present leading to spin-valley locking (triangular lattice with spin dependent complex hoppings conserving C_3 symmetry). Both cases correspond to $n = 1$, $|t| = 8.27$ meV, $U = 80$ meV, $J = 4t^2/U$. Additionally for (b) we take $V = 22$ meV and $D = 0.3$ V/nm. In the lower part of the panel the Fermi surfaces are shown. Note that in the mixed singlet-triplet state considered in (b) there are two different SC gap distributions realized in **k**-space [cf. Eq. (S16)] in contrast to the situation with pure singlet pairing in (a).

from our manuscript (Fig. 2e of the manuscript), where the SOC is taken into account. Here we take $D = 0.3$ V/nm which corresponds to relatively large values of the SC amplitude in the diagram provided in Fig. 2e of the manuscript. Now the hoppings are complex are spin dependent with the form factor $\phi \approx 7\pi/8$. Due to the presence of the spin-valley locking the C_6 symmetry is broken and we are left with a C_3 symmetry and two separate Fermi surfaces; one for spin-up and K' valley, one for spin-down and K valley, as shown in Fig. S5(b). According to our calculations, for this case a stable SC solution corresponds to a mixed $d + id$ and $p - ip$ symmetry of the gap. As one can see in Fig. S5(b) this particular composition of the symmetry components leads to a situation in which the SC gap fulfills

the C_3 symmetry. Moreover, there are two different SC gap distributions realized in $\mathbf{k}$-space [cf. Eq. (S16)] in contrast to the situation with pure singlet pairing in (a). This allows for the SC gap to adjust to the shape of the two separate Fermi surfaces resulting from the spin-valley locking. Therefore, the mixed symmetry of the gap is a straightforward result of the spin-valley locking which leads to reduction of the symmetry from C_6 to C_3 and to two separate Fermi surfaces.

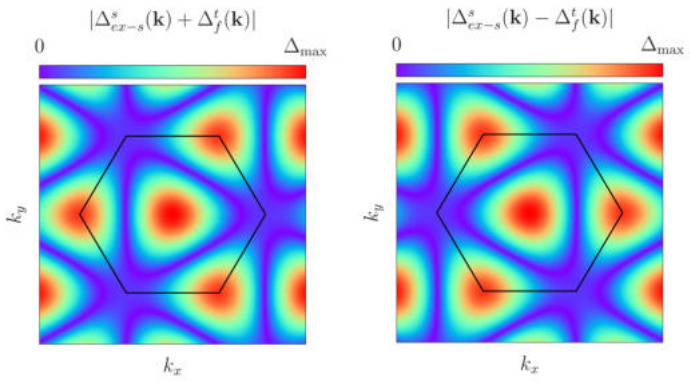

FIG. S6. The $\mathbf{k}$-dependent SC gaps for the case of *extended* s/f mixed state which becomes stable in the low- ($n \approx 0$) and high- ($n \approx 2$) electron concentration regimes and requires $V \approx 0$ and/or high values of J.

The obtained mixed $d+id/p-ip$ state leads to the same free energy as the $d-id/p+ip$ state. Therefore, similarly as in the case of the pure $d \pm id$ pairing in the absence of the spin-valley locking, also here we have a degeneracy. Another pairing channel which is possible in the considered system is a mixed *extended s-wave* and *f-wave* state (cf. Fig. S6). However, it is much more fragile and appears only for the $V = 0$ case and/or for larger values of J. If those conditions are met and *extended s-wave*/f*-wave* state becomes stable for the band fillings close to the empty and fully filled situations. As one can see from Fig. S6 in this case a significant SC gap can be opened if the Fermi surfaces are relatively small and located at the Γ point or the K and K' points of the Brillouin zone. Such situation appears for very low and very high electron concentrations which is not the case considered in our manuscript since we focus on $n \in [0.8, 1.2]$.

It should be emphasized that in the obtained mixed state, the opposite signs of the imaginary part in the $d \pm id$ and $p \mp ip$ amplitudes are of crucial importance. Only in such

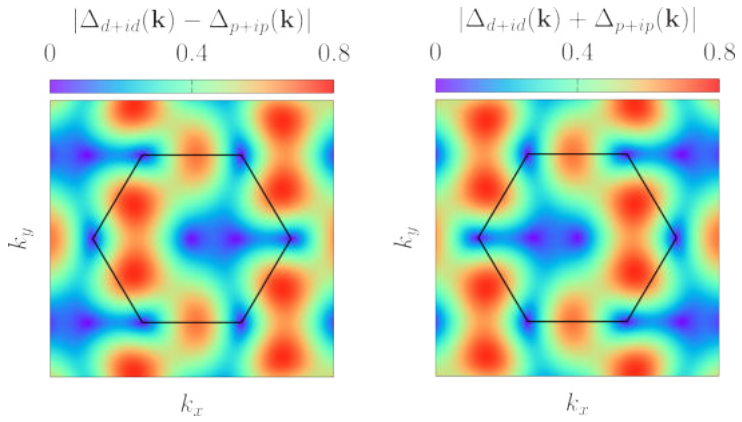

FIG. S7. The **k**-dependent SC gaps for the case of hypothetical $d + id/p + ip$ mixed state. As one can see in such case C_2 symmetry is realized not the C_3 which corresponds to our system with spin-valley locking. Therefore, such pairing channel is not likely to be realized here. The presented distributions have been obtained by setting the amplitudes $\Delta^s_{d+id} = 1$ and $\Delta^t_{p+ip} = 0.5$ and correspond to a representative situation.

case can one obtain an SC gap which realizes the C_3 symmetry resulting from the spin-valley locking. For the sake of clarity, in Fig. S7 we show the **k**-dependence of the SC gap for a hypothetical mixed $d + id/p + ip$ state which is not a result of self-consistent calculations but has been determined by assuming $\Delta^s_{d+id} = 1$ and $\Delta^s_{p+ip} = 0.5$. As one can see here, a C_2 symmetry is realized. Stabilization of such a state would require some additional symmetry breaking, which is not energetically favorable according to our calculations.

It should be noted that instabilities towards mixed singlet-triplet pairing of d/p- as well as *extended* s/f- type have been also reported by using functional renormalization group (FRG) [22, 23] as well as density matrix renormalization group (DMRG) [24] methods for the case of $tWSe_2$ within a single- and three- band pictures. Moreover, recent studies carried out within the continuum model have shown that for non-zero displacement field, the leading pairing instability corresponds to the two-dimensional E representation which similarly gives rise to a chiral mixed singlet/triplet superconducting channels in large regime of parameters [25, 26]. However, in contrast to our results, Ref. [25] shows a transition to a time-reversal symmetric nematic state at high values of displacement field. Such transition might originate from the details of the continuum model which are not captured by the effective single-band approach taken here. Nevertheless, according to the experimental data,

the SC state is contained in a relatively small range of band fillings and displacement fields. Therefore, it is not completely clear if the regime of large D values at which the transition to the namatic phase could appear according to Ref. [25], is reached.

Finally, apart from the symmetry related aspect, the effect of the spin-valley locking on the paired state appears also via the density of states. Namely, as discussed in Section I, the displacement field tunes the spin-valley locking, which affects the location of the Van Hove singularity. As discussed in detail in the main part of the manuscript [cf Fig. 2(e,j) of the manuscript], the SC state is stabilized at the crossing between the Van Hove singularity and the half-filling. This is due to the fact, that high values of the density of states enhance superconductivity, and additionally half-filling provides large renormalization which also stabilizes pairing. The maximal pairing amplitudes and, therefore, the most stable SC state appear for $n \approx 1$ and $D \approx 0.3 - 0.35$ V/nm. As one can see in Fig. S5(b) which corresponds to this regime, the Fermi surfaces almost reach the K and K' points and the spin splitting is well pronounced. This is due to the fact that the Fermi energy is in the proximity of thee Van Hove singularity, hence, we are close to the transition point between the closed electron-like Fermi surfaces and opened hole-like Fermi surfaces.

III. TOPOLOGICAL PROPERTIES

To identify the topological properties of the obtained paired state we have calculated the Chern number by using the the Brillouin zone triangulation method [27]. According to our calculations in the relevant range of parameters corresponding to Fig. 2(e,j) in the main text of the manuscript, the superconducting state is nontrivial topologically with the Chern number $C = \pm 4$. For clarity we revisit here the mentioned diagram slightly zoomed in Fig. S8. As one can see, the sign change of C appears at the line representing the Van Hove singularity.

To analyze further the topological nature of the obtained paired state we consider two representative sets of parameters which are marked by green dots in Fig. S8(a). In Fig. S9 we provide the corresponding **k**-dependent SC gap as well as the normal state Fermi surfaces. As one can see, there are points at which the SC gap closes which are called nodal points. Each nodal point carries a topological charge (Chern charge). The Chern number of the superconducting state is equal to the sum of the topological charge contained in the

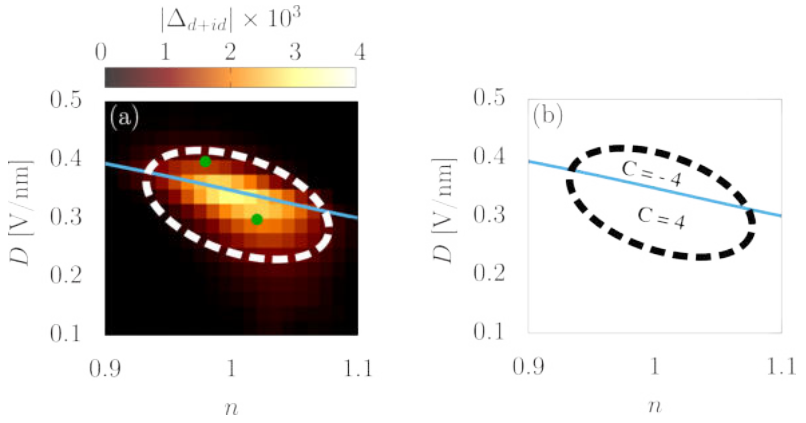

FIG. S8. (a) The SC gap amplitude as a function of band filling and displacement field for the case of $U = 80$ meV, $J = 4t^2/U$, $V = 22$ meV (the same model parameters as in Fig. 2e in the main text of the manuscript). Here we provide only the $d + id$ singlet component since the triplet one shows the same behavior but is approximately twice smaller. The white dashed line is a guide to the eye denoting the stability range of the SC state. The two green points correspond to the two representative n and D values leading to $C = \pm 4$ and selected for the detailed analysis of the topological features provided on Fig. S9. (b) The phase diagram which shows the calculated values of the Chern number characterizing the obtained superconducting state.

normal-state Fermi surface. Namely,

$$C = \sum_{i \in \Omega_{FS}} (-1)^w C_i, \tag{S20}$$

where C_i is the topological charge of a given nodal point which can be determined by calculating the winding number of the order parameter around it. The sign of the Chern charge depends on whether it is enclosed by an electron- ($w = 0$) or hole-like ($w = 1$) Fermi surface. The i index runs only over the nodal points that are contained inside the Fermi surface.

As one can see, the spin up and spin down Fermi surfaces introduce the Chern number equal ± 2 each, which in total gives ± 4. Moreover, the positive (negative) Chern number corresponds to electron-like (hole-like) Fermi surfaces centered at Γ point (K and K' points). That is why the sign change of the Chern number in the diagram presented in Fig. S8(b) appears at the line representing the Van Hove singularity. As discussed in detail in Section I, the Van Hove singularity line represents the transition between the electron-like and hole-like

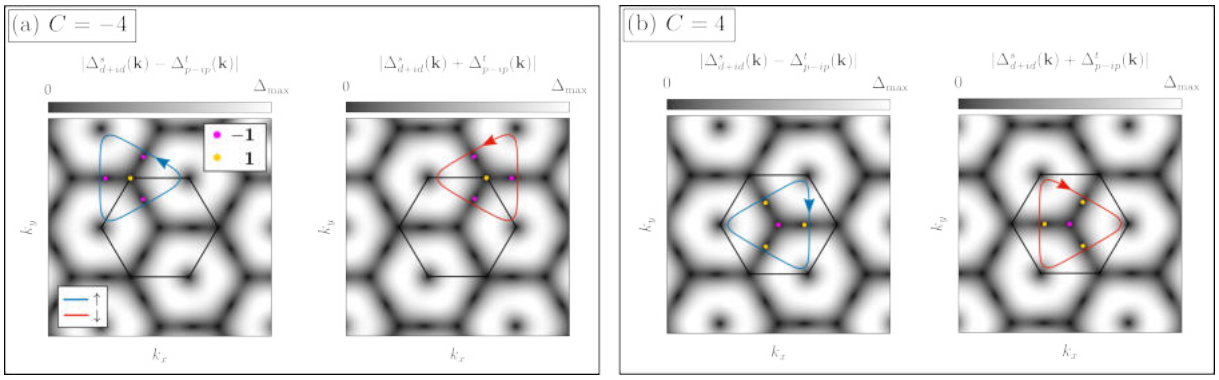

FIG. S9. The normal-state Fermi surfaces for spin-up and -down (blue and red solid lines) electrons as well as the **k**-dependent SC gaps for two selected values of n and D, which are marked by green dots in Fig. S8 and correspond to following values of the Chern number: $C = -4$ (a), $C = 4$ (b). Note, that the value of the Chern number is simply the sum of the Chern charges contained inside the spin-up and -down Fermi surfaces (marked by the colored dots). The arrows at the Fermi surfaces represent the winding direction which is counterclockwise (clockwise) for the electron-like (hole-like) Fermi surfaces. Note that the signs of the Chern charges depend on the winding direction.

Fermi surfaces, which, as shown here, also leads to sign change of the Chern number.

[1] L. Wang, E.-M. Shih, A. Ghiotto, L. Xian, D. A. Rhodes, C. Tan, M. Claassen, D. M. Kennes, Y. Bai, B. Kim, K. Watanabe, T. Taniguchi, X. Zhu, J. Hone, A. Rubio, and C. R. Pasupathy, Abhay N. amd Dean, Correlated electronic phases in twisted bilayer transition metal dichalcogenides, Nature Materials **19**, 861 (2020).

[2] D. Xiao, G.-B. Liu, W. Feng, X. Xu, and W. Yao, Coupled spin and valley physics in monolayers of mos_2 and other group-vi dichalcogenides, Phys. Rev. Lett. **108**, 196802 (2012).

[3] Y. Zhang, L. Li, J.-H. Sun, D.-H. Xu, R. Lü, H.-G. Luo, and W.-Q. Chen, Kondo effect in monolayer transition metal dichalcogenide ising superconductors, Phys. Rev. B **101**, 035124 (2020).

[4] H. Pan, F. Wu, and S. Das Sarma, Band topology, hubbard model, heisenberg model, and dzyaloshinskii-moriya interaction in twisted bilayer wse_2, Phys. Rev. Res. **2**, 033087 (2020).

[5] Y.-T. Hsu, F. Wu, and S. Das Sarma, Spin-valley locked instabilities in moiré transition metal

dichalcogenides with conventional and higher-order van hove singularities, Phys. Rev. B **104**, 195134 (2021).

[6] J. Zang, J. Wang, J. Cano, and A. J. Millis, Hartree-fock study of the moiré hubbard model for twisted bilayer transition metal dichalcogenides, Phys. Rev. B **104**, 075150 (2021).

[7] M. Bélanger, J. Fournier, and D. Sénéchal, Superconductivity in the twisted bilayer transition metal dichalcogenide wse_2: A quantum cluster study, Phys. Rev. B **106**, 235135 (2022).

[8] J. Zang, J. Wang, J. Cano, A. Georges, and A. J. Millis, Dynamical mean-field theory of moiré bilayer transition metal dichalcogenides: Phase diagram, resistivity, and quantum criticality, Phys. Rev. X **12**, 021064 (2022).

[9] F. Wu, T. Lovorn, E. Tutuc, and A. H. MacDonald, Hubbard model physics in transition metal dichalcogenide moiré bands, Phys. Rev. Lett. **121**, 026402 (2018).

[10] Y. and D. N. Sheng, Topological chiral and nematic superconductivity by doping mott insulators on triangular lattice, Phys. Rev. X **12**, 031009 (2022).

[11] S. Daul, D. J. Scalapino, and S. R. White, Pairing correlations on $t - U - J$ ladders, Phys. Rev. Lett. **84**, 4188 (2000).

[12] S. Basu, R. J. Gooding, and P. W. Leung, Enhanced bound-state formation in two dimensions via stripelike hopping anisotropies, Phys. Rev. B **63**, 100506 (2001).

[13] E. Plekhanov, S. Sorella, and M. Fabrizio, Increasing d-wave superconductivity by on-site repulsion, Phys. Rev. Lett. **90**, 187004 (2003).

[14] T. Xiang, H. G. Luo, D. H. Lu, K. M. Shen, and Z. X. Shen, Intrinsic electron and hole bands in electron-doped cuprate superconductors, Phys. Rev. B **79**, 014524 (2009).

[15] M. Abram, J. Kaczmarczyk, J. Jędrak, and J. Spałek, d-wave superconductivity and its coexistence with antiferromagnetism in the t–j–u model: Statistically consistent gutzwiller approach, Phys. Rev. B **88**, 094502 (2013).

[16] R. B. Laughlin, Gossamer superconductivity (2002), arXiv:cond-mat/0209269 [cond-mat.supr-con].

[17] F. C. Zhang, Gossamer superconductor, mott insulator, and resonating valence bond state in correlated electron systems, Phys. Rev. Lett. **90**, 207002 (2003).

[18] J. Spałek, M. Zegrodnik, and J. Kaczmarczyk, Universal properties of high-temperature superconductors from real-space pairing: $t - j - u$ model and its quantitative comparison with experiment, Phys. Rev. B **95**, 024506 (2017).

[19] J. Bünemann, T. Schickling, and F. Gebhard, Variational study of fermi surface deformations in hubbard models, Europhysics Letters **98**, 27006 (2012).

[20] J. Spałek, M. Fidrysiak, M. Zegrodnik, and A. Biborski, Superconductivity in high-tc and related strongly correlated systems from variational perspective: Beyond mean field theory, Physics Reports **959**, 1 (2022).

[21] J. Kaczmarczyk, Comparison of two approaches for the treatment of gutzwiller variational wave functions, Philosophical Magazine **95**, 563 (2015), https://doi.org/10.1080/14786435.2014.965235.

[22] L. Klebl, A. Fischer, L. Classen, M. M. Scherer, and D. M. Kennes, Competition of density waves and superconductivity in twisted tungsten diselenide, Phys. Rev. Res. **5**, L012034 (2023).

[23] A. Fischer, L. Klebl, V. Crépel, S. Ryee, A. Rubio, L. Xian, T. O. Wehling, A. Georges, D. M. Kennes, and A. J. Millis, Theory of intervalley-coherent afm order and topological superconductivity in $twse_2$ (2024), arXiv:2412.14296 [cond-mat.str-el].

[24] F. Chen and D. N. Sheng, Singlet, triplet, and pair density wave superconductivity in the doped triangular-lattice moiré system, Phys. Rev. B **108**, L201110 (2023).

[25] D. Guerci, D. Kaplan, J. Ingham, J. H. Pixley, and A. J. Millis, Topological superconductivity from repulsive interactions in twisted wse_2 (2024), arXiv:2408.16075 [cond-mat.supr-con].

[26] C. Schrade and L. Fu, Nematic, chiral and topological superconductivity in transition metal dichalcogenides (2024).

[27] T. Fukui, Y. Hatsugai, and H. Suzuki, Chern numbers in discretized brillouin zone: Efficient method of computing (spin) hall conductances, Journal of the Physical Society of Japan **74**, 1674 (2005), https://doi.org/10.1143/JPSJ.74.1674.

4.3 Superconductivity in moiré transition metal dichalcogenide bilayers: comparison of two distinct theoretical approaches

This work investigates SC in $tWSe_2$ bilayer within two distinct theoretical frameworks, the negative-U Hubbard model and the t-J-U model. The study is motivated by recent experimental observations of SC in TMD moiré bilayers.

The negative-U Hubbard model represents a conventional approach based on onsite attractive interaction, leading to an isotropic s-wave superconducting gap. In this framework, SC is primarily governed by the DOS and is enhanced near the VHS. However, this behavior does not fully reproduce experimental observations, which indicate SC predominantly near half filling and only in relatively small range of displacement fields. In contrast, the t-J-U model incorporates strong electron correlations through onsite Coulomb repulsion and intersite kinetic exchange interactions. Within this approach, SC emerges from an unconventional pairing mechanism with mixed $d+id$ (singlet) and $p-ip$ (triplet) symmetry. The inclusion of correlation effects via the Gutzwiller approximation leads to significant renormalization of the electronic parameters, particularly near half filling. These renormalization effects favor SC in the moderately correlated regime ($U \lesssim W$), while strong correlations suppress pairing at half-filling due to proximity to an insulating state. A key outcome of this work is that, while both models predict enhancement of SC near the VHS, only the t-J-U framework captures the experimentally observed localization of the superconducting state at the crossing between VHS and half-filling where both strong correlations and high DOS cooperate. Overall, the comparison highlights the importance of electronic correlations and unconventional pairing mechanisms in describing SC in $tWSe_2$, suggesting that the t-J-U model provides a more realistic description of the experimental phase diagram.

The manuscript presented below corresponds to the arXiv preprint version of this work. The article has been accepted for publication in Acta Physica Polonica B and is currently in press.

Superconductivity in moiré transition metal dichalcogenide bilayers: comparison of two distinct theoretical approaches

Waseem Akbar and Michał Zegrodnik

Academic Centre for Materials and Nanotechnology, AGH University of Krakow, al. A. Mickiewicza 30, 30-059 Krakow, Poland

Received May 7, 2026

Superconductivity has recently been observed in moiré transition-metal dichalcogenide bilayers. Here, we investigate the superconducting state in twisted WSe_2 using two complementary theoretical approaches. The first is based on the negative U-Hubbard model and represents a relatively conventional pairing scenario, in which strong electron–electron repulsion does not directly affect the paired state and an isotropic *s-wave* gap emerges. The second approach employs the t-J-U model, allowing for unconventional gap symmetries and incorporating strong correlation effects via substantial renormalization induced by Coulomb repulsion. We compare the key properties of the superconducting states obtained within these two frameworks and discuss their implications in light of available experimental observations.

1. Introduction

Moiré transition metal dichalcogenide (TMD) bilayers have emerged as a highly tunable platform for exploring correlated electron physics in two dimensions. When two monolayers are stacked with a small twist angle or lattice mismatch, long-wavelength moiré superlattices form, leading to flat electronic bands. These systems combine strong spin–orbit coupling, valley degrees of freedom, and reduced dielectric screening, giving rise to a rich variety of interaction-driven ground states including correlated insulators[1, 2, 3], topological phases[4, 5, 6, 7, 8, 9, 10], generalized Wigner crystals[11, 12] and tunable excitonic complexes[13, 14, 15]. Moreover, recent experiments on twisted bilayer WSe_2 and $MoTe_2$ have revealed the appearance of the superconducting phase (SC)[16, 17, 18, 19, 20, 21]. It should be noted that TMD moiré bilayers are characterized by significant advantages in comparison to the canonical strongly correlated electron systems such as cuprates, in which superconductivity was also identified many years ago[22, 23]. Namely, by varying the twist angle between the layers, one

directly controls the bandwidth and thus the strength of electronic correlations, enabling continuous tuning from weak- to strong-coupling regimes. Independent electrostatic control of the band filling through gate voltages further allows superconductivity to be probed across distinct carrier-density regimes. In addition, the strong spin–orbit coupling intrinsic to WSe_2 can be modified via an applied displacement field, altering the spin–valley locking and possibly modifying the available pairing channels. Together, these tuning knobs make twisted bilayer WSe_2 a uniquely flexible platform for investigating unconventional superconductivity in two dimensions, where both the interaction scale and internal electronic structure can be engineered in an *in situ* manner.

According to the experimental data gathered so far, the superconductivity in twisted WSe_2 appears close to the correlated insulator, which lies at half-filling. The paired state shows dome-like behavior as a function of electronic concentration with the maximal critical temperature below 1 K. For small twist angles ($\sim 2^\circ$) the SC state stability appears close to zero displacement fields, while for relatively larger angles ($\sim 5^\circ$) some non-zero displacement field is necessary to induce the pairing[19, 21]. Also, depending on the twist angle and the value of displacement field, both one and two superconducting domes can be observed with changing band filling.

So far the pairing mechanism and the complete theoretical description of the fundamental features of the superconducting phase in $tWSe_2$ has not been established. Most of the theoretical analysis emphasize the Coulomb-interaction driven pairing both within strong and weak-to moderate interaction regime which leads to an anisotropic gap in $\mathbf{k}$-space and singlet-triplet mixing[24, 25, 26, 27, 28, 29, 30, 31, 32, 33]. However, pure spin-singlet channel has also been considered[34, 35] and a more standard phonon mediated pairing still remains a possibility and has been discussed in Ref. [36].

The main aim of this paper is to confront two distinct approaches to the description of superconductivity as applied to the study of $tWSe_2$ and to discuss them in the context of available experimental data. Within the first scenario, we apply the so-called negative-U Hubbard model which was originally proposed by Robaszkiewicz et al. and analyzed in the context of superconducting state and charge ordering[37, 38]. Here we combined it with an effective description of a single moié band of $tWSe_2$ with the Ising-type spin orbit coupling taken into account by the spin dependent complex hoppings. This constitutes a relatively conventional approach and leads in a straightforward manner to an isotropic *s-wave* type of pairing. Such description can be considered as compatible with momentum independent pairing potential similar to the one considered in the standard BCS theory but without limiting the pairing to a narrow range of energies around the Fermi level.

In the second case, we revisit our recent considerations in which we employ the *t*-*J*-*U* model that refers to electron pairing induced by kinetic exchange leading to an unconventional form of the superconducting gap realizing a mixed $d + id/p - ip$ symmetry, which is due to the presence of Ising type spin-orbit coupling in $tWSe_2$[39, 33]. It should be noted that the *t*-*J*-*U* model has been extensively applied to superconducting cuprates already some time ago[40, 23] and it can be considered as evolving from the canonical Hubbard[41, 42] and *t*-*J*[43, 44] model based theories within the paradigm of strong electronic correlations. Here, we use the Gutzwiller approximation method in order to analyze the influence of the correlation induced renormalization effects and their influence of the resulting physical picture.

2. Model and Method

To describe the single moiré band of twisted WSe_2 with Ising type spin orbit coupling in an effective manner, we consider the following single-particle Hamiltonian

$$\hat{H}_0 = t \sum_{\langle ij \rangle \sigma} e^{i\sigma\nu_{ij}\phi} \, \hat{c}^{\dagger}_{i\sigma} \hat{c}_{j\sigma}, \tag{1}$$

where $\hat{c}^{\dagger}_{i\sigma}$ and $\hat{c}_{i\sigma}$ are the creation and annihilation operators for the electron with spin σ at the site i while $\langle i, j \rangle$ corresponds to the nearest neighbor lattice sites at the triangular lattice. As one can see, the hoppings are both spin- and direction-dependent with $\sigma = 1$ ($\sigma = -1$) corresponding to spin up (spin down) and $\nu_{ij} = \pm 1$ depending on the hopping direction [cf. Fig. 1 (a)].

It should be noted that within such an effective single band picture, the hopping amplitude t and the phase factor ϕ depend on the displacement field (D) as shown in Refs. [16, 45]. Here we take the values provided in [16]. By changing the displacement field, one can enhance the strength of the Ising type spin orbit coupling and influence the profile of the density of states in the system. In Fig. 1 (b) we show the resulting evolution of the Van Hove singularity in the (n, D)-plane, where $n = \sum_{\sigma} \langle \hat{n}_{i\sigma} \rangle$. The presented curve divides the diagram into two regimes with closed (left-bottom) and opened (right-upper) spin-split Fermi surfaces. For the sake of clarity in Fig. 1 (c) and (d) we provide the density of states at the Fermi level as a function of band filling for two selected displacement fields, where the shift of the Van Hove singularity from higher to lower band fillings is visualized with increasing D.

In this study, the single particle part provided above is supplemented with an interaction part in order to analyze the fundamental features of the

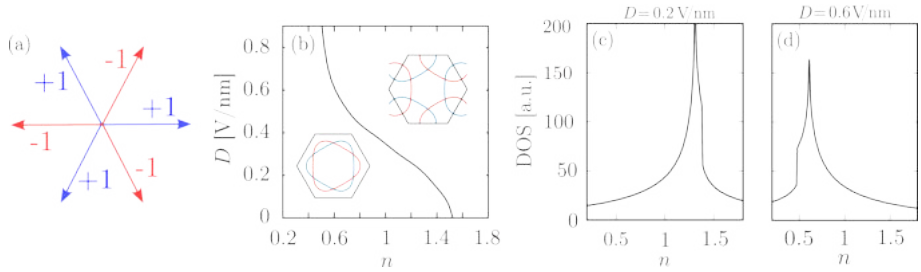

Fig. 1. (a) The values of the direction dependent factor $\nu_{ij} = \pm 1$ corresponding to the nearest neighbor hoppings on a triangular lattice which determines the sign of the complex phase appearing in Eq. (1). (b) The evolution of the Van Hove singularity in the (n, D)-plane. Note that the resulting curve divides the diagram into two regimes with closed (left-bottom) and opened (right-upper) spin-split Fermi surfaces. (c) and (d) Density of states at the Fermi level as a function of band filling for two selected values of the displacement field, D.

superconducting state. Therefore the resulting Hamiltonian has the general form

$$\hat{H} = \hat{H}_0 + \hat{H}_I, \tag{2}$$

where $\hat{H}_I$ constitutes the interaction part. In the following, we describe the two theoretical approaches which differ by the form of the interaction term and correspond to the negative U-Hubbard model in connection with the Hartree-Fock method as well as the t-J-U model with the application of the Gutzwiller approximation method.

2.1. Negative U-Hubbard model

First we consider the interaction part of our model in the form of the negative U-Hubbard term

$$\hat{H}_I = U \sum_i \hat{n}_{i\uparrow}\hat{n}_{i\downarrow}, \tag{3}$$

where $\hat{n}_{i\sigma} = \hat{c}^\dagger_{i\sigma}\hat{c}_{i\sigma}$ and $U < 0$ leading to an attractive onsite interaction which results in superconducting pairing in a straightforward manner as shown below. After the application of the Hartree-Fock approximation with the inclusion of the anomalous expectation values, the interaction term takes the form

$$\hat{H}_I = \sum_i \left(\tilde{\Delta}^* \hat{c}_{i\uparrow}\hat{c}_{i\downarrow} + \tilde{\Delta}\hat{c}^\dagger_{i\downarrow}\hat{c}^\dagger_{i\uparrow}\right) + U\frac{n}{2}\sum_{i\sigma}\hat{n}_{i\sigma} - \frac{N}{U}|\tilde{\Delta}|^2 - NU\frac{n^2}{4}, \tag{4}$$

where N is the number of lattice sites and we have introduced the onsite pairing amplitude $\tilde{\Delta}_i = U\langle \hat{c}_{i\downarrow}\hat{c}_{i\uparrow}\rangle$. Also, since we consider a homogeneous, non-magnetic state, we take $\tilde{\Delta}_i \equiv \tilde{\Delta}$ and $\langle \hat{n}_{i\sigma}\rangle \equiv n/2$. For the sake of convenience, we additionally determine the pure anomalous expectation value $\Delta = \tilde{\Delta}/U$, which is going to be useful further on when comparing the results coming from the two considered here approaches. Moreover, the second summation in the above equation can be dropped since it only shifts the energy scale of the considered band and therefore in the considered single band case it does not have any influence on the physics of the model.

After the transformation to reciprocal space we can write the full Hamiltonian in a compact form

$$\begin{aligned}\hat{H} = \frac{1}{2}\sum_{\mathbf{k}\sigma} & \begin{pmatrix} \hat{c}^{\dagger}_{\mathbf{k}\sigma} & \hat{c}_{-\mathbf{k}\bar{\sigma}} \end{pmatrix} \begin{pmatrix} \epsilon_{\mathbf{k}\sigma} - \mu & \sigma\tilde{\Delta} \\ \sigma\tilde{\Delta}^{*} & -\epsilon_{-\mathbf{k}\bar{\sigma}} + \mu \end{pmatrix} \begin{pmatrix} \hat{c}_{\mathbf{k}\sigma} \\ \hat{c}^{\dagger}_{-\mathbf{k}\bar{\sigma}} \end{pmatrix} \\ & + \sum_{\mathbf{k}\sigma}(\epsilon_{\mathbf{k}\sigma} - \mu) - \frac{N}{U}|\tilde{\Delta}|^2 - NU\frac{n^2}{4},\end{aligned} \tag{5}$$

where $\bar{\sigma} = -\sigma$ and we have supplemented the model with the chemical potential contribution $(-\mu\sum_i \hat{n}_{i\sigma})$. As one can see, onsite pairing amplitudes $\tilde{\Delta}$ correspond to coupling between the electron- and hole-like dispersion relations which leads to gap opening in the resulting band structure. The standard Bogolubov-de Gennes approach can be applied to the Hamiltonian given by Eq. (5) in order to derive the self consistent equations for the superconducting gap and chemical potential, which than can be solved numerically.

2.2. The t-J-U model

As the second scenario considered here we revisit the *t-J-U* model as applied to the single band effective description of the twisted WSe_2[25, 33]. In this case the interaction part of the model is taken in the form

$$\begin{aligned}\hat{H}_I = & J\sum_{\langle ij\rangle}{}' \Bigg(\hat{S}^z_i\hat{S}^z_j + \cos(2\nu_{ij}\phi)\sum_{\alpha=x,y}\hat{S}^{\alpha}_i\hat{S}^{\alpha}_j \\ & + \sin(2\nu_{ij}\phi)(\hat{\mathbf{S}}_i \times \hat{\mathbf{S}}_j)\cdot\hat{z}\Bigg) + U\sum_i \hat{n}_{i\uparrow}\hat{n}_{i\downarrow},\end{aligned} \tag{6}$$

where $\hat{\mathbf{S}}_i$ is the spin-$\frac{1}{2}$ operator while $J > 0$ and $U > 0$ correspond to intersite kinetic exchange and onsite Coulomb repulsion, respectively. The presented form of the kinetic exchange term can be obtained when deriving the *t-J* model form the Hubbard model description of a single moiré band

of $tWSe_2$. The considered t-J-U Hamiltonian can be viewed as an effective framework appropriate for regimes where U is large but finite, and double occupancies remains small yet nonvanishing. Under these conditions, the Hubbard U term must be retained in the Hamiltonian, while the kinetic spin–spin exchange interaction already starts to develop. The t-J-U model is therefore used to explicitly capture both contributions. It should be noted that, here the kinetic exchange term differs from the one obtained originally by Spałek et al[43] due to the appearance of the additional Dzyaloshinskii-Moriya-type of term. Such a form is a straightforward result of the Ising type spin orbit coupling which is characteristic to $tWSe_2$ and is taken into account via spin and direction dependent complex hoppings.

In order to take into account the electron-electron correlations within such approach we consider the Gutzwiller variational wave function in the following form

$$|\Psi_G\rangle = \prod_i \sum_\Gamma \lambda_{i,\Gamma} |\Gamma\rangle_{i\,i}\langle\Gamma|\Psi_0\rangle, \tag{7}$$

where $|\Psi_0\rangle$ is the uncorrelated (mean-field) state and i runs over all the lattice sites, $|\Gamma\rangle$ corresponds to the local basis $|\Gamma\rangle \in \{|\emptyset\rangle,\ |\uparrow\rangle,\ |\downarrow\rangle,\ |\uparrow\downarrow\rangle\}$, and $\lambda_{i,\Gamma}$ are the variational parameters. Similarly as in the previous subsection, also here we consider a homogeneous, non-magnetic state, thus $\lambda_{i,\Gamma} \equiv \lambda_\Gamma$ and $\lambda_\sigma \equiv \lambda_s$. As shown by Bünemann et al., one can impose an additional condition to the correlation operator, in order to reduce the complexity of the numerical calculations [46]. Within the infinite dimensions approximation (Gutzwiller approximation), the expectation value of our Hamiltonian in the $|\Psi_G\rangle$ state takes the form

$$\begin{aligned}\langle\hat{H}\rangle_G = \sum_{ij} q^2 t_{ij\sigma}\langle\hat{c}^\dagger_{i\sigma}\hat{c}_{j\sigma}\rangle_0 + \lambda_s^4\, J \sum_{\langle ij\rangle}{}' \Bigg(\frac{1}{2}\sum_\sigma e^{i\sigma 2\phi_{ij}}\langle\hat{c}^\dagger_{i\sigma}\hat{c}_{i\bar{\sigma}}\hat{c}^\dagger_{j\bar{\sigma}}\hat{c}_{j\sigma}\rangle_0 \\ + \frac{1}{4}\sum_{\sigma\sigma'}\sigma\sigma'\langle\hat{n}^{HF}_{i\sigma}\hat{n}^{HF}_{j\sigma'}\rangle_0\Bigg) + \lambda^2_{\uparrow\downarrow}U\sum_i\langle\hat{n}_{i\uparrow}\hat{n}_{i\downarrow}\rangle_0,\end{aligned} \tag{8}$$

where $q = \lambda_s\big(\lambda_{\uparrow\downarrow}n/2 + \lambda_\emptyset(1-n/2)\big)$ and $\langle\hat{o}\rangle_0$ stands for the expectation value of the $\hat{o}$ operator in the state $|\psi_0\rangle$. Using the standard Wick's theorem, all four-operator expectation values appearing on the right-hand side of the above equation can be decomposed. As a result, $\langle\hat{H}\rangle_G$ can be written as a function of n, the electron hopping $[P_{ij\sigma} = \langle\hat{c}^\dagger_{i\sigma}\hat{c}_{j\sigma}\rangle_0]$ and Cooper pairing mean-field parameters $[S^{\sigma\sigma'}_{ij} = \langle\hat{c}_{i\sigma}\hat{c}_{j\sigma'}\rangle_0]$. In order to determine the values of those mean fields we apply the Effective Hamiltonian Scheme[47]. Within such approach the minimization condition of the ground state energy, $\langle\hat{H}\rangle_G$, leads to an effective Hamiltonian which can be treated within the Bogilubov-de Gennes formalism as shown in some more detail in Refs. [25, 33].

It should be noted that the anomalous expectation values in the correlated state can be extracted from the non-correlated counterparts with the use of the following relation: $\Delta_{ij}^{\sigma\sigma'} = \langle \hat{c}_{i\sigma}\hat{c}_{j\sigma'}\rangle_G = q^2\langle \hat{c}_{i\sigma}\hat{c}_{j\sigma'}\rangle_0$. After determining the correlated pairing amplitudes to all nearest neighbors one can extract the so-called symmetry resolved gap amplitudes corresponding to different pairing symmetries, which are going to be analyzed in the following Section.

3. Results

At first we analyze the results obtained from the negative U-Hubbard model as applied to the $tWSe_2$. As mentioned in the introduction from the experimental perspective the considered twisted bilayer structure is placed in between two electrodes which allows to change the band filling (n) as well as the bias voltage across the bilayer (D) in an *in situ* manner. In order to relate our theoretical results with the available experimental data we have calculated the amplitude of the superconducting gap as a function of both n and D which we show in Fig. 2 for three selected values of U. For relatively large negative U the isotropic *s-wave* SC state appears to be stable in a significant area of the phase diagram. Since U plays the role of the pairing strength, while decreasing it, the superconductivity is becoming less and less robust. In particular, for $U = -6$ meV the SC state survives only in close proximity of the Van Hove singularity line which is marked in blue. For such a case, the high values of density of states generated by the Van Hove singularity are necessary to stabilize superconductivity. For completeness, in Fig. 2 (d) and (e) we show the SC gap as a function of n and D separately along the cuts represented by the red arrows in Fig. 2 (c). Note, that the visible dome-like behavior of the gap amplitude Δ with increasing n and D is in qualitative agreement with the experimental data[18, 17]. This is due to a trivial effect related with the enhancement of the SC pairing by large values of the density of states, which correspond to $n \approx 1$ and $D \approx 0.35$ V/nm. Nevertheless, the calculated phase diagram in Fig. 2 does not reproduce the one observed in experiments. Since in the latter case the appearance of the paired state is reported only close to half-filling, while in the former, superconductivity stays stable around the Van Hove singularity line even away from the $n = 1$ situation.

Next, we analyze the results obtained within the t-J-U model in connection with the Gutzwiller approximation method. The first difference with respect to the previous considerations stems from the fact that here the pairing mechanism has an intersite character, meaning that the resulting SC gap is **k**-dependent and can realize various symmetries. In the case considered, the stable paired state corresponds to a mixed $d + id$ (singlet) and

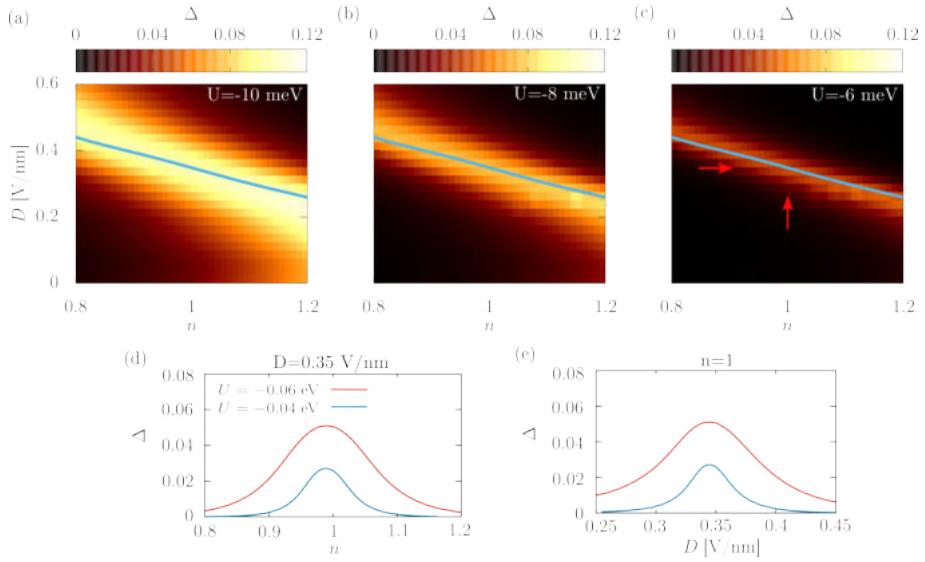

Fig. 2. Superconducting gap amplitude as a function of displacement field (D) and band filling n resulting from the nagative U-Hubbard model for three selected values of the U parameter. The blue solid line marks the evolution of the Van Hove singularity across the phase diagram. In (d) and (e) we show the superconducting gap amplitude as a function of band filling and displacement field, respectively, for two selected values of U along the cuts represented by red arrows in (c).

$p-ip$ (triplet) channel and is topologically non-trivial with Chern number $C = \pm 2, \pm 4$, depending on the particular set of model parameters[25]. In Fig. 3 (a) and (b) we show the calculated singlet and triplet gap amplitudes as a function of band filling for the case of moderate and strong correlations, respectively. As one can see in the former case, also a single SC dome appears similarly as for the negative U-Hubbard model, while in the latter a two-dome structure appears with the SC state being suppressed at half-filling due to the presence of the insulating state. An important difference between this framework and the previous one is that here the strong onsite Coulomb repulsion generates renormalization of subsequent terms of the Hamiltonian [cf. Eq. (8)]. The values of all the renormalization parameters are provided in Figs. 3 (d-f). As can be seen, renormalization is the strongest near half-filling and increases with increasing Coulomb repulsion U. It should be noted that the parameter $\lambda_s^4 > 1$ renormalizes the kintic exchange term that is responsible for pairing, meaning that the correlations work in favor of the SC state stabilization. Nevertheless, for $U/W > 1$ the SC gap is largely suppressed at half filling due to $q^2 \approx 0$ (since $\Delta_{ij}^{\sigma\sigma'} = q^2 \langle \hat{c}_{i\sigma} \hat{c}_{j\sigma'} \rangle$). Therefore, the optimal situation for stabiliza-

tion of the SC state is close to half-filling but in the moderately correlated regime where $U/W \lesssim 1$. For comparison we have carried out calculations with the use of the Hartree-Fock method for $U/W = 1$ by setting all the renormalization parameters to 1, which leads to the resulting SC gap to be few orders of magnitude smaller than the one shown in Fig. 3(a). It should be noted that the effect of Van Hove singularity discussed earlier is going to be operative also here. However, in the moderately correlated regime the half-filled case should create favorable conditions for the appearance of the superconducting state possibly making it especially stable in the close proximity of the $n = 1$ case. This is in contrast with the result presented in Fig. 2 where the value of the SC gap remained unchanged also away from the half-filling provided that D is adjusted to make the Van Hove singularity stay at the Fermi level. As we have shown very recently, after supplementing the considered t-J-U model with a nearest neighbor Coulomb repulsion term, which additionally suppresses the pairing in a large area of the phase diagram[33], the SC state survives only at the crossing of the Van Hove singularity with the half-filling, where the two effects (renormalization and Van Hove singularity) can work simultaneously in favor of the pairing leading to a phase diagram that agrees qualitatively with the experimental data.

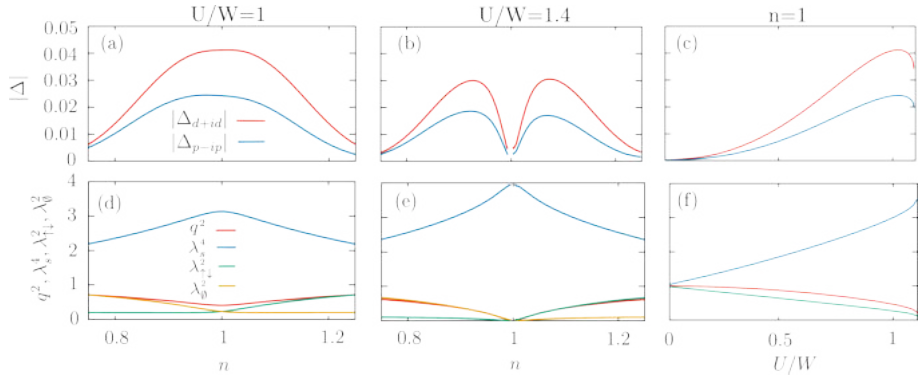

Fig. 3. The gap amplitudes for the obtained mixed singlet-triplet paired state as a function of band filling (a,b) and onsite Coulomb repulsion (c) for one selected value of displacement field $D = 0.35$ V/nm. Note that $W \approx 90$ meV corresponds to the bare band width. In (d-f) we show the corresponding renormalization factors obtained within the Gutzwiller approximation [Eq. (8)].

4. Conclusions

We have compared two distinct approaches to the description of the superconducting phase in a single moiré band of twisted WSe_2. In both

cases, high values of the density of states stabilize superconductivity which creates a tendency for the SC state stability regime to follow the Van Hove singularity line at the (n,D)-phase diagram. For the case of negative U-Hubbard model the paired state realizes a trivial *s-wave* symmetry of the gap and it can become stable even away from the half-filled case provided the displacement field is adjusted so as the high density of states-condition is fulfilled. Such behavior is in contrast with the experimental picture, where the SC state appears as stable only close to the half-filled scenario.

For the case of the t-J-U model calculated with the use of the Gutzwiller approximation method, the pairing appears due to intersite kinetic exchange leading to an exotic $d + id/p - ip$ mixed symmetry state. Moreover, the renormalization effects resulting from a significant onsite Coulomb repulsion can work in favor of the paired state close to half-filling in the moderately correlated state when $U \lesssim W$, for which the Mott insulator is still not well developed. This effect can cause the superconducting pairing to be specifically stable close to half-filling. As shown in more detail in Ref. [33], after the inclusion of the intersite Coulomb repulsion, which suppresses the stability of the superconducting state in a large area of the phase diagram, one obtains a situation in which the SC state survives only at the crossing between the Van Hove singularity line and half-filling at the (n,D) phase diagram. In such a case, the effects of Van Hove singularity as well as correlation induced renormalization can work simultaneously stabilizing the paired phase only in a small area of the phase diagram in qualitative agreement with the experimental observations.

5. Acknowledgment

This work is dedicated to Professor Józef Spałek in recognition of his outstanding contributions to the field of correlated electron systems, as well as his exceptional mentorship. I sincerely thank him for his guidance, support, and the many lessons that have influenced my scientific career (MZ).

This research was supported by the National Science Center, Poland (NCN) according to decision 2021/42/E/ST3/00128.

REFERENCES

[1] Yanhao Tang, Lizhong Li, Tingxin Li, Yang Xu, Song Liu, Katayun Barmak, Kenji Watanabe, Takashi Taniguchi, Allan H Macdonald, Jie Shan, and Kin Fai Mak. Simulation of Hubbard model physics in WSe_2/WS_2 moiré superlattices. *Nature*, 579:353 – 358, 2020.

[2] Zhongdong Han, Yiyu Xia, Zhengchao Xia, Wenjin Zhao, Yichi Zhang, Kenji Watanabe, Takashi Taniguchi, Jie Shan, and Kin Fai Mak. Evidence of topological Kondo insulating state in $MoTe_2/WSe_2$ moiré bilayers, 2025.

[3] Wenjin Zhao, Bowen Shen, Zui Tao, Zhongdong Han, Kaifei Kang, Kenji Watanabe, Takashi Taniguchi, Kin Mak, Fai, and Jie Shan. Gate-tunable heavy fermions in a moiré kondo lattice. *Nature*, 616:61–65, 2023.

[4] Benjamin A. Foutty, Carlos R. Kometter, Trithep Devakul, Aidan P. Reddy, Kenji Watanabe, Takashi Taniguchi, Liang Fu, and Benjamin E. Feldman. Mapping twist-tuned multiband topology in bilayer WSe_2. *Science*, 384(6693):343–347, 2024.

[5] Fan Xu, Zheng Sun, Tongtong Jia, Chang Liu, Cheng Xu, Chushan Li, Yu Gu, Kenji Watanabe, Takashi Taniguchi, Bingbing Tong, Jinfeng Jia, Zhiwen Shi, Shengwei Jiang, Yang Zhang, Xiaoxue Liu, and Tingxin Li. Observation of integer and fractional quantum anomalous hall effects in twisted bilayer $MoTe_2$. *Phys. Rev. X*, 13:031037, Sep 2023.

[6] Fan Zhang, Nicolás Morales-Durán, Yanxing Li, Wang Yao, Jung-Jung Su, Yu-Chuan Lin, Chengye Dong, Xiaohui Liu, Fu-Xiang Rikudo Chen, Hyunsue Kim, Kenji Watanabe, Takashi Taniguchi, Xiaoqin Li, Joshua A. Robinson, Allan H. Macdonald, and Chih-Kang Shih. Experimental signature of layer skyrmions and implications for band topology in twisted WSe_2 bilayers, 2025.

[7] Tingxin Li, Shengwei Jiang, Bowen Shen, Yang Zhang, Lizhong Li, Zui Tao, Trithep Devakul, Kenji Watanabe, Takashi Taniguchi, Liang Fu, Jie Shan, and Kin Fai Mak. Quantum anomalous hall effect from intertwined moiré bands. *Nature*, 600(7890):641–646, December 2021.

[8] Wenjin Zhao, Kaifei Kang, Lizhong Li, Charles Tschirhart, Evgeny Redekop, Kenji Watanabe, Takashi Taniguchi, Andrea Young, Jie Shan, and Kin Fai Mak. Realization of the Haldane Chern insulator in a moiré lattice, 2022.

[9] Palash Saha, Louk Rademaker, and Michał Zegrodnik. Interplay between topology and electron-electron interactions in the moiré $MoTe_2/WSe_2$ heterobilayer. *Phys. Rev. B*, 112:045147, Jul 2025.

[10] Palash Saha and Michał Zegrodnik. Emergent quantum valley hall insulator from electron interactions in transition-metal dichalcogenide heterobilayers, 2025.

[11] Hongyuan Li, Ziyu Xiang, Aidan P. Reddy, Trithep Devakul, Renee Sailus, Rounak Banerjee, Takashi Taniguchi, Kenji Watanabe, Sefaattin Tongay, Alex Zettl, Liang Fu, Michael F. Crommie, and Feng Wang. Wigner Molecular Crystals from Multi-electron Moiré Artificial Atoms, 2023.

[12] Emma C. Regan, Danqing Wang, Chenhao Jin, M. Iqbal Bakti Utama, Beini Gao, Xin Wei, Sihan Zhao, Wenyu Zhao, Zuocheng Zhang, Kentaro Yumigeta, Mark Blei, Johan D. Carlström, Kenji Watanabe, Takashi Taniguchi, Sefaattin Tongay, Michael Crommie, Alex Zettl, and Feng Wang. Mott and generalized wigner crystal states in WSe_2/WS_2 moiré superlattices. *Nature*, 579(7799):359–363, March 2020.

[13] Medha Dandu, Garima Gupta, Pushkar Dasika, Kenji Watanabe, Takashi Taniguchi, and Kausik Majumdar. Electrically tunable localized versus delo-

calized intralayer moiré excitons and trions in a twisted mos2 bilayer. *ACS Nano*, 16(6):8983–8992, 2022. PMID: 35679485.

[14] Haihong Zheng, Biao Wu, Shaofei Li, Junnan Ding, Jun He, Zongwen Liu, Chang-Tian Wang, Jian-Tao Wang, Anlian Pan, and Yanping Liu. Localization-enhanced moiré exciton in twisted transition metal dichalcogenide heterotrilayer superlattices. *Light: Science & Applications*, 12(1):117, May 2023.

[15] Mingfeng Chen, Runtong Li, Haonan Wang, Yuliang Yang, Yiyang Lai, Chaowei Hu, Takashi Taniguchi, Kenji Watanabe, Jiaqiang Yan, Jiun-Haw Chu, Erik Henriksen, Chuanwei Zhang, Li Yang, and Xi Wang. Bichromatic moiré superlattices for tunable quadrupolar trions and correlated states, 2025.

[16] Lei Wang, En-Min Shih, Augusto Ghiotto, Lede Xian, Daniel A. Rhodes, Chengand Tan, Martin Claassen, Dante M. Kennes, Yusong Bai, Bumho Kim, Kenji Watanabe, Takashi Taniguchi, Xiaoyang Zhu, James Hone, Angel Rubio, and Cory R. Pasupathy, Abhay N. amd Dean. Correlated electronic phases in twisted bilayer transition metal dichalcogenides. *Nature Materials*, 19:861, 2020.

[17] Yiyu Xia, Zhongdong Han, Kenji Watanabe, Takashi Taniguchi, Jie Shan, and Kin Fai Mak. Superconductivity in twisted bilayer wse2. *Nature*, 637(8047):833–838, Jan 2025.

[18] Yinjie Guo, Jordan Pack, Joshua Swann, Luke Holtzman, Matthew Cothrine, Kenji Watanabe, Takashi Taniguchi, David G. Mandrus, Katayun Barmak, James Hone, Andrew J. Millis, Abhay Pasupathy, and Cory R. Dean. Superconductivity in 5.0° twisted bilayer wse2. *Nature*, 637(8047):839–845, Jan 2025.

[19] Yiyu Xia, Zhongdong Han, Jiacheng Zhu, Yichi Zhang, Patrick Knüppel, Kenji Watanabe, Takashi Taniguchi, Kin Fai Mak, and Jie Shan. Simulating high-temperature superconductivity in moiré wse2, 2025.

[20] Yinjie Guo, John Cenker, Ammon Fischer, Daniel Muñoz-Segovia, Jordan Pack, Luke Holtzman, Lennart Klebl, Kenji Watanabe, Takashi Taniguchi, Katayun Barmak, James Hone, Angel Rubio, Dante M. Kennes, Andrew J. Millis, Abhay Pasupathy, and Cory R. Dean. Angle evolution of the superconducting phase diagram in twisted bilayer wse2, 2025.

[21] Fan Xu, Zheng Sun, Jiayi Li, Ce Zheng, Cheng Xu, Jingjing Gao, Tongtong Jia, Kenji Watanabe, Takashi Taniguchi, Bingbing Tong, Li Lu, Jinfeng Jia, Zhiwen Shi, Shengwei Jiang, Yuanbo Zhang, Yang Zhang, Shiming Lei, Xiaoxue Liu, and Tingxin Li. Signatures of unconventional superconductivity near reentrant and fractional quantum anomalous hall insulators, 2025.

[22] J. G. Bednorz and K. A. Müller. Possible high T_c superconductivity in the Ba–La–Cu–O system. *Zeitschrift für Physik B: Condensed Matter*, 64:189–193, 1986.

[23] J. Spałek, M. Fidrysiak, M. Zegrodnik, and A. Biborski. Superconductivity in high-tc and related strongly correlated systems from variational perspective: Beyond mean field theory. *Physics Reports*, 959:1–117, 2022.

[24] M. Zegrodnik and A. Biborski. Mixed singlet-triplet superconducting state within the moiré $t-j-u$ model applied to twisted bilayer wse_2. *Phys. Rev. B*, 108:064506, Aug 2023.

[25] Waseem Akbar, Andrzej Biborski, Louk Rademaker, and Michał Zegrodnik. Topological superconductivity with mixed singlet-triplet pairing in moiré transition metal dichalcogenide bilayers. *Phys. Rev. B*, 110:064516, Aug 2024.

[26] Daniele Guerci, Daniel Kaplan, Julian Ingham, J. H. Pixley, and Andrew J. Millis. Topological superconductivity from repulsive interactions in twisted wse_2, 2024.

[27] Chuyi Tuo, Ming-Rui Li, Zhengzhi Wu, Wen Sun, and Hong Yao. Theory of topological superconductivity and antiferromagnetic correlated insulators in twisted bilayer wse_2, 2024.

[28] Lennart Klebl, Ammon Fischer, Laura Classen, Michael M. Scherer, and Dante M. Kennes. Competition of density waves and superconductivity in twisted tungsten diselenide. *Phys. Rev. Res.*, 5:L012034, Mar 2023.

[29] Ammon Fischer, Lennart Klebl, Valentin Crépel, Siheon Ryee, Angel Rubio, Lede Xian, Tim O. Wehling, Antoine Georges, Dante M. Kennes, and Andrew J. Millis. Theory of intervalley-coherent afm order and topological superconductivity in $twse_2$. *Phys. Rev. X*, 15:041055, Dec 2025.

[30] Wei Qin, Wen-Xuan Qiu, and Fengcheng Wu. Topological chiral superconductivity mediated by intervalley antiferromagnetic fluctuations in twisted bilayer wse_2. *Phys. Rev. Lett.*, 135:246002, Dec 2025.

[31] Valentin Crépel, Daniele Guerci, Jennifer Cano, J. H. Pixley, and Andrew Millis. Topological superconductivity in doped magnetic moiré semiconductors. *Phys. Rev. Lett.*, 131:056001, Aug 2023.

[32] Feng Chen and Donna Sheng. Singlet, triplet and pair density wave superconductivity in the doped triangular-lattice moiré system, 2023.

[33] Michał Zegrodnik, Waseem Akbar, Andrzej Biborski, and Louk Rademaker. Optimal superconductivity in twisted bilayer wse_2 where the van hove singularity crosses half-filling, 2025.

[34] Sunghoon Kim, Juan Felipe Mendez-Valderrama, Xuepeng Wang, and Debanjan Chowdhury. Theory of correlated insulators and superconductor at $\nu = 1$ in twisted wse_2, 2025.

[35] Mathieu Bélanger, Jérôme Fournier, and David Sénéchal. Superconductivity in the twisted bilayer transition metal dichalcogenide wse_2: A quantum cluster study. *Phys. Rev. B*, 106:235135, Dec 2022.

[36] Jihang Zhu, Yang-Zhi Chou, Ming Xie, and Sankar Das Sarma. Superconductivity in twisted transition metal dichalcogenide homobilayers. *Phys. Rev. B*, 111:L060501, Feb 2025.

[37] S. Robaszkiewicz, R. Micnas, and K. A. Chao. Hartree theory for the negative-u extended hubbard model: Ground state. *Phys. Rev. B*, 24:4018–4024, Oct 1981.

[38] R. Micnas, J. Ranninger, and S. Robaszkiewicz. Superconductivity in narrow-band systems with local nonretarded attractive interactions. *Rev. Mod. Phys.*, 62:113–171, Jan 1990.

[39] Józef Spałek, Michał Zegrodnik, and Jan Kaczmarczyk. Universal properties of high-temperature superconductors from real-space pairing: $t-j-u$ model and its quantitative comparison with experiment. *Phys. Rev. B*, 95:024506, Jan 2017.

[40] Józef Spałek, Michał Zegrodnik, and Jan Kaczmarczyk. Universal properties of high-temperature superconductors from real-space pairing: $t-j-u$ model and its quantitative comparison with experiment. *Phys. Rev. B*, 95:024506, Jan 2017.

[41] J. Hubbard. Electron correlations in narrow energy bands. *Proceedings of the Royal Society of London. A. Mathematical and Physical Sciences*, 276(1365):238–257, 11 1963.

[42] N. Bulut. d x 2 - y 2 superconductivity and the hubbard model. *Advances in Physics*, 51(7):1587–1667, 2002.

[43] K A Chao, J Spalek, and A M Oles. Kinetic exchange interaction in a narrow s-band. *Journal of Physics C: Solid State Physics*, 10(10):L271, may 1977.

[44] Masao Ogata and Hiroshi Fukuyama. The t-j model for the oxide high-tc superconductors. *Reports on Progress in Physics*, 71(3):036501, March 2008.

[45] Haining Pan, Fengcheng Wu, and Sankar Das Sarma. Band topology, hubbard model, heisenberg model, and dzyaloshinskii-moriya interaction in twisted bilayer wse_2. *Phys. Rev. Res.*, 2:033087, Jul 2020.

[46] Jörg Bünemann, Tobias Schickling, and Florian Gebhard. Variational study of fermi surface deformations in hubbard models. *Europhysics Letters*, 98(2):27006, apr 2012.

[47] J. Kaczmarczyk. Comparison of two approaches for the treatment of gutzwiller variational wave functions. *Philosophical Magazine*, 95(5-6):563–573, 2015.

4.4 Unconventional superconductivity in the presence of long-range interactions in transition metal dichalcogenide moiré heterobilayers

In this work, we present a detailed theoretical investigation of unconventional SC in WS_2/WSe_2 heterobilayer particularly focusing on the role of long range interactions in different correlated regimes. Our analysis examines whether SC can be stabilized in WS_2/WSe_2 heterobilayers, where strong electronic correlations and long-range Coulomb repulsion are believed to play a dominant role. Unlike the $tWSe_2$ homobilayer, which is considered moderately correlated with $U/W \approx 1$, the heterobilayer is expected to reside deeper in the strongly correlated regime ($U/W > 1$). Our study employs extended t-J-U and t-J models to capture the single particle physics of moiré flat bands and correlation induced effects within the Gutzwiller approximation.

As we show in our study, SC survives only in the strongly correlated regime near half filling. Specifically, the effective strength of the exchange interaction is enhanced, while the effect of the V term is reduced near half filling, thereby stabilizing the paired state. This mechanism allows SC to persist even for relatively large V, which correspond to realistic estimates for WS_2/WSe_2 heterobilayers, where $U/V \approx 3$. In this regime, the system develops a two dome superconducting phase structure separated by a Mott insulating state, closely resembling features known from high T_c cuprates [25]. The role of long range hopping and exchange interactions is also carefully examined. Longer range exchange couplings have little effect on the stability of the SC phase, second and third nearest neighbor hoppings reduce the density of states near E_F and thus weaken the pairing strength. Nonetheless, the fundamental character of the superconducting order parameter remains unchanged, with the $p-ip$ triplet component being dominant. This robustness indicates that the real space pairing scenario is stable even when the additional terms are included in the effective Hamiltonian. The superconducting state has a non zero Chern number $C = -4$, indicating its topological nature.

Finally, our numerical calculations indicate that unconventional SC in WS_2/WSe_2 heterobilayers is a realistic possibility in the strongly correlated regime. The persistence of SC against strong V results from the renormalization effects induced by correlations, which simultaneously suppress the detrimental V term and amplify the pairing contribution from exchange. These findings emphasize that the WS_2/WSe_2 heterobilayer, despite lacking direct experimental observation of SC so far, is a highly promising platform for realizing and tuning exotic superconducting states. Experimental verification will likely require probing in the

low-temperature regime (below 1 K) and at carrier concentrations close to half filling, where strong correlation effects are maximized.

 Originally published as W. Akbar, A. Biborski, L. Rademaker, and M. Zegrodnik, *Scientific Reports* (2026) 16:10611. DOI: 10.1038/s41598-026-45510-4.

scientific reports

Check for updates

OPEN

Unconventional superconductivity in the presence of long-range interactions in transition metal dichalcogenide moiré heterobilayers

Waseem Akbar[1], Andrzej Biborski[1], Louk Rademaker[2,3] & Michał Zegrodnik[1]✉

Transition-metal dichalcogenide (TMD) moiré systems have recently garnered much attention as platforms for studying electron-correlation-induced effects as well as unconventional superconductivity (SC). Here we analyze the principal features of the unconventional superconducting state in a TMD moiré flat band in the strongly correlated regime and in the presence of significant intersite Coulomb repulsion as well as long-range hopping and exchange interaction terms. In our study, we use the extended versions of both the *t-J-U* and *t-J* models and apply the Gutzwiller approximation method to incorporate the effects of electron-electron interactions. We show that in the strongly correlated regime and close to half-filling, the superconducting state is strongly immune to the negative effect of the *V*-term on the pairing, and shows a two-dome behavior with a Mott insulating state residing at half-filling. We explain this result as originating from relatively strong renormalization of the intersite interaction terms, caused by the significant value of the onsite Coulomb repulsion. As we show, this mechanism allows the superconductivity to persist even for relatively large values of *V*, which are characteristic for the WS_2/WSe_2 heterobilayer. Such a result emphasizes the potential of the WS_2/WSe_2 heterobilayer as another candidate for unconventional SC in the family of moiré flat band systems.

Keywords Unconventional superconductivity, Electronic correlations, Longer range interactions, Transition metal dichalcogenides, Moiré systems

The moiré transition-metal dichalcogenide (TMD) bilayers have emerged as a versatile platform for studying the correlated and topological phases of matter. It has been reported experimentally that those systems host rich physics and are characterized by a high degree of tunability. The examples of recently evidenced exotic correlated phases in this family of systems are: Mott insulating states[1,2], generalized Wigner crystals[3,4], quantum anomalous Hall insulators[5–7] as well as unconventional superconductivity[2,8,9].

The appearance of moiré pattern of atoms in TMD bilayers can result from rotational misalignment, such as in twisted WSe_2 homobilayer ($tWSe_2$), or due to lattice mismatch between two layers of different kind, like in the WS_2/WSe_2 heterobilayer[10,11]. One common feature of moiré systems is the appearance of flat electronic bands[12] which are believed to be responsible for the observed electron correlation effects. This situation resembles the one known from the so-called copper based high-temperature superconductors (HTS) in which both the Mott insulating state and dome-like superconductivity has been reported already some time ago. The first signatures of the superconducting state in TMD moiré systems have been reported by Wang et al for the case of $tWSe_2$[2]. Very recently strong evidence of the paired state has been shown for the same system in three other experimental papers[8,9,13]. It is believed that $tWSe_2$ is in the moderately correlated regime, with the onsite Coulomb integral being comparable to the flat band width ($U \approx W$)[2,14]. However, the actual strength of electron-electron correlations is influenced by the twist angle, the dielectric environment of the sample, and the so-called displacement field[14].

[1]Academic Centre for Materials and Nanotechnology, AGH University of Krakow, Al. Mickiewicza 30, 30-059 Krakow, Poland. [2]Department of Theoretical Physics, University of Geneva, 1211 Geneva, Switzerland. [3]Institute-Lorentz for Theoretical Physics, Leiden University, PO Box 9506, 2300 Leiden, The Netherlands. ✉email: michal.zegrodnik@agh.edu.pl

Another example of a TMD moiré system, which bears some significant similarities with $tWSe_2$, is the WS_2/WSe_2 heterobilayer. In this case, it is believed that the U/W factor should be larger than in the previous case meaning that the electron correlations are stronger[15,16]. Moreover, the observation of both the Mott insulating state at half-filling as well as the generalized Wigner-Mott crystals at fractional fillings have been reported in recent years[17–21]. This indicates that not only the onsite repulsion but also the longer ranged Coulomb interaction plays a central role. It should be noted that superconductivity has not been reported as of yet for the case of the WS_2/WSe_2 heterobilayer.

When it comes to theoretical description of TMD moiré bilayers, the usual starting point is based on the continuum model describing the topmost valley bands of the two layers (in terms of the effective mass approximation) as well as the moiré potential and interlayer tunneling[14,22]. The resulting many-band structure can than be mapped onto a few selected bands leading to a low-energy effective model. In order to take into account effects related with electronic correlations such approach has to be supplemented with interaction terms leading to a Hubbard-like description. So far, the effective single-, two-, and three-band models have been analyzed for the TMD based moiré systems[14,22–24]. Moreover, motivated by the experimental observation of SC in $tWSe_2$, different pairing mechanisms have been studied theoretically based on the paradigm of strong electronic correlations[25], interlayer excitonic effects[26], or spin fluctuations in weak-to-moderate correlated regime[24,27].

In our previous study, we have analyzed the fundamental features of the paired state within effective single band models (*t-J*, *t-J-U*, and Hubbard) applied to the description of the $tWSe_2$ system[28–31] in which superconductivity has been experimentally reported in recent years[2,8,9]. According to our analysis, the effective description of the homobilayer case leads to an exotic form of the superconducting state with mixed $d + id$-*wave* singlet and $p - ip$-*wave* triplet symmetry of the gap. Moreover, the paired state shows a non-trivial topology with the Chern number being $C = \pm 4, \pm 2$ depending on the value of the perpendicular electric field (so-called displacement field). Also, depending on the specifics of the model, both single- and two-dome behavior of the superconducting phase has been obtained.

Here we extend our previous analysis by taking into account the intersite Coulomb repulsion as well as long-range hopping and exchange interaction terms both within the *t-J-U* and *t-J* models. Moreover, due to the similarities between the theoretical description of $tWSe_2$ and WS_2/WSe_2, we analyze here the possibility of the appearance of paired states in the latter, which has not yet been reported experimentally. The additional motivation for considering the heterobilayer case is that both experimental observations and theoretical analysis indicate that in this system both onsite and intersite Coulomb repulsion play significant role[15–19,21,32]. Therefore, we aim at determining the influence of such circumstance on the paired state and most importantly analyze if the considered unconventional superconducting state can still persist in the range of significant values of the intersite Coulomb integral within the real-space pairing scenario.

According to our analysis focused on the heterobilayer case, the SC state is predominantly of triplet character with the stability regime residing mainly on the hole doped side of the phase diagram which is in contrast with the homobilayer scenario. Also, pairing appears to be significantly immune to the destructive effect of the inter-site Coulomb term for relatively large values of U and close to half filling where the correlations are the strongest. This allows for the formation of the SC state in the parameter regime corresponding to the WS_2/WSe_2 heterobilayer. We explain this result as originating from relatively strong renormalization of the intersite interaction terms, caused by the significant value of the onsite Coulomb repulsion. These findings suggest that the WS_2/WSe_2 heterobilayer can be considered as a promising platform to realize unconventional superconductivity. However, this would require some fine tuning of the electron-electron correlation strength, possibly by applying a twist between the layers and/or proper selection of the dielectric environment of the system.

Model and method

We start with the effective single band *t-J-U-V* Hamiltonian of the general form

$$\hat{H} = \hat{H}_0 + \hat{H}_J + \hat{H}_{UV}, \tag{1}$$

with the first term being the single-particle part

$$\hat{H} = \sum_{\langle ij \rangle \sigma} t_{ij\sigma}\, \hat{c}^{\dagger}_{i\sigma} \hat{c}_{j\sigma}, \tag{2}$$

where $\hat{c}^{\dagger}_{i\sigma}$ and $\hat{c}_{i\sigma}$ are the creation and annihilation operators of an electron with spin $\sigma = \{1, -1\}$ occupying a moiré orbital located at site i of a triangular lattice. The hopping parameters, $t_{ij\sigma}$, to the l-th nearest neighbor can be expressed in the following form

$$t_{ij\sigma} = |t_l| e^{i\sigma\nu_{ij}\phi_l}, \tag{3}$$

with $\nu_{ij} = \pm 1$, depending on the direction of the bond. The resulting complex phase of the hoppings have opposite sign for opposite hopping direction, fulfilling the Hermiticity condition ($t_{ij\sigma} = t^{*}_{ji\sigma}$) and threefold rotational symmetry (C_3) condition. Additionally, by changing the spin to the opposite one also has to reverse all the signs of the phases, which results from the time-reversal symmetry requirement ($t_{ij\sigma} = t^{*}_{ij\bar{\sigma}}$). In the following we take into account maximally up to the third nearest-neighbor hoppings.

A single particle Hamiltonian of the form given by Eq. (2) can be used as an effective tight binding representation of the flat valence band of a TMD heterobilayer. This has been shown by using a continuum model approach for the WSe_2/WS_2 system [22]. It should be noted that a single TMD monolayer (WX_2 with X =

S, Se) creates a hexagonal lattice with C_3 rotational symmetry and corresponds to a relatively large direct band gap at the K and K' points. After two different TMD monolayers are joint in a heterobilayer a moiré pattern emerges with a new lattice constant $a_M = 1/\sqrt{\frac{1}{a_1^2} + \frac{1}{a_2^2} - \frac{2\cos\theta}{a_1 a_2}}$ (where a_1 and a_2 are the monolayer lattice constants and θ is the twist angle). Moreover, a mini Brillouin zone is created with the high-symmetry points $\gamma = (0,0)$, $\kappa = (\frac{4\pi}{3a_M}, 0)$, $\kappa' = (\frac{2\pi}{3a_M}, \frac{2\pi}{\sqrt{3}a_M})$. Because the two monolayers have different band gaps, the top of the valence band of the resulting structure consists of states localized in a single layer. Within the continuum model approach, the valence band states can be described per spin/valley, by using a moiré potential $V(\mathrm{r})$. This leads to the following continuum Hamiltonian[22]

$$H = -\frac{\hbar^2 \mathrm{Q}^2}{2m^*} + V(\mathrm{r}), \quad V(\mathrm{r}) = \sum_{\mathrm{g}_i} V_j \exp[i\,\mathrm{g}_i \mathrm{r}], \tag{4}$$

where Q is the momentum relative to the K and $\mathbf{K}'$ points of the monolayer and $\mathrm{g}_j = 4\frac{\pi}{\sqrt{3}}(-\sin\frac{2\pi(j-1)}{6}, \cos\frac{2\pi(j-1)}{6})$ are the reciprocal moiré vectors. Due to the C_3 symmetry of the moiré lattice one obtains: $V_1 = V_3 = V_5$ and $V_2 = V_4 = V_6 = V_1^*$. After carrying out a proper momentum backfolding procedure to the moiré mini-Brillouin zone, the moiré band structure can be calculated and than used during the Wannierization procedure to obtain the absolute values and the complex phases of the hoppings appearing in Eq. (2). The following values have been obtained in Ref.[22] for the top valence moiré flat band of the aligned AA-stacking of the WSe_2/WS_2 heterobilayer with the contunuum model parameters $(V, \psi) = (7.8\,\mathrm{meV}, -106^\circ)$, where $V_1 = Ve^{i\psi}$,

$$\begin{aligned} |t_1| &= 1.81\,\mathrm{meV}; \quad \phi_1 = 2\pi/3, \\ |t_2| &= 0.28\,\mathrm{meV}; \quad \phi_2 = \pi, \\ |t_3| &= 0.11\,\mathrm{meV}; \quad \phi_3 = \pi/3. \end{aligned} \tag{5}$$

For the sake of completeness, the resulting dispersion relation together with the density of states of the top valence moiré band is shown in Fig. 1. It should be emphasized that such single band description corresponds to the absence of a perpendicular electric field. In such case the top moiré band consists of states originating exclusively from one of the layers and it is separated by a gap from the remaining bottom bands. Since we are focused on studying the fundamental features of the superconudcitng phase in the range of partially filled upper band (between $n = 0.5$ and $n = 1.2$) the single band approach should be sufficient. However, for considering the situation with non-zero displacement fields when the lower moiré bands are pushed towards the top one, a multi-band description would be more appropriate since significant band mixing takes place. For example, it has been shown for TMD heterobilayers that above some value of the displacement field an anomalous Quantum Hall state can be formed[5] which can be reproduced only within a minimal two-band model[33,34].

The second term in Eq. (1) introduces the exchange interactions and has the following form

$$\hat{H}_J = \sum_{\langle ij \rangle}{}' J_{ij} \left(\hat{S}_i^z \hat{S}_j^z + \cos(2\phi_{ij\uparrow}) \sum_{\alpha=x,y} \hat{S}_i^\alpha \hat{S}_j^\alpha + \sin(2\phi_{ij\uparrow})(\hat{\mathbf{S}}_i \times \hat{\mathbf{S}}_j) \cdot \hat{z} \right), \tag{6}$$

where $\hat{\mathbf{S}}_i = (\hat{S}_i^x, \hat{S}_i^y, \hat{S}_i^z)$ is the spin-$\frac{1}{2}$ operator and $\phi_{ij\uparrow}$ is the complex phase corresponding to spin-up hopping between i and j lattice sites. As one can see in the above equation, the exchange interaction term is supplemented by the Dzyaloshinskii-Moriya term which results from the fact that the phases of the hoppings are spin-dependent. The primed summation means that each bond appears only once. In the following we take into

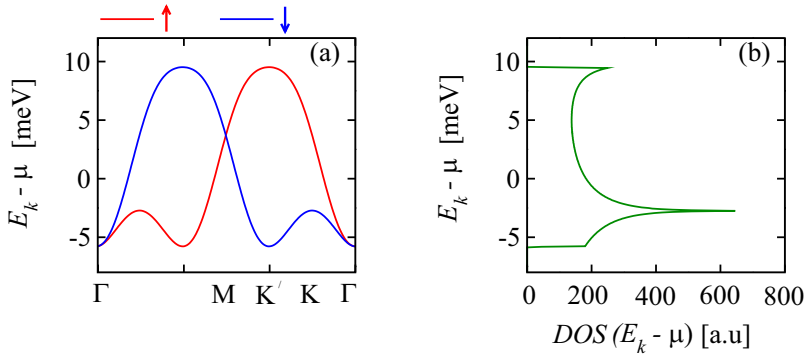

Fig. 1. Dispersion relation (**a**) and the density of states (**b**) resulting from the single particle part of our Hamiltonian ($\hat{H}_0$), with the inclusion of hoppings up to the third nearest neighbor. Zero energy on the vertical axis corresponds to Fermi energy level for the half-filled case. Note that the van Hove singularity is accessible for the hole-doped situation.

account maximally up to the third nearest neighbor exchange interaction terms. We will use the notation within which J_1, J_2, and J_3 correspond to the first, second, and third nearest neighbor exchange interaction integral. In our calculations the value of J_l is determined by the equation

$$J_l = \frac{4|t_l|^2}{U}, \tag{7}$$

where U is the onsite Coulomb repulsion (cf. below).

The last term of our Hamiltonian corresponds to both onsite and intersite Coulomb repulsion terms, i.e.,

$$\hat{H}_{UV} = U \sum_i n_{i\uparrow} n_{i\downarrow} + V \sum_{\langle ij \rangle}{}' n_i n_j, \tag{8}$$

where $\hat{n}_{i\sigma} = \hat{c}^{\dagger}_{i\sigma}\hat{c}_{i\sigma}$ is the occupation operator at site i for an electron with spin σ, and $\hat{n}_i = \hat{n}_{i\uparrow} + \hat{n}_{i\downarrow}$ is the total occupation operator at site i. The U- and V- terms correspond to onsite and intersite Coulomb repulsion, respectively. It should be emphasized that in this study we include onsite U, nearest-neighbor V, as well as hopping and exchange up to third neighbors. For the sake of simplicity, we use the term "long-range" in reference to all the terms that are beyond onsite, but it does not correspond to a truly long-range Coulomb tail.

In the following Section we study the moderately ($U \approx W$) and strongly correlated regime ($U \gg W$) of the model with the emphasis placed on the latter. Eq. (7) originates from the strong coupling expansion; therefore, the J values should be considered as well defined for the case of $U \gg W$. At the same time for $U \approx W$ the spin-spin kinetic exchange interaction already begins to develop; however, its strength might be weaker. Hence, in the moderately correlated regime, Eq. (7) should be regarded as an effective parameterization of the exchange interaction, and the results in this regime should be viewed as qualitative. Deviations of the effective exchange from Eq. (7), or an explicit dependence of J on the intersite interaction V, would mainly shift the quantitative boundaries of the obtained phase diagrams but are not expected to change the overall physical trends discussed in this work. Moreover, the main conclusion of our study presented in the following Section is related with the strongly correlated regime where Eq. 7 is much more justified.

It should be noted that an effective low-energy model of similar structure as described above can be applied to the description of the twisted WSe_2 homobilayer which was studied by us previously and for which superconductivity has been identified experimentally. As already mentioned due to similarities between the two systems it is reasonable to analyze if the superconducting state can also appear in the heterobilayer case. However, there are also differences between the heterobilayer and homobilayer situations. Within the single-band picture applied here, those differences lie in the values of the complex hopping parameters, the resulting band width and the distribution of the density of states as a function of band filling. Moreover, for the case of WSe_2/WS_2, the onsite Coulomb repulsion is considered to be larger (stronger correlations) and most importantly the longer-ranged interactions are significantly more pronounced (larger values of V). As we show in the following Section all those aspects have influence on the stability and the character of the superconducting state.

Since the considered system corresponds to a situation for which $U \gtrsim W$, where W is the bare bandwidth, we should take into account the electron-electron correlation effects by going beyond the simple mean-field approach. In order to do that, we utilize the variational wave function of the Gutzwiller type which has the following form

$$|\Psi_G\rangle = \hat{P}|\Psi_0\rangle. \tag{9}$$

Here, $|\Psi_0\rangle$ represents the non-correlated (mean-field) state, and $\hat{P}$ denotes the correlation operator.

$$\hat{P} = \prod_i \sum_{\Gamma} \lambda_{i,\Gamma} |\Gamma\rangle_{i\,i}\langle\Gamma|. \tag{10}$$

In this expression, the index i iterates over all lattice sites, while $|\Gamma\rangle$ belongs to the set $\{|\emptyset\rangle, |\uparrow\rangle, |\downarrow\rangle, |\uparrow\downarrow\rangle\}$, and $\lambda_{i,\Gamma}$ represent the respective variational parameters. Previous studies have demonstrated[35] that for this particular form of the correlation operator, it is advantageous to impose an additional condition on the $\hat{P}_i$ operator, namely:

$$\hat{P}_i^2 = 1 + x\hat{d}_i^{HF}, \tag{11}$$

where $\hat{d}_i^{HF} = \hat{n}_{i\uparrow}^{HF}\hat{n}_{i\downarrow}^{HF}$, $\hat{n}_{i\sigma}^{HF} = \hat{n}_{i\sigma} - n_{i\sigma}$, with $n_{i\sigma} = \langle\Psi_0|\hat{n}_{i\sigma}|\Psi_0\rangle$, and x represents another variational parameter. It can be easily demonstrated that the relation between the x and the λ parameters appearing in Eq. (10) is the following

$$\begin{aligned} \lambda_{\uparrow\downarrow}^2 &= 1 + x(1-n_s)^2, \\ \lambda_s^2 &= 1 - xn_s(1-n_s), \\ \lambda_{\emptyset}^2 &= 1 + xn_s^2, \end{aligned} \tag{12}$$

where for simplicity we have assumed a homogeneous system devoid of any magnetic or charge ordering. Consequently, we have $\lambda_{i,\Gamma} \equiv \lambda_\Gamma$ and $\lambda_\uparrow = \lambda_\downarrow \equiv \lambda_s$, $n_{i\uparrow} = n_{i\downarrow} \equiv n_s$. As one can see from Eq. 12 one can treat x as the only variational parameter which determines the values of all the λ parameters.

Next, in order to obtain the formula for the expectation value of our Hamiltonian,

$$E_G = \frac{\langle \Psi_G | \hat{H} | \Psi_G \rangle}{\langle \Psi_G | \Psi_G \rangle} = \langle \hat{H} \rangle_G, \tag{13}$$

we utilize the diagrammatic expansion of the Gutzwiller wave function (DE-GWF)[36] in the zeroth order, which is equivalent to the Statistically Consistent Gutzwiller Approximation (SGA)[37]. Consequently, we obtain

$$\begin{aligned}
\langle \hat{H}_0 \rangle_G &= \sum_{ij} q^2 t_{ij\sigma} \langle \hat{c}^\dagger_{i\sigma} \hat{c}_{j\sigma} \rangle_0, \\
\langle \hat{H}_J \rangle_G &= \lambda_s^4 {\sum_{\langle ij \rangle}}' J_{ij} \left(\frac{1}{2} \sum_\sigma e^{i\sigma 2\phi_{ij}} \langle \hat{c}^\dagger_{i\sigma} \hat{c}_{i\bar{\sigma}} \hat{c}^\dagger_{j\bar{\sigma}} \hat{c}_{j\sigma} \rangle_0 + \frac{1}{4} \sum_{\sigma\sigma'} \sigma\sigma' \langle \hat{n}^{HF}_{i\sigma} \hat{n}^{HF}_{j\sigma'} \rangle_0 \right), \\
\langle \hat{H}_{UV} \rangle_G &= \lambda^2_{\uparrow\downarrow} U \sum_i \langle n_{i\uparrow} n_{j\downarrow} \rangle_0 + V {\sum_{\langle ij \rangle}}' \left((1 - g_v^2) \langle \hat{n}_i \rangle_0 \langle \hat{n}_j \rangle_0 + g_v^2 \langle \hat{n}_i \hat{n}_j \rangle_0 \right).
\end{aligned} \tag{14}$$

where,

$$\begin{aligned}
q &= \lambda_s \left(\lambda_d n_s + \lambda_\emptyset (1 - n_s) \right), \\
g_v &= 1 + x n_s (1 - n_s),
\end{aligned} \tag{15}$$

and $\langle \hat{o} \rangle_0$ represents the expectation value of the operator $\hat{o}$ in state $|\psi_0\rangle$. Employing the standard Wick's theorem decomposition allows us to express all four-operator expectation values that appear on the right-hand side of the equations above. As one can see from Eq. (14) the expectation value of the total energy in the correlated state ($|\Psi_G\rangle$) can be expressed in terms of the expectation values in the non-correlated state ($|\Psi_0\rangle$). By comparing the Hamiltonian given by Eq. (1) and its expectation value in the Gutzwiller correlated state, one can distinguish between the original bare hopping amplitudes $t_{ij\sigma}$ and the renormalized correspondants determined by $q^2 t_{ij\sigma}$. Similarly, the bare interaction parameters J, U, V are going to be renormalized by the λ_s^4, $\lambda^2_{\uparrow\downarrow}$, and g_v^2 factors, respectively. Through such renormalization, the effects related with electron-electron interactions are taken into account. Eventually, the resulting E_G becomes dependent on the variational parameter x, on the average number of particles, n_s, as well as the mean field parameters for electron hopping and Cooper pairing

$$P_{ij\sigma} = \langle \hat{c}^\dagger_{i\sigma} \hat{c}_{j\sigma} \rangle_0, \quad S^{\sigma\sigma'}_{ij} = \langle \hat{c}_{i\sigma} \hat{c}_{j\sigma'} \rangle_0, \tag{16}$$

It is important to recognize that the expectation values in the non-correlated state, along with the variational parameters, determine the corresponding expectation values in the correlated state. Specifically,

$$\begin{aligned}
\Delta^{\sigma\sigma'}_{ij} &= \langle \hat{c}_{i\sigma} \hat{c}_{j\bar{\sigma}} \rangle_G = q^2 \langle \hat{c}_{i\sigma} \hat{c}_{j\sigma'} \rangle_0, \\
\Lambda_{ij\sigma} &= \langle \hat{c}^\dagger_{i\sigma} \hat{c}_{j\sigma} \rangle_G = q^2 \langle \hat{c}^\dagger_{i\sigma} \hat{c}_{j\sigma} \rangle_0.
\end{aligned} \tag{17}$$

In our analysis, we consider $S^{\uparrow\downarrow}_{ij}$ and $S^{\downarrow\uparrow}_{ij}$ separately, allowing for both pure spin-singlet pairing ($S^{\uparrow\downarrow}_{ij} = -S^{\downarrow\uparrow}_{ij}$), pure spin-triplet pairing ($S^{\uparrow\downarrow}_{ij} = S^{\downarrow\uparrow}_{ij}$), as well as their combination ($|S^{\uparrow\downarrow}_{ij}| \neq |S^{\downarrow\uparrow}_{ij}|$). Meanwhile, we disregard the possibility of $\uparrow\uparrow$ and $\downarrow\downarrow$ pairing, as the pairing mechanism is based on the kinetic exchange term, which exhibits an antiferromagnetic nature. Additionally, pairing channels with $S^z = \pm 1$ would result in a mismatch of Fermi wave vectors, which is detrimental to the formation of the superconducting state.

To determine the values of the mean fields, we utilize the Effective Hamiltonian Scheme[38]. More details of the approach are provided in Appendix. It entails minimizing the ground state energy (13) and results in an effective Hamiltonian which can than be treated in a standard manner analogous to the Bogoliubov-de Gennes approach as shown by us in Ref.[29]. This leads to a set of self-consistent equations governing the mean-field parameters [Eq. (16)] as well as an additional condition for the minimization of energy in the variational parameter x. Through a numerical solution of the set of self-consistent equations, we ascertain the hopping and pairing amplitudes for the six nearest neighbors in the non-correlated state. Subsequently, to derive the correlated state counterparts, we employ Eq. (17). Similarly to our previous investigations[28,29], we discern the symmetry of the resulting paired state by converting the six real-space nearest neighbor pairing amplitudes into six symmetry-resolved pairing amplitudes.

Within the described procedure which we apply for the t-J-U-V Hamiltonian, the number of double occupancies can be non-zero, however, it is suppressed significantly by the presence of the onsite U-term via the

minimization procedure over the variational parameter x. On the other hand, for the case of the t-J-V model which should be considered as describing a large U-limit, the double occupancies are completely projected out. This requires the x parameter to have a particular value which depends only on n_s via the following equations

$$\begin{aligned} &\text{for } n_s < 0.5 : \lambda_{\uparrow\downarrow} = 0 \Rightarrow x = -\frac{1}{(1-n_s)^2}, \\ &\text{for } n_s > 0.5 : \lambda_{\emptyset} = 0 \Rightarrow x = -\frac{1}{n_s^2}. \end{aligned} \tag{18}$$

By fulfilling above equations we impose the constraint that below (above) half-filling the doublons (holons) are prohibited.

Results

Superconductivity in the *t-J-U-V* model

The actual values of the onsite (U) and intersite (V) Coulomb repulsion integrals of our model depend on the dielectric environment of the sample and are very difficult to be determined exactly. However, the experimental observation of the generalized Wigner crystals and Mott insulating states in WS_2/WSe_2 heterobilayers indicates at least $U \gtrsim W$ ($W \approx 16.3$ meV) and a significant value of the parameter $V \gg t$[17–19,21,32]. More concrete experimental estimates of the onsite Coulomb repulsion give $U \approx 20 - 30$ meV[19,39]. At the same time, a rough estimate can also be determined by using the following equation $U \approx e^2/(4\pi\epsilon_0\epsilon_{\text{eff}}L)$, where, $L = 8$ nm corresponds to angle-aligned moiré lattice constant ($\approx$ Wannier orbital size scale), and $\epsilon_{\text{eff}} \approx 3 - 5$ (for hBN[19]). This leads to $U \approx 36 - 60$ meV. Furthermore, according to previous theoretical estimates, one should consider $U/V \approx 3$[15] as realistic.

In the following we examine the properties of an angle-aligned system in the absence of the displacement field as a function of both U and V. In our discussion we focus mainly on the strongly correlated regime with $30\,\text{meV} \lesssim U \lesssim 40\,\text{meV}$ and the $V = U/3$ case. Nevertheless, one should keep in mind that the actual values of the Coulomb interaction strength can be tuned experimentally by applying an additional twist angle (smaller angles lead to larger U) and changing the dielectric environment of the sample (stronger screening gives smaller U).

We start with the calculated gap amplitudes as a function of n in Fig. 2 for three selected values of U which correspond to the moderately correlated regime with $U \lesssim W$ (a), and $U \gtrsim W$ (b), as well as to the strongly correlated regime with $U > W$ (c). In this particular case we set $V = 0$ and we take into account only the nearest neighbor hopping and exchange interaction terms, as the starting point of our analysis. Influence of those additional factors is going to be analyzed later on. For each value of U we determine J by using the formula $J = 4|t|^2/U$.

As one can see, the obtained solution represents a mixture of *d+id* (singlet) and *p-ip* (triplet) symmetry of the gap. This situation is similar to the one which we have obtained previously in Ref.[28,29] where the $tWSe_2$ homobilayer has been considered. Nevertheless, here the dominant contribution comes from the triplet pairing. As one can see for the strongly correlated case (c), the superconducting order parameter is suppressed at half-filling, which is caused by the presence of the Mott insulating state. On the other hand, in the moderately correlated regime (a,b) a single superconducting dome appears which covers the half-filled situation and now the Mott insulating state is absent. The maximum of the pairing amplitudes seen in the low concentrations regime corresponds to the van Hove singularity, where the high value of the density of states enhances SC. Moreover, according to the numerical determination of the Chern number, the obtained SC state is topologically non-trivial. The Chern number is evaluated following exactly the same procedure as adopted in our previous work[29] where the Bogoliubov–de Gennes Hamiltonian is constructed in momentum space and the Chern number is computed from the occupied (negative-energy) BdG bands using the Brillouin zone triangulation method[40].

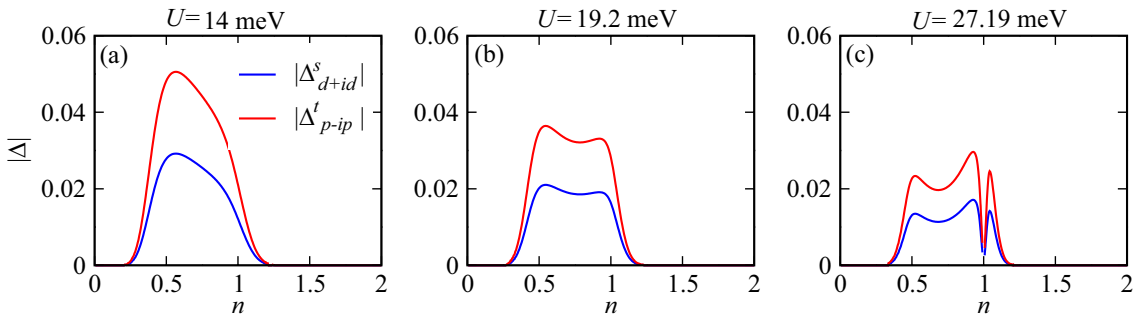

Fig. 2. Symmetry resolved superconducting gap amplitudes corresponding to the spin-singlet $d + id$ and spin-triplet $p - ip$ symmetries as functions of band filling n for selected values of the on-site Coulomb repulsion $U = 14$ meV ($J = 0.936$ meV) (**a**), $U = 19.2$ meV ($J = 0.682$ meV) (**b**) and $U = 27.19$ meV ($J = 0.482$ meV) (**c**). The results have been obtained with the inclusion of the nearest neighbor hoppings and exchange interaction terms only.

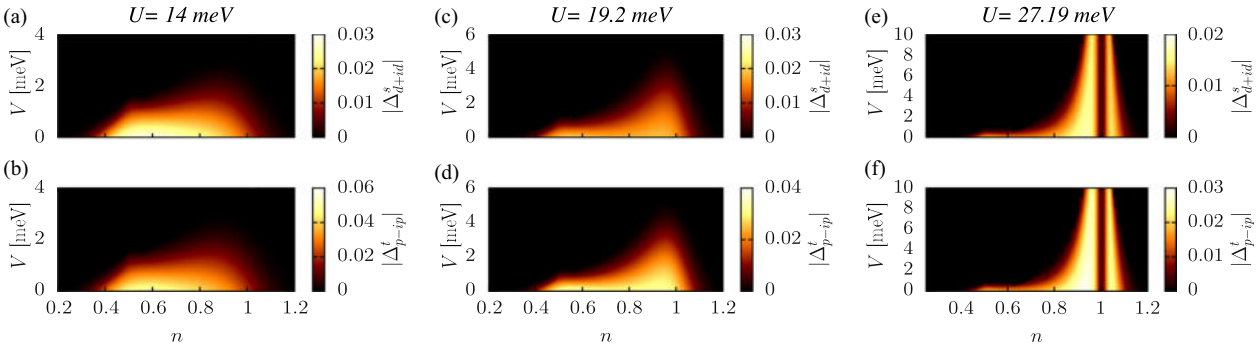

Fig. 3. Symmetry resolved superconducting gap amplitudes for the spin-singlet $d + id$ and spin-triplet $p - ip$ pairing as a function of band filling n and intersite Coulomb integral V for selected values of the on-site Coulomb repulsion $U = 14$ meV ($J = 0.936$ meV) (**a**, **b**), $U = 19.2$ meV ($J = 0.682$ meV) (**c**, **d**), and $U = 27.19$ meV ($J = 0.482$ meV) (**e**, **f**).

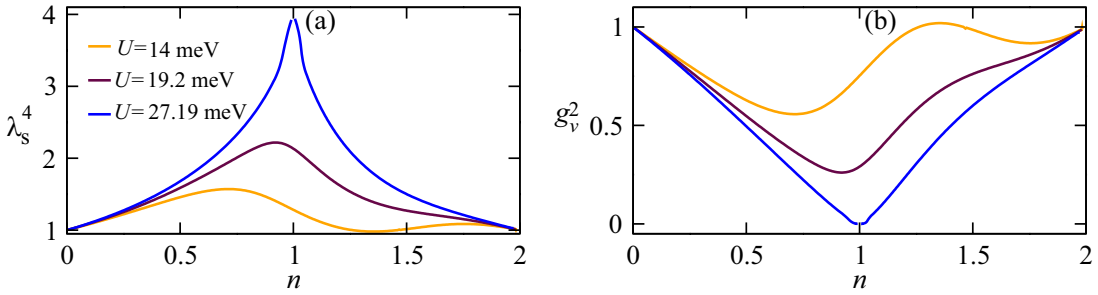

Fig. 4. The renormalization parameters which correspond to the exchange interaction term (**a**) and the intersite Coulomb repulsion term (**b**) for three selected values of the onsite Coulomb repulsion term (shown in the Figure). The results correspond to the $V = 10$ meV situation within the *t*-*J*-*U*-*V* model.

The obtained value of the Chern number $C = -4$ persists throughout the entire obtained stability region of the superconducting phase in all the cases considered in the present work.

Subsequently, we analyze the influence of the intersite Coulomb repulsion term ($\sim V$) on the superconducting state. In Fig. 3 we show both the spin-singlet and spin-triplet gap amplitudes as functions of n and V again for the three selected values of U. As one can see from Fig. 3, the intersite Coulomb repulsion term suppresses the pairing. Such situation is expected since we are considering a real-space pairing scenario in which the opening of the gap in the superconducting state results from nonzero nearest neighbor intersite pairing amplitudes defined by Eq. (17). Therefore, the repulsive V-term which also operates at the nearest-neighbor lattice sites should introduce a pair-breaking mechanism. Hence, there is a competition between the exchange interaction term $\sim J$ which stabilizes the superconducting state and the V-term which suppresses it. Interestingly, the negative influence of the intersite Coulomb term on the pairing is the strongest for the case where the SC gap is the highest among the three considered situations (the smallest values of U). It should be noted that the experimental observation of the generalized Wigner-Mott crystals at fractional fillings of WS_2/WSe_2 heterobilayer indicates a significant value of the parameter V[17–19,21,32]. According to previous theoretical estimates, one should consider $U/V \approx 3$[15] as realistic, which would mean that in the moderately correlated regime (a,b,c,d) the pairing would be completely suppressed by Coulomb repulsion between neighboring sites. However, according to our calculations, in the strongly correlated regime (e,f) and close to half-filling, the superconducting phase is very persistent against the destructive character of the V-term. As we show here, the SC phase survives even above the value of $V = U/3$. Based on the mechanism shown here it is possible to determine an analytical formula which determines the area of the (n,V) phase diagram in which the SC state can be stable. However, this can only be done for a simplified case of purely real hoppings and when the double occupancies are completely projected out from the system (*t*-*J*-*V* model case). We show those considerations in the Appendix for completeness.

To analyze the origin of the effect shown in Fig. 3e, f where SC seems to be strongly immune to the negative influence of the V-term, we show in Fig. 4 the renormalization parameters which tune the actual values of the exchange interaction integral (a) and the intersite Coulomb repulsion integral (b) [cf. Eq. (14)]. Via those renormalization parameters, the electron-electron correlation effects are taken into account within the Gutzwiller approximation applied here. As can be seen in the figure, for the strongly correlated case ($U = 27.19$ meV) and

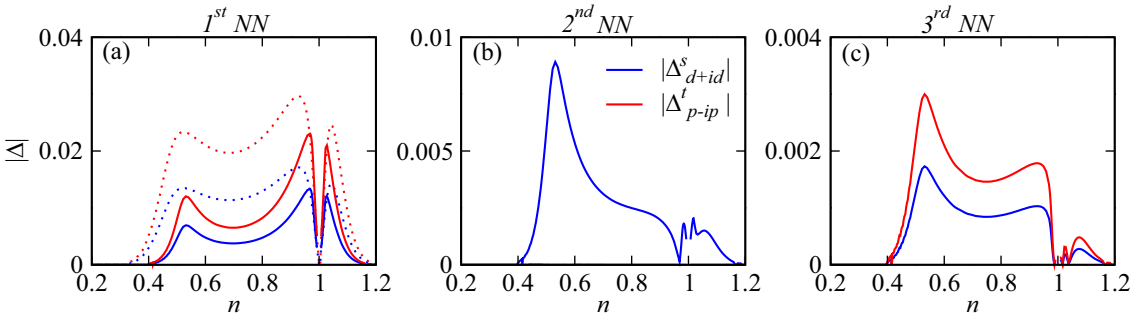

Fig. 5. Symmetry resolved superconducting gap amplitudes corresponding to the first (**a**), second (**b**) and third (**c**) nearest neighbors pairings as functions of band filling (n) for selected values of the on-site Coulomb repulsion $U = 27.19$ and for $V = 0$ (t-J-U model calculations). The solid line corresponds to the case when the hopping and exchange interaction terms are taken into account up to the third nearest neighbor. For comparison we also show the results corresponding to a limited case when only the nearest neighbor terms are included [dashed line in (**a**)].

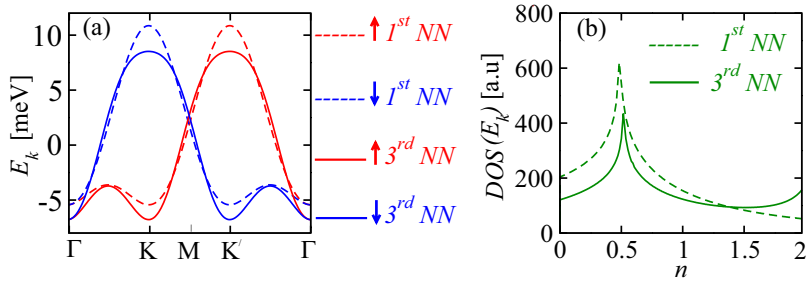

Fig. 6. (**a**) Dispersion relations along the high symmetry directions in the Brillouin zone. (**b**) Density of states at the fermi level as a function of band filling. The dashed and solid lines correspond to the single-particle Hamiltonian $\hat{H}_0$ with the hoppings taken up to the first nearest-neighbor and up to the third nearest neighbor.

close to half-filling ($n \approx 1$), the destructive influence of the V-term is significantly reduced due to significant negative renormalization (small values of g_v^2). At the same time, the J-term is enhanced via positive renormalization (large values λ_s^4). Both effects work in favor of stabilizing the superconducting pairing close to half-fillings for strong enough correlations. Also, as we move away from half filling the renormalization parameters approach the value of $\lambda_s = 1$, $g_v = 1$ meaning that no renormalization takes place due to suppression of the electron-electron correlation effects.

Next, we take into account the effect of long-range exchange and hopping terms on the paired state. In this analysis, we focus on the strongly correlated regime ($U = 27.19$ meV) since as we show above, it corresponds to the most promising case when it comes to the appearance of the SC state. In Fig. 5 we present the superconducting gap amplitudes as functions of band filling calculated with the inclusion of both the hopping and exchange interaction terms up to the third nearest neighbor. The first, second and third exchange interaction integrals have been set to $J_1 = 0.482$ meV, $J_2 = 0.0115$ meV, $J_3 = 0.00178$ meV, respectively. These values have been obtained using the equation $J_l = 4|t_l|^2/U$, where $l = 1, 2, 3$, and t_l corresponds to the hopping to the l-th nearest-neighbor defined by Eq. (5). In the considered case, apart from the symmetry-resolved nearest-neighbor (NN) gap amplitudes shown in (a), we have also calculated the second and third nearest-neighbor counterparts, which are provided in (b) and (c). As can be seen, the NN gap amplitude is still the dominant one, and the inclusion of longer-range terms has not changed the resultant gap symmetry, which is still a mixture of d+id (singlet) and p-ip (triplet). To determine the significance of the long-range terms in Fig. 5a, we provide a comparison between the data obtained with (solid line) and without (dashed line) those additional terms. As one can see, the results did not change qualitatively; however, the long-range terms seem to be suppressing the paired state. As we show in Fig. 6, this negative effect is due to the second and third nearest-neighbor hoppings, which lead to a decrease of the density of states at the Fermi level in the band filling range corresponding to the stability of the SC state. Smaller values of the density of states weakens the pairing similarly as in the conventional superconductors. For the sake of completeness, in Appendix we show explicitly how the SC gap amplitudes depend on particular additional longer-range terms. Our detailed analysis shows that, apart from inducing pairing between additional lattice sites, the longer-range exchange interactions terms do not have a significant influence on the values of the nearest-neighbor SC amplitudes and the stability range of the paired state.

Finally, to determine the necessary conditions for the pairing to appear within the considered approach, we calculate the gap amplitudes as a function of both n and U with the inclusion of all the considered long-range

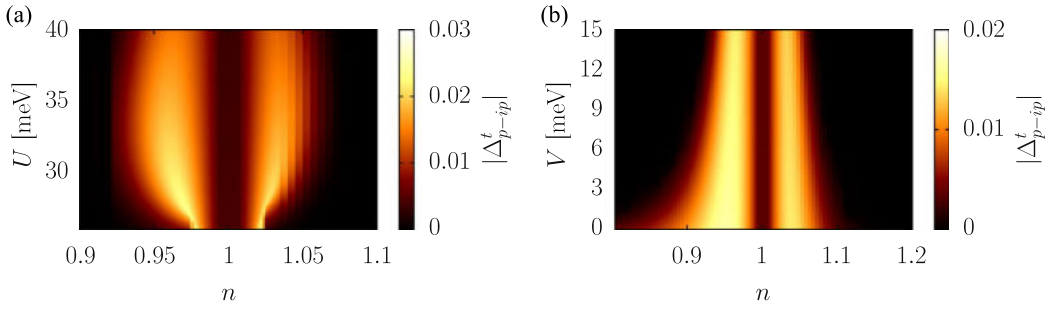

Fig. 7. (**a**) Superconducting gap amplitude for the spin-triplet $p-ip$ pairing channel as a function onsite Coulomb repulsion integral and band filling. Here we keep $U/V = 3$ and $J_l = 4|t_l|^2/U$; (**b**) Superconducting gap amplitude for the spin-triplet $p-ip$ pairing channel as a function intersite Coulomb repulsion integral and band filling for $U = 40$ meV. In (**a**) and (**b**) we show only the dominant triplet contribution to the pairing since the singlet one shows the same behavior but is smaller by factor of ~ 1.5.

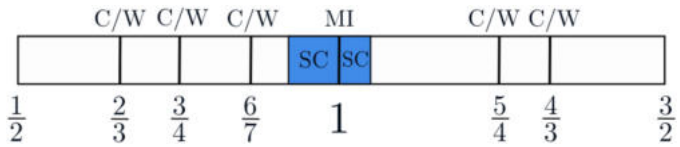

Fig. 8. Schematic phase diagram showing the band filling range of the superconducting phase as obtained here within the *t-J-U-V* model (marked in blue) for optimal model parameters [for $U \approx 30-35$ meV in Fig. 7a] in comparison with the fractional fillings for which the charge/Wigner ordering (C/W) and Mott insulating (MI) states have been reported experimentally[18,19] and/or theoretically[15,41] in the range between $n = 0.5$ and $n = 1.5$.

terms. The data are presented in Fig. 7 where for each U value the exchange couplings, J, have been determined by using Eq. (7) and V have been set by assuming a realistic $U/V = 3$ relation. As can be seen, in the range 25 meV $\lesssim U \lesssim$ 40 meV the SC state is stable in a relatively wide range of band fillings, $0.9 \lesssim n \lesssim 1.0$ and $1.0 \lesssim n \lesssim 1.05$. For $U \approx 25$ meV the SC state covers a very narrow area of the phase diagram. For the sake of completeness, in Fig. 7b we show the phase diagram in the (n,V)-plane for the case of strong Coulomb repulsion $U = 40$ meV also with the inclusion of all the long-range terms. Here we see a similar behavior to that shown in Fig. 3e, f. The final results from Fig. 7 show that by tuning the U parameter one should be able to induce the appearance of the superconducting state in the WSe_2/WS_2 heterobilayer. The U-range in which we obtain a stable SC state is located in the strongly-correlated regime, with the optimal value being $U \approx 2W$.

It should be noted that for significant strength of the V-term one should expect the charge ordered states and generalized Wigner crystals for certain fractional band fillings. Such states are, in fact, observed experimentally[17–19,21,32] and identified theoretically[15] for the WS_2/WSe_2 heterobilayer. As mentioned in the previous section we assume a homogeneous situation, therefore, these effects are not taken into account within our study. Nevertheless, as shown in Fig. 8 the stability range of the SC state, which corresponds to our result from Fig. 7a (for $U \approx 30-35$ meV), does not coincide with the fractional filings that lead to the charge order and Wigner-like states as reported experimentally and theoretically in other studies of the same system[15,18,19,41]. Therefore, the paired state obtained by us should not be significantly altered by the presence of the mentioned effects.

Since the considered Gutzwiller wave function corresponds to the ground state only, our results reflect the $T = 0$ case. To obtain a rough estimate of the critical temperature of the obtained SC state, we apply the standard relation known from BCS theory $\Delta(T=0) = 1.764 k_B T$. The calculated maximum of the joint singlet and triplet superconducting gap amplitude ($\Delta(T=0) = \Delta_{\max} J \approx 0.016$ meV) in the strongly correlated regime [$U = 32$ meV from Fig. 7a] leads to $T_c \approx 1.0$ K. This value should be viewed as a rough upper bound because our calculation is mean field in nature and neglect fluctuations. However in two-dimensional systems such as moiré heterobilayers, thermal and phase fluctuations are expected to further suppress the actual experimental transition temperature below the mean field estimate leading to a sub kelvin range. Although this estimate is simple, it can be useful for experimental comparison while acknowledging the limitations of the method.

Superconductivity in the *t-J-V* model

For the sake of completeness, here, we provide the results obtained within the *t-J-V* model which corresponds to the limit where the double occupancies are completely projected out. For this situation, we impose the conditions given by Eq. (18) which determines the value of variational parameter x. The symmetry-resolved gap amplitudes as functions of the band filling are provided in Fig. 9. Similarly as in Fig. 5, in (a) we show the results of the calculations for which all the longer-range terms are taken into account (solid line) together with those

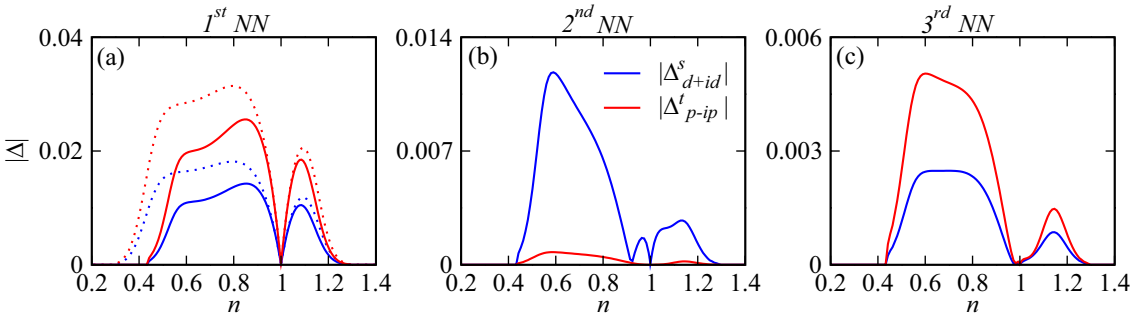

Fig. 9. Symmetry resolved superconducting gap amplitudes corresponding to the first (**a**), second (**b**) and third (**c**) nearest neighbor pairings as functions of band filling (n) for the case of t-J model with the inclusion of both hoppings and exchange interactions up to the third nearest neighbor (solid lines). For comparison we also show the results corresponding to a limited case when only the nearest neighbor hoppings and exchange interactions are included [dashed line in (a)].

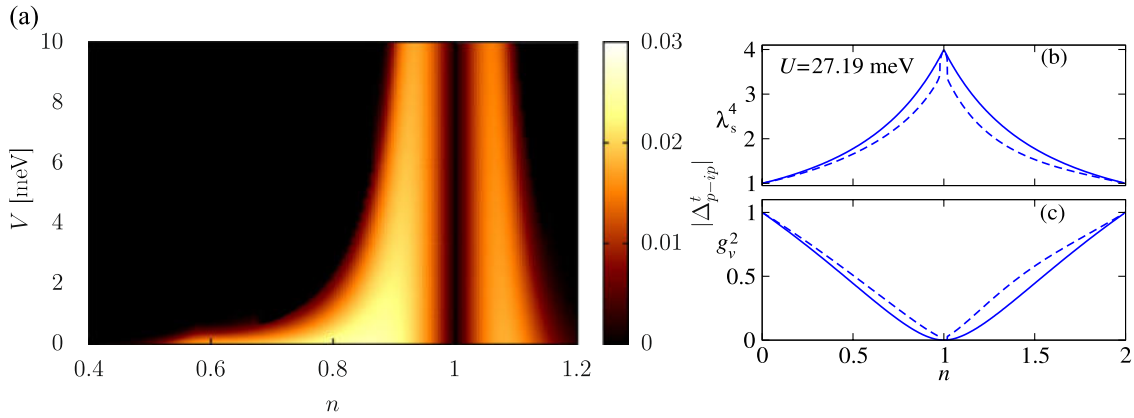

Fig. 10. Superconducting gap amplitude for spin-triplet $p-ip$ symmetry pairing channel as a function of band filling n and intersite Coulomb potential (v) for selected $J = 0.482$ ($U \sim 27.19$ meV) with the inclusion of hoppings up to the third nearest neighbor which corresponds to the case referred in 9(**a**) (solid line) within t-J-V model of WS_2-WSe_2 heterobilayer. The renormalization parameters associated with the exchange interaction (**b**) and inter-site Coulomb repulsion (**c**) are shown. Solid and dashed lines correspond to calculations within the t-J-V and t-J-U-V models, respectively for the inter-site Coulomb repulsion integral of $V = 9$ meV.

obtained with the inclusion of only the nearest-neighbor terms (dotted line). As before, the long-range terms weaken the superconducting phase, but they do not change the qualitative picture with mixed d+id (singlet) and p-ip (triplet) type of pairing.

In Fig. 10, we analyze the influence of the intersite Coulomb repulsion term by showing the gap amplitudes as functions of both n and V. Again, the situation is similar as in the case of the t-J-U-V model. However, here the SC state is more persistent with respect to the negative influence of the V-term on superconductivity. This can be understood in terms of the renormalization factors that modulate the interaction parameters responsible for both the stabilization of the SC state (J) and its suppression (V). As one can see in Fig. 10b, c the renormalization parameters work in favor of the SC state in close proximity of the half-filled case. This mechanism is stronger within the t-J-V model in comparison to the t-J-U-V model case. This is due to the fact that in the former the double occupancies are fully projected out and maximal renormalization is realized as shown in Fig. 10b, c where we compare both theoretical approaches.

Conclusions

We have carried out the analysis of principal features of the superconducting state in the TMD moiré flat band in the strongly correlated regime and in the presence of significant intersite Coulomb repulsion as well as long-range hopping and exchange interaction terms. In our considerations, we have focused on the effective single-band model appropriate for the WS_2/WSe_2 heterobilayer. Our study reveals the stability of a topological superconducting state characterized by a mixed singlet-triplet pairing, with the spin-triplet contribution playing a dominant role. The long-range exchange interaction terms do not have a significant influence on the superconducting phase, whereas the corresponding hopping terms have a visible negative effect on the pairing.

This is because after the inclusion of the additional hoppings, the density of states at the Fermi level decreases in the band-filling range, which corresponds to the stability of the SC state.

The intersite Coulomb term suppresses the pairing completely for the case of the moderately correlated regime for realistic values of V, which are relatively high for the case of the considered system (WS_2/WSe_2 heterobilayer). However, in the strongly correlated regime ($U > W$), the SC state is still able to survive up to the realistic values of the model parameters. This can be understood in terms of the renormalization induced by the electron-electron correlations. Namely, the renormalized nearest neighbor repulsion is reduced while the renormalized exchange is enhanced, allowing superconductivity to persist even when bare V is relatively large. As a result, the SC state appears to be significantly immune to the destructive effect of the inter-site Coulomb term for relatively large values of U and close to half filling where the correlations are the strongest. These findings suggest that the WS_2/WSe_2 heterobilayer can be considered as a promising platform to realize unconventional superconductivity. Nevertheless, this would require a detailed experimental analysis with emphasis placed on the low-temperature regime (below 1K) and close to half-filling. The possibly necessary enhancement of electron-electron correlations, which should stabilize the SC state according to our analysis, can be realized by tuning the twist angle and/or modifying the dielectric environment of the sample to adjust the onsite Coulomb repulsion. According to our analysis the optimal value of U for the stabilization of the paired state is $U \approx 2W$.

An additional comment is in place here. Namely, as shown in Section "Model and method" within the considered approach the correlation effects are included through Gutzwiller renormalization factors capturing the Mott physics and other related effects arising from strong onsite repulsion, U. Nevertheless, for a more complete description which takes into account also non-local correlations, one should go above the considered method by taking into account Jastrov correlators within the Variational Monte Carlo (VMC) approach or carry out the Density Matrix Renormalization Group (DMRG) analysis. The additional effects can promote competing ordered states in certain band filling ranges, making the situation much more complex. In partricular, the significant value of the V-term for the WS_2/WSe_2 heterobilayer should generate charge ordering or in an extreme situation generalized Wigner crystals, which are, in fact, observed experimentally for certain fractional fillings of the system[17–19,21,32]. This effect has been extensively analyzed by us recently by using the DMRG method[41]. Nevertheless, the stability range of the SC state obtained here does not seem to coincide with the fractional filings that lead to the charge order/Wigner-like states as reported experimentally and theoretically in other studies of the same system. Moreover, in close proximity of half-filling where the stability of the SC state has been obtained here, the onsite correlations should play the decisive role, and the physical picture stemming from our analysis should hold. Still, it would be interesting to analyze the possible interaction/competition between Wigner crystal formation (or charge ordering) and SC state within a single theoretical framework taking also into account the possibility of pair-density-wave[42] formation by going above the Gutzwiller approximation method. This requires much more involved analysis and is beyond the scope of this work. Here, we provide a baseline physical mechanism for correlation driven suppression of V and enhancement of pairing near half filling on which future studies can build.

Data availability

The data behind the figures, as well as the code that has been used for the calculations are available in open repository[43].

Appendix

Effective Hamiltonian and comparison with analytical estimates

Here we provide explicitly the form of the effective Hamiltonian as obtained in the considered situation. From the minimization condition imposed on the ground state energy (13) one can derive the following form of the effective Hamiltonian[38]

$$\hat{\mathscr{H}}_{\text{eff}} = \sum_{ij\sigma} \tilde{t}_{ij\sigma} \hat{c}^{\dagger}_{i\sigma} \hat{c}_{j\sigma} - \tilde{\mu} \sum_{i\sigma} \hat{n}_{i\sigma} + \sum_{\langle ij \rangle \sigma}{}' \left((\tilde{\Delta}_{ij\sigma\bar{\sigma}})^* \hat{c}_{j\sigma} \hat{c}_{i\bar{\sigma}} + h.c. \right), \tag{19}$$

where the effective hopping, effective chemical potential, and the effective superconducting gap parameters are defined through the corresponding relations

$$\tilde{t}_{ij\sigma} \equiv \frac{\partial \mathscr{F}}{\partial P_{ij\sigma}}, \quad (\tilde{\Delta}_{ij\sigma\bar{\sigma}})^* \equiv \frac{\partial \mathscr{F}}{\partial S^{\sigma\bar{\sigma}}_{ji}}, \quad \tilde{\mu} \equiv -\frac{\partial \mathscr{F}}{\partial n_s}, \tag{20}$$

where $\mathscr{F} = E_G - 2\mu_G n_s$ and μ_G is the chemical potential in the correlated state. The effective model parameters have the following form

$$\tilde{t}_{ij\sigma} = q^2 t_{ij\sigma} - J \frac{\lambda_s^4}{4} \left[2(P_{ij\bar{\sigma}})^* e^{i2\phi^{\sigma}_{ij}} + (P_{ij\sigma})^* \right] + g_v^2 V (P_{ij\sigma})^*, \tag{21}$$

$$(\tilde{\Delta}^{\sigma\bar{\sigma}}_{ij})^* = -J \frac{\lambda_s^4}{2} \left[2(S^{\sigma\bar{\sigma}}_{ij})^* e^{i2\phi^{\sigma}_{ij}} - (S^{\bar{\sigma}\sigma}_{ij})^* \right] + 2V g_V^2 (S^{\bar{\sigma}\sigma}_{ij}), \tag{22}$$

$$\tilde{\mu} = \mu_G - U\lambda_d^2 n_s - 6V n_s. \tag{23}$$

From Eq. 22 one can explicitly see that both λ_s^4 and g_v^2 parameters modulate the two contributions to the pairing originating from the $\sim J$ and $\sim V$ terms, respectively.
To analyze in more detail the influence of the $\sim V$ term on superconductivity, here, we consider a simplified situation for which $\phi = \pi$, meaning that we have purely real, negative hoppings and an exchange interaction term without the contribution originating from the Dzyaloshinskiiâ€“Moriya interaction. In such a case, the pairing is of spin-singlet character only[28,29] and the SC gap in the effective Hamiltonian has the following form

$$(\tilde{\Delta}_{ij}^{\sigma\bar{\sigma}})^* = -J_{\text{eff}} S_{ij}^{\sigma\bar{\sigma}}, \quad J_{\text{eff}} = J\frac{3\lambda_s^4}{2} - 2g_v^2 V. \tag{24}$$

Hence, the effective interaction works in favor of Cooper pairing when $J_{\text{eff}} > 0$, meaning that $3J\lambda_s^4/2 > 2g_v^2 V$. For the case of $t-J-V$ model when the double occupancies are projected out from the system, one can use Eqs. (12, 15 and 18) to derive the following simple form of the renormalization parameters

$$\begin{aligned} &\text{for} \quad n_s > 0.5: \quad \lambda_s = 1 + \frac{1-n_s}{ns}; \quad g_v = 1 - \frac{1-n_s}{ns}, \\ &\text{for} \quad n_s < 0.5: \quad \lambda_s = 1 + \frac{n_s}{1-ns}; \quad g_v = 1 - \frac{n_s}{1-ns}. \end{aligned} \tag{25}$$

Substituting the above expressions to Eq. (24) we obtain the n_s dependence of the effective pairing parameter in the form

$$\begin{aligned} &\text{for} \quad n_s > 0.5: \quad J_{\text{eff}} = \frac{3(J-2V)}{2(1-n_s)^2} + 8V\frac{n_s}{1-n_s}, \\ &\text{for} \quad n_s < 0.5: \quad J_{\text{eff}} = \frac{3(J-2V)}{2n_s^2} + 8V\frac{1-n_s}{n_s}. \end{aligned} \tag{26}$$

This allows us to analytically determine the area in the (n, V) plane for a given J, for which the necessary condition for the pairing to appear is fulfilled ($J_{\text{eff}} > 0$). In Fig. 11, the solid red line marks the boundary between the attractive interaction that leads to pairing (below the curve) and the repulsive interaction in which the SC state cannot be stable (above the curve). It is clearly shown that the higher the V, the narrower the stability range of the SC state when it comes to band filling. For the sake of completeness, we also show the numerical calculations for the considered case in the figure. The bright region which marks the stability region of the numerically determined SC state does not exceed the analytical requirement for the pairing to exist. The numerical data do not exactly coincide with the analytically determined condition because the latter does not take into account the details of the electronic structure itself. Namely, the stability of the SC state is significantly determined by the value of the density of states around the Fermi energy. For the $\phi = \pi$ situation considered here, the van Hove singularity appears at the Fermi energy for $n > 1$. That is why the SC stability region determined numerically is wider at the $n > 1$ side of the diagram. Nevertheless, the general feature of narrowing the SC stability region with increasing V is seen both in the necessary analytic condition and the numerical result.

Influence of the long-range hoppings and exchange interaction terms

For the sake of completeness, we analyze the significance of long-range hoppings and exchange interactions separately, for the case of the *t-J-U* model. In Fig. 12, we show the influence of the longer-range hoppings without the inclusion of the terms J_2 and J_3. Furthermore, in Fig. 13 we present the dependence of the J_2 and J_3 of the SC gap amplitudes up to the values corresponding to ten times the realistic ones. As one can see, the influence of the long-range hoppings is significant, while exchange terms can be neglected for the case of realistic set of parameters, which are marked by the dashed vertical line. Therefore, the suppression of the SC gap seen in Fig. 5(a) is caused mainly by the second and third nearest-neighbor hoppings. The fact that the additional hoppinngs

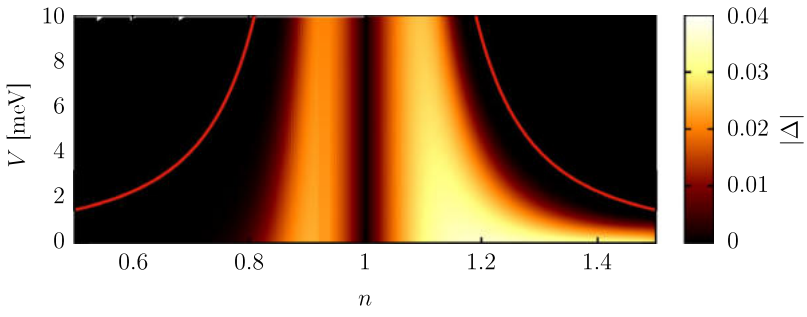

Fig. 11. The superconducting gap amplitude of the spin-singlet $d + id$ symmetry as a function of band filling n and intersite Coulomb integral (V) for selected $J = 0.482$ ($U \sim 27$ meV) for the case of hoppings up to the first nearest neighbor with the phase $\phi = \pi$ (purely real hoppings).

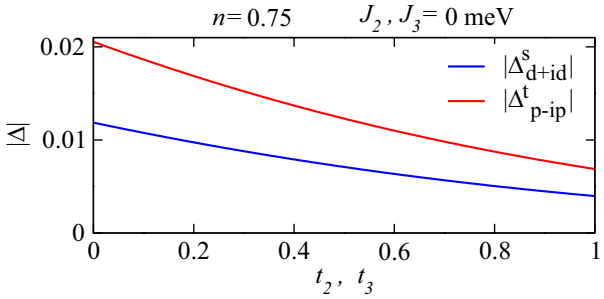

Fig. 12. Symmetry resolved gap amplitudes as a function of the 2nd and 3rd nearest neighbor hopping for selected value of band filling ($n = 0.75$). Here we set $J_2 = J_3 = 0$ since we aim at determining the sole effect resulting from the longer range hoppings. The t_2 and t_3 amplitudes are changed proportionally where 0 means $t_2 = t_3 = 0$ and 1 corresponds to the values determined by Eq. (5).

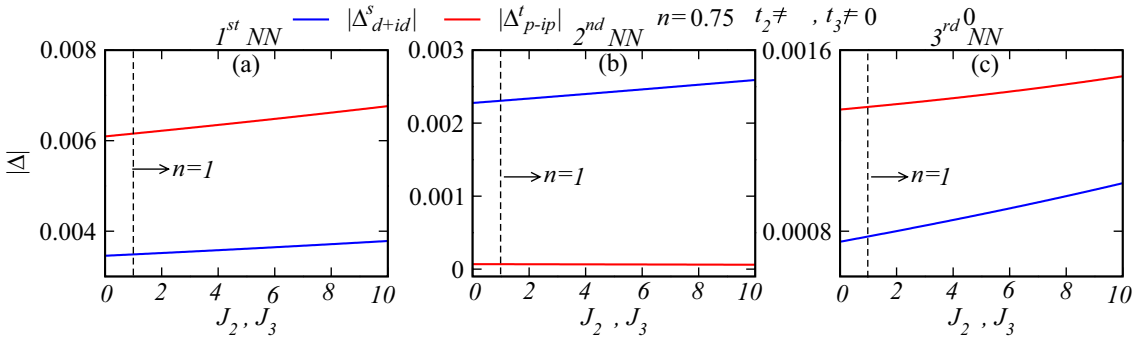

Fig. 13. Symmetry resolved gap amplitudes as a function of the 2nd and 3rd nearest neighbor exchange interaction integrals for a selected value of band filling ($n = 0.75$). Here t_2 and t_3 are set to the values determined by Eq. (5). The J_2 and J_3 amplitudes are changed proportionally where 0 means $J_2 = J_3 = 0$ and 1 corresponds to the values determined by Eq. (7).

suppress the SC gap can be understood by looking at the density of states. Namely, as we show in Fig. 6 the density of states acquires smaller values in the band-filling range of the SC phase for the case where the additional hoppings are taken into account.

Received: 9 November 2025; Accepted: 19 March 2026
Published online: 30 March 2026

References

1. Ghiotto, A. et al. Quantum criticality in twisted transition metal dichalcogenides. *Nature* **597**, 345–349. https://doi.org/10.1038/s41586-021-03815-6 (2021).
2. Wang, L. et al. Correlated electronic phases in twisted bilayer transition metal dichalcogenides. *Nat. Mater.* **19**, 861. https://doi.org/10.1038/s41563-020-0708-6 (2020).
3. Jin, C. et al. Stripe phases in wse2/ws2 moiré superlattices. *Nat. Mater.* **2**, 940. https://doi.org/10.1038/s41563-021-00959-8 (2021).
4. Ghiotto, A. et al. Correlated insulating states at fractional fillings of the ws2/wse2 moiré lattice. *Nat. Phys.* **17**, 715. https://doi.org/10.1038/s41567-021-01171-w (2021).
5. Li, T. et al. Quantum anomalous hall effect from intertwined moiré bands. *Nature* **600**, 641–646. https://doi.org/10.1038/s41586-021-04171-1 (2021).
6. Tao, Z. et al. Valley-coherent quantum anomalous hall state in AB-stacked $MoTe_2/WSe_2$ bilayers. *Phys. Rev. X* **14**, 011004. https://doi.org/10.1103/PhysRevX.14.011004 (2024).
7. Tao, Z. et al. Giant spin hall effect in ab-stacked mote2/wse2 bilayers. *Nature* **19**, 28–33. https://doi.org/10.1038/s41565-023-01492-2 (2024).
8. Guo, Y. et al. Superconductivity in 5.0° twisted bilayer wse2. *Nature* **637**, 839–845. https://doi.org/10.1038/s41586-024-08381-1 (2025).
9. Xia, Y. et al. Superconductivity in twisted bilayer wse2. *Nature* **637**, 833–838. https://doi.org/10.1038/s41586-024-08116-2 (2025).
10. Shi, B. et al. Exotic physical properties of 2d materials modulated by moiré superlattices. *Mater. Adv.* **2**, 5542–5559. https://doi.org/10.1039/D1MA00263E (2021).
11. Stansbury, C. H. et al. Visualizing electron localization of ws2/wse2 moiré superlattices in momentum space. *Sci. Adv.* **7**, eabf4387. https://doi.org/10.1126/sciadv.abf4387 (2021).
12. Gatti, G. et al. Flat Γ moiré bands in twisted bilayer WSe_2. *Phys. Rev. Lett.* **131**, 046401. https://doi.org/10.1103/PhysRevLett.131.046401 (2023).
13. Xia, Y. et al. Bandwidth-tuned mott transition and superconductivity in moiré wse2. *Nature* https://doi.org/10.1038/s41586-025-10049-3 (2026).

14. Pan, H. et al. Band topology, hubbard model, heisenberg model, and dzyaloshinskii-moriya interaction in twisted bilayer wse2. *Phys. Rev. Res.* **2**, 033087. https://doi.org/10.1103/PhysRevResearch.2.033087 (2020).
15. Tan, Y. et al. Doping a wigner-mott insulator: Exotic charge orders in transition metal dichalcogenide moiré heterobilayers. *Phys. Rev. Res.* **5**, 043190. https://doi.org/10.1103/PhysRevResearch.5.043190 (2023).
16. Motruk, J. et al. Kagome chiral spin liquid in transition metal dichalcogenide moiré bilayers. *Phys. Rev. Res.* **5**, L022049. https://doi.org/10.1103/PhysRevResearch.5.L022049 (2023).
17. Regan, E. C. et al. Mott and generalized wigner crystal states in wse2/ws2 moiré superlattices. *Nature* **579**, 359–363. https://doi.org/10.1038/s41586-020-2092-4 (2020).
18. Xu, Y. et al. Correlated insulating states at fractional fillings of moiré superlattices. *Nature* **587**, 214–218. https://doi.org/10.1038/s41586-020-2868-6 (2020).
19. Huang, X. et al. Correlated insulating states at fractional fillings of the ws2/wse2 moiré lattice. *Nat. Phys.* **17**, 715–719. https://doi.org/10.1038/s41567-021-01171-w (2021).
20. Li, T. et al. Continuous mott transition in semiconductor moiré superlattices. *Nature* **596**, 350. https://doi.org/10.1038/s41586-021-03853-0 (2021).
21. Zhou, H. et al. Spotlight: Visualization of moiré quantum phenomena in transition metal dichalcogenide with scanning tunneling microscopy. *ACS Appl. Electron. Mater.* **6**, 1530–1541. https://doi.org/10.1021/acsaelm.3c01328 (2024).
22. Rademaker, L. Spin-orbit coupling in transition metal dichalcogenide heterobilayer flat bands. *Phys. Rev. B* **105**, 195428. https://doi.org/10.1103/PhysRevB.105.195428 (2022).
23. Crepel, V. et al. Bridging the small and large in twisted transition metal dichalcogenide homobilayers: A tight binding model capturing orbital interference and topology across a wide range of twist angles. *Phys. Rev. Res.* **6**, 033127. https://doi.org/10.1103/PhysRevResearch.6.033127 (2024).
24. Fischer, A. et al. Theory of intervalley-coherent afm order and topological superconductivity in twse_2. *Phys. Rev. X* **15**, 041055. https://doi.org/10.1103/gfzx-rrcr (2025).
25. Bélanger, M. et al. Superconductivity in the twisted bilayer transition metal dichalcogenide wse_2: A quantum cluster study. *Phys. Rev. B* **106**, 235135. https://doi.org/10.1103/PhysRevB.106.235135 (2022).
26. Crépel, V., Guerci, D., Cano, J., Pixley, J. H. & Millis, A. Topological superconductivity in doped magnetic moiré semiconductors. *Phys. Rev. Lett.* **131**, 056001. https://doi.org/10.1103/PhysRevLett.131.056001 (2023).
27. Schrade, C. & Fu, L. Nematic, chiral and topological superconductivity in transition metal dichalcogenides. *Phys. Rev. B* https://doi.org/10.1103/PhysRevB.110.035143 (2024).
28. Zegrodnik, M. & Biborski, A. Mixed singlet-triplet superconducting state within the moiré t- j- u model applied to twisted bilayer wse_2. *Phys. Rev. B* **108**, 064506. https://doi.org/10.1103/PhysRevB.108.064506 (2023).
29. Akbar, W., Biborski, A., Rademaker, L. & Zegrodnik, M. Topological superconductivity with mixed singlet-triplet pairing in moiré transition metal dichalcogenide bilayers. *Phys. Rev. B* **110**, 064516. https://doi.org/10.1103/PhysRevB.110.064516 (2024).
30. Biborski, A. & Zegrodnik, M. Signatures of superconducting pairing driven by electron-electron interactions in moiré $\mathrm{wse}_2/\mathrm{wse}_2$ homobilayer modeled by hubbard hamiltonian. *Phys. Rev. B* **112**, L161122. https://doi.org/10.1103/kdpn-5g9d (2025).
31. Zegrodnik, M., Akbar, W., Biborski, A. & Rademaker, L. Optimal superconductivity in twisted bilayer wse_2 where the van hove singularity crosses half-filling. *Phys. Rev. Res.* **8**, L012070. https://doi.org/10.1103/pkf3-fkv4 (2026).
32. Li, H. et al. Imaging two-dimensional generalized wigner crystals. *Nature* **597**, 650–654. https://doi.org/10.1038/s41586-021-03874-9 (2021).
33. Devakul, T. & Fu, L. Quantum anomalous hall effect from inverted charge transfer gap. *Phys. Rev. X* **12**, 021031. https://doi.org/10.1103/PhysRevX.12.021031 (2022).
34. Saha, P., Rademaker, L. & Zegrodnik, M. Interplay between topology and electron-electron interactions in the moiré $\mathrm{mote}_2/\mathrm{wse}_2$ heterobilayer. *Phys. Rev. B* **112**, 045147. https://doi.org/10.1103/phn6-8sbj (2025).
35. Bünemann, J., Schickling, T. & Gebhard, F. Variational study of fermi surface deformations in hubbard models. *Europhys. Lett.* **98**, 27006. https://doi.org/10.1209/0295-5075/98/27006 (2012).
36. Spałek, J., Fidrysiak, M., Zegrodnik, M. & Biborski, A. Superconductivity in high-tc and related strongly correlated systems from variational perspective: Beyond mean field theory. *Phys. Rep.* **959**, 1–117. https://doi.org/10.1016/j.physrep.2022.02.003 (2022).
37. Abram, M., Kaczmarczyk, J., Jędrak, J. & Spałek, J. d-wave superconductivity and its coexistence with antiferromagnetism in the t-j-u model: Statistically consistent gutzwiller approach. *Phys. Rev. B* **88**, 094502. https://doi.org/10.1103/PhysRevB.88.094502 (2013).
38. Kaczmarczyk, J. Comparison of two approaches for the treatment of gutzwiller variational wave functions. *Philos. Mag.* **95**, 563–573. https://doi.org/10.1080/14786435.2014.965235 (2015).
39. Lian, Z. et al. Quadrupolar excitons and hybridized interlayer mott insulator in a trilayer moiré superlattice. *Nat. Commun.* **14**, 4604. https://doi.org/10.1038/s41467-023-40288-9 (2023).
40. Fukui, T., Hatsugai, Y. & Suzuki, H. Chern numbers in discretized brillouin zone: Efficient method of computing (spin) hall conductances. *J. Phys. Soc. Jpn.* **74**, 1674–1677. https://doi.org/10.1143/JPSJ.74.1674 (2005).
41. Biborski, A. & Zegrodnik, M. Charge and spin properties of a generalized wigner crystal realized in the moiré $\mathrm{wse}_2/\mathrm{ws}_2$ heterobilayer. *Phys. Rev. B* **111**, 075116. https://doi.org/10.1103/PhysRevB.111.075116 (2025).
42. Zegrodnik, M. & Spałek, J. Incorporation of charge- and pair-density-wave states into the one-band model of d-wave superconductivity. *Phys. Rev. B* **98**, 155144. https://doi.org/10.1103/PhysRevB.98.155144 (2018).
43. Zegrodnik, M. Unconventional superconductivity in tmd heterobilayers: effect of long range terms [data set]. zenodo. https://doi.org/10.5281/zenodo.18646779.

Author contributions

W.A. did the numerical calculations. W. A. and M. Z. wrote the initial version of the manuscript. M.Z. has proposed the main idea behind this work. W.A., M.Z., L.R., and A.B. analyzed and discussed the results and took part in the conceptual work. All authors reviewed the manuscript.

Funding

This research was funded by National Science Centre, Poland (NCN) according to decision 2021/42/E/ST3/00128. We gratefully acknowledge Polish high-performance computing infrastructure PLGrid (HPC Center: ACK Cyfronet AGH) for providing computer facilities and support within computational grant no. PLG/2024/017372. LR is funded by the Swiss National Science Foundation through Starting Grant No. TMSGI2_211296.

Declarations

Competing interests

The authors declare no competing interests.

Additional information

Correspondence and requests for materials should be addressed to M.Z.

Reprints and permissions information is available at www.nature.com/reprints.

Publisher's note Springer Nature remains neutral with regard to jurisdictional claims in published maps and institutional affiliations.

Chapter 5

Summary

The research presented in this doctoral thesis explores the intricate interplay between electron electron interactions, topological effects and superconducting pairing in TMD bilayers. Motivation comes from recent experimental discoveries of correlated insulating and SC states in the moiré structures based on TMDs [8–10, 50]. These findings have opened a new frontier in condensed matter physics, where strongly interacting electrons confined within flat moiré minibands exhibit emergent phenomena reminiscent of high T_c SC in cuprates, but within a highly tunable 2D platform. The central aim of this research is to construct and analyze microscopic models that capture the essence of paired and insulating states, to identify possible superconducting symmetries and to provide a unified theoretical framework for interpreting the experimentally observed tunable SC in moiré TMD systems.

Our theoretical analysis is based on the t–J and t–J-U models in which superconducting pairing results from kinetic exchange and the single particle part reconstruct is a single moiré band with SOC characteristic for TMD-based systems. Within such effective approach, the interplay between strong electronic correlations and SOC gives rise to exotic character of unconventional SC characterized by mixed parity and nontrivial topological properties. In order to treat these models, we employ the Gutzwiller variational projection technique which lead to systematic renormalization of hopping amplitudes and interaction energies in the presence of different degrees of electron-electron correlations and allows for the description of unconventional superconductivity enabling direct comparison with experimental phase diagrams.

The first major part of the research investigates topological superconductivity with mixed singlet–triplet pairing in tWSe_2 homobilayer. By applying the t–J model on a triangular lattice with complex spin dependent hopping integrals, it is demonstrated that superconducting domes naturally emerge on both sides of a Mott like insulating phase at half-filling. The resulting order parameter exhibits a mixed $(d+id)$ spin-singlet and $(p-ip)$ spin-triplet

gap structure, breaking time-reversal symmetry and giving rise to topologically nontrivial phases characterized by Chern numbers $C = \pm 2, \pm 4$. These findings provide a microscopic explanation for the experimentally observed two-dome superconducting structure and highlight how the displacement field can tune both the singlet–triplet balance and the topological invariant of the superconducting phase. Additionally, the study predicts extended s-wave and f-wave phases at the edges of the phase diagram, although these are topologically trivial. The theoretical phase transitions between topologically distinct superconducting states under variations of carrier filling or external displacement field represent one of the first demonstrations of tunable topological superconductivity in moiré materials.

The second main component of the research refers to the subsequent experimental reports which showed SC for various twist angles in close proximity of half-filling in a relatively narrow range of displacement field for $tWSe_2$. In this part of the analysis we applied the t–J–U–V model. In such framework, V competes with superconducting pairing, while electronic correlations renormalize its effective impact. The calculations reveal that near half-filling the correlation effects, mitigate the pair breaking influence of V, allowing SC to persist even in the presence of substantial intersite repulsion. At the same time, the enhanced density of states near VHS amplifies pairing tendencies. The displacement field tuning is shown to shift the VHS relative to half-filling. As a result the stability of the SC state appears in a small range of the phase diagram at the crossing between the VHS and half-filling, where the two effects can act simultaneously, creating favorable conditions for the paired state in a qualitative agreement with experiments.

Additionally we have also investigated the SC phase in $tWSe_2$ by comparing two distinct theoretical approaches *i.e.,* negative-U Hubbard model and the t-J-U framework. The analysis demonstrates that the negative-U model yields a conventional isotropic s-wave pairing concentrated around VHS. However, this behavior does not fully reproduce the experimental observation which point to SC appearing predominantly near half-filling. The t–J–U approach treated with the use of Gutzwiller method captures the role of strong electronic correlations, leading to an unconventional mixed $d + id$ and $p - ip$ SC state enhanced in the proximity of half-filling due to maximized renormalization effects. These results highlight that the interplay between VHS and electronic correlations is essential for reproducing experimentally observed SC behavior. Overall, the study establishes that strongly correlated frameworks provide a more realistic description of SC in moiré TMD bilayers.

Motivated by the fact that WS_2/WSe_2 moiré heterobilayer share key flat band and correlation features with $tWSe_2$ but differs in their hopping amplitudes and phase, we investigated the possibility of an unconventional SC in this system. For this, we used extended t-J-U-V and t-J-V models across moderate to strong correlation regimes, taking into account

the long range interactions. We find that topological superconductivity survives near half-filling only in the strong coupling regime driven by correlation induced renormalization and dominated by $p-ip$ triplet pairing despite the suppressing effect of V. In this regime, the phase diagram shows two SC domes separated by a Mott insulating phase, reminiscent of cuprates and tWSe_2 moiré bilayers. This part of our analysis indicates that unconventional SC in WS_2/WSe_2 heterobilayers is a realistic possibility in the strongly correlated regime even though it has not been experimentally reported as yet.

Collectively, the research establishes that moiré TMD bilayers are a uniquely versatile platform to explore the intersection of strong correlations, SOC, and topological order. The presence of flat bands due to twist angle or lattice mismatch creates the ideal environment for realizing interaction induced pairing. Across all models studied, the results converge on a common theme *i.e.,* the paired state emerges as a result of unconventional pairing mechanism based on kinetic exchange where the spin-valley locking leads to exotic forms of order parameter with singlet-triplet mixing and non-trivial topology. Moreover, the stability of the paired state is determined by the interplay between the renormalization effects induced by electron correlations and the position of the Van Hove singularity.

Future Outlook. The research presented in this thesis opens numerous pathways for further theoretical and experimental investigations. One promising direction is to extend the models to include explicit multiorbital and valley degrees of freedom, which could reveal additional forms of unconventional SC pairing. Incorporating dynamical mean field theory or quantum Monte Carlo simulations could also provide quantitative estimates of critical temperatures and allow to take into account electronic correlation beyond the Gutzwiller approximation.

Another important direction for future research is to combine moiré TMD superconductors with other 2D materials to make hybrid structures. Additionally, it would be interesting to investigate the interplay between SC and other symmetry broken states such as charge- or spin-density waves, nematic states which are observed in various moiré structures.

References

[1] Y. Cao *et al.*, Nature **556**, 43 (2018).

[2] Y. Cao *et al.*, Nature **556**, 80 (2018).

[3] G. Chen *et al.*, Nature **572**, 215 (2019).

[4] G. Chen *et al.*, Nature Physics **15**, 237 (2019).

[5] X. Liu *et al.*, Nature **583**, 221 (2020).

[6] X. Lu *et al.*, Nature **574**, 653 (2019).

[7] A. L. Sharpe *et al.*, Science **365**, 605 (2019).

[8] L. Wang *et al.*, Nature Materials **19**, 861 (2020).

[9] Y. Xia *et al.*, Nature **637**, 833 (2024).

[10] Y. Guo *et al.*, Nature **637**, 839 (2025).

[11] M. Ogata and H. Fukuyama, Reports on Progress in Physics **71**, 036501 (2008).

[12] H. Kamerlingh Onnes, Communications from the Physical Laboratory of the University of Leiden **120b**, 1 (1911).

[13] W. Meissner and R. Ochsenfeld, Naturwissenschaften **21**, 787 (1933).

[14] J. Bardeen *et al.*, Physical Review **108**, 1175 (1957).

[15] F. Steglich *et al.*, Physical Review Letters **43**, 1892 (1979).

[16] N. M. Plakida, Journal of Magnetism and Magnetic Materials **258-259**, 401 (2003).

[17] C. Duan *et al.*, Nature **600**, 636 (2021).

[18] J. G. Bednorz and K. A. Müller, Zeitschrift für Physik B **64**, 189 (1986).

[19] C. C. Tsuei and J. R. Kirtley, Reviews of Modern Physics **72**, 969 (2000).

[20] A. P. Mackenzie and Y. Maeno, Reviews of Modern Physics **75**, 657 (2003).

[21] K. Umezawa *et al.*, Physical Review Letters **108**, 037002 (2012).

[22] D. Li *et al.*, Nature **572**, 624 (2019).

References

[23] B. R. Ortiz *et al.*, Physical Review Letters **125**, 247002 (2020).

[24] N. P. Armitage *et al.*, Reviews of Modern Physics **82**, 2421 (2010).

[25] B. Keimer *et al.*, Nature **518**, 179 (2015).

[26] J. Hubbard, Proceedings of the Royal Society A **276**, 238 (1963).

[27] F. Steglich *et al.*, Physical Review Letters **43**, 1892 (1979).

[28] P. W. Anderson, Science **235**, 1196 (1987).

[29] T. D. Stanescu and P. Phillips, Physical Review Letters **91**, 017002 (2003).

[30] P. P. Orth *et al.*, npj Quantum Materials **4**, 4 (2019).

[31] W.-W. Yang *et al.*, arXiv preprint arXiv:2101.10611 (2021), arXiv:2101.10611 .

[32] X. Lu *et al.*, Nature **574**, 653 (2019).

[33] M. Yankowitz *et al.*, Science **363**, 1059 (2019).

[34] Y. Tang *et al.*, Nature **579**, 353 (2020).

[35] E. C. Regan *et al.*, Nature **579**, 359 (2020).

[36] A. L. Sharpe *et al.*, Science **365**, 605 (2019).

[37] M. Serlin *et al.*, Science **367**, 900 (2020).

[38] R. Su *et al.*, Nature Materials **22**, 1332 (2023).

[39] Y. Cao *et al.*, Science **372**, 264 (2021).

[40] K. P. Nuckolls *et al.*, Nature **588**, 610 (2020).

[41] T. Devakul *et al.*, Nature Communications **12**, 6730 (2021).

[42] Y. Xu *et al.*, Nature Nanotechnology **17**, 934 (2022).

[43] E. Y. Andrei *et al.*, Nature Reviews Materials **6**, 201 (2021).

[44] D. Zhai *et al.*, Reports on Progress in Physics **88**, 084501 (2025).

[45] M. Angeli *et al.*, Physical Review B **106**, 235159 (2022).

[46] C. Jin *et al.*, Nature **567**, 76 (2019).

[47] N. Gupta *et al.*, RSC Advances **14**, 2878 (2024).

[48] G. Scuri *et al.*, Physical Review Letters **124**, 217403 (2020).

[49] Y. Xia *et al.*, Nature **637**, 833 (2025).

[50] Y. Xia *et al.*, Nature **650**, 585 (2026).

[51] M. Oh *et al.*, Nature **622**, 63 (2023).

[52] Y. Chen *et al.*, Nature Communications **17**, 1077 (2026).

[53] M. Chhowalla *et al.*, Nature Chemistry **5**, 263 (2013).

[54] L. An *et al.*, Nanoscale Horizons **5**, 1309 (2020).

[55] M. Bélanger *et al.*, Physical Review B **106**, 235135 (2022).

[56] M. Christos *et al.*, Physical Review Letters **135**, 046503 (2025).

[57] J. Tuo *et al.*, Nature Communications **16**, 9525 (2025).

[58] X. Huang and et al., Nature Physics **17**, 715 (2021).

[59] Z. Zhang *et al.*, Nature Physics **18**, 1214 (2022).

[60] S. Becker and M. Yang, arXiv preprint arXiv:2401.06078 (2024), arXiv:2401.06078 [cond-mat.str-el] .

[61] Y. Tan and et al., Physical Review Research **5**, 043190 (2023).

[62] J. Motruk and et al., Physical Review Research **5**, L022049 (2023).

[63] Y. Xu *et al.*, Nature **587**, 214 (2020).

[64] H. Zhou *et al.*, ACS Applied Electronic Materials **6**, 1530 (2024).

[65] H. Li and et al., Nature **597**, 650 (2021).

[66] S. Miao *et al.*, Nature Communications **12**, 3608 (2021).

[67] J. Spałek *et al.*, Physical Review B **95**, 024506 (2017).

[68] M. Imada *et al.*, Rev. Mod. Phys. **70**, 1039 (1998).

[69] A. Georges *et al.*, Rev. Mod. Phys. **68**, 13 (1996).

[70] A. Auerbach, *Interacting Electrons and Quantum Magnetism* (Springer, 1994).

[71] D. J. Scalapino, Rev. Mod. Phys. **84**, 1383 (2012).

[72] T. A. Maier *et al.*, Rev. Mod. Phys. **77**, 1027 (2005).

[73] S. R. White and D. J. Scalapino, Phys. Rev. Lett. **80**, 1272 (1998).

[74] F. F. Assaad and H. G. Evertz, Lect. Notes Phys. **739**, 277 (2008).

[75] P. A. Lee *et al.*, Rev. Mod. Phys. **78**, 17 (2006).

[76] T. A. Maier *et al.*, Phys. Rev. Lett. **95**, 237001 (2005).

[77] P. Fazekas, *Lecture Notes on Electron Correlation and Magnetism* (World Scientific, 1999).

[78] K. A. Chao, J. Spałek, and A. M. Oleś, J. Phys. C: Solid State Phys. **10**, L271 (1977).

[79] S. Daul *et al.*, Physical Review Letters **84**, 4188 (2000).

[80] S. Basu *et al.*, Physical Review B **63**, 100506 (2001).

[81] E. Plekhanov *et al.*, Physical Review Letters **90**, 187004 (2003).

[82] T. Xiang *et al.*, Physical Review B **79**, 014524 (2009).

[83] M. Abram *et al.*, Physical Review B **88**, 094502 (2013).

[84] R. B. Laughlin, arXiv preprint arXiv:cond-mat/0209269 (2002), arXiv:cond-mat/0209269 [cond-mat.supr-con] .

[85] F. C. Zhang, Physical Review Letters **90**, 207002 (2003).

[86] H. Pan *et al.*, Physical Review Research **2**, 033087 (2020).

[87] L. Rademaker, Physical Review B **105**, 195428 (2022).

[88] J. Bünemann *et al.*, Europhysics Letters **98**, 27006 (2012).

[89] J. Spałek *et al.*, Physics Reports **959**, 1 (2022).

[90] J. Kaczmarczyk, Philosophical Magazine **95**, 563 (2015), https://doi.org/10.1080/14786435.2014.965235 .

[91] M. Zegrodnik and A. Biborski, Phys. Rev. B **108**, 064506 (2023).